GLYCODENDRIMER MEDIATION OF GALECTIN-3 CANCER PROCESSES AND INDIUM(III) AS A GLYCOSYLATION PROMOTER

by

Anna Kaczmarek Michel

A dissertation submitted in partial fulfillment
of the requirements for the degree

of

Doctor of Philosophy

in

Chemistry

MONTANA STATE UNIVERSITY
Bozeman, Montana

April 2014

©COPYRIGHT

by

Anna Kaczmarek Michel

2014

All Rights Reserved

DEDICATION

For my parents.

ACKNOWLEDGEMENTS

I would like to thank my advisor, Dr. Mary Cloninger, for all of her support and for her faith in me. For all her priceless advice along the way, from avoiding public speaking disasters, to sharing her wealth of knowledge in all things chemistry; to her I am eternally grateful. I would like to thank Dr. Ronald Brisbois for inspiring me with his own love of chemistry. I thank the Cloninger lab for creating a wonderful working environment, and for all your collective guidance along the way. I especially thank Candace, Jessica, and Amanda for always being there for every issue in my life, chemistry or otherwise, big or small. Your friendship means a lot to me. To Kristian's enormous help at the start, and to Garrett's immeasurable help at the end. Thanks to Brad, Ryan, Ky, Sarah, and especially Tyson for all the non-chemistry related distractions. And I thank Martha and my family for always making sure I know that they are proud of me.

I thank you all.

TABLE OF CONTENTS

1. INTRODUCTION TO GALECTIN-3, MUC1, MULTIVALENCY, AND DENDRIMERS 1

Galectins 1
Galectin-3 2
The Roles of Galectin-3 in Types of Cancer 5
Galectin-3 Induced Homotypic Aggregation of Cancer Cells 8
Differences in Healthy and Cancer-Associated Epithelial Cells 9
The Roles of Mucin 1 in Healthy and Cancerous Epithelial Cells 10
Multivalent Systems as a Means to Study Galectin-3 Binding 12
The Dendrimer Framework 15
Conclusion 17

2. THE SYNTHESIS OF LACTOSE FUNCTIONALIZED DENDRIMERS 18

Introduction 18
Results and Discussion 19
Synthesis of Lactose-Functionalized Dendrimers 19
Conclusion 21
Experimental Procedures 21
General Methods 21
Equations Used to Determine Carbohydrate Incorporation on to Dendrimers 25

3. USING GLYCODENDRIMERS TO ARBITRATE GALECTIN-3 CANCER CELL AGGREGATES 30

Introduction 30
Dendrimers Used 32
Cell Lines Used 33
Results and Discussion 33
Cellular Aggregation Assays with A549 Cells and Lactose Functionalized Dendrimers **9-12** 34
Cellular Aggregation Assays with DU-145 and HT-1080 Cells and Lactose Functionalized Dendrimers **9-12** 36
Cellular Aggregation Assays with Fixed Cells 39
Fluorescence Microscopy to Determine the Effect of the Glycodendrimer on the Cell Surface Localization of Galectin-3 41
Conclusion 44
Experimental Procedures 45

TABLE OF CONTENTS – CONTINUED

4. MATRIX METALLOPROTEINASE SUBSTRATE-LINKED DENDRIMERS....52

Introduction....52
Dendrimers as a Drug Delivery System....52
The Roles of Matrix Metalloproteinases in Cancer....55
Using MMP Substrates for Dendritic Drug Design....57
Results and Discussion....59
Conclusion....60
Experimental Procedures....61
General Methods....61

5. INDIUM(III) AS A PROMOTER FOR GLYCOSYLATION....66

Introduction....66
Glycosylation....66
Rationale and Approach....69
Results and Discussion....70
Conclusion....78
Experimental Procedures....78
General Methods....78

6. SUMMARY AND CONCLUSIONS....88

APPENDICES....90

APPENDIX A: Tempo-Lactose Functionalized Dendrimers....91
APPENDIX B: Relevant Spectral Data....100
APPENDIX C: Copyright Information for Reprinted Figures....164

REFERENCES CITED....166

LIST OF TABLES

Table Page

1. MALDI data for lactose functionalized dendrimers 27

2. Degree of functionalization as calculated by equations (a), (b), and (c), and NMR analysis 29

3. A summary of glycosylation yields for tetra-benzylated galactose 72

4. Reactions testing the reversibility of In(III)-promoted glycosylation 73

5. A summary of glycosylation yields for tetra-acetylated mannose 74

6. $In(OTf)_3$ promoted disaccharide formations 75

7. Preparation of pyranoside derivatives in the presence of a proton scavenger 77

8. Conditions for glycosylation of trichloroacetimidates **16-17** 80

9. Conditions for formation of disaccharides **29** and **30** 83

10. Experimental reactant amounts used toward the synthesis of TEMPO-labeled lactose functionalized dendrimers 96

11. M_W determined by MALDI for compounds listed 98

12. Average carbohydrate loading calculated by four methods 98

LIST OF FIGURES

Figure Page

1. Schematic depiction of structural subtypes of galectins 2

2. Crystal structure of the carbohydrate recognition domain of galectin-3 3

3. A representation of N-terminal-associated galectin-3 inducing cellular aggregation through interactions of β–galactosides at the cell surface 4

4. Ligands for galectin-3 5

5. A summary of the roles of galectin-3 in different cancers 6

6. A schematic representation of Mucin-1, relative to the plasma membrane 11

7. Interaction of galectin-3 with MUC1 at the cell surface 12

8. A summary of multivalent interactions 14

9. Structure of a PAMAM dendrimer 15

10. Close-up of the N-H region of an acetylated G2 glycodendrimer 28

11. Proposed dendrimer interactions with galectin-3 in homotypic aggregation 32

12. Lactose-functionalized dendrimers used in homotypic cell assays 33

13. Effect of lactose-functionalized dendrimers on untreated and galectin-3-induced homotypic aggregates of A549 cells 35

14. Representative images taken from cellular assays using A549 cells 36

15. Effect of lactose-functionalized dendrimers on untreated and galectin-3 induced homotypic aggregates of DU-145 cells 37

LIST OF FIGURES - CONTINUED

Figure Page

16. Effect of lactose-functionalized dendrimers on untreated and galectin-3 –induced homotypic aggregates of HT-1080 cells 38

17. Western blot depicting relative amounts of endogenous galectin-3 across cell lines 39

18. Effect of lactose-functionalized dendrimers **9** and **12** on fixed cells with and without added galectin-3 40

19. Micrographs of A549 cells in the absence or presence of galectin-3 and lactose-functionalized dendrimers probed with fluorescent anti-galectin-3 41

20. Western blots demonstrating cross-reactivity of primary antibodies 43

21. Schematics describing cancer cell surface environments in the absence and in the presence of glycodendrimers 44

22. Selected primary data from the controls in cellular aggregation assays on A549 cells 47

23. Selected primary data from cellular aggregation assays of A549 cells in which no additional galectin-3 was added 48

24. Selected primary data from cellular aggregation assays of A549 cells in the presence of additional galectin-3 49

25. Structure of the catalytic domain of MMP-9 generated imaging software 56

26. Fluorescent intensity of MMP-substrates incubated with A549 cells 59

27. Full ^{1}H NMR spectrum for compound **5** 102

28. Smoothed MALDI-TOF spectrum for **5**. 103

29. Full ^{1}H NMR spectrum for compound **6** 104

LIST OF FIGURES - CONTINUED

Figure Page

30. Smoothed MALDI-TOF spectrum for **6**. 105

31. Full ^{1}H NMR spectrum for compound **7**....106

32. Smoothed MALDI-TOF spectrum for **7** 107

33. Full ^{1}H NMR spectrum for compound **8**....108

34. Full ^{13}C NMR spectrum for compound **8** 109

35. Smoothed MALDI-TOF spectrum for **8** 110

36. Full ^{1}H NMR spectrum for compound **9**....111

37. Full ^{13}C NMR spectrum for compound **9** 112

38. Smoothed MALDI-TOF spectrum for **9**. 113

39. Full ^{1}H NMR spectrum for compound **10**....114

40. Smoothed MALDI-TOF spectrum for **10** 115

41. Full ^{1}H NMR spectrum for compound **11**....116

42. Smoothed MALDI-TOF spectrum for **11** 117

43. Full ^{1}H NMR spectrum for compound **12**....118

44. Smoothed MALDI-TOF spectrum for **12** 119

45. Full ^{1}H NMR spectrum for compound **13**....120

46. Full ^{13}C NMR spectrum for compound **13** 121

47. Smoothed MALDI-TOF spectrum for **13** 122

48. Full ^{1}H NMR spectrum for compound **14**....123

49. Full ^{13}C NMR spectrum for compound **14**. 124

LIST OF FIGURES - CONTINUED

Figure Page

50. Smoothed MALDI-TOF spectrum for **14** 125

51. Full ^{1}H NMR spectrum for compound **15**.....126

52. Smoothed MALDI-TOF spectrum for **15** 127

53. Full ^{1}H NMR spectrum for compound **22**.....128

54. Expansion of the ^{1}H NMR carbohydrate region for **22**. 129

55. Full ^{13}C NMR spectrum for compound **22**. 130

56. Full ^{1}H NMR spectrum for compound **23**.....131

57. Expansion of ^{1}H NMR carbohydrate region for **23** 132

58. Full ^{13}C NMR spectrum for compound **23**. 133

59. Full ^{1}H NMR spectrum for compound **24.**.....134

60. Full ^{1}H NMR spectrum for compound **24**.....135

61. Full ^{13}C NMR spectrum for compound **24**.. 136

62. Full ^{1}H NMR spectrum for compound **25**.....137

63. Expansion of the ^{1}H NMR carbohydrate region for **25** 138

64. Full ^{13}C NMR spectrum for compound **25** 139

65. Full ^{1}H NMR spectrum for compound **26**.....140

66. Expansion of ^{1}H NMR carbohydrate region for **26**. 141

67. Full ^{13}C NMR spectrum for compound **26** 142

68. Full ^{1}H NMR spectrum for compound **27**.....143

69. Expansion of the ^{1}H NMR carbohydrate region for **27** 144

LIST OF FIGURES - CONTINUED

Figure Page

70. Full ^{13}C NMR spectrum for compound **27** 145

71. Full ^{1}H NMR spectrum for compound **29**.....146

72. Expansion of the ^{1}H NMR carbohydrate region for **29** 147

73. Full ^{13}C NMR spectrum for compound **29** 148

74. Full ^{1}H NMR spectrum for compound **30**.....149

75. Expansion of the ^{1}H NMR carbohydrate region for **30**. 150

76. Full ^{13}C NMR spectrum for compound **30** 151

77. Smoothed MALDI-TOF spectrum for **31** 152

78. EPR spectrum for **31** 153

79. Smoothed MALDI-TOF spectrum for **32** 154

80. EPR spectrum for **32** 155

81. Smoothed MALDI-TOF spectrum for **33** 156

82. EPR spectrum for **33** 157

83. Smoothed MALDI-TOF spectrum for **34** 158

84. EPR spectrum for **34** 159

85. Smoothed MALDI-TOF spectrum for **35** 160

86. Smoothed MALDI-TOF spectrum for **36** 161

87. Smoothed MALDI-TOF spectrum for **37**. 162

88. Smoothed MALDI-TOF spectrum for **38** 163

LIST OF SCHEMES

Scheme Page

1. Synthesis of lactose-functionalized PAMAM dendrimers 20

2. Final steps in the synthesis of MMP-substrate labeled lactose functionalized dendrimers 58

3. General scheme for glycosylation.....67

4. Solvent effects in glycosylation 68

5. General scheme of reactions 70

6. The formation of disaccharides **29** and **30** using In(III) as a promoter 75

7. Brønsted acid-promoted glycosylation of a sugar 76

8. Synthesis of lactose-functionalized dendrimers labeled with TEMPO 93

9. Synthesis for the TEMPO-labeled lactose monomer.....94

ABSTRACT

Galectin-3 is a carbohydrate-binding protein that is found inside and at the surface of most healthy cells, where it plays a role in cellular differentiation, proliferation, and death. Galectin-3 is also overexpressed in many forms of cancer, where it interacts with β-galactosides on the surface of the transmembrane protein Mucin 1 (MUC1), which is also upregulated in many cancers. The interaction between MUC1 and galectin-3 leads to enhanced tumor formation, invasion, and metastasis.

Glycodendrimers were synthesized and used as tools to probe the galectin-3/MUC1 mediated cancer cellular aggregation. Cellular aggregation assays were designed and performed using three different cancer cell lines. Results indicate that cellular aggregation can either be inhibited or intensified depending on the size of the dendrimer and on the number of carbohydrate endgroups present. Confocal micrographs of cancer cells confirm that the pattern of galectin-3 on the outside of the cell is altered in the presence of glycodendrimers. These finding indicate that glycodendrimers mediate cellular aggregation properties, giving insight into the mechanism of action. The results also establish glycodendrimers as potential targeting agents and prodrug delivery systems when considering cancer drug design. A dendrimer bearing a matrix metalloproteinase (MMP) substrate was synthesized to explore dendritic potential as drug delivery systems. Results show that the substrate can be cleaved from the dendrimer when incubated with cancer cells known to overexpress MMP, indicating a potential for glycodendrimers as a prodrug carrier.

A novel method for glycosylation was also explored. Indium(III) provides many advantages over standard glycosylation promoters (such as $BF_3 \bullet OEt_2$) in that it is not air- or water-sensitive, and there is no need for additional purification of In(III) before use. Carbohydrate donors with a variety of protecting groups were tested against a range of glycosyl acceptors, including a carbohydrate. Results show that using In(III) as a glycosylation promoter gives comparable yields in less time when compared to a common glycosylation promoter.

CHAPTER 1

INTRODUCTION TO GALECTIN-3, MUC1, MULTIVALENCY, AND DENDRIMERS

Galectins

Lectins are a family of proteins that specifically recognize and reversibly bind carbohydrates and are found in most plants and animals, indicating that they have an important role in basic biological functions.[1, 2] In animals, lectins have known roles in cell adhesion processes, immune response, and protein recognition.[3, 4] Lectins can be further broken down into subfamilies, including the Ca^{2+}-dependant, or C-type, lectin family of selectins, collectins, and hyalectans. I-type lectins belong to the immunoglobulin superfamily of lectins, which includes siglecs.[5] S-type lectins (sulphydryl-dependent), now more commonly known as galectins, are a class of lectins that bind specifically to β-galactosides. Galectins are not membrane-bound and are implicated in both intra- and extracellular roles. Fifteen galectins have been reported in the literature and are named in the order of their discovery; each includes a conserved carbohydrate recognition domain (CRD) of roughly 130 amino acids arranged in a folded β-sheet.[5] These 15 galectins can be further broken down into the three distinct structure types shown in Figure 1.

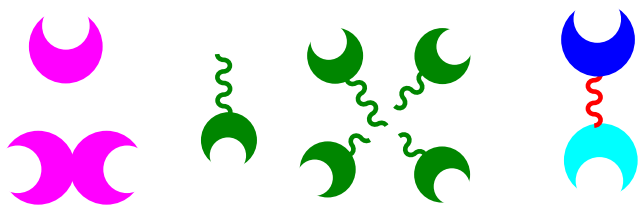


Figure 1. Schematic depiction of the structural subtypes of galectins. Prototype galectins contain a single carbohydrate recognition domain (CRD) that can form homodimers. Chimera-type contain an extended collagen-like tail capable of oligomerization in addition to the CRD. Tandem repeat types contain two unique CRDs bound by a short peptide chain.[5]

Prototype galectins consist of galectins- 1, 2, 5, 7, 10, 11, 13, 14, and 15 and contain a single CRD, although they are capable of forming homodimers. Galectin-3 is the only known chimera-type galectin,[5, 6] and its extended N-terminus collagen-like tail distinguishes it from the other members of the galectin family. The third structure type includes galectins-4, 6, 8, 9, and 12 and is defined by having two CRDs bound by a short peptide sequence that forms a heterodimer.[6] Though the CRD is conserved across structure types, galectins are expressed in different parts of the body. For example, galectin-2 is expressed exclusively in the liver, galectin-5 in erythrocytes, and galectin-11 in the lens.[7] The expression amount and type of galectin also varies greatly depending on developmental stage; galectins-1, -3, and -9 are all implicated in early embryonic development and are highly expressed at the maternal-fetal interface.[8]

Galectin-3

Of the galectins, galectin-3 is the most studied. Though it is involved in normal biological functions and is found in most healthy animal cells,[9] it is the implication of galectin-3 in cancer processes that makes the protein an interesting target when

considering investigations into cancer pathways and developing cancer markers and targets.

Galectin-3 is the only known chimeric lectin with the conserved carbohydrate binding domain specific for β-galactosides found in all galectins (Figure 2). It has a collagen-like tail rich in proline, lysine, and tyrosine and is capable of forming pentamers and other oligomers at high concentrations or when interacting with multivalent frameworks.[9, 10, 13-17] Galectin-3 is expressed in the intestine, kidney, neurons, testes, prostate, leukocytes, bone, and breast tissues.[7] The oligomeric state of galectin-3 is concentration-dependent, but it has been reported as a monomer, dimer, and pentamer.[14,18, 19] Oligomerization occurs through the association of the collagen-like tails on different molecules of galectin-3, which leads to the induction of cellular aggregation (Figure 3).[14, 20]

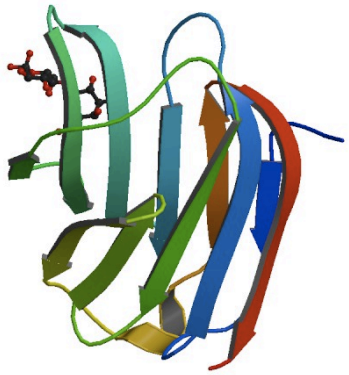


Figure 2. A crystal structure of the carbohydrate recognition domain of galectin-3. Lactose is shown interacting in the shallow binding pocket.[10-12]

The effect described in Figure 3 has been shown through protein fragmentation studies. Isolated fragments of the N-terminal domain have been shown to self-associate,

but no agglutination occurs without the CRD.[21] Similarly, studies using the CRD without the tail show β-galactoside binding still occurs, but without the tail present, no agglutination activity is observed.[22]

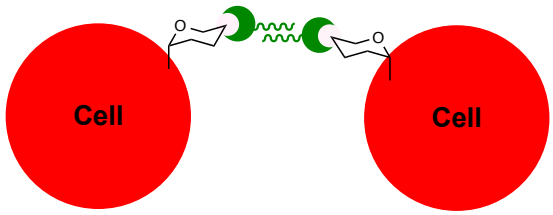


Figure 3. A representation of N-terminal-associated galectin-3 (green) inducing cellular aggregation through interactions of β-galactosides at the cell surface.

In healthy animal cells, galectin-3 is found in both the intracellular and extracellular regions and is involved in a number of processes, including regulation of cell adhesion, immuno- and inflammation response, and apoptosis.[9] The function and activity of galectin-3 are directly related to its ability to effectively and selectively bind to β-galactosides. Three β-galactoside binding partners have been extensively researched: lactose, *N*-acetyllactosamine, and cancer-associated Thomsen-Friedenreich antigen (TF antigen), shown in Figure 4.[13, 23-26] Though monovalent binding of these ligands by galectin-3 is relatively weak, the oligomeric nature of the protein enhances binding. Increasing the local concentration of ligands near galectin-3 also enhances binding.[27] Multivalent frameworks as a means to study the binding of galectin-3 are discussed in more detail later in the chapter.

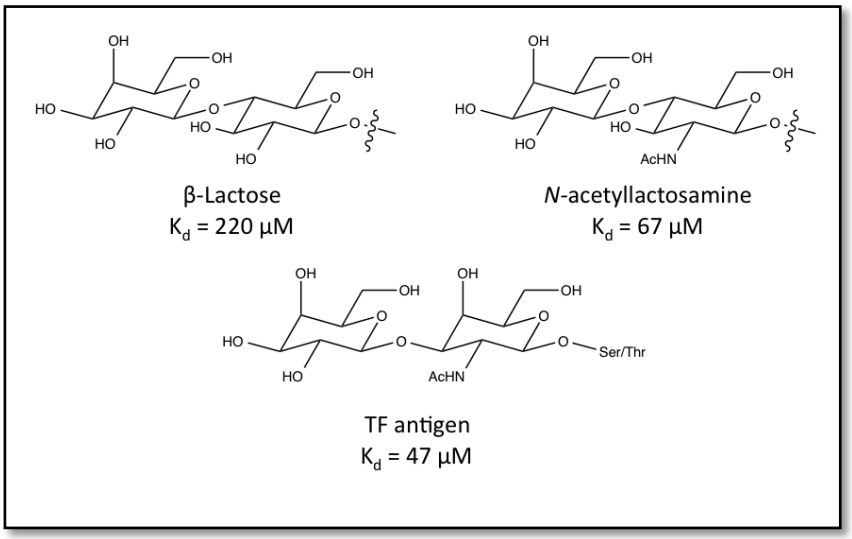


Figure 4. Ligands for galectin-3. Listed K_d values were determined by competitive fluorescence polarization.[25, 28]

The Roles of Galectin-3 in Types of Cancer

Though galectins are necessary for basic biological functions, they have also been implicated in many cancer processes and have emerged as potential biomarkers in certain types of cancer.[6] Galectin-3 has been found to be overexpressed in many forms of cancer[29, 30] and has been implicated in an abundance of processes (as shown in Figure 5).[29] In general, there is a correlation between the amount of circulating galectin-3 and the aggressiveness of the cancer.[23, 31-33]

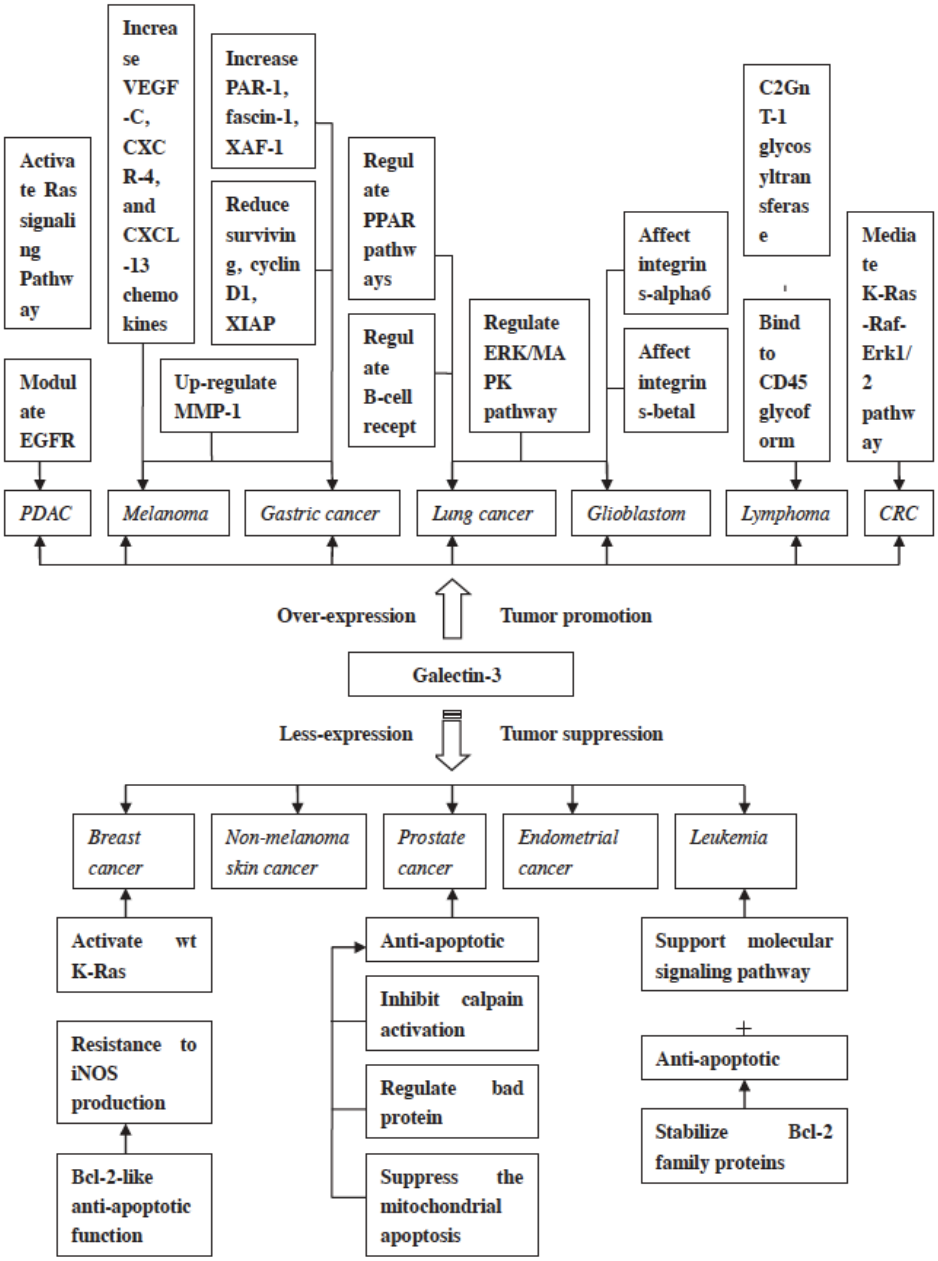


Figure 5. A summary of the roles of galectin-3 in different cancers. Abbreviations: PDAC, pancreatic carcinoma; CRC, colorectal cancer; Bcl-2, B-cell lymphoma-2; CXCR-4/13, C-X-C chemokine receptor type 4/13; MMP-1, matrix metalloproteinase-1; PPAR, peroxisome proliferator-activated receptor; C2GnT1, core 2 β 1,6-N-acetylglucosaminyl transferase 1; PAR-1, Protease-activated receptors-1; ERK, extracellular regulated protein kinases; MAPK, mitogen-activated protein kinases. Reprinted with permission from Tang, et al. [39]

Galectin-3 is known to be upregulated in many forms of cancer and has been explored as a potential diagnostic marker. In thyroid cancer, galectin-3 is highly overexpressed in relation to healthy thyroid cells and to benign thyroid lesions.[34, 35] Overexpression of galectin-3 is also reported for renal neoplasia, and galectin-3 has been suggested as a prognostic indicator in both of these forms of cancer.[34, 36] Expression levels have also been found to be downregulated in certain forms of cancer, such as cervical cancer and some forms of brain cancer.[6, 34, 37] In hormone-sensitive prostate cancers, galectin-3 expression has been shown to be significantly downregulated compared to healthy prostate cells, a phenomenon directly correlated with the progression of the cancer. [34, 38]

Galectin-3 can be used as a prognostic tool for certain types of cancer. In addition to those already discussed, the expression of galectin-3 in tumors from colorectal cancers correlated with the progression of cancer, with higher levels correlating to poorer patient prognoses. The same results were found with gastric and laryngeal cancers.[34, 40, 41]

Galectin-3 is involved in many cancer-specific pathways (Figure 5).[30] In breast cancer, an increase in galectin-3 expression correlates with vascular invasion and metastasis by means of an invasive mechanism as opposed to acting as a proliferation promoter. As with prostate cancer, breast cancer patients had poorer prognoses when downregulation of galectin-3 expression was observed.[42] *In vitro* studies using the breast cancer cell line BT-549 demonstrated that oncogenic and metastatic potential were enhanced through the activation by galectin-3 of wild-type K-*Ras,* a protein that recruits growth factors that lead to cancer progression.[43, 44] The *Ras* protein is also bound to and activated by galectin-3 in pancreatic tumor tissues, where galectin-3 is significantly

overexpressed, leading to both cancer cell proliferation and increased invasion in this case.[45] In colorectal cancer, galectin-3 binding proteins like LGALS3BP are overproduced, which acts to remove galectin-3 from the system, thereby advancing the cancer through increasing cell motility and migration.[46] Among its many functions in gastric cancer, it is proposed that galectin-3 increases metastasis by promoting the expression of protein-activated receptor PAR-1 and matrix metalloproteinase-1 (MMP-1).[47] In the blood cancer leukemia, upregulation of galectin-3 stabilizes anti-apoptotic Bcl-2 proteins, preventing cells from undergoing apoptosis, thereby advancing the cancer.[48]

The collagen-like tail on galectin-3 can be cleaved by MMP-2 and MMP-9 between the Gly^{32}-Ala^{33} and Ala^{62}-Tyr^{63} amino acids, resulting in a truncation to about 27 and 22 KDa, respectively. It is hypothesized that the truncated form of the protein contributes to tumorigenic potential of breast cancer cell line BT-549. In that same cell line, it was also shown that the cleaved galectin-3 had enhanced chemotactic properties toward endothelial cells, which aided in the onset of angiogenesis.[49] MMPs are often overexpressed in cancer and involved in cancer processes such as angiogenesis and metastasis, and presence of the cleaved form of galectin-3 can be used as an *in vivo* diagnostic measure of MMP activity.[50]

Galectin-3 Induced Homotypic Aggregation of Cancer Cells

As shown in Figure 3, galectin-3 is capable of cross-linking cells by oligomerization through association of multiple N-termini. In cancer, this event is implicated in metastatic advancement through the interaction of galectin-3 oligomers

with glycoconjugates found on the surface of multiple cancer cells, inducing homotypic cell adhesion.[50, 51] It is believed that this process is due, in part, to the interaction of galectin-3 with the TF antigen, a β-galactoside expressed on the surface of cancer cells in 90% of cancers.[52] It has been shown that a natural ligand of galectin-3 is cancer-associated Mucin 1 (MUC1), a large, heavily glycosylated transmembrane glycoprotein that displays TF antigen and is overexpressed on epithelial cancer cells.[31, 53-56]

Differences in Healthy and Cancer-Associated Epithelial Cells

Of the four major tissue types in animals (connective, muscle, epithelial, and nervous), epithelial cells are the most abundant. They act to line body cavities and coat smooth surfaces. They line veins and the digestive tract, as well as most organs, and comprise most of the tissue in the lungs and skin. The surface of epithelial cells is inherently polar, with apical (upper), lateral (central) and basal (lower) membrane domains. Epithelial cells form tight junctions with other epithelial cells at their lateral membrane domains to form epithelial sheets, called the epithelium, which has the primary function of protection from outside toxins and trauma. The epithelial sheet also acts as a conduit between the inside and outside of an organ requiring a highly polarized surface. The epithelium is avascular and receives nutrients through the basal layer.

The three domains of the epithelial cell are unique in their structure, purpose, and the proteins they express. The lateral membrane contains adhesion molecules that allow for tight junctions. The basal membrane absorbs nutrients from the basement membrane, which consists of extracellular matrix proteins that mark the junction between the epithelium and connective tissues.[57, 58] The apical surface contains heavily glycosylated

mucin proteins that protect the cell surface from outside toxins. The basal and lateral membranes are often grouped together as the basolateral membrane, which acts as a junction between cell surfaces and contains many adhesion molecules including E-cadherin, α- and β-catenin (unlike the apical face, which is contact-free).[57] Epithelial cell polarity directs the tissue formation of epithelial sheets, resulting in planar cell polarity.[59,60] Cell polarity is also vital for basic organ functions, and a disturbance in this polarity is indicative of disease.[61] When polarity is disrupted, there is a breakdown in cell-cell signaling, apoptosis, cell differentiation, and other basic functions may be evaded.[60] In fact, loss of cell polarity is a critical step toward disease progression, with studies showing that genes involved in inducing and regulating polarity in the epithelium also operate as tumor suppressors and proto-oncoproteins.[57, 59, 60] Over 80% of human tumors are epithelial in origin, and the downregulation of these polarity-regulating proteins is an important hallmark of tumor progression and invasion.[60]

The Roles of Mucin 1 in Healthy and Cancerous Epithelial Cells

In healthy epithelial cells, MUC1 is a very large, heavily glycosylated protein that has a mass up to 500 kDa once glycosylated (Figure 6). It is constrained to the apical side of the cell (Figure 7a) and extends away from the cell surface, providing a mucosal-membrane surface that coats the interior of respiratory, gastrointestinal, and reproductive tracts and keeps irritants from interacting with the cell surface.[62-64] It is involved in signal transduction through its heavily glycosylated surface and is also an actor in the prevention of bacterial infections. MUC1 not only acts as a steric barrier between the infecting bacteria and the cell surface, but it intercepts the bacteria before it can interact

with the cell. After binding to bacteria, the MUC1-bacterial moiety is shed from the cell surface and discarded in digestive fluids.[63, 64] MUC1 serves in many important biological roles in healthy systems, but much like galectin-3, it is the implications of MUC1 in cancer mechanisms and the glycoprotein's potential as a cancer biomarker that are currently of particular interest to the scientific community.[65, 66]

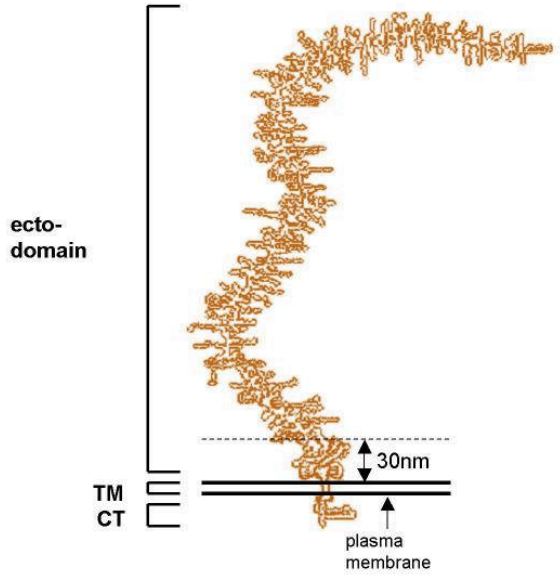


Figure 6. A schematic representation of Mucin-1, relative to the plasma membrane. The C-terminal (CT) and ectoplasmic (ecto) domain are both shown, as well as the single trans-membrane domain (TM). Reprinted with permission from Brayman, *et al*.[62]

In epithelial cancer cells, cell polarity is minimized, and MUC1 is no longer confined to the apical surface, but is overexpressed across the entire surface of cancer cells and is aberrantly glycosylated (Figure 7b).[23] Cancer-associated MUC1 acts to shield the adhesion molecules on the surface of the cell, increasing vascular invasion potential. The truncated glycosylation exposes TF antigen, a serine- or threonine-linked disaccharide (Galβ1-3GalNAc-α-O-Ser/Thr) that is thought to be a natural ligand for

galectin-3.[24, 31] Circulating galectin-3 interacts with the TF antigen on MUC1, polarizing the trans-membrane mucin on the cell surface, exposing adhesion molecules and allowing for increased homotypic (tumor formation) and heterotypic (metastasis) cellular adhesions to occur (Figure 7c).[23]

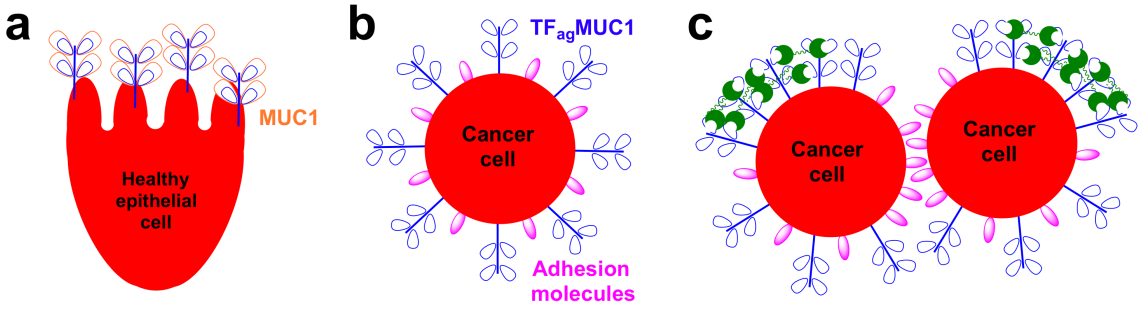


Figure 7. Interaction of galectin-3 with MUC1 at the cell surface. (a) A healthy epithelial cell with a normal distribution of MUC1. (b) The cell surface of a cancer cell with over-expressed and aberrantly glycosylated MUC1. (c) When circulating galectin-3 (green) is introduced to the cancer cell surface, its interaction with cancer-associated MUC1 causes adhesion molecules to be exposed, inducing aggregation. Schematic adapted from Yu, *et al*.[24]

Multivalent Systems as a Means to Study Galectin-3 Binding

One molecule of galectin-3 binds monovalently to a β-galactoside, and a relatively weak interaction results, with dissociation constants in the low μM range (see Figure 4). The characteristic chimeric N-terminal collagen-like tail, however, allows galectin-3 to associate with other galectin-3 proteins resulting in an oligomer. The number of galectin-3 molecules that oligomerize is debated, but found largely to be concentration-dependent, ranging from a dimer to pentamer.[14, 18, 19] Having the ability to form a multivalent quaternary structure, galectin-3 is an excellent target for the study of multivalent binding. Multivalency is a common effect that increases the affinity a

substrate has for its ligand. When multiple ligands are bound into a single moiety, this is commonly called the cluster effect, a concept investigated by Y.C. Lee who initially demonstrated a dramatically enhanced affinity for mammalian hepatic lectin to both synthetically-created glycoclusters as well as natural oligosaccharides derived from proteins.[67] Lee, *et al.* went on to further explore this idea by varying the sugar density on bovine serum albumin (BSA) and surveyed its binding affinity to rabbit hepatocytes. They found that, while only one sugar is required for binding, a multivalent carbohydrate framework is required for efficient binding; that for every linear increase in carbohydrate density on BSA, the binding affinity actually increases logarithmically up to 20 sugars per protein.[68,69]

It has been previously demonstrated that galectin-3 shows a higher affinity for multivalent networks of β-galactosides than for monomeric carbohydrates.[70] A structured, octavalent lactose scaffold enhanced the affinity of galectin-3 to lactose by over 500 times on a per-lactose basis.[70, 71] Multivalency provides a number of beneficial characteristics, those of particular interest when applying multivalency to the study of galectin-3 are highlighted in Figure 8.

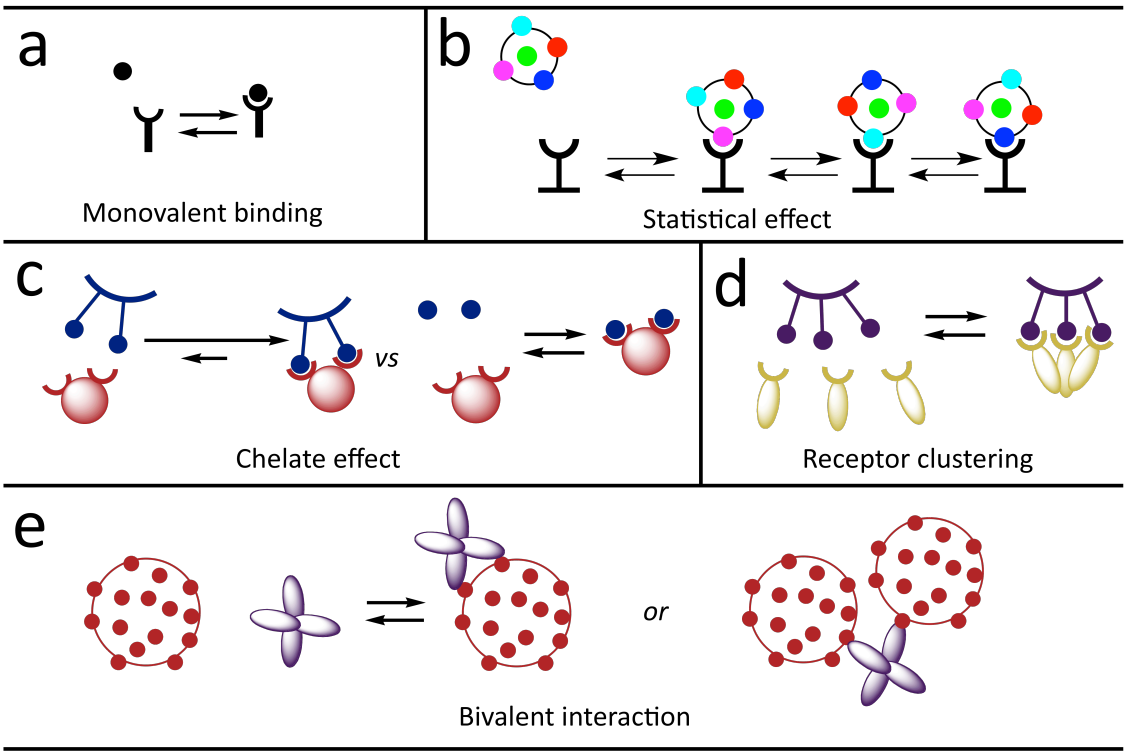
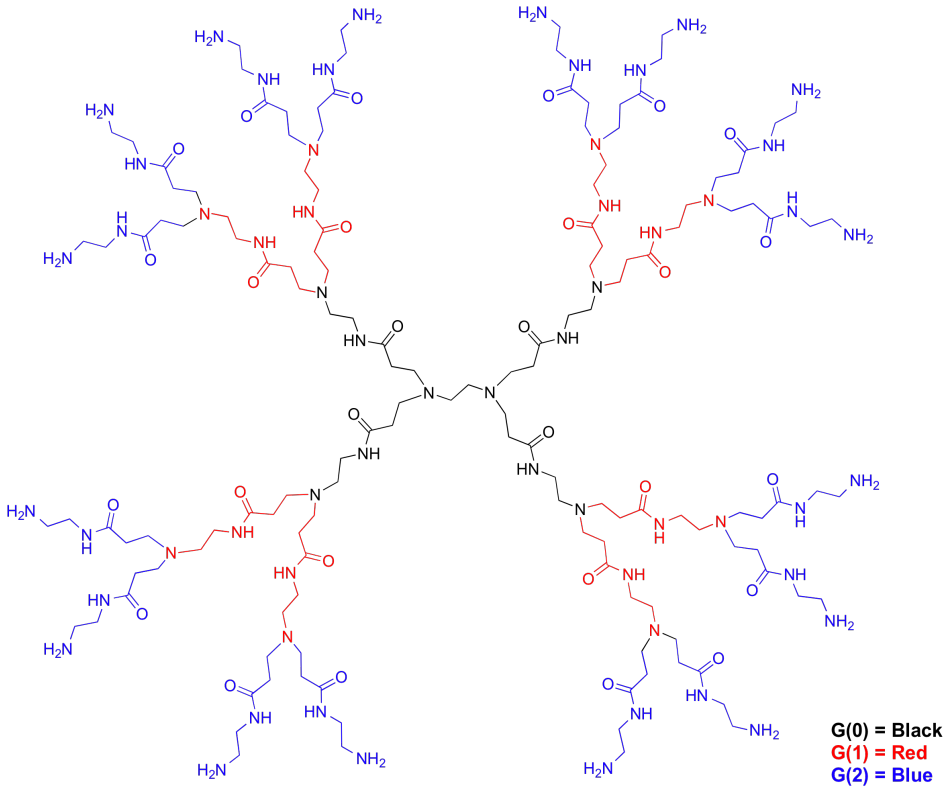


Figure 8. A summary of multivalent interactions.

Typical monovalent binding is depicted in Figure 8a, compared to the statistical effect in Figure 8b, which allows for enhanced binding through the use of a framework with multiple ligands and effectively increases the time a ligand will interact with a receptor. There is also an entropic gain from the chelate effect (Figure 8c); a bivalent ligand binding to a dual receptor is more entropically favorable than two separate ligands binding in the same footprint. Both Figure 8d and 8e show how ligands can be re-patterned in their environment, causing either receptor clustering or clustering of the framework via an oligomeric receptor.

The Dendrimer Framework



Generation 2 PAMAM Dendrimer

Figure 9. The structure of a PAMAM dendrimer. Black shows a generation zero (G0) dendrimer with 4 amino-endgroups. In red is the G1 dendrimer with 8 endgroups, and G2 in blue with 16 endgoups.

Dendrimers are a valuable framework that can be utilized in the exploration of the significance of multivalency in carbohydrate-protein interactions. They are symmetrical, highly branched, polymeric constructs. They contain a variable amount of end groups that can be synthetically modified with a number of functionalities.[72] This versatility in functionalization makes them an attractive scaffold for many purposes, including drug delivery, tissue repair, and cellular imaging.[73, 74] A widely used framework has a polyamido amine (PAMAM) core, with amine endgroups that can be easily synthetically

modified in a number of ways (Figure 9). PAMAM dendrimers are spheroidal in nature, and each increase in generation doubles the amount of amino-endgroups, starting with a generation zero (G0) PAMAM dendrimer containing 4 terminal amines, up to a G10, with 4096 theoretical end groups.

Specifically, the PAMAM scaffold can be functionalized with carbohydrates, creating glycodendrimers. This area of dendrimer research has a number of biological implications, primarily that of monitoring intercellular signaling through protein-carbohydrate interactions.[75] Dendrimers are ideal scaffolds to study these interactions due to their adjustable size and multivalency.[76] Glycosyl receptors, such as galectin-3, have low affinities for their monovalent substrates, but when multiple glycosides are fixed to a biological or synthetic scaffold, this interaction is greatly enhanced.[77] Studies have already been performed that utilize PAMAM dendrimer scaffolds to study protein-carbohydrate interactions. Woller, *et al.* showed that mannose-functionalized PAMAM dendrimers can exhibit control over the binding activity of the mannose-binding plant lectin Concanavalin A (Con A) depending on the amount of carbohydrates present on the dendrimer framework. They also demonstrated that re-patterning the Con A in its environment is possible by causing the lectin to cluster around the dendrimers in a generation-dependent manner.[78] Mannose or *N*-acetylglucosamine functionalized PAMAM dendrimers were used to study their binding affinity with lymphocyte rat receptors NKR-P1A and NKR-P1B. Compared to the monomeric form of the sugars, binding was dramatically increased for the oligomeric forms of the receptors.[79] Goodman, *et al.* have used lactose-functionalized dendrimers to study the aggregating

behavior of galectin-3, demonstrating that protein aggregate size and polydispersity were dependent on the size of the multivalent platform used and carbohydrates available.[80]

Conclusion

To summarize, upregulation and downregulation of galectin-3 has been shown to correlate to tumor formation, cancer progression, and metastasis. A particularly interesting effect of cancer-associated galectin-3 is that the protein can induce cellular adhesion through binding β-galactosides on the surface of cells. In epithelial cancers, MUC1 displays the β-galactoside TF antigen. Circulating galectin-3 interacts with TF antigen on the surface of MUC1, which polarizes the cell surface and exposes adhesion molecules, leading to homotypic and heterotypic cellular aggregation. The cellular aggregation then leads to cancer progression. Because both MUC1 and galectin-3 play integral roles in important processes related to cancer progression, they are important targets when considering the design of therapeutics. Through the use of a multivalent framework with a β-galactoside display of lactose, the role of galectin-3, and by extension MUC1, can be further elucidated as described in the remaining chapters of this thesis.

CHAPTER 2

THE SYNTHESIS OF LACTOSE FUNCTIONALIZED DENDRIMERS

Introduction

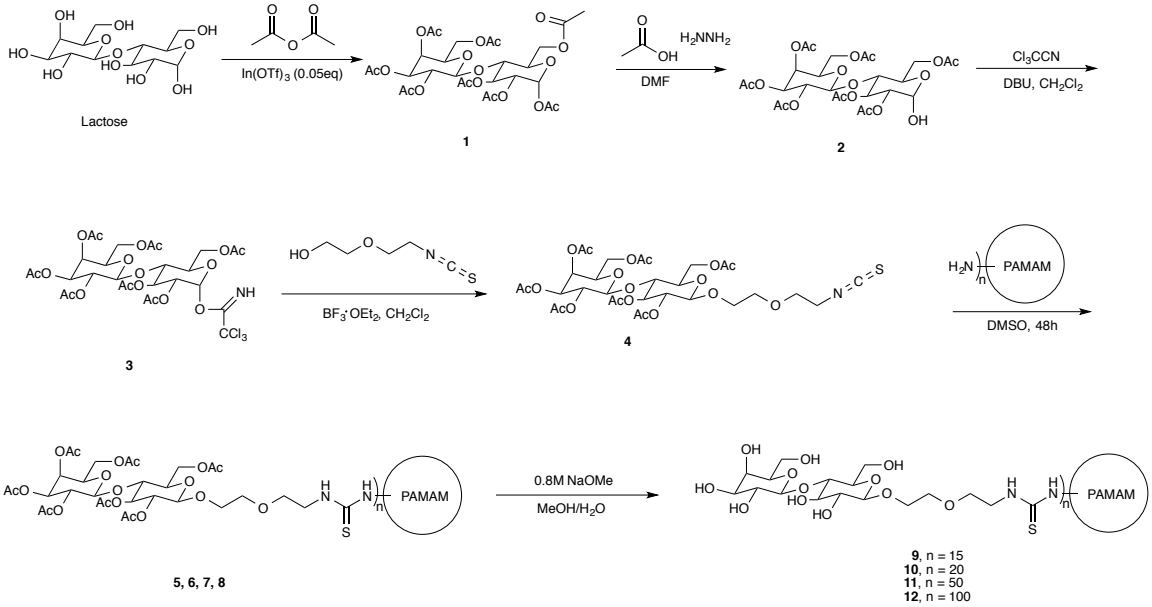
Previous work has established lactose-functionalized frameworks as valuable tools to study carbohydrate-carbohydrate (CCI) and protein-carbohydrate interactions (PCI). Nishimura, *et al.* reported the synthesis and activities of cyclodextrin-based lactose glycoclusters against several lectins. Their results showed an increased potency of the glycoclusters over monomeric lactose when it came to the inhibition of lectin-induced hemagglutination.[81] Benzoic-acid-derived dendrimers were functionalized with lactose to differing valences then evaluated via fluorescence for their affinity to the cholera toxin B subunit. Affinity was increased in a generation-dependent manner up to nearly a factor of ten for the K_d of the multivalent dendrimers over monovalent lactose.[82] Fluorescently-active silica particles have been functionalized with lactose, amongst other carbohydrates, and screened for lectin-binding activity via fluorescence. The results showed a high specificity of peanut lectin to lactose-functionalized particles by means of the clustering effect.[83] In one of the earliest examples of using dendrimers to probe CCIs, Basu, *et al.* used lactose-PAMAM dendrimers with Langmuir monolayers of melanoma cell glycolipid GM3 (a known lactose binder), and found the interaction between the two to be generation-dependent, dependent on the density of the glycolipid, and required the presence of calcium ions.[84]

It has been demonstrated that lactose-functionalized polymeric frameworks can be successfully utilized in the study multivalent protein-carbohydrate interactions. Lactose is an inexpensive, readily available β-galactoside that effectively binds to galectin-3. As shown in Figure 4, TF antigen has the strongest binding with galectin-3 at 47 μM, and is on the same order as the *N*-acetyllactosamine, at 67 μM. There is a decrease in binding capability when considering lactose (220 μM), but it can be purchased economically and directly from common chemical manufacturers. Using lactose also offers a straightforward synthesis, thus it is an attractive starting point for multivalent studies with galectin-3. Herein, the synthesis of lactose-functionalized PAMAM dendrimers is described. The dendrimers will be used to probe protein-carbohydrate interactions discussed in subsequent chapters.

Results and Discussion

Synthesis of Lactose-Functionalized Dendrimers

The synthesis was carried out in accordance with previously established methods.[80,85] A generalized scheme is provided below (Scheme 1).



Scheme 1. Synthesis of lactose-functionalized PAMAM dendrimers.

Lactose was peracetylated using an In(III)-promoted reaction that uses acetic anhydride as both solvent and reagent to produce intermediate **1**. Selective deprotection at the anomeric position was achieved using hydrazine acetate to afford **2**. Acetylated lactose intermediate **2** was transformed into the corresponding trichloroacetimidate **3**, which is an excellent glycosyl donor. Intermediate **3** was reacted with glycosyl acceptor 2-(2-isothiocyanatoethoxy)ethanol using BF_3•$(OEt)_2$ acting as the promoter, yielding peracetylated isothiocyanato intermediate **4**. Neighboring group participation in this step yields the β-product almost exclusively. Intermediate **4** was reacted with the terminal amines on PAMAM dendrimers to afford thiourea-linked acetylated glycodendrimers **5-8**. These dendrimers were deprotected using NaOMe to afford glycodendrimers **9-12**. The degree of functionalization listed in Scheme 1 for glycodendrimers **9-12** was determined using calculations based on the weighted average molecular weights (M_w)

and NMR integrations of the acetylated and deacetylated products. This process is described in the Experimental Procedures.

Conclusion

Four generations of lactose-functionalized dendrimers bearing between ten and one hundred lactoside units were prepared, purified, and characterized. Lactose functionalized generations three, four, and six dendrimers were previously prepared by Wolfenden,[85] but lactose functionalized generation two dendrimers were first synthesized by Michel. All syntheses rely on methodology for global acetylation that was developed by Bizier, *et al*.[86] The four generations of lactose functionalized dendrimers will be used to investigate the interaction of multivalent β-galactosides with galectin-3 in cancer processes, which is described in the next chapter.

Experimental Procedures

General Methods

Generations 3, 4, and 6 lactose functionalized dendrimers **10, 11,** and **12** were prepared, purified, and characterized using previously described methods.[80, 85] This procedure was adapted toward the synthesis of G2-lactose dendrimer **9**. Procedures and experimental values for generation 2 dendrimers are provided below. Procedures and characterization for lactose precursors were prepared as previously reported.[80] As acetylated G6 intermediate **8** was used in syntheses and analyses presented in subsequent chapters, characterization data for this compound is also presented here.

General reagents were purchased from Acros and Aldrich Chemical Companies. PAMAM dendrimers were purchased from Dendritech. Purified compounds were analyzed by ^{13}C and ^{1}H NMR with a Bruker DRX 500 MHz Spectrometer using trimethyl silane as an internal standard. For peak assignments, the following nomenclature was employed: s = singlet, d = doublet, t = triplet, dd = doublet of doublets, m = multiplet, bs = broad singlet. MALDI mass spectra were acquired using a Bruker Autoflex III time-of-flight mass spectrometer in positive linear mode with an acceleration voltage of 19 kV. Spectra of all dendrimers and dendrimer intermediates were obtained with a matrix: analyte ratio of 10,000:1 to 500:1 using a *trans*-3-indoleacrylic acid matrix and dimethyl formamide (DMF) as the solvent. Bovine serum albumin (MW 66,431 g/mol), myoglobin (MW 16,952 g/mol), and trypsinogen (MW 23,982 g/mol) were used as external standards. A 1 μL aliquot of matrix : analyte was used. Molecular mass data of the broad peaks were calculated using a peak centroid based on a peak width of approximately 2000 for G2 dendrimers, 5000 for G3 and G4 dendrimers, and 10,000 for G6 dendrimers. Relevent spectra can be found in Appendix B.

Synthesis of Acetyl-Protected Lactose Functionalized G2 (**5**). An aqueous solution of amine terminated G(2)-PAMAM dendrimer was frozen and lyophilized to yield a white, fluffy solid. In a half-dram glass scintillation vial, an 18.5 mM solution of this solid (30 mg, 9.2 μmol) was made in DMSO (0.5 mL) and a teflon-coated stirbar was added. To this solution, 0.52 mL of a 300 mM solution of **4** (157 μmol, 120 mg, 17 equiv in DMSO) was added. The reaction mixture was then stirred for 24 h at 20°C. The reaction mixture was then dialyzed using 3500 Da molecular weight cutoff (MWCO)

dialysis membrane in 250 mL DMSO for 8 h, replacing the DMSO with fresh every 2 h. The contents of the dialysis membrane were then frozen and lyophilized to yield the purified product as a yellow viscous oil and analyzed by MALDI-TOF and NMR. ^{1}H NMR (500 MHz, DMSO-D_6) δ 7.98 (bs, 1H), 7.80 (bs, 0.9H), 7.50 (bs, 1.1H), 5.18 (s, 0.8H), 5.15-5.07 (m, 1.3H), 4.83-4.76 (m, 1.0H), 4.74-4.67 (m, 1.1H), 4.65-4.60 (m, 0.6H), 4.29-4.23 (m, 0.8H), 4.20-4.15 (m, 0.9H), 4.10-3.93 (m, 3.0H), 3.80-3.69 (m, 2.3H), 3.60-3.34 (m, 7.5H), 3.13 (bs, 2.3H), 3.04 (bs, 2.0H), 2.68-2.57 (m, 4.5H), 2.43-2.35 (m, 1.7H), 2.39 (bs, 2.1H), 2.16 (bs, 3.6H), 2.06 (s, 2.4H), 2.04 (s, 2.6H), 1.97 (s, 5.2H), 1.93 (s, 3.1H), 1.86 (s, 2.1H) ppm. MALDI-TOF (pos) m/z 11290.

Acetylated Lactose Functionalized G6 (**8**). ^{1}H NMR (500 MHz, DMSO-D_6) δ 7.97 (bs, 1.0H), 7.74 (bs, 0.7H), 7.47 (bs, 1.0H), 5.27 – 5.06 (m, 2.2H), 4.87-4.59 (m, 2.6H), 4.33 – 4.11 (m, 1.9H), 4.11 – 3.90 (m, 2.8H), 3.83-3.65 (m, 2.3H), 3.64 – 3.36 (m, 5.7H), 3.22-2.97 (m, 2.6H), 2.78 – 2.34 (m, solvent-obstructed), 2.25 – 2.00 (m, 7.3H), 2.01 – 1.90 (m, 7.9H), 1.90-1.81 (m, 2.2H) ppm. ^{13}C NMR (125 MHz, DMSO-D_6) δ 170.66, 170.29, 169.91, 169.76, 169.59, 169.47, 121.40, 100.50, 100.36, 99.71, 93.95, 89.28, 88.66, 76.95, 76.70, 75.76, 73.22, 73.11, 72.88, 72.20, 72.00, 71.67, 71.52, 70.76, 70.72, 70.12, 69.91, 69.68, 69.39, 68.90, 68.54, 67.90, 67.52, 63.59, 63.03, 62.86, 62.64, 61.34, 61.27, 49.94, 45.50, 21.07, 20.87, 20.77, 20.71 ppm. MALDI-TOF (pos) m/z 113904. Proton NMR in agreement with literature values.[80]

Generalized Deacetylation Procedure
to Afford Lactose Functionalized G2 (**9**). A half-dram glass scintillation vial was charged with lyophilized solid peracetylated dendrimer **5** and a teflon-coated stirbar, then

1 mL of 1:1 water:methanol was added, which resulted in an undissolved white suspension. To this suspension, 0.2 equivalents of sodium methoxide (0.8 M in methanol) was added for each peripheral carbohydrate, and let stir for 3 h at 20°C. If, at this time, particulates had not dissolved and the suspension had not become a clear solution, a further 0.2 equivalents of sodium methoxide (0.8 M in methanol) was added and this step was repeated until the suspension became a clear and colorless solution. Aqueous hydrochloric acid solution (0.1 M) was then added slowly until the pH was ~ 7. At this point, the reaction mixture was purified by dialysis in 3500 Da MWCO tubing and dialyzed in 250 mL of deionized water for 8 h, replacing the deionized water with fresh every 2 h. The contents of the dialysis tubing were then frozen and lyophilized to yield the purified product as a white fluffy solid and analyzed by MALDI-TOF and NMR. ^{1}H NMR (500 MHz, DMSO-D_6) δ 8.16 (bs, 1H), 7.76-7.40 (m, 1.2H), 5.21-4.90 (m, 1.0H), 4.88-4.38 (m, 3.6H), 4.31-4.25 (m, 0.3H), 4.24-4.07 (m, 1.2H), 3.92-3.59 (m, 1.0H), 3.74-3.07 (m, solvent-obstructed), 3.04-2.82 (m, 3.0H), 2.46 (s, 2.3H) ppm. ^{13}C NMR (125 MHz, DMSO-D_6) δ 172.14-170.50 (bs), 104.28, 103.09, 97.12, 92.50, 81.78, 81.45, 81.17, 75.97, 75.42, 75.29, 75.17, 74.98, 73.71, 73.57, 72.60, 71.80, 71.04, 70.24, 69.95, 69.25, 68.59, 68.40, 61.12, 60.96, 60.84, 60.66, 56.82, 52.29, 49.72, 45.07, 44.00, 38.81. MALDI-TOF (pos) m/z 9230.

Method for Determining Degree
of Dendrimer Functionalization

Dendrimers **5-8** and **9-12** were characterized via NMR and MALDI, and these data were used to establish the degree of functionalization, which are listed in Scheme 1. Though PAMAM dendrimers have reasonably well-defined molecular weights in

comparison to other polymers and dendrons, they still have a significant degree of polydispersity, which makes exact characterization complex. To account for this, the number of carbohydrates present on the dendrimers is represented by an average determined through NMR and a series of equations described below:

Equations Used to Determine
Carbohydrate Incorporation on to Dendrimers

$$\frac{M_W \text{ (acetylated intermediate)} - M_W\text{(PAMAM dendrimer)}}{MW_{\text{acetylated lactose tether}}} \quad \text{(a)}$$

$$\frac{M_W \text{ (acetylated intermediate)} - M_W\text{(deprotected product)}}{MW_{\text{acetylated lactose tether}} - MW_{\text{deacetylated lactose tether}}} \quad \text{(b)}$$

$$\frac{M_W\text{(deprotected product)} - M_W\text{(PAMAM dendrimer)}}{MW_{\text{deacetylated lactose tether}}} \quad \text{(c)}$$

Weighted averages of molecular weights (M_W) for dendrimers and their intermediates are determined by MALDI. The M_W(acetylated intermediate) is the weighted average molecular weight of the acetylated dendrimer intermediate **5, 6, 7,** or **8**. The M_W(deprotected product) is the final deprotected dendrimer product (**9-12**), and M_W(PAMAM dendrimer) refers to the unfunctionalized dendrimer, direct from Dendritech.

Equation (a) represents the M_W added to the dendrimer due to the acetylated carbohydrate loading, and is divided by the molecular weight of the acetylated carbohydrate precurser, in the case of dendrimers **5-8** is **4**, which weighs 766 g/mol. Equation (b) represents the loss in M_W caused by the deprotection of the dendrimer, where the denominator is the difference in M_W of the acetylated and deacetylated sugar

monomer, 294 g/mol (seven acetyl groups are removed and replaced by hydroxyls). The final weighted average-based calculation used is equation (c), which calculates loading by using the weighted average of the deacetylated glycodendrimer, as well as the MW for the deacetylated sugar (plus the (isothiocyanatoethoxy)ethyl tether) which totals 471 g/mol.

Theoretical molecular weights and the number of amino-endgroups for PAMAM dendrimers are presented on the Dendritech website.[87] The values for smaller generation dendrimers G2 and G3 have been verified by MALDI. The larger generations of unfunctionalized PAMAM dendrimers, G4 and G6, have somewhat lower weighted averages when characterized by MALDI than the theoretical ones reported on the Dendritech website. This can be attributed to the method by which the dendrimers are produced. They are synthesized through the repeated reactions of methyl acrylate with ethylene diamine via Michael addition to produce a carboxylic acid-terminated dendrimer (an X.5 generation), followed by the coupling of ethylene diamine to the X.5 generation dendrimer to generate an amine-terminated PAMAM framework. Each iteration of these two steps produces a new generation, and the more times it is performed, the more opportunity there is for imperfections to present in the synthesis. For a G4 dendrimer, the theoretical weight is 14,215 Da, which accounts for 64 endgroups. The actual weighted average as determined by MALDI is closer to 13,600, allowing for 60 endgroups. The experimental MW for G6 is 52,000 Da, which allows for a possible 212 endgroups (in comparison to 256 theoretical endgroups).

The necessary values for using equations (a), (b), and (c) and therefore determining the degree of functionalization for glycodendrimers **9, 10, 11,** and **12** are summarized in Table 1.

Table 1. MALDI data for lactose functionalized dendrimers.

Compound[a]	Generation	Dendrimer M_W	Acetylated M_W	Deacetylated M_W
9	2	3256	11290	9383
10	3	6909	22682	16206
11	4	13610	43465	34453
12	6	52000	113904	95962

[a]Though full characterization data for these dendrimers is not presented, the spectra that correlate to the values presented are provided in Appendix B of the thesis.

Another method for determining the degree of functionalization uses the ^{1}H NMR spectrum for the acetylated glycodendrimers. (Integrations on the deprotected glycodendrimer are less reliable, and not considered when determining functionalization.) The degree of functionalization is determined through analysis of the N-H region in the acetylated glycodendrimer spectrum.

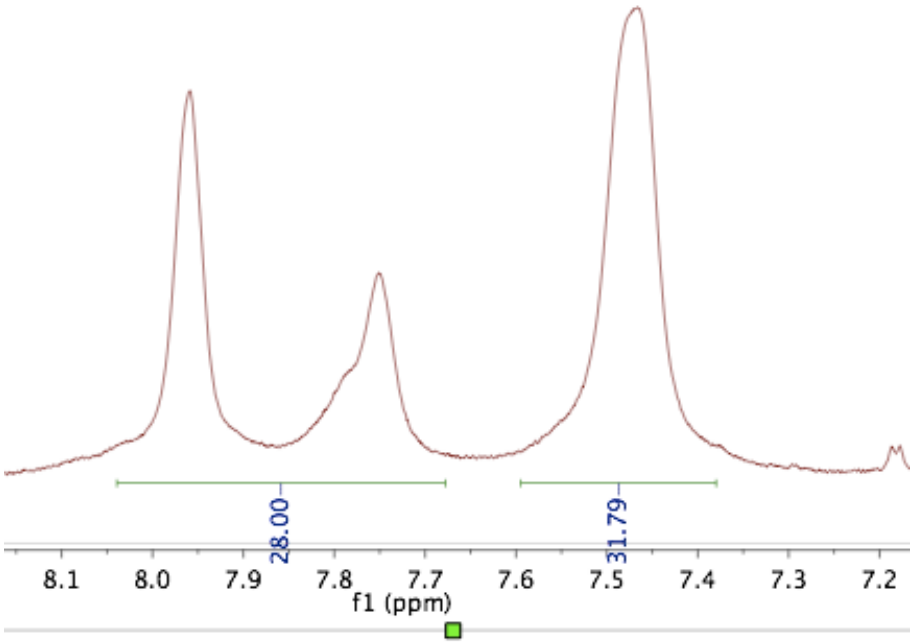


Figure 10. A close-up of the N-H region of an acetylated G2 glycodendrimer.

The two peaks in the ^{1}H NMR spectrum centered at 7.85 ppm shown in Figure 10 are resonances that correspond to the internal amide peaks on the PAMAM dendrimer. This value is absolute and does not change with respect to functionalization. The third peak centered at 7.5 ppm arises due to the thiourea contributions that develop upon functionalization. There are two thiourea protons per carbohydrate endgroup, so when the amide peaks are held constant (in the case of G2, there are 28 internal amide protons), the signal due to the thiourea contribution should increase as incorporation of carbohydrates is increased at a rate of two protons per sugar. The functionalization calculated in this way is shown in Table 2.

Table 2. Degree of functionalization as calculated by equations (a), (b), (c), and NMR analysis.

Compound	a	b	c	NMR[a]	Average
9	10.5	6.5	13.0	14.6	11
10	20.6	22.0	19.7	25.0	22
11	39.0	30.7	44.3	45.0	40
12	80.9	61.0	93.3	159.0	99

[a]The corresponding NMR spectra are included at the end of this chapter.

When the corresponding values from Table 1 are used in equations (a), (b), and (c), average number of carbohydrate endgroups are determined and reported in Table 2. The average of these three values with loading determined from the ^{1}H NMR data for the acetylated dendrimer gives a more accurate approximation of the degree of functionalization than any of the methods separately and is shown in Table 2.

CHAPTER 3

USING GLYCODENDRIMERS TO ARBITRATE GALECTIN-3 CANCER CELL AGGREGATES

Introduction

Cell based assays are an essential precursor to *in vivo* studies and allow for the study of specific pathways in a simplified system. Specifically, homotypic cell aggregation assays are a useful method to study galectin-3/carbohydrate interactions in cancer processes because there is straightforward and quantitative effect: cell aggregation. There is literature precedence for using this method to probe cancer-associated galectin-3 processes. Iurisci, *et al.* used cell-based assays to probe the binding of galectin-1 and galectin-3 to cancer cell surface protein LGalS3BP, a process that leads to cellular adhesion. After synthesizing β-lactoseaminide analogs, homotypic aggregation assays on cancer cells were used to assess the efficiency of the galactosides in inhibiting the binding of galectin-1 and galectin-3 on the surface of the cell.[88] Zou, *et al.* used cell-based assays to look at both homotypic and heterotypic cancer cell aggregation induced by galectin-3 between breast cancer cells and healthy epithelial cells. They identified a series of peptide sequences that act as galectin-3 agonists, inhibiting the interaction between galectin-3 and cell surface, greatly decreasing both types of aggregation.[89] Glinskii, *et al.* used lactulose-L-leucine as a galectin-3 inhibitor *in vitro* with prostate cancer cell line DU-145 and found that the simple carbohydrate mimic was able to inhibit

induced aggregation while not causing any cytotoxic effects, results that were also mirrored *in vivo* by reducing the metastatic effects of cancer in mice.[26]

The increased affinity of galectin-3 to lactose-functionalized PAMAM dendrimers as compared to lactose monomer has been specifically demonstrated. Roy, *et al.* was able to demonstrate that G0-G5 lactose-functionalized dendrimers were more potent than lactose on its own when interacting with galectin-3, with specifically G4 having nearly 300 times the potency of lactose alone.[90]

Here, the focus is to exploit the natural affinity galectin-3 has for multivalent clusters of lactose using tunable multivalent lactose-functionalized dendrimers. Use of these glycodendrimers with different displays of carbohydrates allows for the monitoring of the effects of multivalency on galectin-3 mediated homotypic aggregation in three different cancer cell lines. This allows for exploration into the mechanism by which cancer cellular aggregation occurs. There has been a demonstrated correlation between cancer cells that aggregate *in vitro* and their metastatic potential *in vivo*,[91] suggesting real value in a therapeutic agent that can inhibit galectin-3 mediated cellular aggregation.

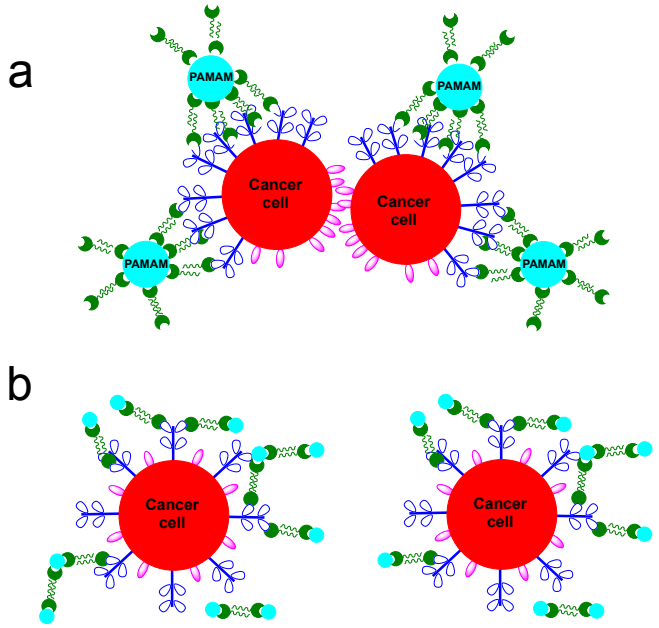
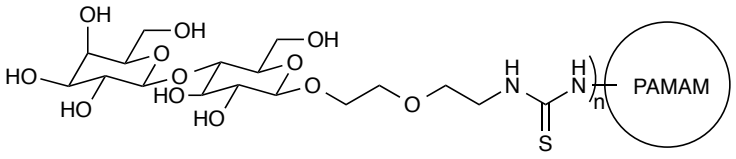


Figure 11. Proposed dendrimer interactions with galectin-3 in homotypic aggregation.

It is proposed that lactose-functionalized glycodendrimers will interact with galectin-3 induced cancer cell aggregates to either enhance or inhibit aggregation (Figure 11). In Figure 11a, large dendrimers induce aggregation of cancer cells. The large dendritic framework supports many sugars. In the case of **12,** a generation 6 dendrimer, there are 99 lactosides, which provides an excess of ligands for galectin-3, and cross-linking results. In Figure 11b, smaller dendrimers provide a competitive binding ligand for galectin-3, prohibiting it from interacting with its putative binding partner, MUC1, on the cell surface, and aggregation is inhibited.

Dendrimers Used

The dendrimers used in these studies were those described in Chapter 2. A summary of their average carbohydrate loading is presented in Figure 12.



9, n = 11
10, n = 22
11, n = 40
12, n = 99

Figure 12. Lactose-functionalized dendrimers used in homotypic cell assays. The value of *n* indicates the degree of carbohydrate loading.

Cell Lines Used

Homotypic cellular aggregation assays were performed using lactose functionalized dendrimers **9-12** with three different cancer cell lines. All cell lines used were chosen for their depth of characterization and robustness as well as the level of galectin-3 expression. The assays were initially run with A549 lung carcinoma cells, a cell line known to upregulate galectin-3.[92] To test the generality of the results obtained with A549 cells, two additional cell lines were used based on the amount of galectin-3 expressed within the cell.[93, 94] Prostate cancer cell line DU-145 expresses more galectin-3 than A549s, and fibrosarcoma cell line HT-1080 express less.

Results and Discussion

Cancer cells were incubated with galectin-3 to induce aggregation in the presence of **9-12** to assess how glycodendrimers affect galectin-3 induced homotypic cellular aggregation. This assay was also performed without added galectin-3 to test the hypothesis presented in Figure 11a, where glycodendrimers cause cellular aggregation. A series of assays were also performed in the presence of an anti-galectin-3 fluorescent antibody and analyzed with confocal microscopy to visualize any polarization changes made to the cell surface.

Cellular Aggregation Assays with A549 Cells
and Lactose- Functionalized Dendrimers **9–12**

As an initial step in testing the effects of different generations of lactose-functionalized dendrimers **9-12** on cellular aggregation, assays using the glycodendrimers were conducted using A549 lung carcinoma cells with and without the addition of galectin-3. The addition of galectin-3 to the A549 cells induced cellular aggregation. When generation two and generation three glycodendrimers **9** and **10** were incubated with galectin-3 and A549 cells, the formation of (galectin-3 induced) cellular aggregates was inhibited. Incubation of the cells with the same glycodendrimers **9** and **10** but in the absence of galectin-3, however, had no impact on cellular aggregation (Figure 13a and b). When larger generation four and generation six glycodendrimers **11** and **12** were used, there was no apparent inhibition of galectin-3 induced aggregation. In the absence of additional galectin-3, however, glycodendrimer-induced aggregation was observed (Figure 13b and c). The smallest and largest lactose functionalized dendrimers that were studied, **9** and **12**, cause the most pronounced effects. More subtle results were obtained when **10** and **11** were present.

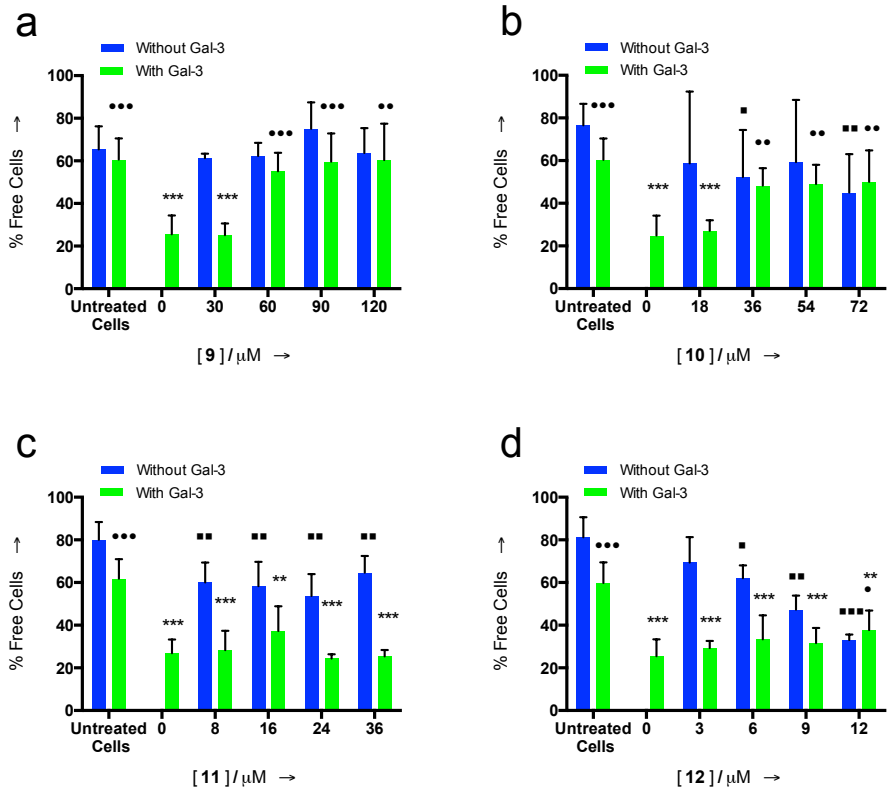


Figure 13**.** Effect of lactose-functionalized dendrimers on untreated and galectin-3-induced homotypic aggregates of A549 cells. In the assays without galectin-3 (gal-3) added, ■ represents a statistical significance with respect to untreated cells. In the assays with galectin-3 added, * represents a statistical significance with respect untreated cells, • represents a statistical significance with respect to the galectin-3 standard ("0"). (a) Compound **9** inhibits galectin-3 aggregates from forming but has no effect on cells without added galectin-3. (b and c) Dendrimers **10** and **11** have little effect on cellular aggregation. (d) Aggregation results from the incubation of untreated cells with **12**.

Example microscope images of control A549 cells, A549 cells for which galectin-3 mediated aggregation has been inhibited by **9**, and aggregates of A549 cells that were formed upon addition of galectin-3 are shown in Figure 14a, 14b, and 14c, respectively.

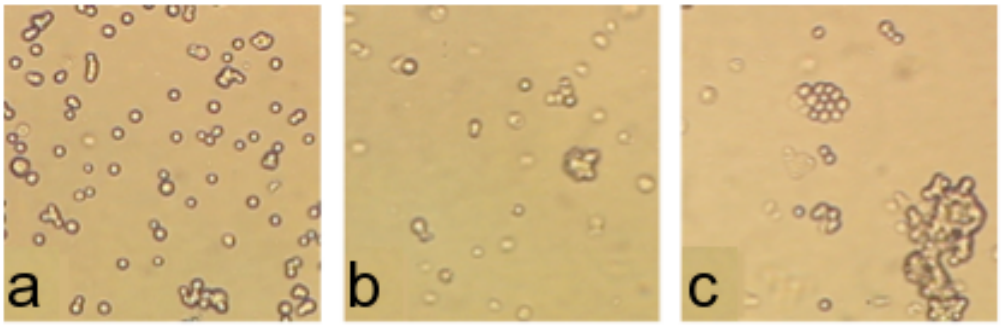


Figure 14. Representative images taken from cellular assays using A549 cells. (a) A micrograph of free cells. (b) A micrograph of cells in the presence of galectin-3 and 60 μM **9**. (c) A micrograph of galectin-3 induced cellular aggregates.

Cellular Aggregation Assays with
DU-145 and HT-1080 Cells and
Lactose Functionalized Dendrimers 9-12

To test the generality of the results obtained using A549 cells in the homotypic aggregation assay, two additional cell lines (DU-145 and HT-1080) were tested. These particular cell lines were chosen because of their expression levels of galectin-3; DU-145 cells express more galectin-3 than A549 cells, and HT-1080 cells express less.

The results of the homotopyic assays using DU-145 prostate carcinoma cells corroborated the results described above using A549 cells. Dendrimers **9** and **10** were also able to inhibit galectin-3 induced aggregation, but had no statistical effect without additional galectin-3 present (Figure 15a and Figure 15b). As with A549 cells, the lactose functionalized generation four and six dendrimers **11** and **12** did not discernibly inhibit cellular aggregation of DU-145 cells when an aggregation-inducing amount of galectin-3 was added (Figure 15c and d). However, when no galectin-3 was added, an increase in aggregation was observed when **12** was used (Figure 15d).

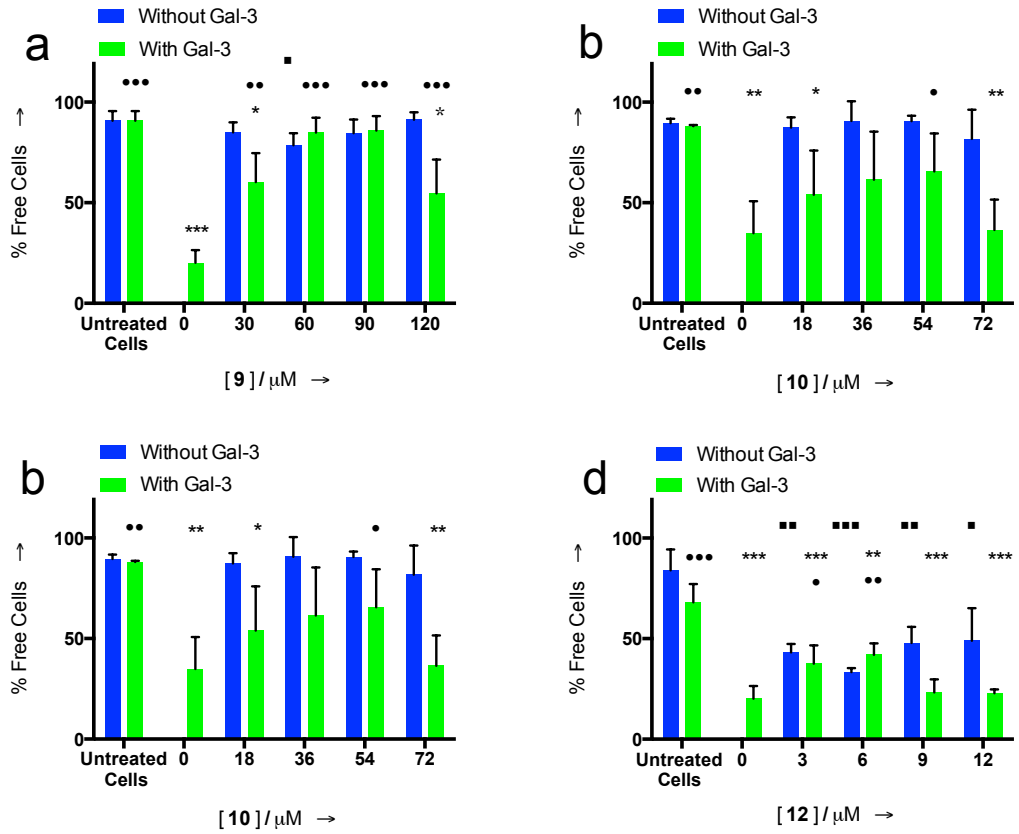


Figure 15. Effect of lactose-functionalized dendrimers on untreated and galectin-3-induced homotypic aggregates of DU-145 cells. In the assays without galectin-3 (gal-3) added, ■ represents a statistical significance with respect to untreated cells. In the assays with galectin-3 added, * represents a statistical significance with respect untreated cells, • represents a statistical significance with respect to the galectin-3 standard ("0"). (a) Compound **9** inhibits galectin-3 aggregates from forming but has no effect on cells without added galectin-3. (b and c) Dendrimers **10** and **11** have little effect on cellular aggregation. (d) Aggregation results from the incubation of untreated cells with **12**.

The same assays were then performed using HT-1080 fibrosarcoma cells. Some results agreed with the results of A549 and DU-145 cell lines with glycodendrimers, but others produced less obvious trends. As in the other two cell lines, the presence of glycodendrimer **9** and **10** inhibited galectin-3 induced aggregates, but without additional galectin-3, no statistically significant effect was observed (Figure 16a and b). With generation four and generation six dendrimers **11** and **12,** there was no statistical effect

with or without added galectin-3 (Figure 16c and d). In the other cell lines, glycodendrimer-induced aggregates were observed using generation six glycodendrimer **12** without added galectin-3.

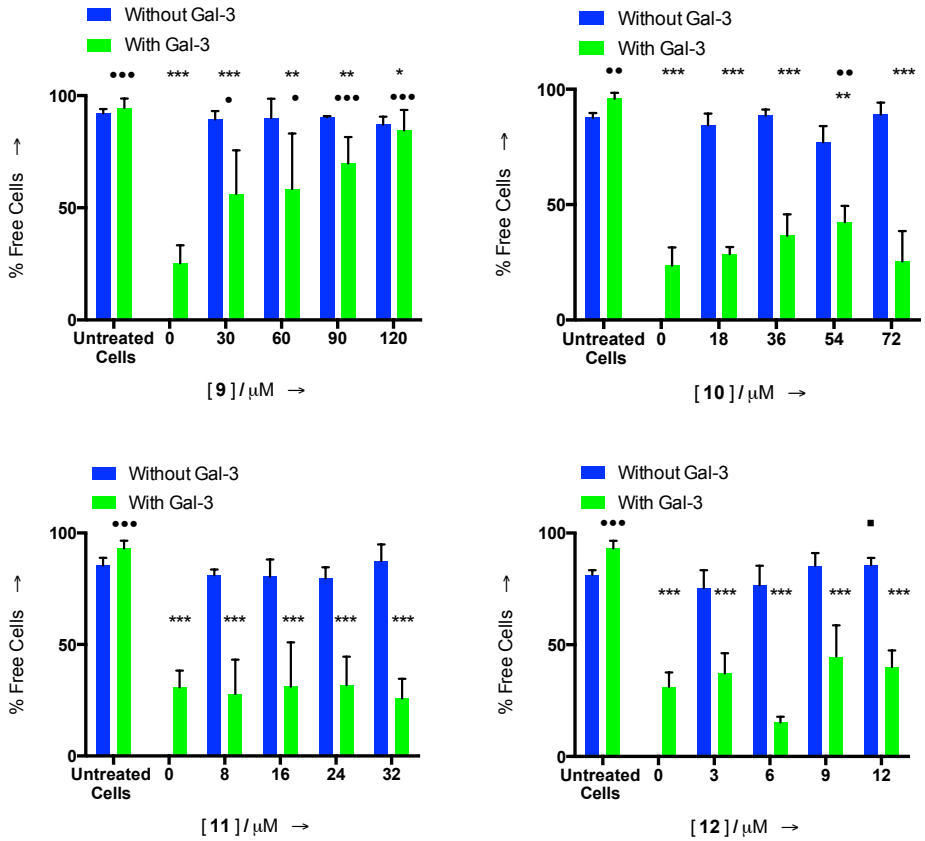


Figure 16. Effect of lactose-functionalized dendrimers on untreated and galectin-3-induced homotypic aggregates of HT-1080 cells. In the assays without galectin-3 (gal-3) added, ■ represents a statistical significance with respect to untreated cells. In the assays with galectin-3 added, * represents a statistical significance with respect untreated cells, • represents a statistical significance with respect to the galectin-3 standard ("0"). (a and b) Compounds **9** and **10** inhibit galectin-3 aggregates from forming but has no effect on cells without added galectin-3. (c and d) Dendrimers **11** and **12** have little effect on cellular aggregation.

A possible explanation for this observation is that the results are impacted by the endogenous amount of galectin-3 in each cell line. Using whole cell lysates (WCLs) of

the three cell lines, the relative amount of endogenous galectin-3 in each cell line was measured by Western blot and it was confirmed that DU-145 cells had more total native galectin-3 than either of the other cell lines. HT-1080 cells had the lowest amount of native galectin-3 (Figure 17). While only the extracellular galectin-3 is thought to be involved in homotypic aggregation processes,[23] it can be inferred that an increase in total galectin-3 for the cell results in an increase of cell surface galectin-3. With less galectin-3 present for interaction with dendrimer **12**, little effect on the cellular aggregation was observable for HT-1080 cells. Since DU-145 and A549 cells had more galectin-3 present, the effect that glycodendrimer **12** had with these cell lines was more pronounced than that observed in the HT-1080.

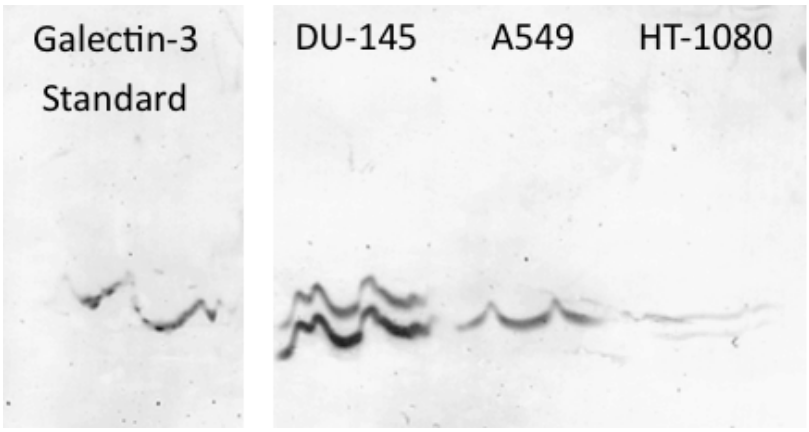


Figure 17. A Western blot depicting relative amounts of endogenous galectin-3 across cell lines. The experiment was performed as described in methods section, and the nitrocellulose membrane was then scanned and analyzed. The first lane contains 10μg galectin-3 standard, while the others contain 16μg of the whole cell lysate indicated.

Cellular Aggregation Assays with Fixed Cells

When assays using glycodendrimers **9**–**12** were run without adding galectin-3, it was observed that **12** (the lactose functionalized G6-dendrimer) caused cellular

aggregation to occur. To determine if reorganization of the cell surface MUC1 by galectin-3 is responsible for the observed aggregation in the presence of **12**, the cellular aggregation assays were performed on fixed A549 cells (Figure 18). With fixed cells, the cell surface is not dynamic, and galectin-3 cannot influence the localization of MUC1. When **12** was added to these fixed cells with or without the presence of added galectin-3, no aggregates formed. This indicates that polarizable MUC1 on the cell surface and galectin-3 are required for cellular aggregation to be induced by **12**. The same assay was performed on fixed cells in the presence of generation 2 dendrimer **9** with and without added galectin-3, with no observed effect in either case.

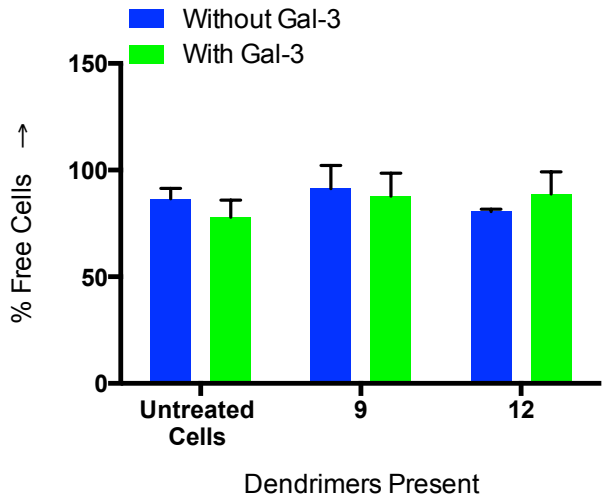


Figure 18. Effect of lactose-functionalized dendrimers **9** and **12** on fixed cells with and without added galectin-3. Dendrimer **9** was used at a concentration of 120 μM, and **12** was used at a concentration of 12 μM. As expected, there is no statistically significant difference between untreated fixed cells and fixed cells in the presence of added galectin-3 (gal-3), regardless of whether either generation glycodendrimer is present.

Fluorescence Microscopy to Determine
the Effect of Glycodendrimers on the
Cell Surface Localization of Galectin-3

To determine the distribution of galectin-3 around the outside of the cell surface, homotypic aggregation assays were performed as described previously for **9** and **12**, then cells were incubated with fluorescently labeled anti-galectin-3 antibody (Dendrimers **9** and **12** were chosen for further study because they elicited the greatest responses in the aggregation assays.) Results are summarized in Figure 19.

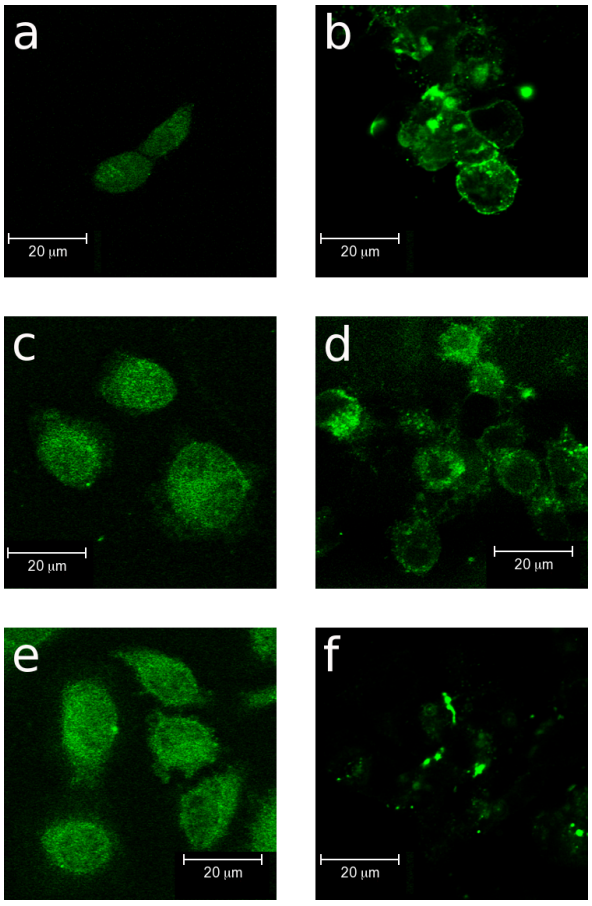


Figure 19. Micrographs of A549 cells in the absence or presence of galectin-3 and lactose-functionalized dendrimers probed with fluorescent anti-galectin-3. (**a**) Untreated cells. (**b**) Cells incubated with galectin-3. (**c**) Cells incubated with 120 μM **9**. (**d**) Cells incubated with 12 μM **12**. (**e**) Cells incubated with galectin-3 and 120 μM **9** (**f**) Cells incubated with galectin-3 and 12 μM **12**.

When untreated cells were incubated with fluorescent anti-galectin-3 antibody, a faint green fluorescence was visible over the entire cell surface indicating that the galectin-3 was distributed evenly throughout the cell surface (Figure 19a). When cells were treated with only galectin-3 and then visualized with fluorescent antibody, the fluorescence appeared much more punctate, indicating that the galectin-3 (when in higher concentrations) was localized around the cells (Figure 19b).

Taken in consideration with the fixation data, these fluorescence images indicate that galectin-3 reorganizes the cell surface to increase the aggregation potential of the cells, most likely by interacting with MUC1 and exposing adhesion molecules on the cell surface as shown when comparing Figure 19a to 19b. When cells were incubated with **9** but no additional galectin-3 was added, the cells looked similar to the untreated cell (Figure 19c), as the galectin-3 pattern remained unchanged. When incubated with **12**, the phenotype looked similar to the galectin-3 induced aggregates (Figure 19d). When the cells were incubated in the presence of **9** and galectin-3, the cells again looked similar to the untreated control (Figure 19e), indicating that the glycodendrimer is interfering with galectin-3 in repatterning the cell surface. Finally, when **12** was incubated with galectin-3 and the cells, large aggregates of galectin-3 were observed between the cell interfaces (Figure 19f). Indeed, a larger network of cells was observed when galectin-3 and **12** were added than were observed in the galectin-3 control. The galectin-3 also looked more punctate when both galectin-3 and **12** were present, suggesting aggregation of galectin-3 into a large multivalent matrix was occurring.

In addition to using confocal microscopy to visualize the patterning of galectin-3 at the cell surface, a fluorescent MUC1 antibody was also used in an effort to evaluate

how polarized the cell surface appeared during the various experimental conditions. After several trials of observing apparent colocalization between MUC1 and galectin-3, it was suspected that the MUC1 antibody was cross-reacting with galectin-3. To confirm this, Western blots were performed using both primary antibodies on purified galectin-3, WCL, and MUC1. As shown in Figure 20a, the primary galectin-3 antibody only stains for galectin-3, however, higher molecular weight bands do appear in the HT-1080 WCL sample. Though not conclusive since the antibody did not stain the MUC1 standard, this could indicate a cross reaction with MUC1, or it could indicate large aggregates of galectin-3 are forming on the gels. In Figure 20b, a blot stained with anti-MUC1 primary antibody is shown, which reacts with the galectin-3 in the standard and the WCL, but interestingly, not with MUC1. As the intended MUC1 staining of the target protein was not observed via Western blot, the fluorescence data gathered *in vitro* was disregarded, and this experimental line of inquiry was dropped.

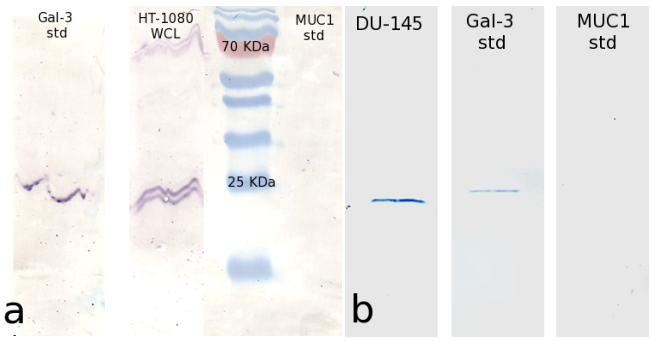


Figure 20. Western blots demonstrating cross-reactivity of primary antibodies. A 10 ng sample of galectin-3 (gal-3) standard was loaded, 16 μg of whole cell lysate (WCL) was loaded, and 4 μg MUC1 standard was loaded. (a) A Western blot stained using a galectin-3 primary antibody. The galectin-3 in HT-1080 WCL as well as the galectin-3 standard were observed, in addition to higher molecular weight bands, but the MUC1 standard was not observed. (b) A MUC1 primary antibody was used to stain the Western blot. The galectin-3 in DU-145 WCL and the galectin-3 standard were stained, but purified MUC1 protein was not observed.

Reiterating the hypothesis presented in Figure 11, schematic representations explaining the fluorescent results observed in Figure 19 are provided in Figure 21. Figure 21a depicts naturally occurring galectin-3 interacting with MUC-1 at the cell surface, which occurs in a distributed fashion. When additional galectin-3 is introduced to the cells, or when galectin-3 is over-expressed by the cells, more galectin-3 is present at the cell-cell interfaces, and cellular aggregation results (Figure 21b). This interaction is disrupted upon the introduction of small glycodendrimer **9** (Figure 21c) since **9** diverts galectin-3 away from the clusters on the cell surface, re-establishing the diffuse pattern of galectin-3 shown in Figure 21a. When large glycodendrimer **12** is added in the presence of high concentrations of galectin-3, the aggregation seen in Figure 21b is augmented as shown in Figure 21d by multivalent crosslinking of the cells through formation of galectin-3/glycodendrimer matrices.

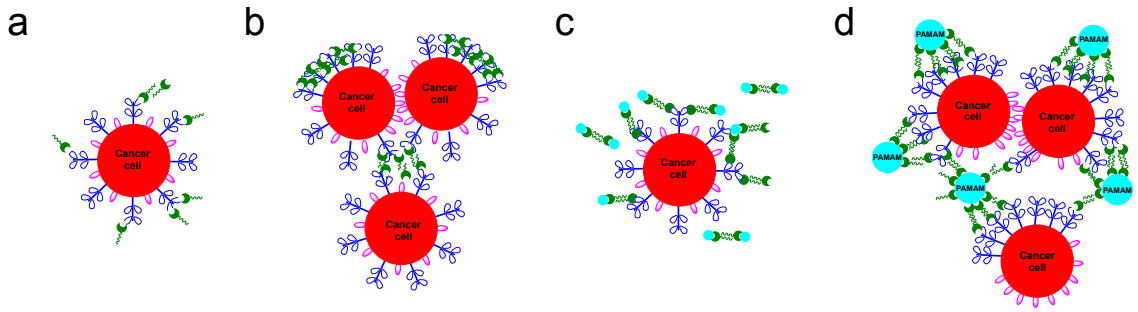


Figure 21. Schematics describing cancer cell surface environments in the absence and in the presence of glycodendrimers. (**a**) Untreated cell. (**b**) Cells incubated with galectin-3. (**c**) Cell incubated with **9** and galectin-3. (**d**) Cells incubated with **12**.

Conclusion

Using lactose functionalized PAMAM dendrimers as a tunable multivalent system, the level of cellular aggregation that occurred for three different cancer cell lines

was mediated. Smaller dendrimer **9** (a generation 2 dendrimer with 11 lactose endgroups) inhibited galectin-3 induced aggregation for all three of the cancer cell lines that were tested. In contrast, dendrimer **12** (a larger, generation 6 dendrimer with 99 lactose endgroups on average) caused cancer cells to aggregate through a galectin-3 pathway. The results of the homotypic cellular aggregation assays indicated that inhibition by dendrimer **9** was accomplished by providing competitive binding sites for galectin-3 (to divert binding from its putative cancer cell ligand, TF antigen on MUC1). Dendrimer **12**, on the other hand, provided so many sites for galectin-3 binding that the cross linking of the cells intensified, enhancing aggregation.

These findings indicate that glycodendrimers effectively mediate cellular aggregation properties by intercepting and modifying the galectin-3/MUC1 pathway. These results establish glycodendrimers as tools to better understand the effects of multivalency on important roles in cancer cellular process. Glycodendrimers that target the galectin-3/MUC1 binding system may also provide important insights for the development of targeting agents, prodrug delivery systems, or diagnostics and imaging systems.

Experimental Procedures

Dendrimer Synthesis

Glycodendrimers used for the experiments in this chapter are summarized in Figure 12 and were synthesized as previously described in Chapter 2.

Galectin-3

Galectin-3 was produced using a protocol developed by the Raz lab.[80, 95] The concentration of galectin-3 was verified via a bicinchoninic acid (BCA) protein assay.[96]

Cell Lines and Cultures

Cell lines were chosen due to their robustness, depth of characterization, and galectin-3 expression level.[92-94] Human lung carcinoma cell line A549, human prostate cell line DU-145, and human fibrosarcoma HT-1080 cells were all purchased from ATCC and cultured as recommended by ATCC. Cells that have been passaged less than 12 times were used for these experiments. Prior to use, cells were dissociated from growth dishes using 0.02% EDTA/0.25% trypsin (SAFC Biosciences).

Homotypic Aggregation Assay

Cells were counted and made into a solution of 16 million/mL in serum-free media (SFM). Dendrimers were made into a solution of 2 mg/mL in ultrapure water. Galectin-3 was used at a concentration of 0.5 mg/mL in PBS. Galectin-3 (13 μL, 16.7 μM, 217 ρmol), dendrimer solution (0 μL, 10 μL, 20 μL, 30 μL, or 40 μL), and enough SFM to total 53 μL per sample were combined and vortexed. Cell suspension (15 μL, 240,000 cells) was then added to each reaction and gently mixed again and incubated at 37 °C for 1 h with gentle rotation. Three 10 μL aliquots of each reaction were viewed and recorded on a Jenco BC-364 inverted microscope. Four images randomly chosen from each aliquot were obtained. Using the image analysis software Pixcavator, the percentage of free and aggregated cells (aggregation indicated by 4 or more cells clumped together) for each experimental condition was determined. Sample primary data using A549 cells

is provided in Figures 22, 23, and 24. Figure 22 shows an example of the untreated cell and galectin-3 standards run with every assay. Figure 23 shows sample data for assays run without additional galectin-3, and Figure 24 shows sample data for assays run in the presence of additional galectin-3. Assays performed on fixed cells were performed the same as described above, using cells fixed in a 4 % PFA solution made in PBS at pH = 8.

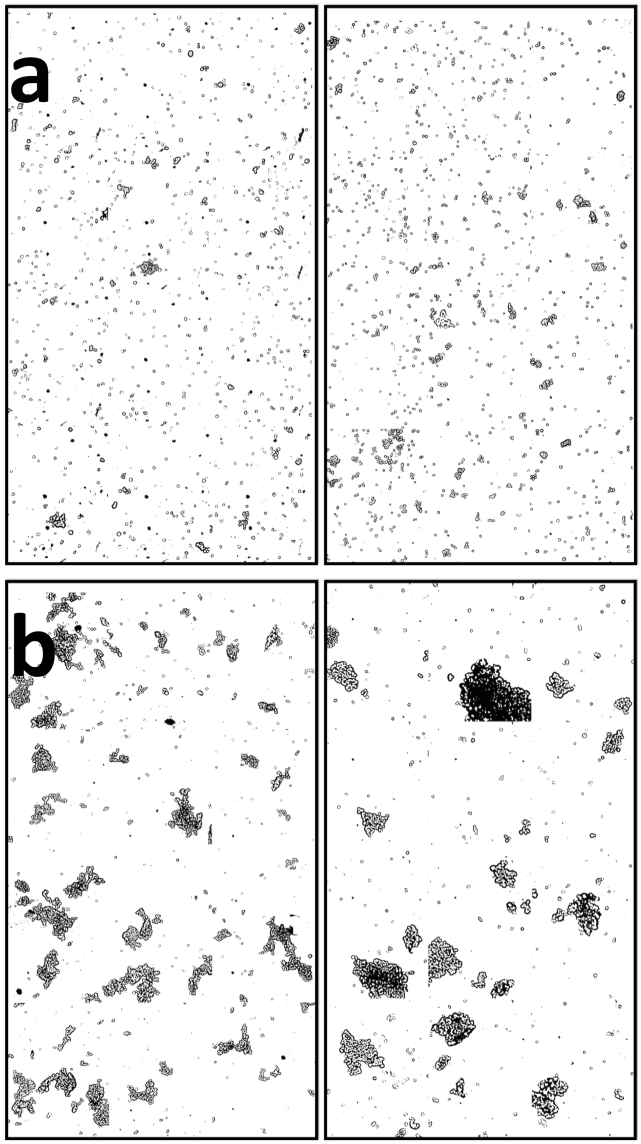


Figure 22. Selected primary data from the controls in cellular aggregation assays on A549 cells. Row (**a**) shows representative images from untreated cell experimentals. Images shown are compressed stills taken at 10x magnification then manipulated to black and white. Row (**b**) shows representative images from galectin-3 control experiments.

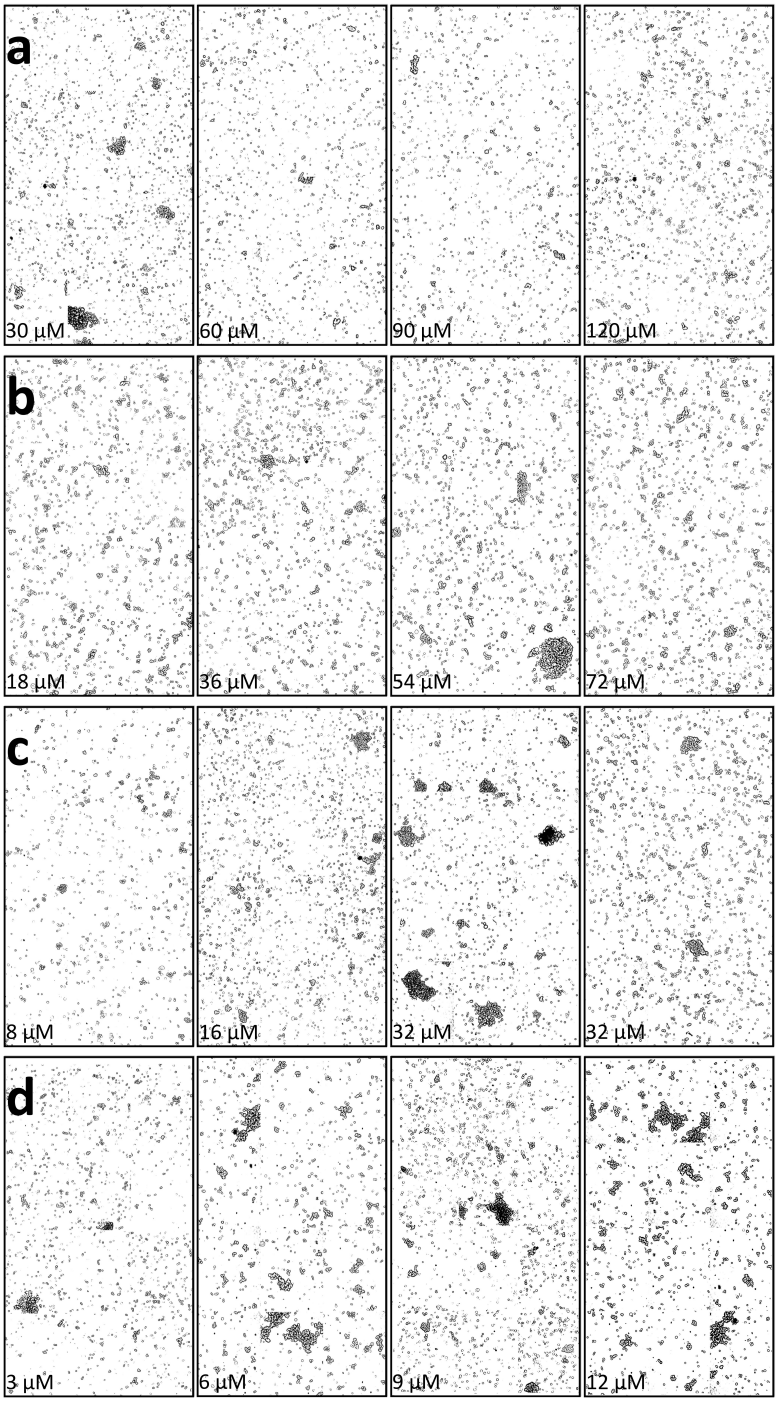


Figure 23. Selected primary data from cellular aggregation assays of A549 cells in which no additional galectin-3 was added. Images shown are compressed stills taken at 10x magnification then manipulated to black and white. Concentrations listed are for added dendrimers. Row (**a)** shows representative images for dendrimer **9**. Row (**b**) shows representative images for dendrimer **10.** Row (**c**) shows representative images for dendrimer **11**. Row (**d**) shows representative images for dendrimer **12**.

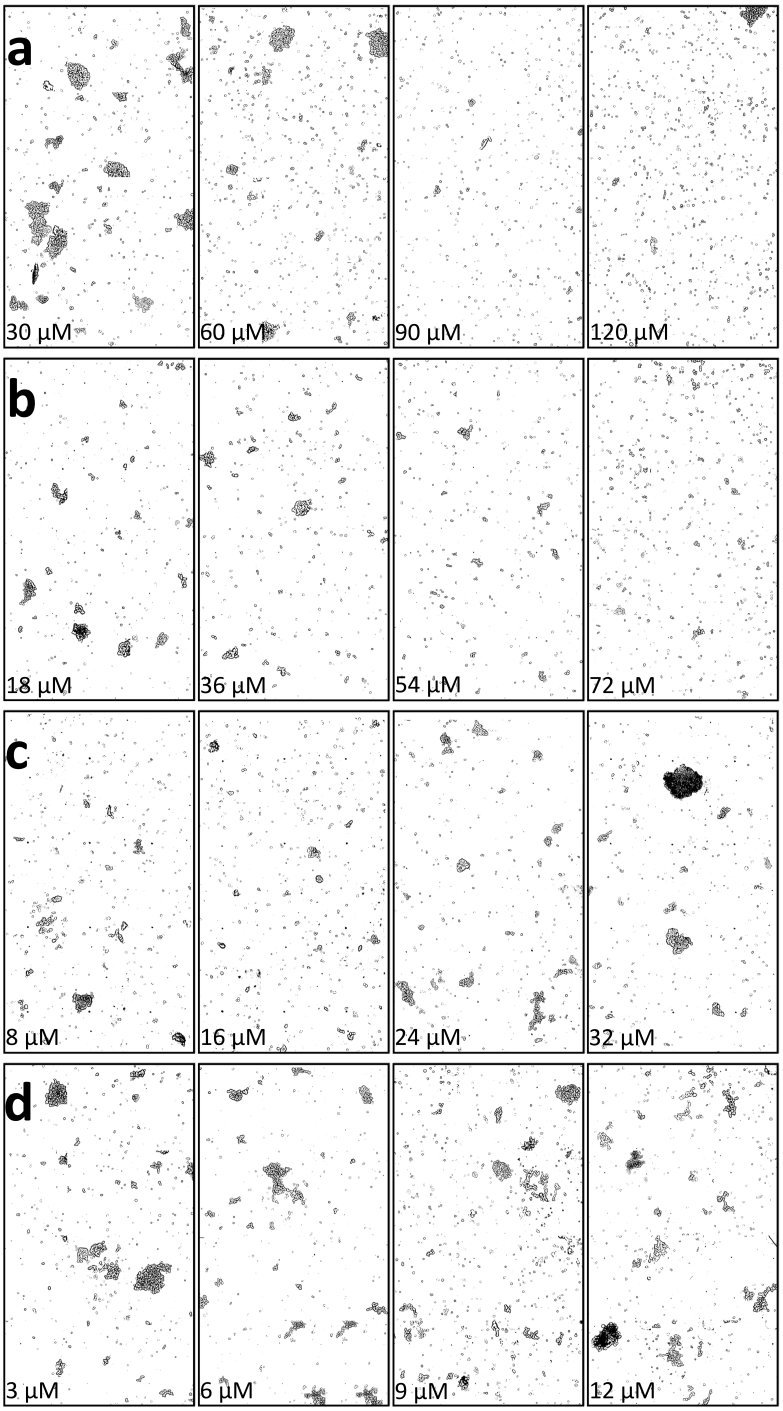


Figure 24. Selected primary data from cellular aggregation assays of A549 cells in the presence of additional galectin-3. Images shown are compressed stills taken at 10x magnification then manipulated to black and white. Concentrations listed are for added dendrimers. Row (**a)** shows representative images for dendrimer **9**. Row (**b**) shows representative images for dendrimer **10.** Row (**c**) shows representative images for dendrimer **11**. Row (**d**) shows representative images for dendrimer **12**.

SDS-PAGE and Western Blots

Each cell line was grown to confluency, and cells were lifted using 0.53 mM EDTA/0.25% trypsin. Cells were washed twice with ice-cold PBS buffer then incubated with NP40 cell lysis buffer and protease inhibitor cocktail (BD Bioscience) for 30 min on ice and vortexed vigorously for 1 min every 5 min. The lysed cells were spun down for 20 min at 10,000 g. The cell pellet was then discarded, and the total protein concentration in the supernatant for each cell line was determined by BCA. Using 16 μg of whole cell lysate for each cell line (A549, HT-1080, and DU-145) with an appropriate amount of 3x SDS sample buffer, samples were loaded onto a 20% SDS gel. A PageRuler Prestained Protein Ladder (5 μL, Thermo Scientific), 10 ng of galectin-3 (produced in-house), and 4 μg MUC1 (Sino) standards were also loaded. Gels were run at 200 V for 20 min, then 100 V until complete, then transferred onto nitrocellulose membranes for 1 h at 100 V. Membranes were then blocked in 4% BSA in TTBS for 1 h at room temperature. Membranes stained for galectin-3 were then incubated overnight at 4 °C in 1% BSA in TTBS with anti-h-galectin-3-biotin (1:3000, eBioscience), then incubated 1 h at ambient temperature in 1% BSA in TTBS with strepaviden-HRP (BD Bioscience, 1:1500). Membranes stained for MUC1 were incubated overnight at 4 °C in 1% BSA in TTBS with Mucin 1 antibody VU4H5 (1: 200, Santa Cruz Biotechnology, Inc.), then incubated 1 h at ambient temperature in 1% BSA in TTBS with rat-anti mouse IgG-HRP (Southern Biotech, 1:2000). Between incubations, membranes were washed 3 x 5 min with TTBS. Membranes were then developed in 1-Step TMB Blotting substrate (ThermoScientific), scanned and analyzed.

Microscopy Experiments

Homotypic aggregation assays were run as described above. A 45 μL sample of each reaction was added to 200 μL complete media. A 1:25 dilution of 488-labeled galectin-3 antibody (R&D Biosystems) was added to each mixture and plated in an 8-chamber Lab-Tek II Chamber Coverglass System (Nunc) and incubated at 37 °C overnight. The following day, cells were washed with SFM and fixed in a 4% PFA solution for 20 min at room temperature. A coverslip was then mounted on the microslide using Prolong Gold with DAPI (Invitrogen) and allowed to cure overnight at room temperature shielded from light. Slides were then analyzed using a Nikon Eclipse TE200-U microscope with 40x oil immersion objective. Slides were also analyzed using a Ziess LSM 510 inverted confocal microscope. Experiments were run as described using a fluorescent MUC1 antibody (1:250, eFluor 615, eBioscience) in addition to the galectin-3 fluorescent antibody (results not shown).

Statistics

Statistical analysis was performed using unpaired two-tailed student's t-test. *, $P < 0.05$; **, $P < 0.01$; ***, $P < 0.001$. Error bars represent the mean ± S.D., $n \geq 3$.

CHAPTER 4

MATRIX METALLOPROTEINASE SUBSTRATE-LINKED DENDRIMERS

Introduction

Dendrimers as a Drug Delivery System

Beyond a tool used for the study of protein-carbohydrate interactions, dendrimers can also be useful in the development of therapeutics. They provide a symmetrical, easily manipulated scaffold that can accommodate a diverse surface chemistry. A relatively insoluble drug fixed to a dendrimer would not only benefit from the increased solubility provided by other functionalities on the dendrimers, but targeted delivery would increase the amount of that drug at the site of interest.[74] PAMAM dendrimers are especially useful in this respect, as the framework itself is water-soluble. Targeting agents can also be attached to the dendrimers, allowing for increased specificity of the drug.[97] However, using a large, synthetically diverse scaffold for a drug delivery system presents the same problems common with other systems including biological compatibility, specifically cytotoxicity and cell permeability. In order to be an effective drug delivery system, dendrimers must access the cytoplasmic region of the cell. For the most part, dendrimers have far too large a molecular weight to easily cross the cell membrane, and this can be further complicated by cross-linking between functional groups, causing large aggregates of dendrimers.[98] For this reason, an artificial translocation domain (ATD) must often be incorporated.[99] Kiessling, *et al.* developed such an ATD for their polymeric scaffolds using small, cationic peptides rich in guanidinium groups, as they are known to promote

cellular uptake. Recent studies have shown that smaller-sized dendrimers can be taken up by the cell through a number of pathways, including caveolae- and clatherin- mediated endocytosis, as well as macropinocytosis. Moreover, it has been noted that the addition of lauroyl chains onto PAMAM dendrimers increases the rate of cellular internalization in intestinal epithelial cells via these pathways.[100]

Another complication with dendrimers and other polymeric scaffolds used as drug delivery systems is their toxicity to the body. The size and diversity of end groups poses a challenge for *in vivo* practicality.[101] Highly cationic dendrimers, for example, are quite cytotoxic. This specific issue has been successfully circumvented through the addition of a polyethylene glycol tether (which also had the positive effect of extending the release of the attached drug).[102] Considering where in the body dendrimers aggregate is another complication. In a study involving polyester dendrimers and their effects on tumors in mice, when subjected to the dendrimers, a large percentage of the dendrimers ended up in the blood, and subsequently, the tumors. A significant buildup of dendrimers was also observed in the liver and spleen, most likely due to the molecular weight and size of the polymer.[103]

An imaging agent can also be incorporated on to a dendrimer scaffold. This can help establish if the cell takes up specific dendrimers, or can elucidate the pathway by which they are internalized. The most common motif for this is the addition of a fluorescent label. Rhodamine, fluorescein, and Alexa-fluor dyes have all been successfully incorporated for the purpose of tracking the biological routes of dendrimers.[100, 104] By using a confocal or epifluorescence microscope, specific localizations where dendrimers congregate in the cell can be determined.

In addition to a targeting agent (like glycosides for lectins), and an imaging agent, a therapeutic agent can also be applied to a denrimer scaffold. Despite the complications involved, dendritic drug delivery systems have been evaluated.[102, 105] A galactose-functionalized polypropylene imine (PPI) glycodendrimer was heterogeneously synthesized with the addition of primaquine phosphate endgroups and targeted the liver. The results showed that almost double (50%) the amount of primaquine phosphate was delivered to liver cells when incorporated on a glycodendrimer, as opposed to a PPI dendrimer functionalized with only primaquine phosphate.[102] PAMAM dendrimers have been functionalized with an inflammatory bowel disease drug 5-aminosalicylic acid (5-ASA) using pH-sensitive azo–linkages, that were then incubated with rat large intestine homogenates to test the specificity of colon-delivery. Compared with the 5-ASA prodrug currently on the market, the dendritic version had a much slower release, with about 50% delivered after 24 h, as opposed to the 80% of the free prodrug at 6 h. It was also shown that very little of the drug was released in homogenates of the stomach and small intestine, indicating real promise for azo-linked dendrimers as colon-specific controlled-release delivery systems.[106] Baker, *et al*. have synthesized acetylated PAMAM dendrimers multifunctionalized with folic acid, methotrexate and fluorescein. The dendrimers were the administered intravenously into immunodeficient mice bearing human tumors that overexpress the folic acid receptor. The fluorescein-imaging agent also confirmed the dendrimers were being taken up by the cell. The folic acid on the dendrimer was shown to act effectively as a targeting agent; compared with a non-targeted dendrimer, the folic acid-incorporated dendrimers were found to be localized in the tumor and liver up to 4 days after administration. Other advantages seen were the

marked increase in antitumor activity of the dendrimer over the free drug, and decreased toxicity.[107] Enzymatically-sensitive linkers have also been explored in drug delivery systems. A dextran was conjugated with methotrexate via a peptide linker that can be cleaved by matrix metalloproteinases (MMP) -2 and -9, hydrolases shown to be upregulated in certain cancers.[108]

The Roles of Matrix Metalloproteinases in Cancer

Matrix metalloproteinases (MMPs) are zinc-dependent protein and peptide hydrolases. So far, 23 unique MMPs have been identified in humans. They all contain a similar catalytic domain (Figure 25), containing ~165 amino acids, a five-stranded β-sheet and three α-helices.[109] They also have three zinc-binding histidines and a glutamate that acts as an acid/base during catalysis. In healthy systems, they are heavily involved in metabolic regulation through protein degradation and are the primary actors in extracellular matrix turnover. Thus, MMPs are involved in many biological processes that require tissue turnover and repair such as ovulation, postpartum involution, embryogenises, and wound healing. But their equilibrium is delicate; uncontrolled MMP activity can lead to arthritis, other forms of inflammation, and cancer.[110]

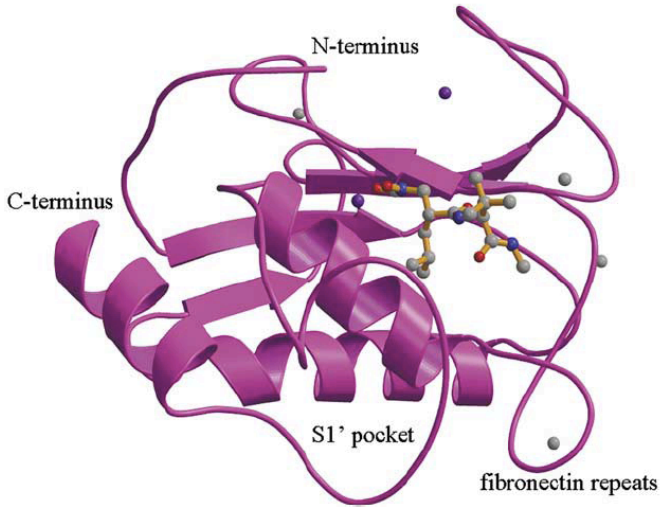


Figure 25. The structure of the catalytic domain of MMP-9 generated by imaging software. Purple zinc and grey calcium ions are also shown.[109]

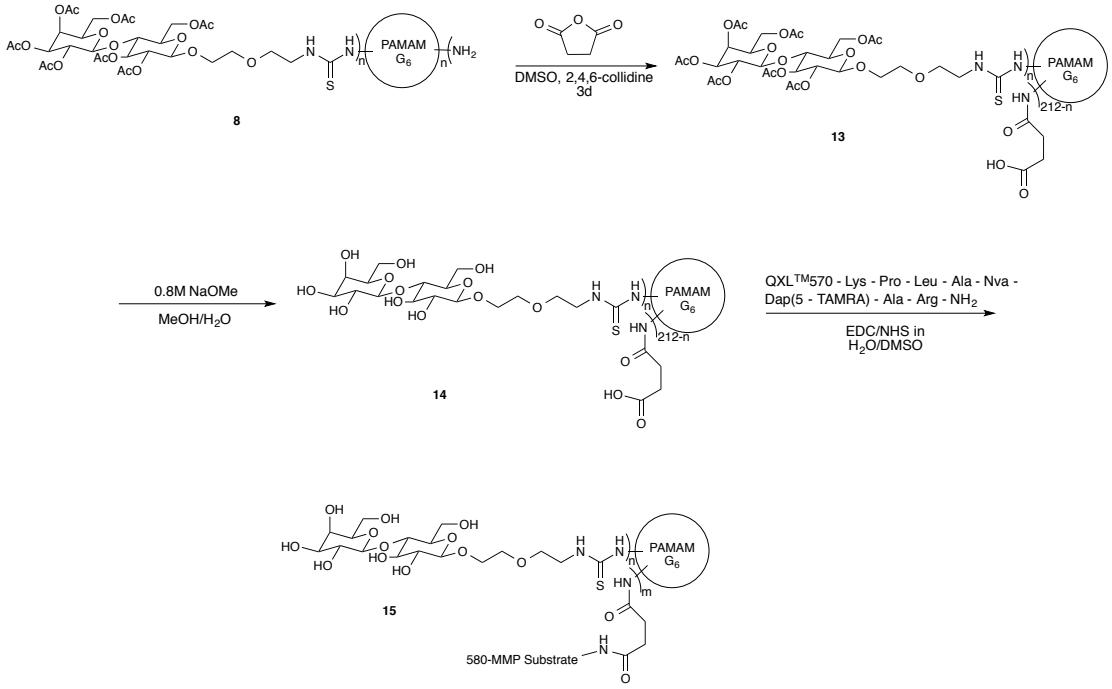
Much like galectin-3, MMPs are heavily upregulated in certain diseases and cancer, and are a viable target for drugs in those diseases. Meyer, *et al.* were able to specifically target and monitor the increased activity of MMP-11 using several different FRET-labeled (fluorescent resonance energy transfer) MMP substrates in pancreatic and mamma adenocarcinoma cells when compared to a line of T lymphocyte cells that do not express MMP-11.[111] Overall, however, drug development has been problematic due to the structural similarites of MMPs. They all have similar catalytic domains making selective targeting difficult, and some MMPs seem to have protective roles in cancer, so if targeting is not specific enough, it could result in a negative impact overall.[110]

Of the known MMPs, MMP-2 and MMP-9 show particular activity in invasion and metastasis, and are viable prognosticators for the aggressiveness of epithelial cancers like colon, breast, and lung cancers, showing low levels in benign tissue, and highly increased levels in malignant tissue.[112] As discussed in chapter 1, MMP-2 and MMP-9

also act to cleave a portion of galectin-3, activating it for some of its roles in breast cancer progression, like heterotypic aggregation and chemoinvasion.[49]

Using MMP Substrates for Dendritic Drug Design

MMPs are known to be upregulated in many forms of cancer and have been established as a tumor marker and target.[49] Substrates for MMPs have even been incorporated into drug design, utilizing their enzymatic activity to release a drug at a targeted location.[108] Here, a FRET-active MMP peptide substrate was incorporated into the synthesis of lactose-functionalized dendrimers for the study of prodrug release. Many MMP substrates are available commercially that target differing MMPs and have various fluorescent properties.[113] The MMP substrate used for the experiments described herein targets MMP-2 and MMP-9 (chosen for their specific implication in cancer processes)[112] and has a FRET signal that is quenched when the peptide is intact, but gives off a fluorescent signal upon cleavage of the peptide. A G6 dendrimer was chosen for the first synthetic target due to its aggregating effect on cancer cells as was described in Chapter 3.



Scheme 2. Final steps in the synthesis of MMP-substrate labeled lactose functionalized dendrimers. The first part of the synthesis is summarized in Scheme 1. The value of *n* was determined via MALDI and NMR, and the value of *m* was determined through absorbance.

The synthesis of MMP-substrate labeled lactose functionalized dendrimer is summarized in Scheme 2. Nucleophilic attack of succinic anhydride by the available terminal amines on dendrimer **8** results in amide-linked carboxylic acid-terminated acetylated-lactose dendrimer **13**. This was followed by deacylation to form **14** before the amine-terminated MMP-substrate was incorporated into the dendrimer via an EDC/NHS coupling, producing MMP-labeled lactose dendrimer **15** at a ratio of ~3 MMP substrate groups per dendrimer.

Results and Discussion

A generation 6 lactose functionalized dendrimer that incorporates a FRET-labeled MMP substrate specific to cancer-associated MMP-2 and MMP-9 was synthesized and incubated *in vitro* with A549 lung carcinoma cancer cells. Upon cleavage of the MMP substrate, a fluorescent signal could be observed. Fluorescence was monitored over time for on-dendrimer MMP substrate (dendrimer **15**), as well as the off-dendrimer free MMP substrate. Generation 6 lactose dendrimer **12** with no MMP substrate present was run as a control, in addition to an experimental condition run with **12** and with free MMP substrate together. Background experiments were performed where no cells were present, and the results are summarized in Figure 26.

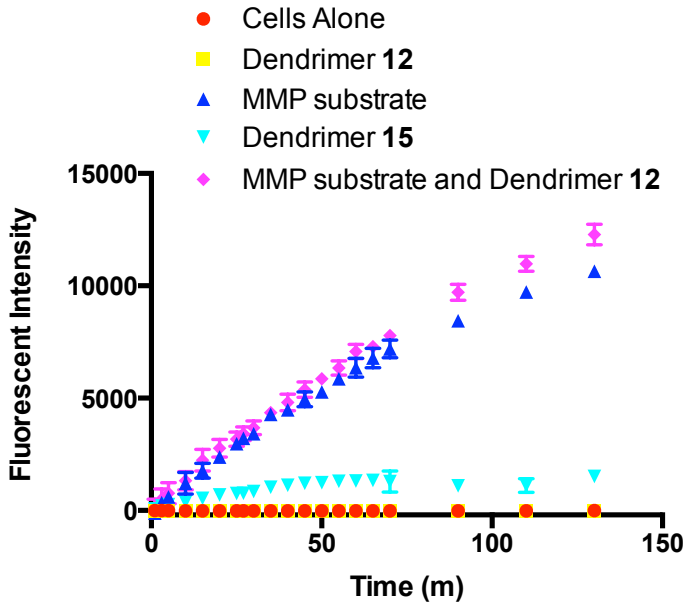


Figure 26. Fluorescent intensity of MMP substrates incubated with A549 cells. Results represent background-subtracted intensities (backgrounds consist of experimental conditions performed in the absence of A549 cancer cells). Results represent the averages of triplicate runs. Error bars represent the square root of the sum of the squares for each data point. Concentration of MMP substrate was roughly held constant for all experimental conditions.

Over time, the fluorescent signal increased, indicating more of the substrate was cleaved by cellular MMP-2 and MMP-9. As expected, the addition of lactose-functionalized G6 dendrimer **12** resulted in no more fluorescence than the negative control where no additional compound was added to A549 cells (Figure 26, ■ and ●, respectively). Off-dendrimer, both in the absence and presence of dendrimer **12**, the MMP substrate gave the largest signal (▲ and ◆, respectively). The MMP-dendrimer substrate **15** gave significantly less signal (▼) than off-dendrimer MMP substrate. Though roughly the same amount of MMP substrate was present in the various experimental conditions, fluorescent intensity stablized after 40 min in the case of **15**, indicating sterics may play a role. With the MMP substrate linked to a large, glycosylated scaffold, it is apparently more difficult for MMP-2 and MMP-9 to acces the peptide in order to cleave it.

Conclusion

A generation 6 lactose dendrimer was functionalized with a FRET-labeled MMP substrate. Upon cleavage of the substrate, a fluorescent signal could be observed. This dendrimer was incubated with MMP-positive lung cancer cell line A549, and the fluorescence was recorded over time. In comparison with a similar concentration of off-dendrimer MMP substrate, significantly less fluorescence was observed, indicating less MMP substrate was cleaved, which signifies that steric hindrance is an issue when considering the cleavage of MMP substrate. The bulk of the carrier scaffold, a ~100,000 Da glycodendrimer, may be blocking MMP-2 and MMP-9 from efficiently cleaving the substrate. It could also indicate that the MMP substrate, with a molecular weight near

2,000 Da, could be providing too much steric bulk itself with 3 moieties present per dendrimer. If the experiment were monitored for longer, it is possible that more MMP substrate is cleaved with time, implicating the dendrimer scaffold as a time-release drug delivery system. Therefore, further investigation of the optimization of the ratio of MMP substrate to dendrimer is needed. That being said, this data still provides real evidence that glycodendrimers could be used to target cancer cells, and MMP substrates can be a method by which a prodrug is cleaved from its scaffold so that it can be delivered. Increased (or decreased) loading of substrate on the glycodendrimer or use of a smaller dendrimer generation could perhaps result in an enhancement of the cleavage of the MMP substrate.

Experimental Procedures

General Methods

General reagents were purchased from Acros and Aldrich Chemical Companies. PAMAM dendrimers were purchased from Dendritech. Purified compounds were analyzed by ^{13}C and ^{1}H NMR with a Bruker DRX 500 MHz Spectrometer using TMS as an internal standard. For peak assignments, the following nomenclature was employed: s = singlet, d = doublet, t = triplet, dd = doublet of doublets, m = multiplet, bs = broad singlet. MALDI mass spectra were acquired using a Bruker Autoflex III time-of-flight mass spectrometer in positive linear mode with an acceleration voltage of 19 kV. Spectra of all dendrimers and dendrimer intermediates were obtained with a matrix: analyte ratio of 10,000:1 to 500:1 using a *trans*-3-indoleacrylic acid matrix and dimethyl formamide as the solvent. Bovine serum albumin (MW 66,431 g/mol), myoglobin (MW 16,952 g/mol),

and trypsinogen (MW 23,982 g/mol) were used as external standards. A 1 μL aliquot of matrix : analyte was used. Molecular mass data of the broad peaks were calculated using a peak centroid based on a peak width of approximately 10,000. Relevant spectra can be found in Appendix B of this thesis.

Carboxylic Acid-Terminated Acetylated Lactose Functionalized Dendrimer (**13**). In a half-dram glass scintillation vial, a teflon-coated stirbar was added to a 25 mg/mL solution of dendrimer intermediate **8** (22.5 mg, 0.196 μmol) in DMSO (0.9 mL), which was made basic by the addition of 2,4,6-collidine (100 uL). An excess of succinic anhydride was then added (11 mg, 110 μmol, 560 equiv) to the reaction mixture, and the resulting reaction mixture was stirred at 20°C for 3 days. The reaction mixture was then purified by dialyzing it in 3500 MWCO dialysis membrane tubing in 250 mL DMSO for 8 h, replacing the DMSO with fresh every 2 h. The contents of the dialysis tubing were then frozen and lyophilized to yield the purified product as white solid, which was then analyzed by NMR and MALDI. ^{1}H NMR (500 MHz, DMSO-D_6) δ 7.96 (s, 1.0H), 7.78 (s, 0.9H), 7.47 (s, 1.2H), 6.08 (m, 0.4H), 5.86 (d, J = 8.2 Hz, 0.2H), 5.35 – 5.05 (m, 3.7H), 4.91 – 4.59 (m, 4.0H), 4.33-4.12 (m, 2.71H), 4.11 – 3.85 (m, 5.1H), 3.78 (s, 3.0H), 3.66 – 2.94 (m, solvent obstructed), 2.71 – 2.55 (m, 4.8H), 2.48 – 2.35 (m, 7H), 2.10-2.01 (m, 7.0H), 2.00-1.90 (m, 12.8H), 1.86 (s, 3.2H) ppm. ^{13}C NMR (125 MHz, DMSO-D_6) δ 173.99, 170.66, 170.30, 169.92, 169.75, 169.48, 100.36, 99.70, 89.28, 76.95, 76.70, 72.87, 72.18, 71.67, 70.75, 70.11, 69.67, 69.38, 68.90, 67.90, 67.50, 63.59, 62.86, 62.64, 61.26, 49.92, 45.50, 33.38, 29.25, 21.04, 20.88, 20.78, 20.72 ppm. MALDI-TOF (pos) m/z 104000.

Deacetylated Lactose Dendrimer (**14**). The generalized procedure outlined in Chapter 2 for the deprotection of dendrimer **8** was used. ^{1}H NMR (500 MHz, DMSO-D_6) δ 8.05 (s, 1.0H), 7.81 (s, 1.3H), 5.38-4.82 (m, 1.0H), 4.82-4.48 (m, 1.8H), 4.32-4.06 (m, 0.5H), 3.77 (m, 0.9H), 3.65 – 2.81 (m, solvent obstructed), 2.81 – 1.93 (m, solvent obstructed), 1.58 (s, 0.4H), 1.20 (s, 0.8H), 0.87-0.69 (m, 0.4H) ppm. ^{13}C NMR (125 MHz, DMSO-D_6) δ 172.48, 104.25, 103.10, 82.86, 81.07, 76.44, 75.96, 75.38, 75.27, 74.20, 73.69, 73.56, 72.56, 71.73, 71.45, 71.03, 69.94, 69.58, 69.25, 68.57, 68.41, 68.10, 60.85, 60.69, 56.84, 49.99, 45.05, 38.73, 37.34, 33.93-33.38, 33.28, 31.40 ppm. MALDI-TOF (pos) m/z 85200.

Addition of MMP Substrate on
Lactose Functionalized Dendrimer (**15**). A half dram glass scintillation vial was charged with dendrimer **14** (3.6 mg, 39.6 nmol) and a teflon-coated stir bar. To this, 100 μL DMSO was added. A solution of 580 MMP FRET Substrate I (Anaspec,[113] 0.3 mg, 170 nmol, 4.3 equiv) in DMSO (50 μL) was added to the dendrimer solution. A 20 mg/mL solution of *N*-hydroxysuccinimide in DMSO was made. From this, 7.0 μL was added to the dendrimer/MMP reaction mixture (0.14 mg, 1.2 μmol, 30 equiv). A 20 mg/mL solution of 1-Ethyl-3-[3-dimethylaminopropyl] carbodiimide hydrochloride (EDC) was made in deionized water, from which 13.0 μL was removed and added to the reaction mixture (0.26 mg, 1.7 μmol, 43 equiv). The final concentration of the reaction mixture was 50 mM with respect to the endgroups on dendrimer **14**. The reaction mixture was shielded from light and allowed to stir at 20°C for 16 h. The reaction solution was then dialyzed while shielded from light in 3500 Da MWCO dialysis tubing in 250 mL

deionized water for 2d, replacing the deionized water with fresh every 12 h. The contents of the dialysis tubing was then frozen and lyophilized, yielding the purified product as a purple fluffy solid analyzed by NMR and MALDI (1.0 mg, 11.0 nmol, 28% yield). The degree of MMP substrate loading was determined using a standard curve of free 580 MMP FRET Substrate I. Absorbance readings were measured at 577 nm (the maximum absorbance of QXL-570, the quencher used in the MMP-substrate). Absorbance readings of purified product **15** (where the concentration with respect to the final product was known) were compared to the absorbances of the standard curve. Through this method, the MMP loading was determined to be 2.9 molecules of MMP substrate per dendrimer on average. ^{1}H NMR (600 MHz, DMSO-D_6) δ 8.48-8.43 (m, 0.2H), 8.17-7.76 (m, 1.8H), 7.56 (bs, 1.0H), 7.46 (s, 0.1H), 7.39 (s, 0.1H), 7.08 (bs, 0.3H), 6.86 (d, J = 9.2 Hz, 0.2H), 6.54-6.47 (m, 0.2H), 5.35-5.06 (m, 1.1H), 4.93-4.41 (m, 2.2H), 4.34-4.16 (m, 0.9H), 3.98 (d, J = 33.7 Hz, 0.6H), 3.90-3.38 (m, 5.3H), 3.27-3.00 (m, 2.0H), 2.95 (s, 0.5H), 2.83-2.59 (m, 2.0H), 2.47-2.33 (m, 0.9H), 2.22 (bs, 1.8H), 1.74-1.40 (m, 1.1H), 1.36-1.17 (m, 0.8H), 0.90 – 0.72 (m, 0.7H) ppm. MALDI-TOF (pos) m/z 83500.

Fluorescence Assay

Lung carcinoma A549 cells were purchased from ATCC and cultured as recommended by ATCC. Prior to use, 4th passage cells were dissociated from growth dishes using 0.02% EDTA/0.25% trypsin (SAFC Biosciences) and diluted to 500,000 cells/mL serum free F12K media (SFM, Gibco). The assay was performed in a standard 96-well quartz plate (Hellma). Five different experimental conditions were observed: SFM (1), dendrimer **12** (2), 580 MMP FRET Substrate I (3), dendrimer **15** (4), and 580

MMP FRET Substrate I with dendrimer **12** (5). Each of these conditions was also performed in the absence of cells, which was used as the appropriate background and subtracted from the overall fluorescence. Experiments were run in triplicate using 100 μL cell solution per well (50,000 cells per experiment). To wells (3) and (5), 5 μL MMP substrate was added (283 μM in Millipore water, 1.42 nmol). To wells (2) and (5), 30 μL dendrimer **12** was added (2 mg/mL in Millipore water, 0.7 nmol). To well (4), 30 μL dendrimer **15** was added (2 mg/mL in Millipore water, 0.7 nmol with respect to the dendrimer, 2.1 nmol with respect to 580 MMP Fret Substrate I). Samples were then monitored every 5 min for 130 min for fluorescent intensity and changes in lifetime using a NovaFluor Fluorescence Lifetime Microplate Reader at 532/556 ex/em with 1s signal averaging taking 3 readings per well per time point.

CHAPTER 5

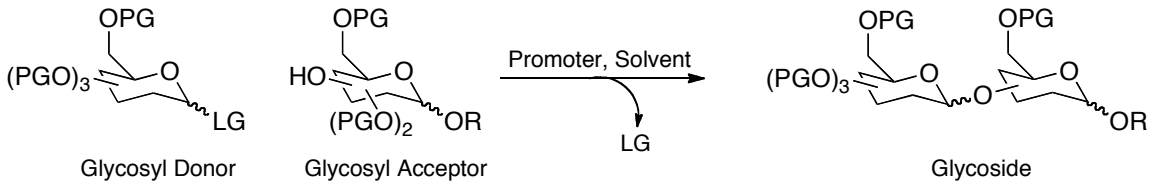
INDIUM(III) AS A PROMOTER FOR GLYCOSYLATION

Introduction

Glycosylation

Carbohydrates decorate proteins, lipids, and phospholipids, and carry the important role of intercellular recognition. Carbohydrates are the receptors responsible for communication with hormones, viruses, and proteins. To study the interactions of these complicated molecules with their receptors, it is necessary target carbohydrates. At the heart of carbohydrate synthesis lays a fundamental reaction: glycosylation. Glycosylation accounts for at least 50% of post-translational modifications on proteins and is the ubiquitous reaction in carbohydrate chemistry, with uses including synthetically functionalizing multivalent macromolecules such as dendrimers.[2]

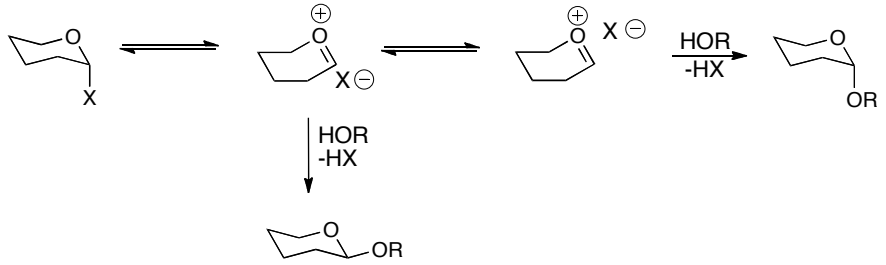
Glycosylation involves a glycosyl donor, the electrophile of the reaction, with a leaving group attached to the anomeric carbon. The donor contains the anomeric carbon of the resulting glycoside. The glycosyl acceptor is the nucleophile of the reaction and is traditionally an alcohol. This reaction is summarized in Scheme 3. Although *N*-, *S*-, and *C*-linked glycosides exist, the vast majority of natural glycosides are *O*-linked. Often a promoter is necessary, usually a Lewis acid, to aid the loss of the leaving group, and various solvents can be chosen based on the desired stereochemical outcome.[114]



Scheme 3. General scheme for glycosylation.

One of the earliest and most successful glycosylation reactions was that developed by Koenigs and Knorr in 1901, which uses a glycosyl halide that is reacted with a deprotected alcohol using silver carbonate as a promoter.[115] Since then, a number of variations have been made to this reaction, most notably the development of more effective heavy metal promoters.[116] Due to the highly water-sensitive nature of a glycosyl halide and the harsh reaction conditions necessary with heavy metals, Schmidt developed a new method that would require milder conditions and less toxic materials. Schmidt's method, which invokes a glycosyl imidate, most commonly a trichloroacetimidate, has been widely adopted since its development in the 1980s.[117, 118] This method is very similar to the Koenigs-Knorr reaction; the key difference is the employment of a more readily formed trichloroacetimidate leaving group on the anomeric carbon rather than a halide. Both of these leaving groups require an activator, but the trichloroacetimidate requires much milder conditions and can be activated without the use of a heavy metal salt. Instead of a mercury or silver salt, the activation occurs with less hazardous reagents, commonly TMSOTf and $BF_3 \bullet OEt_2$. Because these reaction conditions are much more compatible with a variety of substrates and protecting groups commonplace in carbohydrate chemistry, trichloroacetimidates represent a significant advance in carbohydrate chemistry.[117, 118]

While the Koenigs-Knorr and trichloroacetimidate methods remain among the most popular glycosylation reactions, there are no ubiquitous reaction conditions that work for all glycosylations. The variations in acceptor and donor properties, further complicated by protecting groups and neighboring groups, make it difficult for a universal method to be developed.[115] Instead, a wide variety of modifications to these general methods have been developed based on the properties of the substrates and desired product. For example, α versus β selectivity can be affected by the choice of solvent, as it can affect the geometry of the ion pair created by ionization of the glycosyl donor (Scheme 4).[119]



Scheme 4. Solvent effects in glycosylation. Tight ion pairs versus solvent-separated ion pairs produce a different stereochemical outcome.

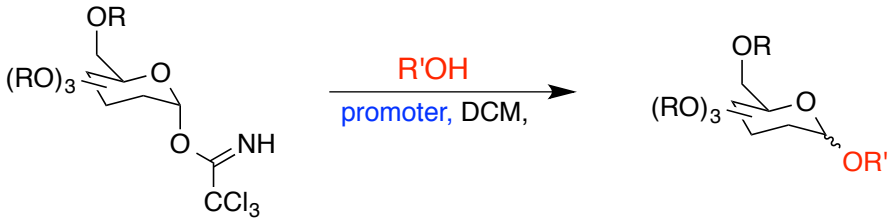
Promoters prevalently employed are usually moisture-sensitive heavy metals, the most common being silver, mercury, and tin Lewis acids.[114] These promoters afford very good yields when optimized but can be impractical on large-scale reactions due to the amount of heavy metal waste generated.[116] Alternative Lewis acid promoters, such as TMSOTf and BF_3•OEt_2, are milder promoters and do not contain toxic heavy metals, but are still quite moisture-sensitive and difficult to work with, as they must be distilled prior to use and kept under argon. They also often require extended reaction times. The milder In(III), on the other hand, is entirely water-tolerant and can be reusable, unlike most other

glycosylation promoters.[120-122] As a Lewis acid, In(III) is less robust when compared to its heavy metal counterparts, and thus is more compatible with a range of protecting groups. The use of In(III) is also quite versatile in the reactions it promotes, as it has been shown to promote reactions ranging from transesterifications to Diels-Alders.[121] It has also been shown to be an effective and efficient promoter in the acetylation of carbohydrates. Because of the success of this reaction and the practicality of In(III) over its heavy metal and moisture-sensitive counterparts, it is proposed that In(III) can also useful as a promoter in glycosylation.[86]

Rationale and Approach

A variety of substrates for the reactions were chosen to highlight the versatility of In(III) as a glycosyl promoter. Sugars with a variety of protecting groups were selected in order to test their compatibility with In(III). A variety of alcohol acceptors, including a carbohydrate, were also chosen to emphasize the flexibility of In(III) as a promoter.

Carbohydrates bearing two different protecting groups (**16** and **17**) were reacted with four different alcohol glycosyl acceptors (**18, 19, 20,** and **21**). Three In(III) promoters ($InCl_3$, $InBr_3$, and $In(OTf)_3$), whose conjugate acids vary in strength, were used to promote these reactions. In addition, $BF_3 \bullet OEt_2$ served as a control. These reactions are summarized in Scheme 5.



16: R = Bn
17: R = Ac

18: R' = 2-(2-azidoethoxy) ethanyl
19: R' = benzyl
20: R' = *n*-butyl
21: R' = *t*-amyl

Promoter = $InCl_3$
$InBr_3$
$In(OTf)_3$
$BF_3 \cdot OEt_2$

Scheme 5. General scheme of reactions.

This chemistry was also used toward the synthesis of dendrimers functionalized with 1,3-diglucose.

Results and Discussion

Overall, little to no product degradation was observed, probably due to the robustness of the benzyl and acetyl protecting groups. When more labile protecting groups are used, overall glycosylation yields suffer.[123] Another variable in these experiments was the degree of substitution presented in the various glycosyl acceptors – alcohols ranging from primary to tertiary, as well as a carbohydrate (Scheme 6) were all tested. The yields using tetra-benzylated galactose **16** are summarized in Table 3 and are similar for all promoters. Yields were lower for the more hindered tertiary glycosyl acceptor **21** with In(III) promoters. Although the varying In(III) promoters also showed little difference in effectiveness in promoting the different glycosides produced, some trends can be elucidated. $InCl_3$, which has a slightly weaker Brønsted acid conjugate, was a consistently better In(III) promoter for **16**. For alcohols **18** and **19**, both $InCl_3$ and $InBr_3$ worked as well as or better than the $BF_3 \bullet OEt_2$ control. The experiments that are

summarized in Table 3 using the perbenzylated galactoside trichloroacetimidate **16** indicate that In(III) promoters can be catalytically used to effectively promote glycosylation reactions. However, since In(III) has been reported as a promoter of Friedel-Crafts chemistry,[124, 125] formation of side products is likely to detrimentally affect reaction yields. Although the side products were not characterized, the increased complexity of the aromatic region in the ^{13}C and ^{1}H NMR spectra of crude product mixtures from **16** indicate their formation.

For reactions using benzylated donor **16**, the β isomer is the major product in every case tested, but α:β ratios vary depending on reaction conditions. Since the conditions were optimized based on overall yield rather than anomeric ratios, it should be noted that time and strength of Brønsted acid promoter (as well as reaction temperature) may have a significant effect on the anomeric ratio of products. While the α-product gains some anomeric stability, benzyl protecting groups are sterically relatively bulky.

Table 3: A summary of glycosylation yields for tetra-benzylated galactose



16

22: R = 2-(2-azidoethoxy)ethanyl
23: R = benzyl
24: R = *n*-butyl
25: R = *t*-amyl

Product	Promoter (equiv.)	Alcohol used	Time (min.)	Yield[a] (%)	α:β ratio[b]
22	$InBr_3$ (0.1)	**18**	30	50	3:7
22	$InCl_3$ (1.0)	**18**	45	61	5:6*
22	$In(OTf)_3$ (0.05)	**18**	20	72	3:5
22	BF_3•OEt_2 (0.2)	**18**	30	74	1:3
23	$InBr_3$ (0.1)	**19**	30	73	2:5*
23	$InCl_3$ (1.0)	**19**	45	96	1:3*
23	$In(OTf)_3$ (0.05)	**19**	20	86	1:2*
23	BF_3•OEt_2 (0.2)	**19**	30	85	1:10*
24	$InBr_3$ (0.1)	**20**	30	76	1:3
24	$InCl_3$ (1.0)	**20**	45	86	2:3
24	$In(OTf)_3$ (0.05)	**20**	20	96	1:2
24[c]	BF_3•OEt_2 (1.0)	**20**	120	95	1:9
25	$InBr_3$ (0.1)	**21**	30	70	1:3
25	$InCl_3$ (1.0)	**21**	45	56	3:10*
25	$In(OTf)_3$ (0.05)	**21**	20	61	1:1
25[c]	BF3•OEt2 (1.0)	**21**	120	80	1:2

[a]Yields determined by ^{1}H NMR spiked with a mesitylene standard.
[b]Ratios determined by ^{1}H NMR or ^{13}C NMR when starred.
[c]BF_3•OEt_2 promotion for this reaction was optimal at 1.0 equiv.

Products **24** and **25** were independently resubjected to the reaction conditions using one equivalent of $InBr_3$, and $InCl_3$, and BF_3•OEt_2, and no interconversion of the α

and β isomers was observed (Table 4). The α:β ratio did change over time in one case, however no additional α product was formed, but rather this ratio change tracked β isomer degredation. Thus, it can be concluded that the reaction occurs under kinetic control.

Table 4. Reactions testing the reversibility of In(III)-promoted glycosylation

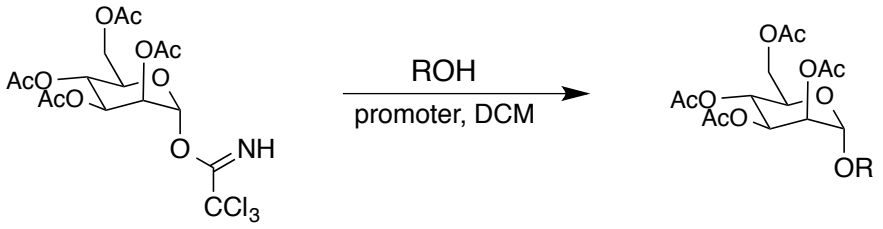
Product	Glycoside mg (α:β)	Alcohol mg (equiv, #[a])	Promoter	Promoter mg (equiv)	Temp. (°C)	α:β Ratio[b]
24	51.8 (0:1)	10.4 (1.8, **20**)	BF_3•OEt_2	15.5 (1.4)	0	0:1
24	50.3 (0:1)	9.6 (1.8, **20**)	$InCl_3$	18.4 (1.1)	0	0:1
24	51.9 (0:1)	9.7 (1.7, **20**)	$InBr_3$	31.1 (1.2)	0	0:1
25	12.4 (1:7)	2.5 (1.4, **21**)	BF_3•OEt_2	3.3 (1.1)	0	1:9
25	12.1 (1:7)	2.5 (1.4, **21**)	$InCl_3$	5.3 (1.2)	0	1:5
25	10.7 (1:7)	2.4 (1.6, **21**)	$InBr_3$	7.7 (1.2)	0	1:2

[a]# refers to compound number, shown in Scheme 5.
[b]Yields determined by ^{1}H NMR spiked with a mesitylene standard.

Results for tetra-acetylated mannose **17** (Table 5) suggest there is no preference for which In(III) promoter is used; $InBr_3$, $In(OTf)_3$, and $InCl_3$ were all shown to perform nearly as well if not better than BF_3•OEt_2. The choice of promoter is independent of the substitution of the glycosyl acceptor (more data available from Mattson, et al.[123]). $In(OTf)_3$ was a less effective promoter, possibly due to the strong Brønsted acid HOTf present, which could cause product degradation. Only the alpha product was observed,

presumably due to the neighboring group participation of the acetyl group at C2 on the mannoside and due to the anomeric effect.

Table 5: A summary of glycosylation yields for tetra-acetylated mannose



17

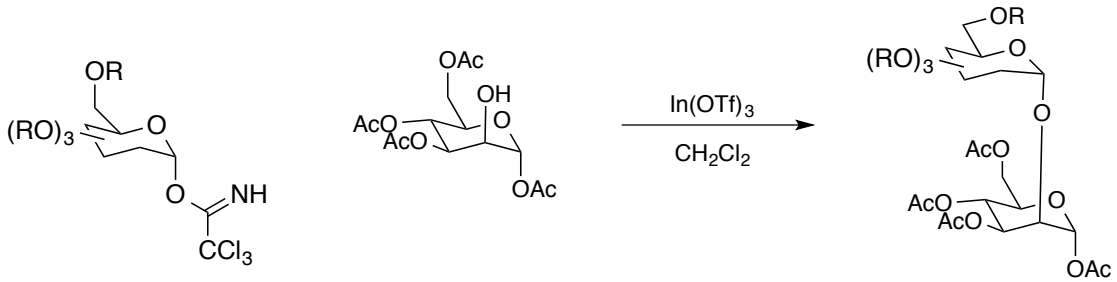
26: R = *n*-butyl
27: R = *t*-amyl

Alcohol	Promoter	Product	Yield[a] (%)
20	$InBr_3$	**26**	77
20	$InCl_3$	**26**	52
20	$In(OTf)_3$	**26**	48
20	BF_3OEt_2	**26**	58
21	$InBr_3$	**27**	86
21	$InCl_3$	**27**	60
21	$In(OTf)_3$	**27**	64
21	BF_3OEt_2	**27**	61

[a]Yields determined by ^{1}H NMR spiked with a mesitylene standard. All α:β ratios are 1:0 due to neighboring group participation.

Overall, glycosylation of peracetylated mannoside trichloroacetimidate **17** with simple alcohols afforded the highest yields using $InBr_3$. Trends were less evident for glycosylation of perbenzylated galactoside trichloroacetimidate **16**. In experiments performed using the same acceptors and promoter against an acetonide protected mannoside trichloroacetimidate, $In(OTf)_3$ was generally the best promoter.[123] Using these results, disaccharide-forming reactions were explored using **16** and **17** with acceptor **28**

(Scheme 6). Initial tests with $InBr_3$ afforded significant amounts of unreacted **17** even when 20 mol % was used (rather than the 10 mol % that was used with **18-21**) and the reaction time was extended six-fold. $In(OTf)_3$ proved to be the preferred promoter for all three donors in disaccharide formation with **28**, and the results are shown in Table 6. Acetyl protected mannoside trichloroacetimidate gave a reasonable yield of disaccharide formation (53%) with only α-linked products observed. Benzylated galactoside trichloroacetimidate afforded a lower yield of α-linked product (36% yield) due to β product also being formed.



16: R = Bn
17: R = Ac

28

29: R = Bn
30: R = Ac

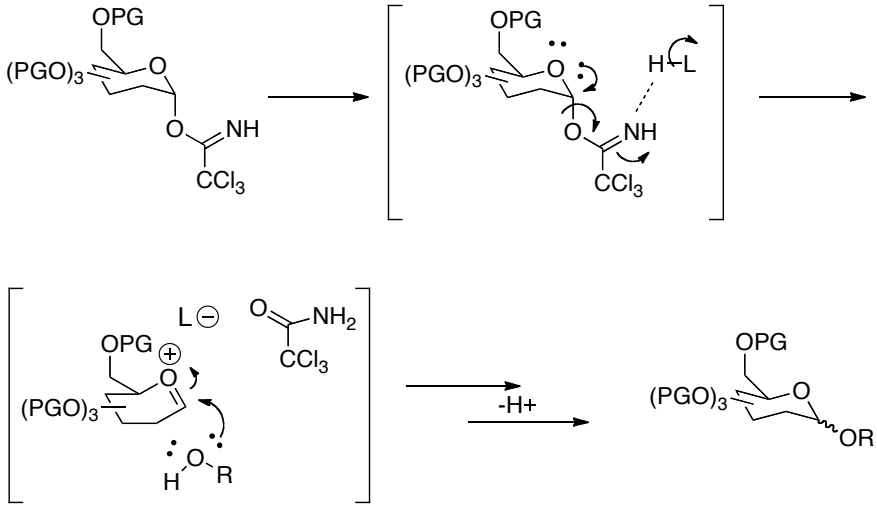
Scheme 6. The formation of a disaccharides **29** and **30** using In(III) as a promoter.

Table 6. $In(OTf)_3$ promoted disaccharide formations

Product	Promoter (equiv.)	Temp (°C)	Time (min.)	Yield[a] (%)
29	$In(OTf)_3$ (0.05)	0	30	36[b]
30	$In(OTf)_3$ (0.05)	0	20	53

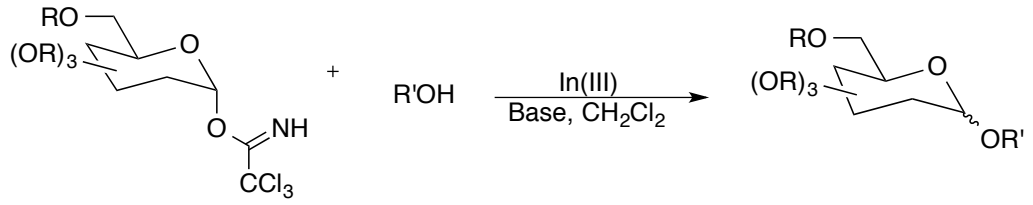
[a]Yields determined by ^1H NMR spiked with a mesitylene standard.
[b]Yield is for α-linked product only.

In addition to testing the effectiveness of In(III) as a promoter of glycosylation reactions, a series of experiments were also carried out in order to test the mechanism of this reaction. It was initially hypothesized that this reaction would follow the same Lewis acid-promoted pathway as previously proposed for other trichloroacetimidate methods.[126] To confirm this, each reaction using benzylated-galactose donor **16** was tested with one equivalent of hindered base added, and while trace amounts of product did form, the rate was greatly hindered (Table 7). The base acts as a proton sponge in these reactions, which indicates that the glycosylation is driven not only by Lewis acid catalysis, but also by the Brønsted acid adduct that is created by the In(III) promoter, which eventually drives the reaction to completion (Scheme 7).[127] Bizier, et al. tested this theory by adding a Brønsted acid (HOTf) in catalytic amounts, however little or no product was obtained.[86] Based on these data, it is believed that the metal salt is a mild provider of the Brønsted acid.



Scheme 7. Brønsted acid-promoted glycosylation of a sugar. PG = protecting group, R=alkyl group.

Table 7. Preparation of pyranoside derivatives in the presence of a proton scavenger



Product[b]	Trichloro-acetimidate mg (#[a])	Alcohol mg (equiv. #)	Promoter	Promoter mg (equiv.)	Base mg (equiv)
22	28.9 **(16)**	6.1 (1.1, **18**)	InBr3	18.3 (1.2)	7.4 (1.4)
22	29.1 **(16)**	6.5 (1.2, **18**)	InCl3	14.1 (1.5)	7.4 (1.4)
23	25.1 **(16)**	5.2 (1.3, **19**)	InBr3	18.2 (1.4)	7.4 (1.7)
23	28.3 **(16)**	5.3 (1.2, **19**)	InCl3	13.2 (1.4)	7.4 (1.5)
24	22.3 **(16)**	3.2 (1.3, **20**)	InBr3	16.1 (1.4)	7.4 (1.9)
24	27.1 **(16)**	3.6 (1.2, **20**)	InCl3	13.7 (1.6)	7.4 (1.5)
25	31.0 **(16)**	4.2 (1.1, **21**)	InBr3	17.5 (1.1)	7.4 (1.4)
25	30.2 **(16)**	4.4 (1.1, **21**)	InCl3	12.9 (1.3)	7.4 (1.4)
26	102.8 **(17)**	16.2 (1.4, **20**)	InBr3	77.3 (1.0)	43.0 (1.0)[c]
26	105.5 **(17)**	17.3 (1.1**, 20**)	InCl3	49.9 (1.1)	46.2 (1.1)[c]
26	107.0 **(17)**	22.7 (1.0, **20**)	In(OTf)3	116.1 (1.0)	41.3 (0.9)[c]
26	51.3 **(17)**	8.5 (1.1, **20**)	BF3•OEt2	14.8 (1.0)	21.4 (1.0)[c]

[a]# refers to compound number, shown in Scheme 5.

[b]All product yields were trace as determined by ^{1}H NMR spiked with a mesitylene standard.

[c]Where indicated, base used was DTBMP, otherwise collidine was used.

Conclusion

In summary, a novel variation to the trichloroacetimidate method of glycosylation has been demonstrated on a number of glycosyl acceptor substrates, including a carbohydrate. While the yields reported are comparable to those found using the already established promoter BF_3•OEt_2, In(III) offers a more practical alternative to the highly hygroscopic and hazardous promoters often employed for this method. This reaction is not very selective when both α- or β-products could be observed, but the more sterically stable product is favored. The ability to vary ligands on In(III) also provides a broad range of promotion strength, enabling optimization of the conditions for desired reactions.

Experimental Procedures

General Methods

To obtain pure products, crude products were combined and purified by column chromatography on 60 Å silica gel with hexane: ethyl acetate mobile phase in the indicated ratio. An ice bath was used for reactions performed at 0 °C. A Bruker DRX 500 MHz Spectrometer was used to record ^{13}C and ^{1}H NMR for purified compounds and trimethyl silane was used as an internal standard. For peaks assigned, the following nomenclature was employed: s = singlet, d = doublet, t = triplet, dd = doublet of doublets, m = multiplet, bs = broad singlet. Mass spectra were obtained using a high-resolution Bruker micro-TOF system, except for dendrimers, which were obtained were acquired using a Bruker Autoflex-III time-of-flight mass spectrometer in positive linear mode with

an acceleration voltage of 19 kV. Spectra were obtained with a matrix: analyte ratio of 10,000:1 to 500:1 using a *trans*-3-indoleacrylic acid matrix and dimethyl formamide as the solvent. Bovine serum albumin (MW 66,431 g/mol), myoglobin (MW 16,952), and trypsinogen (MW 23,982 g/mol) were used as external standards. A 1 μL aliquot of matrix : analyte was used. Molecular mass data of the broad peaks were calculated using a peak centroid based on a peak width of approximately 2000 for G2 dendrimers, 5000 for G3 and G4 dendrimers, and 10,000 for G6 dendrimers. Yields were calculated from crude ^{1}H NMR spectra using an internal mesitylene standard (1,3-diglucose dendrimers were not). Trichloroacetimidate starting materials[128] and acceptor **28**[129] were synthesized using previously described methods. Relevant spectra are located in Appendix B of this thesis.

General Procedure For the Preparation of Mannopyranoside and Galactopyranoside Derivatives. A dry 4 mL scintillation vial was charged with the trichloroacetimidate starting material, a slight excess of alcohol, and a teflon-coated stir bar. To this, dry dicholoromethane was added to obtain a 50 mM solution of the trichloroacetimidate. The mixture was cooled if specified, and the promoter was added. Reactions run with BF_3•OEt_2 were additionally purged with argon and performed under an argon atmoshpere. The reaction mixture then stirred for the specified time. Any unreacted promoter was then quenched with approximately 0.2 g dry sodium bicarbonate and stirred for 20 min, then 2 mL dichloromethane was added. The resulting suspension was filtered over a bed of glass wool to remove any remaining sodium bicarbonate particulates and flushed with additional dichloromethane. The

solvent was removed under reduced pressure. Yields of crude products were obtained from ^{1}H NMR spectra using an internal mesitylene standard. Chromatographic purification was performed (galactopyranoside products 8:2 hexane:ethyl acetate; acetyl protected mannopyranoside products either 6:4 hexane : ethyl acetate or 1:1 hexane : ethyl acetate) to obtain pure samples for characterization purposes. Amounts of reagents used and exact reaction conditions are provided in Table 8.

*Table 8. Conditions for glycosylation of trichloroacetimidates **16**–**17**.*

Pro-duct	Trichloro-acetimidate mg (#[a])	Alcohol mg (equiv, #)	Promoter	Promoter mg (equiv)	Time[a] (min)	Yield[b] (%)	α:β Ratio
22	27.9 (**16**)	6.9 (1.2, **18**)	$InBr_3$	1.7 (0.1)	30	50	3:7
22	28.8 (**16**)	7.4 (1.2, **18**)	$InCl_3$	9.4 (1.0)	45	618	5:6[c]
22	31.1 (**16**)	7.7 (1.2, **18**)	$In(OTf)_3$	1.5 (0.6)	20	72	3:5
22	29.5 (**16**)	7.6 (1.2, **18**)	BF_3•OEt_2	1.2 (0.2)	30	74	1:3
23	34.8(**16**)	6.6 (1.2, **19**)	$InBr_3$	1.5 (0.08)	30	73	2:5[c]
23	32.0 (**16**)	6.0 (1.2, **19**)	$InCl_3$	9.7 (0.9)	45	96	1:3[c]
23	36.5 (**16**)	6.9 (1.2, **19**)	$In(OTf)_3$	1.5 (0.03)	20	86	1:2[c]
23	35.1 (**16**)	6.7 (1.2, **19**)	BF_3•OEt_2	1.5 (0.2)	30	85	1:10[c]
24	32.7 (**16**)	4.2 (1.2, **20**)	$InBr_3$	1.6 (0.1)	30	76	1:3
24	32.2 (**16**)	4.2 (1.2, **20**)	$InCl_3$	9.9 (1.0)	45	86	2:3
24	28.6 (**16**)	3.7 (1.2, **20**)	$In(OTf)_3$	1.3 (.06)	20	96	1:2

*Table 8. Conditions for glycosylation of trichloroacetimidates **16–17** - continued*

Pro-duct	Trichloro-acetimidate mg (#[a])	Alcohol mg (equiv, #)	Promoter	Promoter mg (equiv)	Time[a] (min)	Yield[b] (%)	α:β Ratio[c]
24	31.8 (**16**)	7.4 (2.2, **20**)	BF_3•OEt_2	7.0 (1.1)	120	95	1:9
25	34.0 (**16**)	5.3 (1.2, **21**)	$InBr_3$	1.7 (0.1)	30	70	1:3
25	33.2 (**16**)	5.1 (1.2, **21**)	$InCl_3$	10.4 (1.0)	45	56	3:10[c]
25	29.9 (**16**)	4.6 (1.2, **21**)	$In(OTf)_3$	1.4 (0.06)	20	61	1:1
25	30.7 (**16**)	5.4 (1.4, **21**)	BF_3•OEt_2	6.6 (1.0)	120	80	1:2
26	47.4 (**17**)	8.6 (1.2, **20**)	$InBr_3$	3.9 (0.1)	30	85	1:0
26	53.0 (**17**)	9.6 (1.2, **20**)	$InCl_3$	23.0(1.0)	60	50	1:0
26	51.5 (**17**)	9.3 (1.2, **20**)	$In(OTf)_3$	3.2 (0.05)	15	58	1:0
26	52.5 (**17**)	9.5 (1.2, **20**)	BF_3•OEt_2	3.1 (0.2)	30	56	1:0
27	54.0 (**17**)	11.6 1.2, **21**)	$InBr_3$	3.8 (0.1)	30	74	1:0
27	54.4 (**17**)	11.7 (1.2, **21**)	$InCl_3$	23.2 (1.0)	60	67	1:0
27	49.5 (**17**)	10.6 (1.2, **21**)	$In(OTf)_3$	3.2 (0.06)	15	74	1:0
27	100.1 (**17**)	28.9 (1.6, **21**)	BF_3•OEt_2	121.4(1.1)	120	61	1:0

[a]All reactions performed at 0 °C.
[b]Yields determined by ^{1}H NMR spiked with a mesitylene standard.
[c]Ratios determined by ^{13}C NMR. The remainder were by ^{1}H NMR when specified.

General Procedure for Evaluation of the Reversibility of the Reaction. A dry 2 mL scintillation vial was charged with the glycoside, a slight excess of alcohol, and a Teflon-coated stir bar. Dry dichloromethane was then added to yield a 50 mM solution of the trichloroacetimidate. The reaction mixture was cooled to 0°C, and the promoter was

added. Reactions run with BF_3•OEt_2 were additionally purged with argon and performed under an argon atmoshpere. The reaction mixture then stirred for 2 h while the temperature was held at 0°C, then any unreacted promoter was quenched by the addition of 4 mL saturated aqueous sodium bicarbonate and the mixture was warmed to 20°C. The resulting mixture was washed with 4 mL brine, then dried over magnesium sulfate and filtered over a bed of glass wool. The solvent was removed under reduced pressure. The α:β ratios of crude products were obtained from ^{1}H NMR spectra. Specific amounts of reagents used for these reactions are summarized in Table 4.

General Procedure for Reactions Including Collidine or DTBMP. Using selected trichloroacetimidates, the procedure for preparation of mannoside and galactosides derivatives was modified such that a slight excess of collidine or DTBMP was added prior to addition of the promoter. Reactions were performed for 2 h and were worked up in the same manner as other glycosylation products described above. Exact reagent amounts and reaction details are summarized in Table 7.

General Procedure for Preparation of Disaccharides. A dry 4 mL scintillation vial was charged with the trichloroacetimidate starting material **16** or **17** with a slight excess of acceptor **28** and a teflon-coated stirbar. Dry dichloromethane was added to obtain a 50 mM solution of the trichloroacetimidate. The mixture was cooled if specified, and the promoter was added. The reaction then stirred for the specified time at the specified temperature, then any unreacted promoter was quenched by the addition of 2 mL of saturated aqueous sodium bicarbonate and was stirred for 20 min. To the resulting

solution, 2 mL dichloromethane was added, then the solution was washed with 4 mL brine, dried over magnesium sulfate and filtered over a bed of glass wool. The solvent was removed under reduced pressure. Yields of crude products were obtained from ^{1}H NMR spectra using an internal mesitylene standard. Chromatographic purification was performed (galactopyranoside product 6:4 hexane : ethyl acetate; acetyl protected mannopyranoside product 4:6 hexane : ethyl acetate) to obtain pure samples for characterization purposes. Exact reaction conditions and amounts of reagents used are provided in Table 9.

*Table 9. Conditions for formation of disaccharides **29** and **30**.*

Product	**Trichloro-acetimidate mg (#[a])**	**Acceptor Sugar (28) mg (equiv)**	**In(Otf)$_3$ mg (equiv)**	**Time[b] (min)**	**Yield[c] (%)**	**α:β Ratio[d]**
29	30.7 (**16**)	17.4 (1.1)	1.1 (0.04)	30	36	--
30	22.5 (**17**)	17.8 (1.1)	1.3 (0.05)	20	53	1:0

[a]# means the compound number, shown in Scheme 5.
[b]All reactions run at 0 °C
[c]Yields determined by ^{1}H NMR spiked with a mesitylene standard, and are for the α-linked product.
[d]Ratios determined by ^{1}H NMR.

2,3,4,6-tetra-*O*-benzyl-α-D-galactopyranosyl Trichloroacetimidate (**16**). Confirmed via ^{1}H NMR.[130]

2,3,4,6-tetra-*O*-acetyl-α-D-mannopyranosyl Trichloroacetimidate (**17**). Confirmed via ^{1}H NMR.[131]

5-Azido-3-oxapentyl 2,3,4,6-tetra-*O*-benzyl-D-galactopyranoside (**22**). The values listed are for the β-product. ^{1}H NMR (500 MHz, $CDCl_3$) δ 7.39-7.22 (m, 20H, $CH_2Ph\mathbf{H}$), 4.95-4.91 (m, 2H, $C\mathbf{H_2}Ph$), 4.76 (d, 1H, *J* = 11.3 Hz, $C\mathbf{H_2}Ph$), 4.72 (q, 2H, *J* = 11.8 Hz, $C\mathbf{H_2}Ph$), 4.61 (d, 1H, *J* = 11.3 Hz, $C\mathbf{H_2}Ph$), 4.41-4.37 (m, 3H, $C\mathbf{H_2}Ph$ and H-1), 4.02 (dt, *J* = 10.3, 4.1 Hz, 1H, H-5), 3.88 (d, 1H, *J* = 2.7 Hz, H-4), 3.81 (dd, 1H, *J* = 7.7, 9.7 Hz, H-2), 3.77-3.71 (m, 1H, H-6a), 3.71-3.66 (m, 1H, H-6b), 3.61 (ddd, 2H, *J* = 2.8, 4.4, 6.0 Hz, $OC\mathbf{H_2}CH_2OCH_2$), 3.58-3.50 (m, 5H, H-3 and $CH_2C\mathbf{H_2}OC\mathbf{H_2}CH_2$) 3.27 (dd, 2H, *J* = 4.4, 9.2 Hz, $CH_2C\mathbf{H_2}N_3$); ^{13}C NMR (125 MHz, $CDCl_3$) 138.9, 138.6, 138.5, 137.9, 127.5-128.4 (20C), 104.1, 82.1, 79.4, 75.0, 74.5, 73.5, 73.5, 73.4, 73.0, 70.4, 69.9, 69.0, 68.8, 50.7 ppm; HRMS (micro-TOF) *m/z* 676.2964 (calculated *m/z* M+Na = 676.2999 g/mol for $C_{38}H_{43}N_3O_7Na$).

Phenyl 2,3,4,6-tetra-*O*-benzyl-D-galactopyranoside (**23**). ^{1}H NMR (500 MHz, $CDCl_3$) Spectrum is not readily assignable due an unresolvable mixture of α:β products. ^{13}C NMR (125 MHz, $CDCl_3$) 102.88 (C1- β), 96.06 (C1-α); ^{13}C peaks used to assign α:β ratios, and are consistent with literature.[132] HRMS (micro-TOF) *m/z* 653.2840 (calculated *m/z* M+Na = 653.2879 for $C_{41}H_{42}O_6Na$).

Butyl 2,3,4,6-tetra-*O*-benzyl-D-galactopyranoside (**24**). The values listed are for the β-product. ^{1}H NMR (500 MHz, $CDCl_3$) δ 7.43-7.24 (m, 20H, $CH_2Ph\mathbf{H}$), 4.95 (m, 2H, $C\mathbf{H_2}Ph$), 4.79-4.73 (m, 2H, $C\mathbf{H_2}Ph$), 4.73 (d, 1H, *J* = 11.8 Hz, $C\mathbf{H_2}Ph$), 4.64 (d, 1H, *J* = 11.8 Hz, $C\mathbf{H_2}Ph$), 4.49-4.41 (m, 2H, $C\mathbf{H_2}Ph$), 4.37 (d, 1H, *J* = 7.7, H-1), 4.01-3.93 (m, 1H, H-5), 3.90 (d, 1H, *J* = 2.7 Hz, H-4), 3.83 (dd, 1H, J *J* = 7.7, 9.7 Hz, H-2), 3.60 (dd,

2H, *J* = 1.6, 6.3 Hz, H-6a and H-6b), 3.55-3.50 (m, 3H, H-3 and OC**H$_2$**CH$_2$), 1.71-1.57 (m, 2H, CH$_2$C**H$_2$**CH$_2$), 1.50-1.35 (m, 2H CH$_2$C**H$_2$**CH$_3$), 0.93 (t, 3H, *J* = 7.4 Hz, CH$_2$C**H$_3$**); ^{13}C NMR (125 MHz, CDCl$_3$) 138.8, 138.7, 138.6, 138.0, (4C, quat. Cs) 127.6-128.4 (20C, aromatic Cs), 104.0 (C$_1$), 82.3, 79.6, 75.2, 74.5, 73.6 (2C), 73.4, 73.1, 69.6, 68.9, 31.8, 19.4, 13.9 ppm; HRMS (micro-TOF) *m/z* 619.2865 (calculated *m/z* M+Na = 619.3036 for C$_{38}$H$_{44}$O$_6$Na).

1,1-Dimethylpropyl 2,3,4,6-tetra-*O*-benzyl-D-galactopyranoside (**25**). The values listed are for the α-product. ^{1}H NMR (500 MHz, CDCl$_3$) δ 7.38-7.20 (m, 20H, CH$_2$Ph**H**), 5.15 (d, 1H, *J* = 3.6 Hz, H-1), 4.94 (d, 1H, *J* = 11.4 Hz, C**H$_2$**Ph), 4.79 (d, 1H, *J* = 11.7 Hz, C**H$_2$**Ph), 4.73 (t, 2H, *J* = 12.0 Hz, C**H$_2$**Ph), 4.67 (d, 1H, *J* = 11.7 Hz, C**H$_2$**Ph), 4.54 (d, 1H, *J* = 11.4 Hz, C**H$_2$**Ph), 4.46-4.37 (m, 2H, C**H$_2$**Ph), 4.15-4.09 (m, 1H, H-5), 4.01-3.97 (m, 2H, H-4 and H-2), 3.94 (dd, 1H, *J* = 2.6, 10.2 Hz, H-3), 3.58-3.52 (m, 1H, H-6a) 3.46 (dd, 1H, *J* = 5.7, 9.1 Hz, H-6b), 1.61-1.45 (m, 2H, CC**H$_2$**CH$_3$), 1.17 (s, 6H, OC(C**H$_3$**)$_2$), 0.88 (t, 3H, *J* = 7.5 Hz, CH$_2$C**H$_3$**); ^{13}C NMR (125 MHz, CDCl$_3$) 140.0, 138.9, 138.8, 138.1, 127.3-128.3 (20C), 91.9, 79.2, 77.2, 76.7, 75.2, 74.7, 73.4, 73.2, 72.8, 69.0, 68.8, 34.6, 25.8, 25.5, 8.6 ppm; HRMS (micro-TOF) *m/z* 633.3163 (calculated *m/z* M+Na = 633.3192 for C$_{39}$H$_{46}$O$_6$Na).

Butyl 2,3,4,6-tetra-*O*-acetyl-α-D-mannopyranoside (**26**). ^{1}H NMR (500 MHz, CDCl$_3$) δ 5.32 (dd, 1H, *J* = 3.1, 10.0 Hz, H-3), 5.25 (t, 1H, *J* = 10.0 Hz, H-4), 5.21 (ap. s, 1H, H-2), 4.78 (s, 1H, H-1), 4.25 (dd, 1H, *J* = 5.3, 12.2 Hz, H-6a), 4.08 (appt. d, 1H, *J* = 12.2, H-6b), 3.99-3.92 (m, 1H, H-5), 3.70-3.61 (m, 1H OC**H$_2$**CH$_2$), 3.47-3.39 (m, 1H,

OC**H₂**CH_2), 2.13 (s, 3H, COC**H₃**), 2.08 (s, 3H, COC**H₃**), 2.02 (s, 3H, COC**H₃**), 1.97 (s, 3H, COC**H₃**), 1.59-1.50 (m, 2H, OCH_2C**H₂**CH_2), 1.42-1.31 (m, 2H, CH_2C**H₂**CH_3), 0.91 (t, 3H, J = 7.4 Hz, CH_2C**H₃**); ^{13}C NMR (125 MHz, $CDCl_3$) 170.7, 170.1, 169.9, 169.8, 97.6, 69.7, 69.1, 68.4, 68.2, 66.3, 62.5, 31.3, 20.9, 20.7, 19.3, 13.8 ppm; HRMS (micro-TOF) *m/z* 427.1565 (calculated *m/z* M+Na = 427.1580 for $C_{18}H_{28}O_{10}Na$).

1,1-Dimethylpropyl 2,3,4,6-tetra-*O*-acetyl-α-D-mannopyranoside (**27**). ^{1}H NMR (500 MHz, $CDCl_3$) δ 5.37 (dd, 1H, *J* = 3.0, 10.0 Hz, H-3), 5.23 (t, 1H, *J* = 10.0 Hz, H-4), 5.07 (s, 1H, H-1), 5.02 (ap. s, 1H, H-2), 4.24 (dd, 1H, *J* = 5.4, 12.0 Hz, H-6a), 4.17-4.11 (m, 1H, H-5), 4.03 (d, 1H, *J* = 12.0 Hz, H-6b), 2.13 (s, 3H, COC**H₃**), 2.06 (s, 3H, COC**H₃**), 2.02 (s, 3H, COC**H₃**), 1.97 (s, 3H, COC**H₃**), 1.61-1.44 (m, 2H, CC**H₂**CH_3), 1.18 (d, 6H, *J* = 3.9 Hz, OC(C**H₃**)**₂**), 0.87 (t, 3H, *J* = 7.4 Hz, CH_2C**H₃**); ^{13}C NMR (125 MHz, $CDCl_3$) 170.7, 170.3, 170.0, 169.8, 92.0, 78.9, 71.3, 69.1, 68.1, 66.5, 62.7, 34.0, 25.8, 25.3, 21.0, 20.7, 8.4 ppm; HRMS (micro-TOF) *m/z* 441.1719 (calculated *m/z* M+Na = 441.1737 for $C_{19}H_{30}O_{10}Na$).

2,3,4,6-Tetra-*O*-(benzyl)-α-D-galactopyranosyl-(1→2)-1,3,4,6-tetra-*O*-acetyl-α-D-mannopyranose (**29**). ^{1}H NMR (500 MHz, $CDCl_3$) δ 7.42-7.19 (m, Ph**H,** 20H), 5.78 (s, 1H), 5.51 (t, *J* =9.6 Hz, 1H), 5.24 (d, *J* = 2.7 Hz, 1H), 5.13 (d, *J* = 9.6 Hz, 1H), 4.91 (dd, *J* = 11.7, 22.12 Hz, 2H), 4.82 (d, *J* = 11.6 Hz, 1H), 4.74-4.70 (m, 2H), 4.53 (d, *J* = 11.4 Hz, 1H), 4.39-4.35 (m, 3H), 4.28 (dd, *J* = 5.1, 12.2 Hz, 1H), 4.23 (s, 1H), 4.15 (d, *J* = 11.6 Hz, 1H), 4.09-4.06 (m, 2H), 4.01 (s, 1H), 3.80-3.78 (m, 1H), 3.53 (t, *J* = 8.2 Hz, 1H), 3.45-3.42 (m, 1H), 2.09 (s, 3H), 1.99 (s, 3H), 1.98 (s, 3H), 1.93 (s, 3H) ppm;

^{13}C NMR (125 MHz, $CDCl_3$) 170.8, 169.8, 169.3, 168.8, 138.8, 138.8, 138.6, 137.8, 128.4,127.3-128.4 (Ar-C, 20C), 97.5, 91.3, 78.6, 76.2, 73.5, 73.4, 73.3, 73.1, 72.8, 71.4, 69.8, 68.7, 66.1, 62.2, 20.7, 20.6 (3C) ppm; HRMS (micro-TOF) *m/z* 893.3347 (calculated *m/z* M+Na = 893.3360 for $C_{48}H_{54}O_{15}Na$). ^{1}H NMR is consistent with literature values.[133]

2,3,4,6-Tetra-*O*-acetyl-α-D-mannopyranosyl-(1→2)-1,3,4,6-tetra-*O*-acetyl-α-D-mannopyranose (**30**). This reaction was performed by Amanda L. Mattson and the purified product was obtained and characterized by the author. ^{1}H NMR (500 MHz, $CDCl_3$) δ d 5.76 (s, 1H), 5.48-5.45 (m, 1H), 5.36–5.28 (m, 3H), 5.09 (dd, *J* =2.4, 9.7 Hz, 1H), 4.98 (s, 1H), 4.41-4.39 (m, 1H), 4.31 (dd, *J* = 4.1, 12.2 Hz, 1H), 4.23 (dd, *J* = 4.29, 12.5 Hz, 1H), 4.16-4.14 (m, 2H), 4.03-4.01 (m, 1H), 3.78-3.76 (m, 1H), 2.13-1.99 (m, 24H) ppm; ^{13}C NMR (125 MHz, $CDCl_3$) 170.9, 170.6, 170.2, 169.8, 169.7, 169.5, 169.3, 168.3, 98.3, 90.9, 74.7, 73.1, 72.1, 69.9, 68.8, 68.3, 66.1, 65.6, 62.1, 61.7, 20.9, 20.8, 20.6, 20.5 ppm; HRMS (micro-TOF) *m/z* 701.1873 (calculated *m/z* M+Na = 701.1900 for $C_{28}H_{14}O_{11}Na$).

CHAPTER 6

SUMMARY AND CONCLUSIONS

Glycosylation is a ubiquitous reaction in nature, and there is always a need to develop the efficiency of this reaction in a laboratory setting. By using In(III) to promote glycosylation, a more convenient method has been demonstrated because it can be performed under atmospheric conditions (as opposed to many common options available, such BF_3•OEt_2, which must be run under inert conditions), and in many cases the reaction is faster and cleaner, with fewer side products forming. This chemistry can be applied to the synthesis of carbohydrate-decorated molecules designed to probe protein-protein or carbohydrate-protein interactions.

Using previously established methods, four generations of lactose-functionalized PAMAM dendrimers were synthesized with valences ranging from 11 to 100 carbohydrates. The method by which this carbohydrate loading is determined was described. These dendrimers were then used as a tunable multivalent platform through which galectin-3 mediated cancer cell aggregation was studied in three different cell lines (A549, DU-145 and HT-1080). It was shown that small lactose functionalized G2 dendrimer **9** inhibited galectin-3 induced aggregation of the cancer cells. In contrast, dendrimer **12** (a larger, generation 6 dendrimer with 100 carbohydrate endgroups) caused cancer cells to aggregate through a galectin-3 pathway. This study indicates that inhibition of cellular aggregation occurred because dendrimer **9** provided competitive

binding sites for galectin-3 (compared to its putative cancer cell ligand, TF-antigen on MUC1). Dendrimer **12**, on the other hand, provided an excess of ligands for galectin-3 binding which caused crosslinking and aggregation of cells to be increased.

Following the studies demonstrating that glycodendrimers indeed target and repattern galectin-3 on the surface of cancer cells, it was shown that glycodendrimers also have potential as a drug delivery system. Functionalizing dendrimers with a substrate cleavable by a protein upregulated in many cancers (MMP-2 and MMP-9) proved that a payload could be delivered to cancer cell. Further exploration of this topic will show whether this is a directed and selective event, and if an actual drug like doxorubicin can be delivered and enter the cell.

These studies provide a foundation for glycodendrimer-lectin interactions that can be further investigated. Galectin-1 is also implicated in many of the same cancer-related pathways as galectin-3, but its slightly different structure and oligomeric patterning may cause differing results. In the same vein, glycodendrimers functionalized with better and more complex galectin-3 ligands, such as *N*-acetyllactosamine or TF antigen may provide even more pronounced results than those presented here.

Another potential avenue to explore could be to label glycodendrimers with a fluorescent tag, and use confocal microscopy to monitor the behavior of the dendrimers in relation to galectin-3 and the cell surface.

The research described herein lays the groundwork for many future studies involving multivalent effects of carbohydrates binding to galectins.

APPENDICES

APPENDIX A

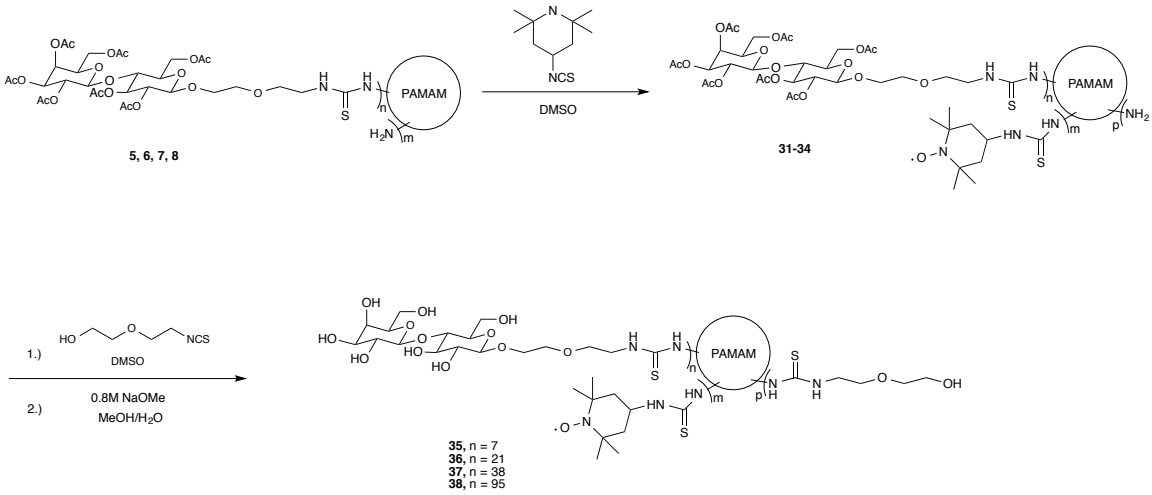
TEMPO-LACTOSE FUNCTIONALIZED DENDRIMERS

Introduction and Synthetic Approach

Monovalent lactose binding to galectin-3 is well characterized.[28] However, because galectin-3 is prone to oligomerization, binding studies using multivalent frameworks often result in precipitate formation, making accurate data collection difficult. An accurate method to measure the binding between proteins and multivalent glycoforms is needed. Previously, attempts to quantify the multivalent binding of lactose functionalized glycodendrimers with galectin-3 using fluorescence lifetime techniques were unsuccessful at determining anything other than the monovalent binding affinity for lactose because of the location of tryptophan in the galectin-3 binding site (unpublished results). Therefore, multivalent binding activities for the different generations of lactose functionalized glycodendrimers cannot be determined and compared using fluorescence lifetime measurements. A new method of studying multivalent binding to lectins that involves affinity chromatography in an EPR spectrometer was proposed, necessitating the synthesis of lactose functionalized dendrimers bearing nitroxide spin labels.

A spin label was incorporated into the lactose-functionalized dendrimer synthesis described in chapter 2, Scheme 1. This label allows the dendrimers to be tracked via EPR spectroscopy. The spin-labeled dendrimers will be monitored by EPR while they are run through a column of galectin-3 tagged beads, and binding constants can be derived. Binding studies will be performed by Dr. Eric Walter, a collaborator at Pacific Northwest National Laboratories. The radical compound 2,2,6,6-tetramethylpiperidine)*N*-oxide (TEMPO) was chosen for its stability and ease of functionalization at the 4-position, allowing for facile incorporation into dendrimer synthesis.

The synthesis of TEMPO-labeled lactose-functionalized dendrimers is very similar to the synthesis described in Scheme 1 in chapter 2 and is summarized in Scheme 8.

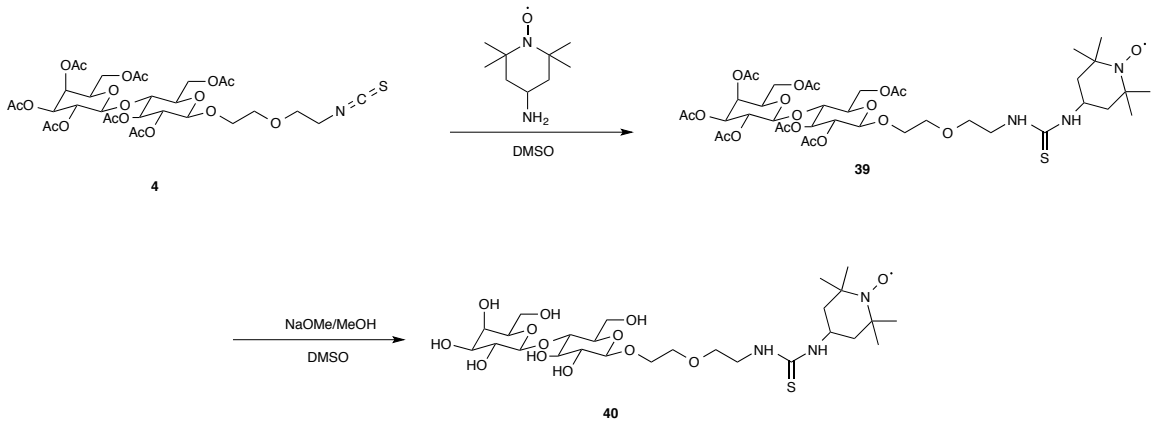


Scheme 8. Synthesis of lactose-functionalized dendrimers labeled with TEMPO and capped with 2-(2-isothiocyanatoethoxy)ethanol. The value of *n* was determined via NMR and MALDI and is summarized in the methods section. The value of *m* was not quantified, but incorporation of the radical was verified using EPR. The value of *p* is defined as (total endgroups)-*m*-*n*.

Results

Acetylated lactose dendrimers **5-8** were synthesized as described in chapter 2. Stable radical compound 4-isothiocyanato-TEMPO was reacted with dendrimers **5-8**, then tested for paramagnetic activity before capping any accessible and unfunctionalized amino endgroups with 2-(2-isothiocyanatoethoxy)ethanol and removing the acetyl protecting groups. The products **31-34** were then purified and once again confirmed to have unpaired electrons by EPR. Since TEMPO-functionalized dendrimers **35-38** have

radicals, they were not characterized by NMR and instead were confirmed using EPR signal and MALDI.



Scheme 9. Synthesis for the TEMPO-labeled lactose monomer.

To assess the differences in binding between multivalent glycoforms and monovalent lactose, it was necessary to label lactose with TEMPO (Scheme 9). In this case, the peracetylated lactose isothiocyanate **4** was reacted with 4-amino TEMPO. Flash chromatography could not be performed because quenching of the radical could occur on silica, so care was taken to use a very slight excess of **4** in the preparation of **39**. Deacetylation of **39** to afford TEMPO functionalized lactose **40** was achieved using NaOMe.

Conclusion

Molecules with unpaired electrons give a reliable and predictable signal via EPR. Because of this, radical-labeled molecules can be utilized in carbohydrate-protein binding studies monitored via EPR. In order to determine binding constants for galectin-3 with lactose-functionalized dendrimers as compared to a lactose monomer, four generations of

TEMPO-labeled lactose functionalized dendrimers were produced in addition to TEMPO-functionalized lactose monomer.

Experimental Procedures

General Methods

General reagents were purchased from Acros and Aldrich Chemical Companies. PAMAM dendrimers were purchased from Dendritech. Purified compounds were analyzed by ^{13}C and ^{1}H NMR with a Bruker DRX 500 MHz Spectrometer using trimethyl silane as an internal standard. For peak assignments, the following nomenclature was employed: s = singlet, d = doublet, t = triplet, dd = doublet of doublets, m = multiplet, bs = broad singlet. Small molecule mass spectra were obtained using a high-resolution Bruker micro-TOF system. Dendrimer M_W were determined using MALDI mass spectra, which were acquired using a Bruker Autoflex III time-of-flight mass spectrometer in positive linear mode with an acceleration voltage of 19 kV. Spectra of all dendrimers and dendrimer intermediates were obtained with a matrix: analyte ratio of 10,000:1 to 500:1 using a *trans*-3-indoleacrylic acid matrix and dimethyl formamide as the solvent. Bovine serum albumin (MW 66,431 g/mol), myoglobin (MW 16,952 g/mol), and trypsinogen (MW 23,982 g/mol) were used as external standards. A 1 μL aliquot of matrix : analyte was used. Molecular mass data of the broad peaks were calculated using a peak centroid based on a peak width of approximately 2000 for G2 dendrimers, 5000 for G3 and G4 dendrimers, and 10,000 for G6 dendrimers. EPR spectra were obtained on a Varian E-109

X-band spectrometer with a lab-built interface. Relevant spectra are presented in Appendix B of this thesis.

Preparation of TEMPO-Labeled Acetylated Lactose Functionalized Dendrimers **31-34**. The products **31-34** were prepared using a procedure adapted from that used to prepare dendrimer **5.** A one-dram glass scintillation vial was charged with dendrimer and a teflon-coated stirbar, then DMSO was added to yield a 50 mM solution with respect to the number of endgroups. To this, 4-isothiocyanato-TEMPO (TCI America) was added and reactions were stirred at 20°C shielded from light for 48 h. The reaction mixture was then dialyzed shielded from light in 3500 Da MWCO dialysis tubing in 250 mL DMSO for 8 h, replacing the DMSO with fresh every 2 h. The contents of the dialysis tubing were then frozen and lyophilized to yield a fluffy orange solid. Exact amounts of reactants used are summarized in Table 10.

Table 10. Experimental reactant amounts used toward the synthesis of TEMPO-labeled lactose functionalized dendrimers.

Compound Number	PAMAM Generation	Ac-lactose dendrimer (μmol)	TEMPO-NCS (μmol)	TEMPO-NCS (equiv.)
31	2	4.5	57	12
32	3	1.1	18	16
33	4	0.8	16	20
34	6	0.2	6.3	30

TEMPO-Labeled Acetylated Lactose Functionalized G2 (**31**). EPR spectrum confirms radical is unquenched. MALDI-TOF (pos) m/z 8536.

TEMPO-Labeled Acetylated Lactose Functionalized G3 (**32**). EPR spectrum confirms radical is unquenched. MALDI-TOF (pos) m/z 22834.

TEMPO-Labeled Acetylated Lactose Functionalized G4 (**33**). EPR spectrum confirms radical is unquenched. MALDI-TOF (pos) m/z 42795.

TEMPO-Labeled Acetylated Lactose Functionalized G6 (**34**). EPR spectrum confirms radical is unquenched. MALDI-TOF (pos) m/z 116587.

Deacetylation of TEMPO-Labeled Lactose Functionalized Dendrimers **35-38.** Dendrimers were deacetylated using the same procedure outlined for the preparation of **9** in Chapter 2.

TEMPO-Labeled Lactose Functionalized G2 (**35**). EPR spectrum confirms radical is unquenched (performed at PNNL by Dr. Eric Walter). MALDI-TOF (pos) m/z 6854.

TEMPO-Labeled Lactose Functionalized G3 (**36**). EPR spectrum confirms radical is unquenched (performed at PNNL by Dr. Eric Walter). MALDI-TOF (pos) m/z 16330.

TEMPO-Labeled Lactose Functionalized G4 (**37**). EPR spectrum confirms radical is unquenched (performed at PNNL by Dr. Eric Walter). MALDI-TOF (pos) m/z 30791.

TEMPO-Labeled Lactose Functionalized G6 (**38**). EPR spectrum confirms radical is unquenched (performed at PNNL by Dr. Eric Walter). MALDI-TOF (pos) m/z 91055.

Determination of Carbohydrate Loading on **35-38**. Following the method laid out in the experimental section of Chapter 2, dendrimers were characterized via MALDI and NMR, and loading was determined using equations (a), (b), and (c). Weighted averages are summarized in Table 11, and average loading for those equations is summarized in Table 12, with the average number of carbohydrates incorporated found in the last column of Table 12.

Table 11. M_W determined by MALDI for compounds listed

Compound	Generation	Dendrimer M_W	Acetylated M_W	Deacetylated M_W
35	2	3256	8536	6854
36	3	6909	22834	16330
37	4	13610	42795	30791
38	6	52000	116587	91055

The acetylated weighted averages were obtained for lactose functionalized dendrimers prior to addition of TEMPO. The deacetylated molecular weight refers to the final products, the molecular weight added from TEMPO and 2-(2-isothiocyanatoethoxy)ethanol added to dendrimers **31-34** is negligible in comparison with their large molecular weights and was ignored when determining degree of functionalization for dendrimers **35-38**.

Table 12. Average carbohydrate loading calculated by four methods

Compound	a	b	c	NMR	Average
35	6.9	5.7	7.6	8.0	7
36	20.8	22.1	20.0	22.1	21
37	38.2	40.8	36.5	38.0	38
38	84.4	86.8	82.9	127.0	95

2,3,4,6-Tetra-*O*-acetyl-β-D-galactopyranosyl-(1→4)-,2,3,6-tetra-*O*-acetyl-1-*O*-(5-(4-thiourea-2,2,6,6-tetramethylpiperidine-*N*-oxide)-3-oxopentyl)-β-D-glucopyranose (**39**). A half-dram glass scintillation vial was charged with isothiocyanato-peracetylated lactose **4** (0.27 g, 35 μmol) and a teflon-coated stirbar and 0.5 mL DMSO was added to make a 50 mM solution. To this, 0.005 g 4-NH_2-TEMPO (TCI America, 30 μmol, 0.9 equiv) was added. The reaction stirred at 20°C shielded from light for 48 h. A sample was removed for MS analysis, and the rest of the reaction mixture was taken directly to the next step. EPR spectrum confirms radical is unquenched (performed at PNNL by Dr. Eric Walter). HRMS (micro-TOF) *m/z* 937.3711 (calculated *m/z* M+ = 937.3720 for $C_{40}H_{63}N_3O_{20}S$).

β-D-galactopyranosyl-(1→4)-1-*O*-(5-(4-thiourea-2,2,6,6-tetramethylpiperidine-*N*-oxide)-3-oxopentyl)-β-D-glucopyranose (**40).** A 0.3M solution of sodium methoxide was prepared from sodium and methanol. This was slowly added to the reaction mixture described in the synthesis of **43** in 0.1 mL aliquots, still shielded from light. The pH was monitored after every added aliquot, and the reaction was deemed complete after the pH stabilized at ~9. The solution was then neutralized using 0.1 M aqueous hydrochloric acid solution, and a small aliquot was removed for MS and EPR analysis. The rest of the reaction was frozen and lyophilized (shielded from light) to yield an orange solid with salts present, so no yield could be determined. EPR spectrum confirms radical is unquenched (performed at PNNL by Dr. Eric Walter). HRMS (micro-TOF) *m/z* 644.3018 (calculated *m/z* M+H = 644.3059 for $C_{26}H_{49}O_{13}N_3S$).

APPENDIX B

RELEVANT SPECTRAL DATA

Notes

^{13}C and ^{1}H NMR with a Bruker DRX 500 MHz Spectrometer, except where noted. MALDI mass spectra were acquired using a Bruker Autoflex III time-of-flight mass spectrometer in positive linear mode with an acceleration voltage of 19 kV. MALDI spectra were then smoothed using a Gaussian algorithm with a smoothing width of 1.0-18 Da m/z for 100 cycles. Molecular mass data of the broad peaks were then calculated using a peak centroid based on a peak width of approximately 2000 for G2 dendrimers, 5000 for G3 and G4 dendrimers, and 10,000 for G6 dendrimers. EPR spectra were obtained on a Varian E-109 X-band spectrometer with a lab-built interface.

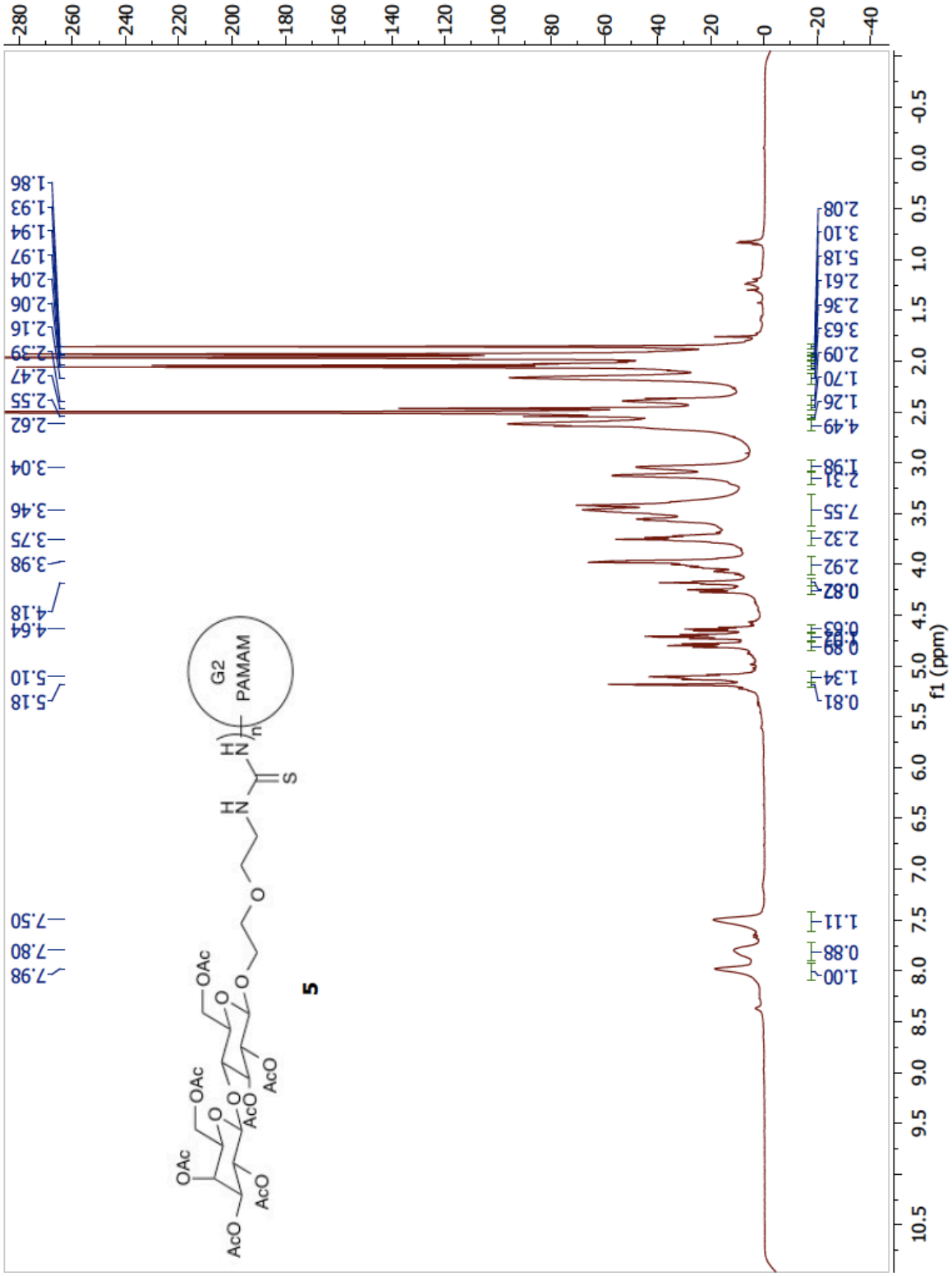


Figure 27. Full ^{1}H NMR spectrum for compound **5**.

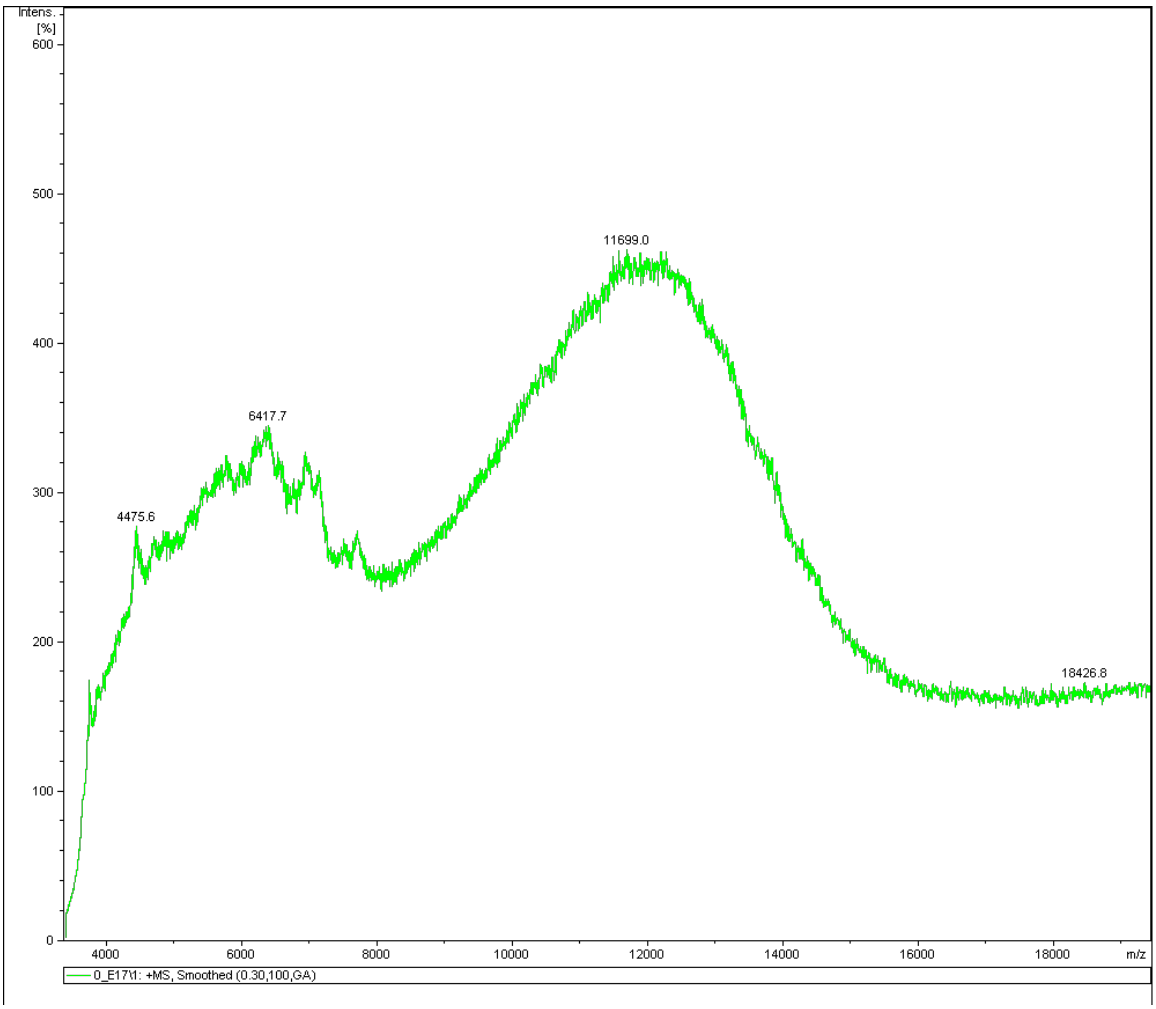


Figure 28. Smoothed MALDI-TOF spectrum for **5**. M_W = 11,290 g/mol.

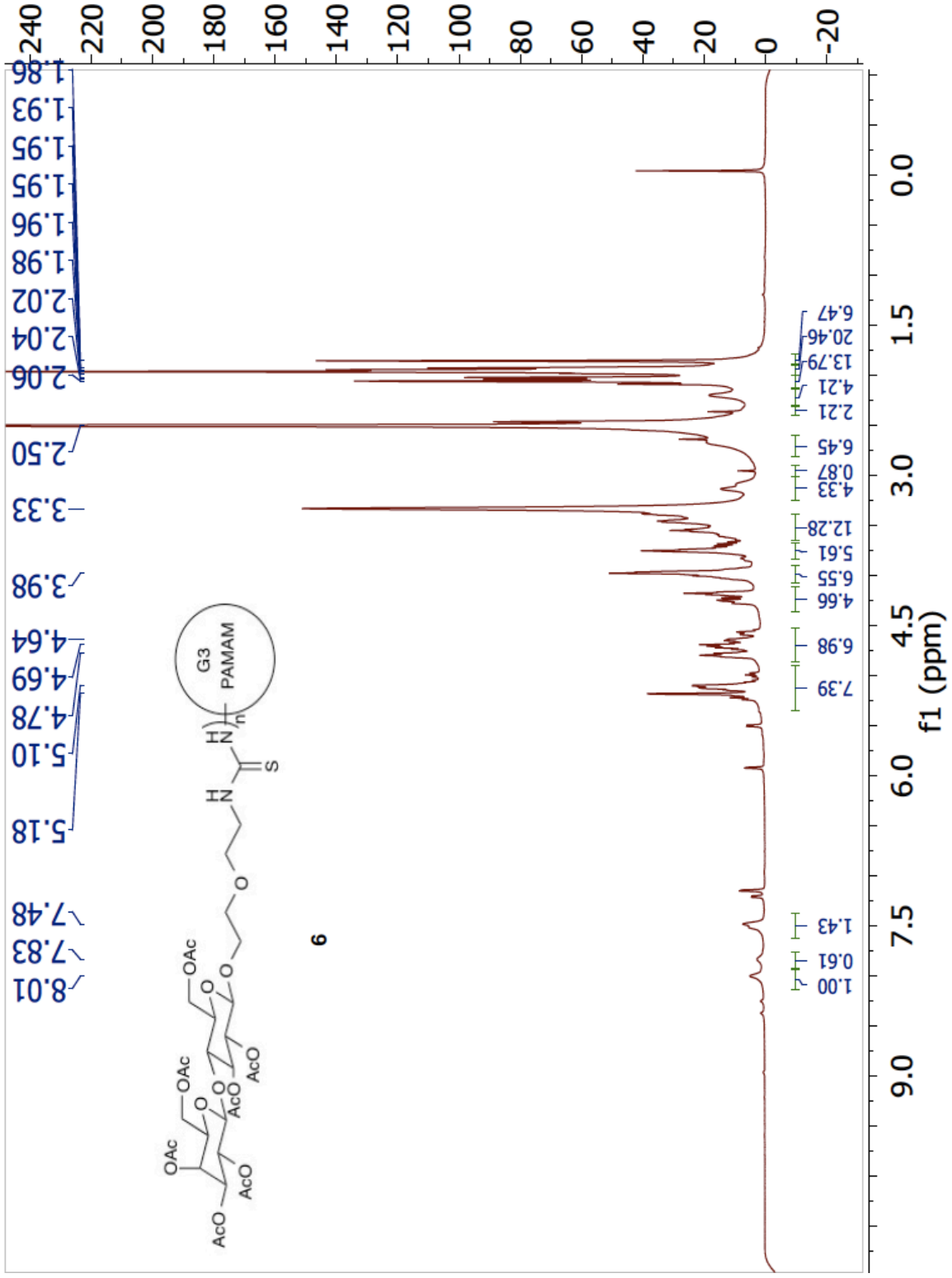


Figure 29. Full ^{1}H NMR spectrum for compound **6**.

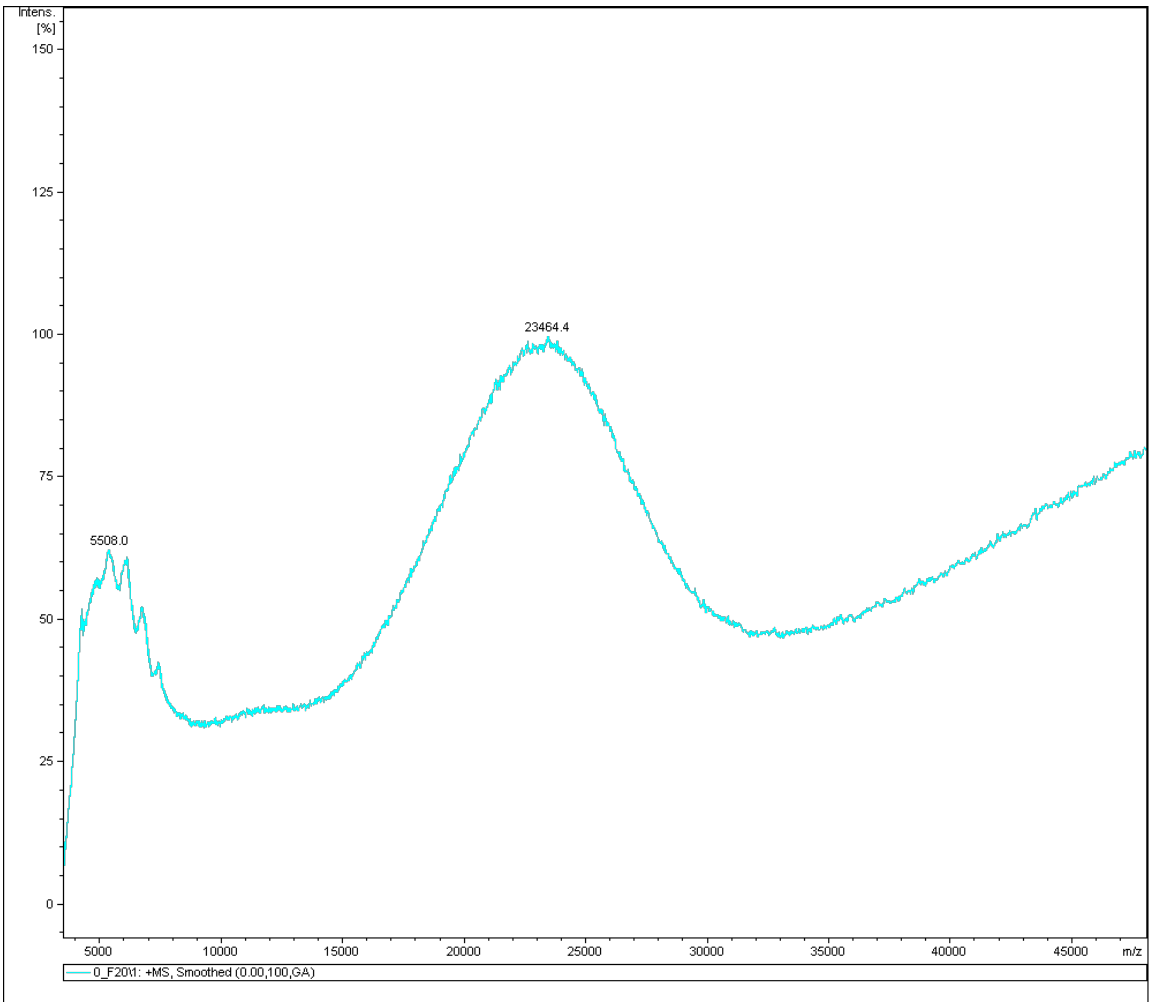


Figure 30. Smoothed MALDI-TOF spectrum for **6**. M_W = 22,682 g/mol.

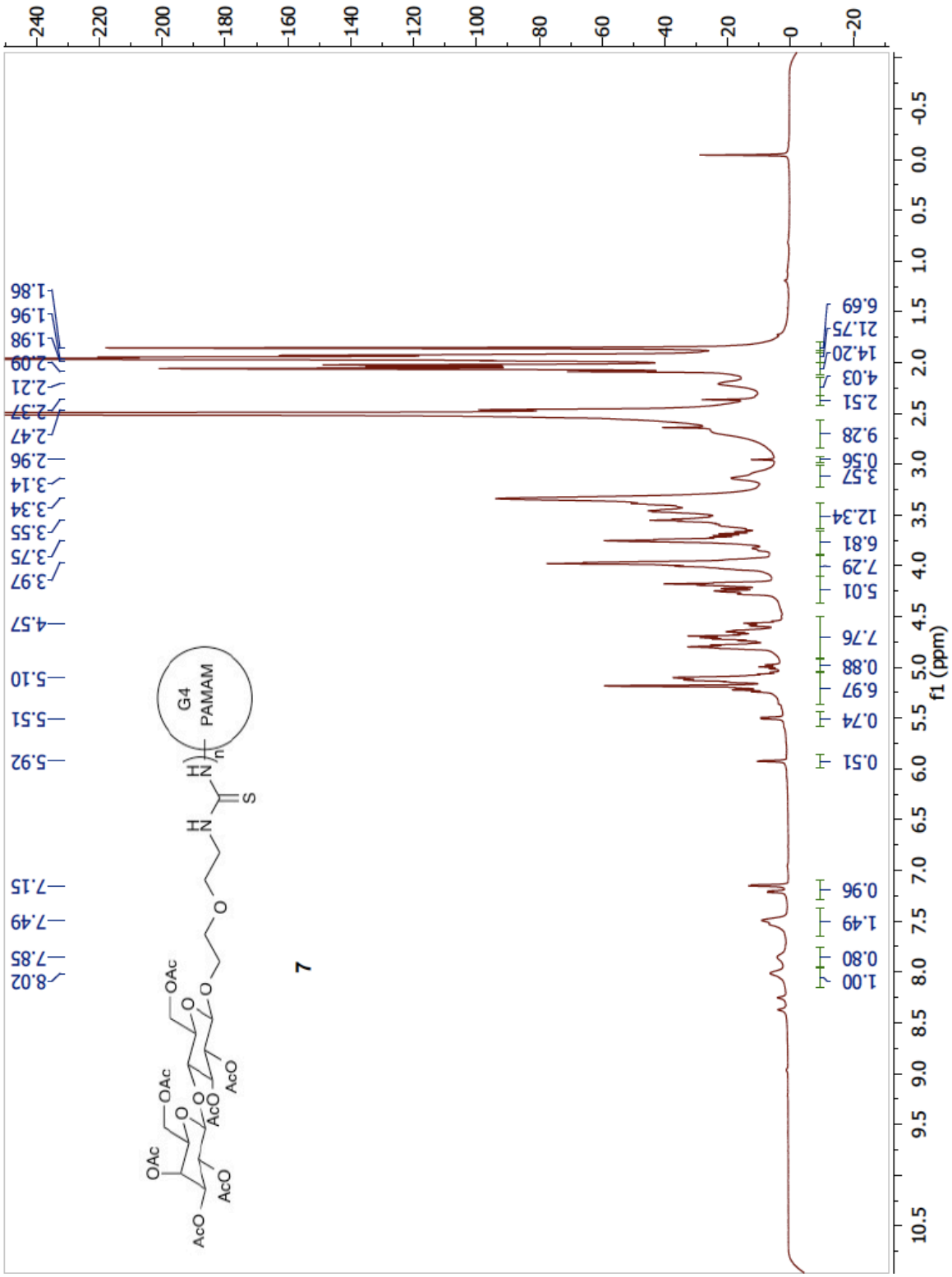


Figure 31. Full ^{1}H NMR spectrum for compound **7**.

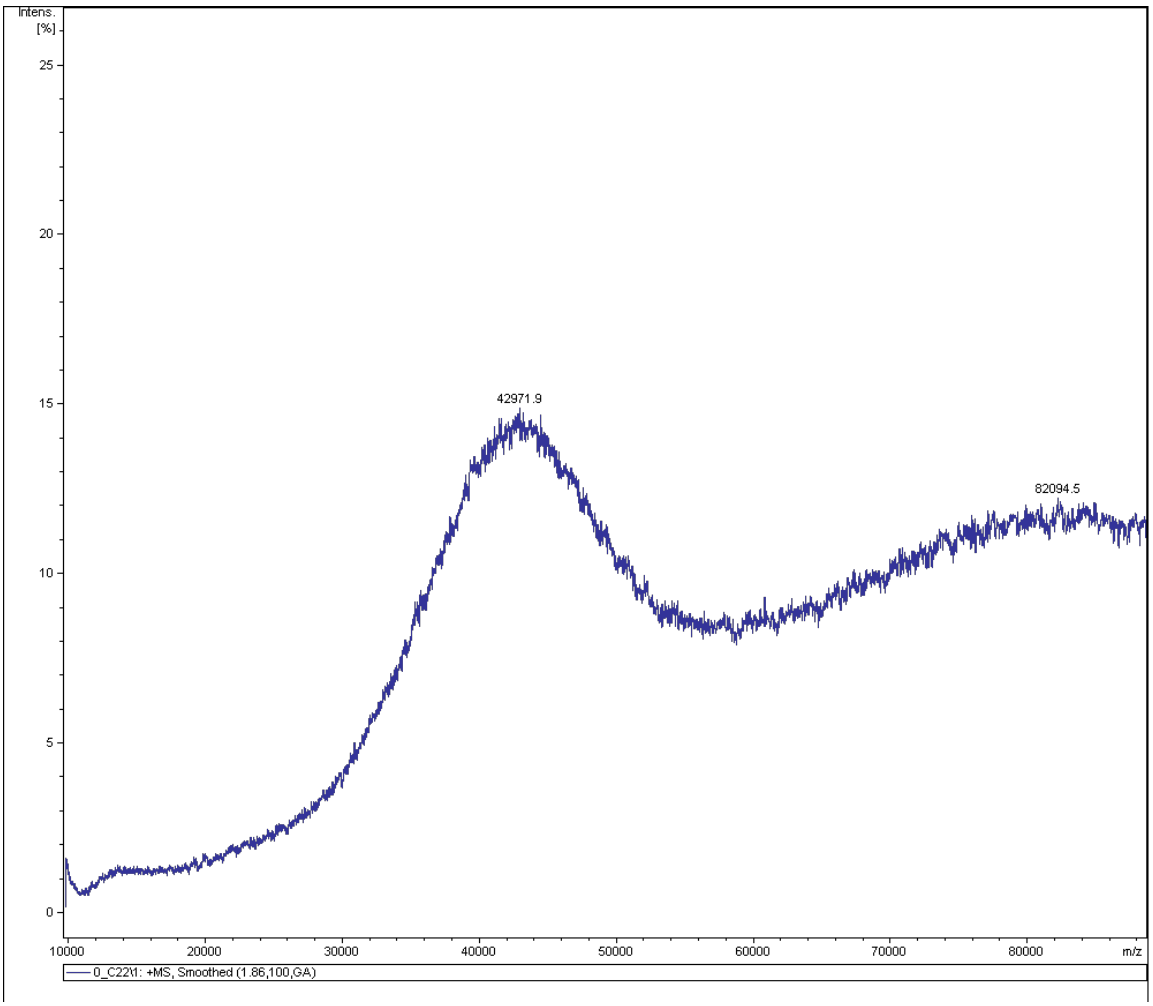


Figure 32. Smoothed MALDI-TOF spectrum for **7**. M_W = 43,465 g/mol.

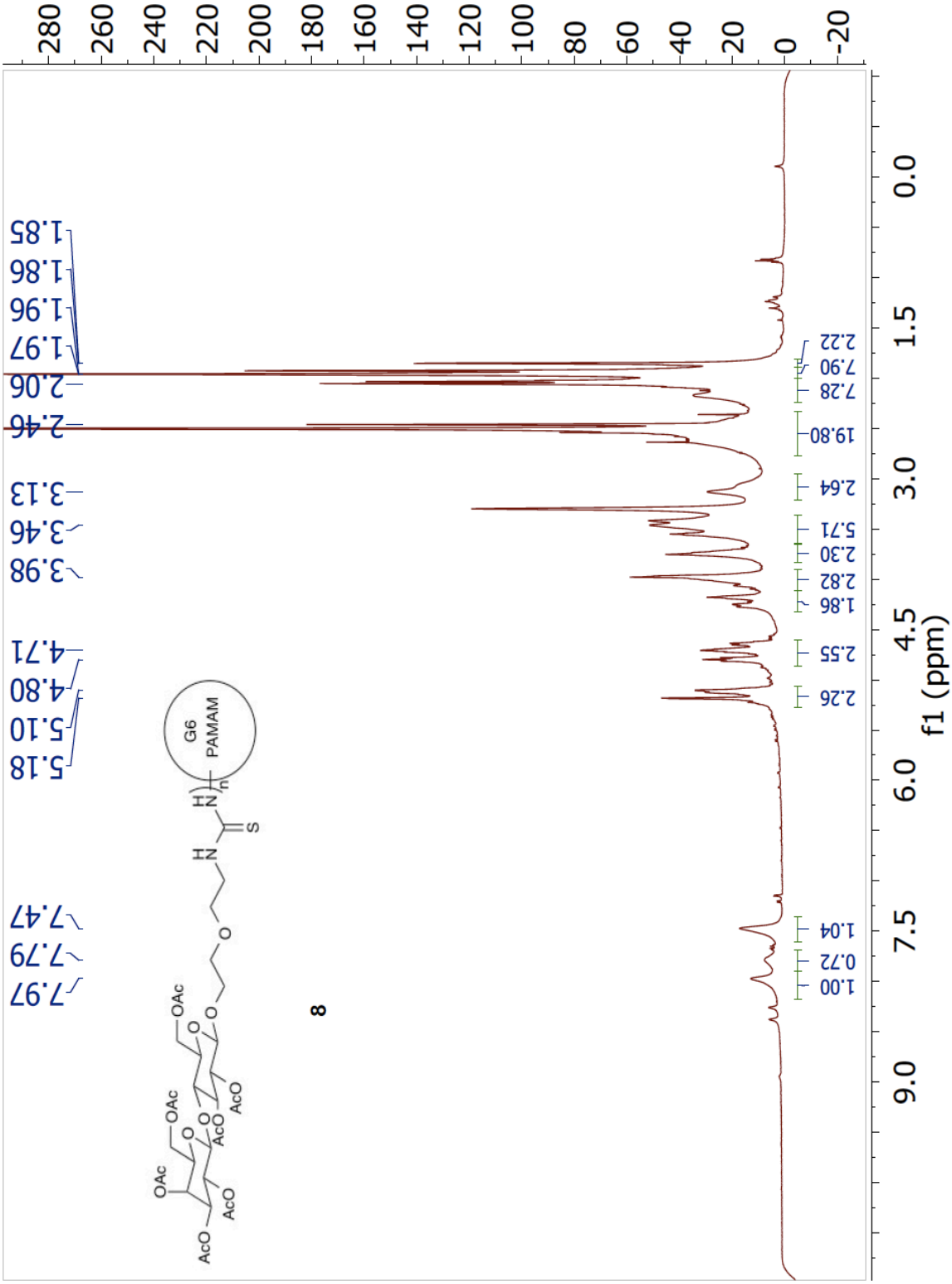


Figure 33. Full ^{1}H NMR spectrum for compound **8**.

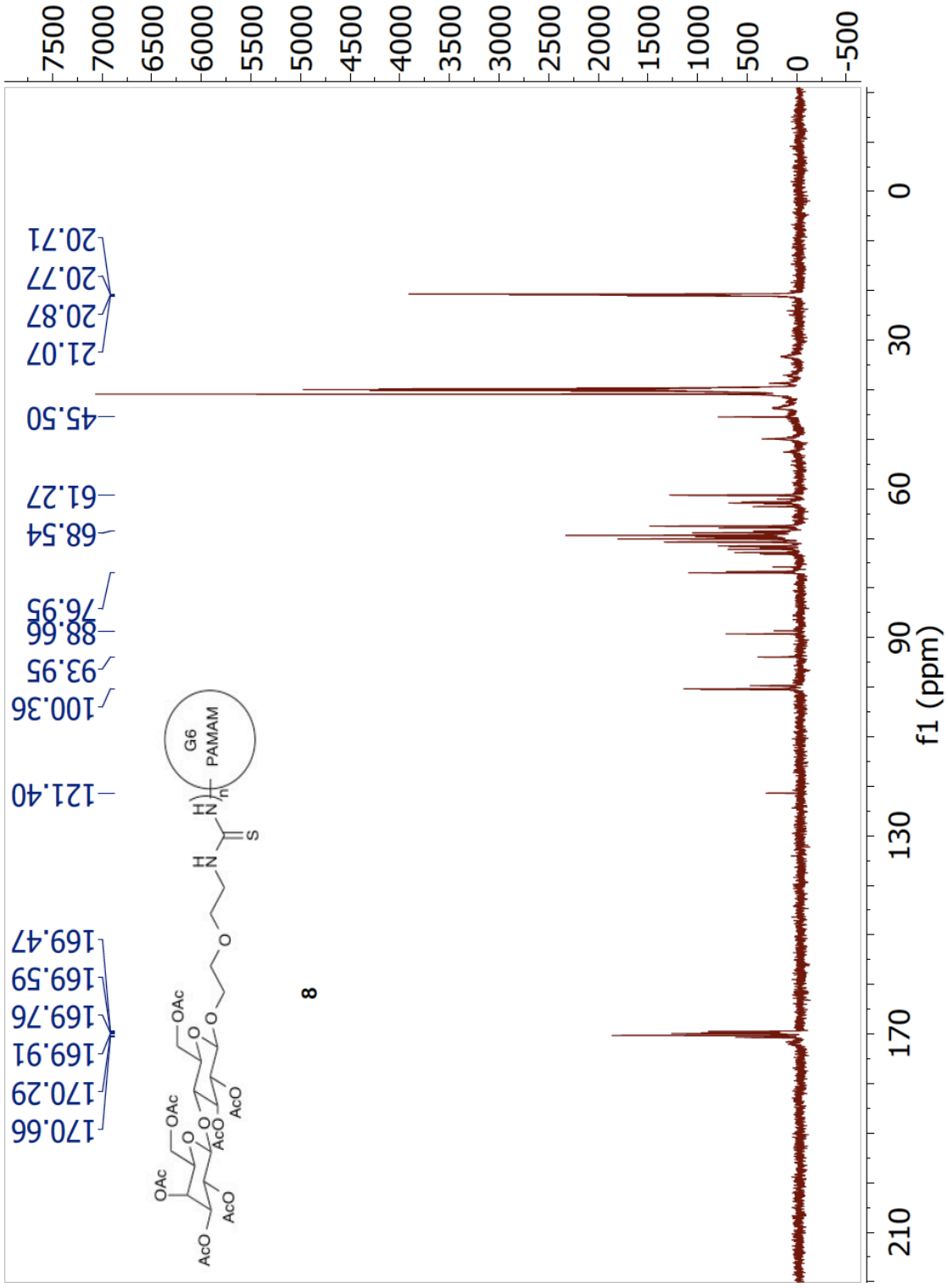


Figure 34. Full ^{13}C NMR spectrum for compound **8**.

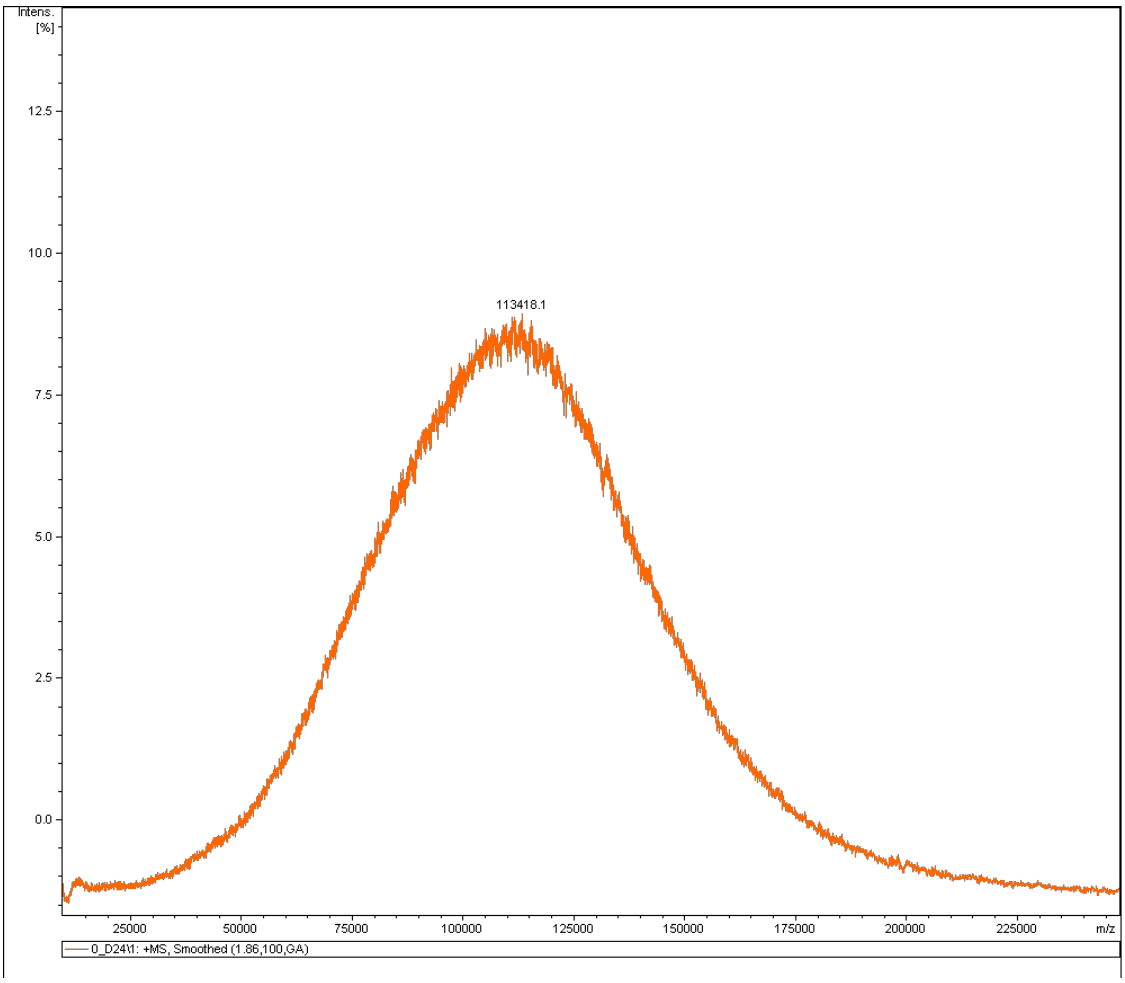


Figure 35. Smoothed MALDI-TOF spectrum for **8**. M_W = 113,904 g/mol.

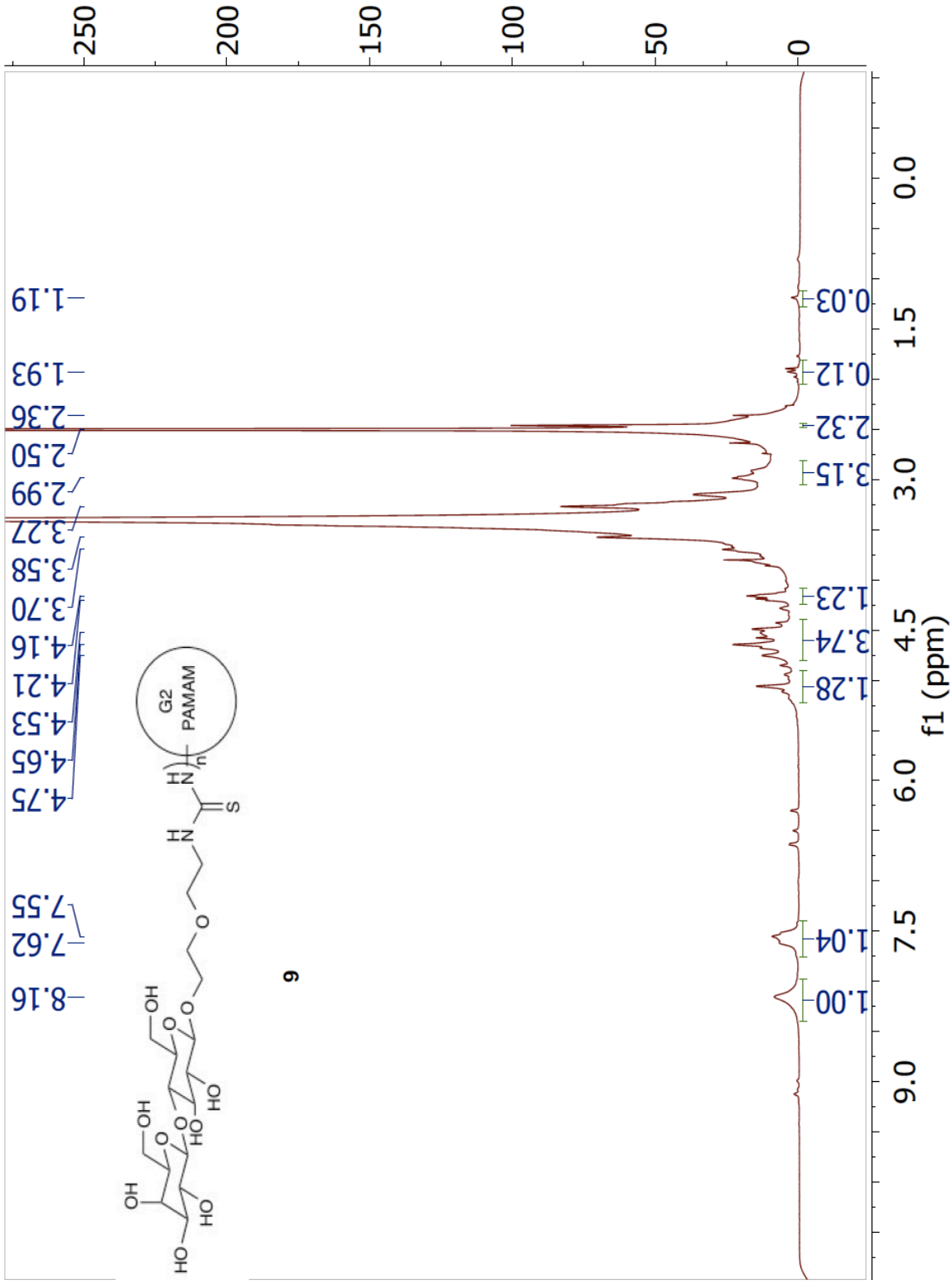


Figure 36. Full ^{1}H NMR spectrum for compound **9**.

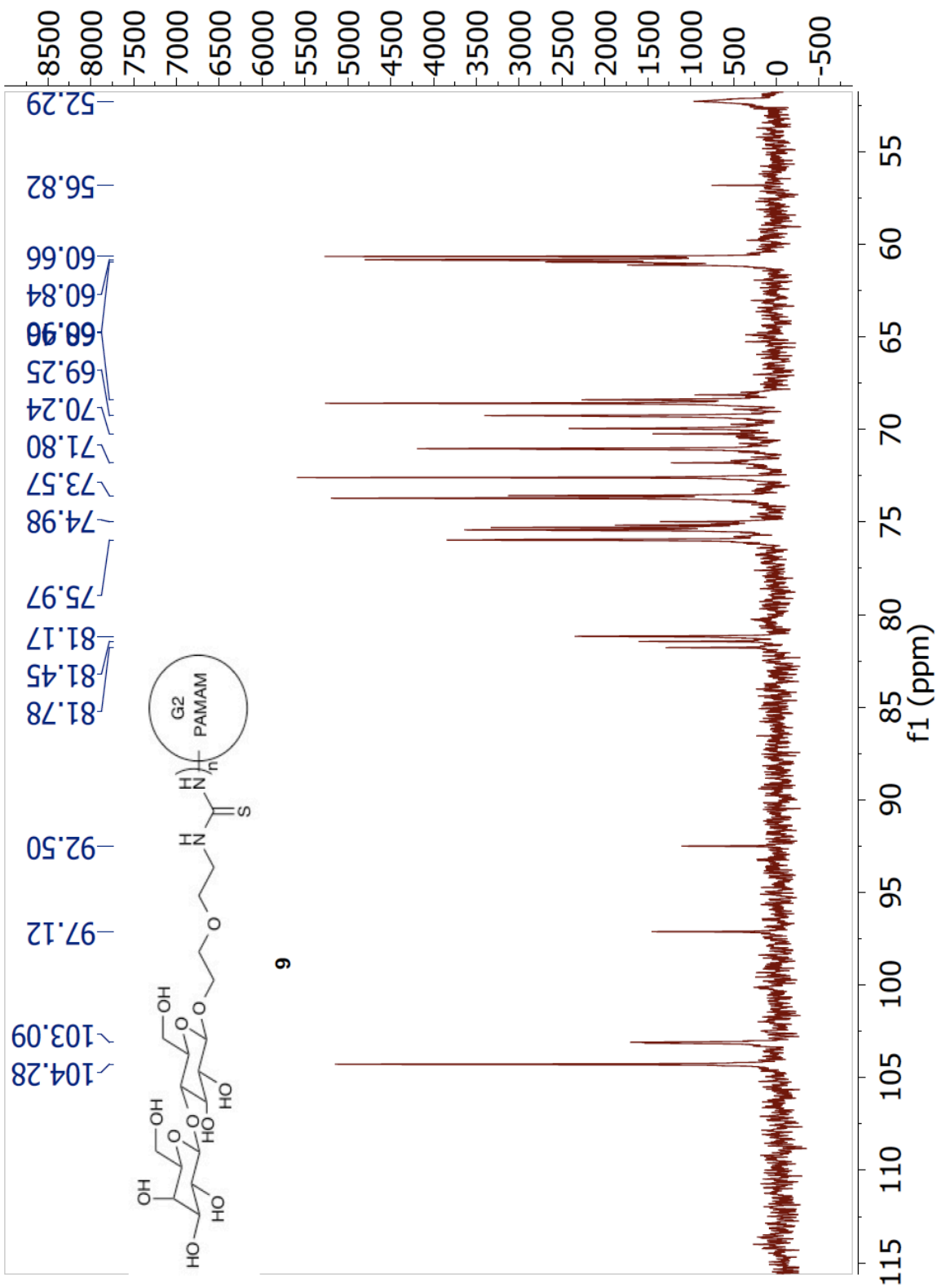


Figure 37. Full ^{13}C NMR spectrum for compound **9**.

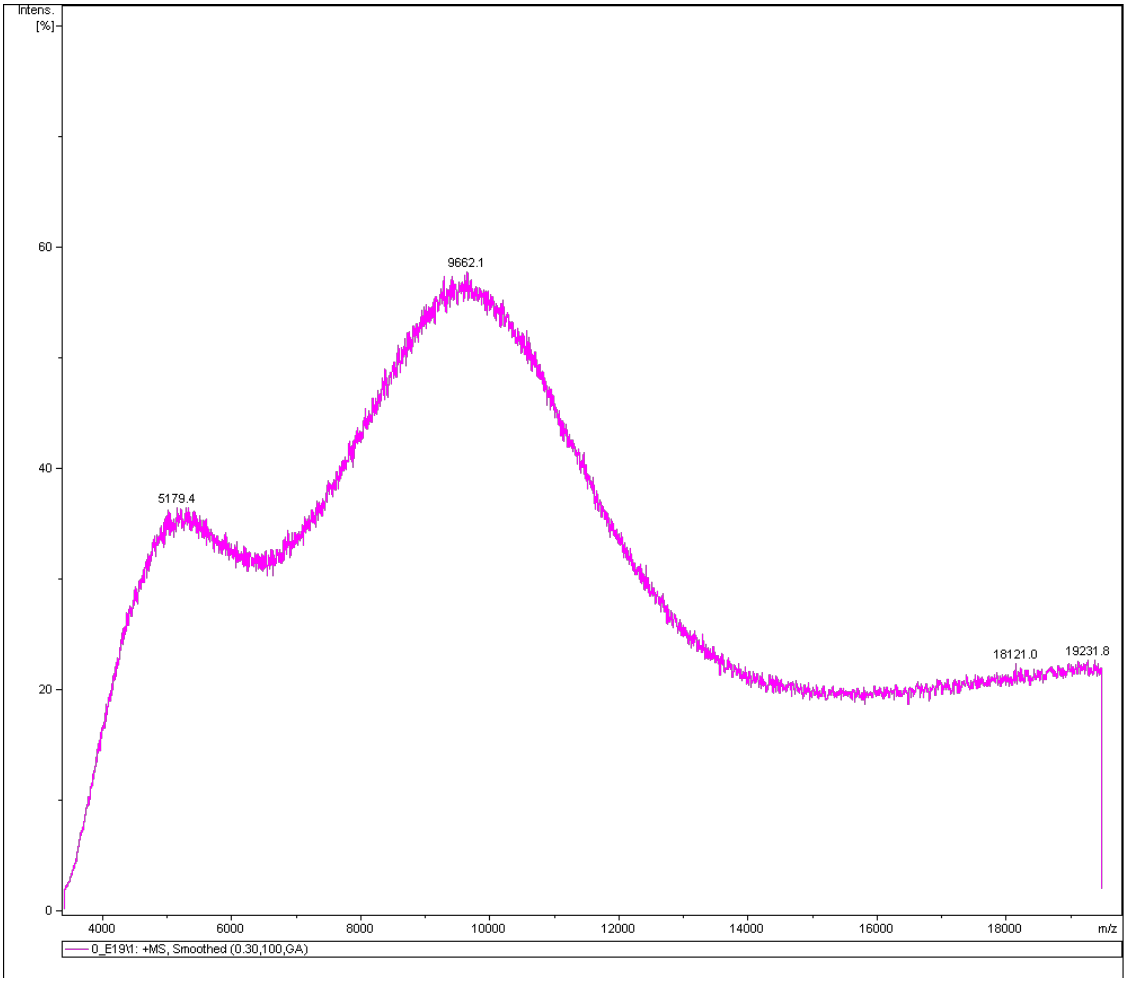


Figure 38. Smoothed MALDI-TOF spectrum for **9**. M_W = 9,383 g/mol.

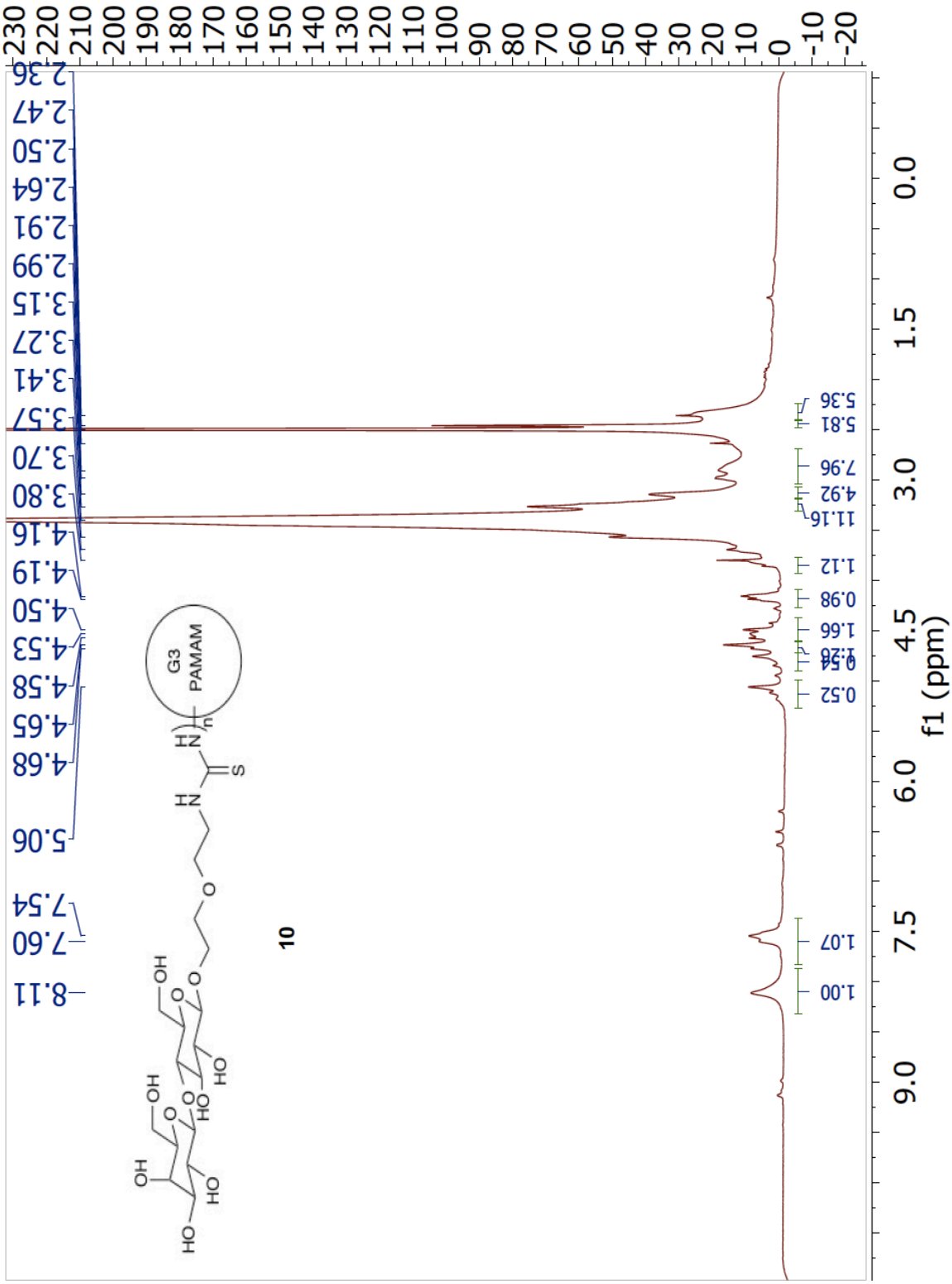


Figure 39. Full ^{1}H NMR spectrum for compound **10**.

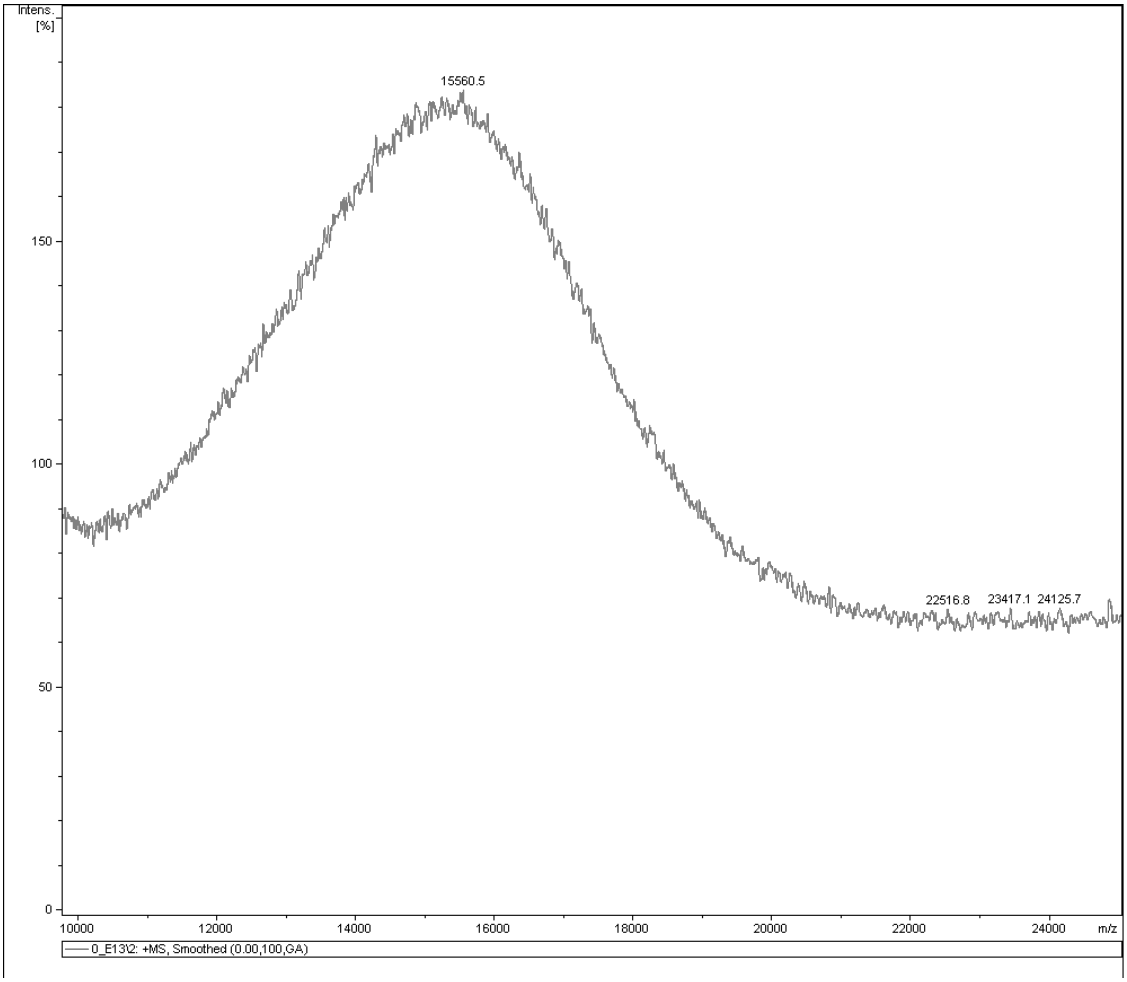


Figure 40. Smoothed MALDI-TOF spectrum for **10**. M_W = 16,206 g/mol.

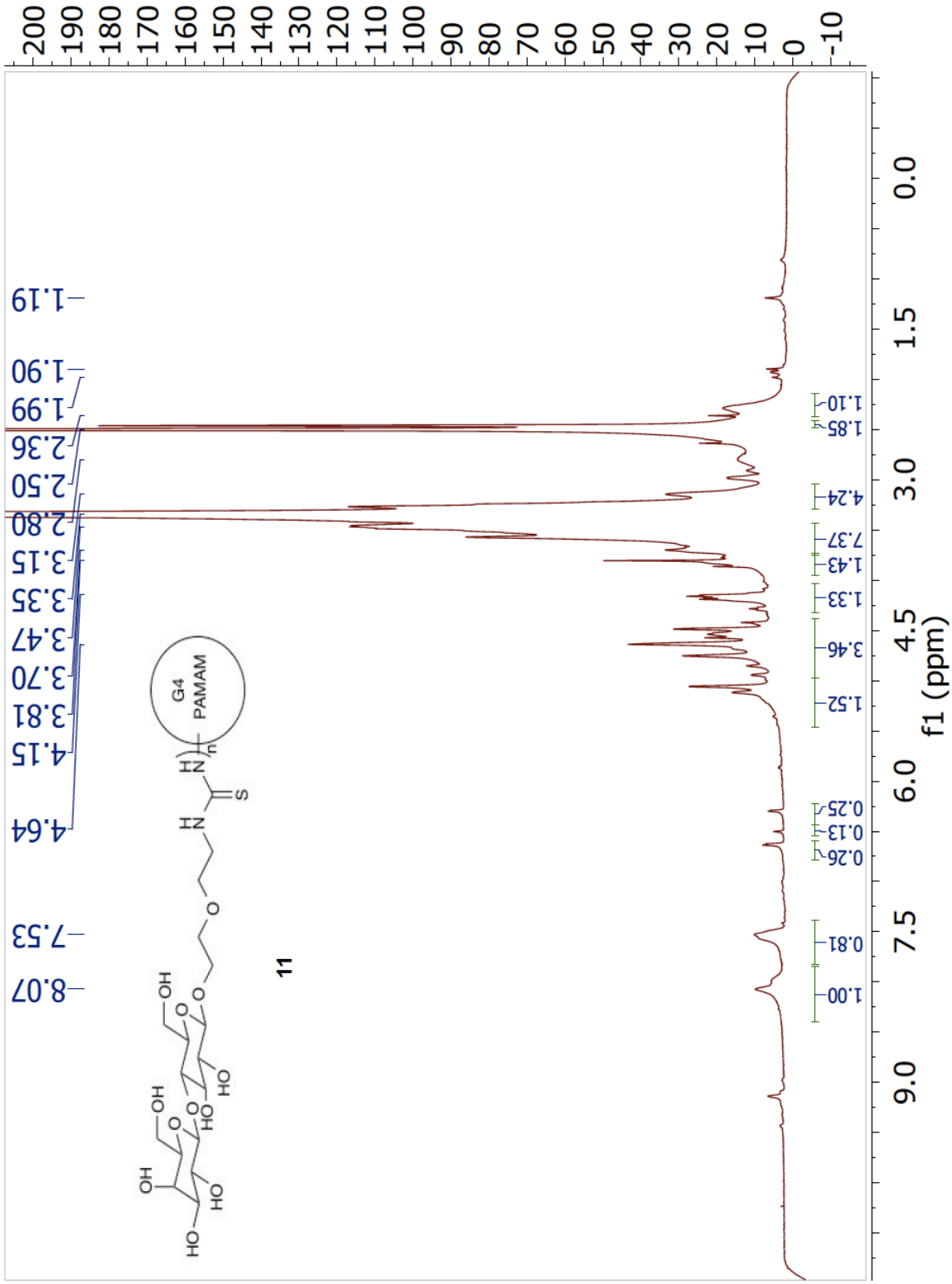


Figure 41. Full ^{1}H NMR spectrum for compound **11**.

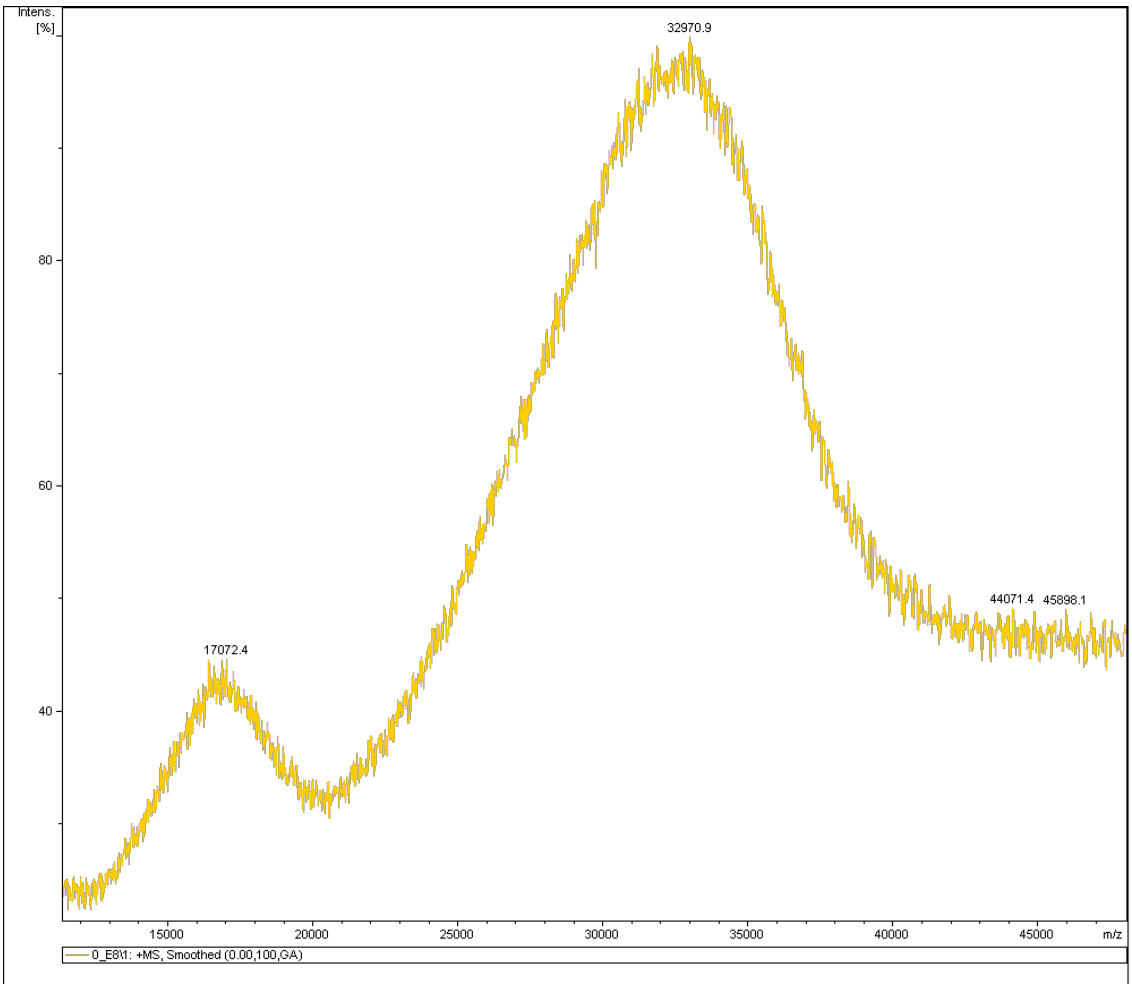


Figure 42. Smoothed MALDI-TOF spectrum for **11**. M_W = 34,453 g/mol.

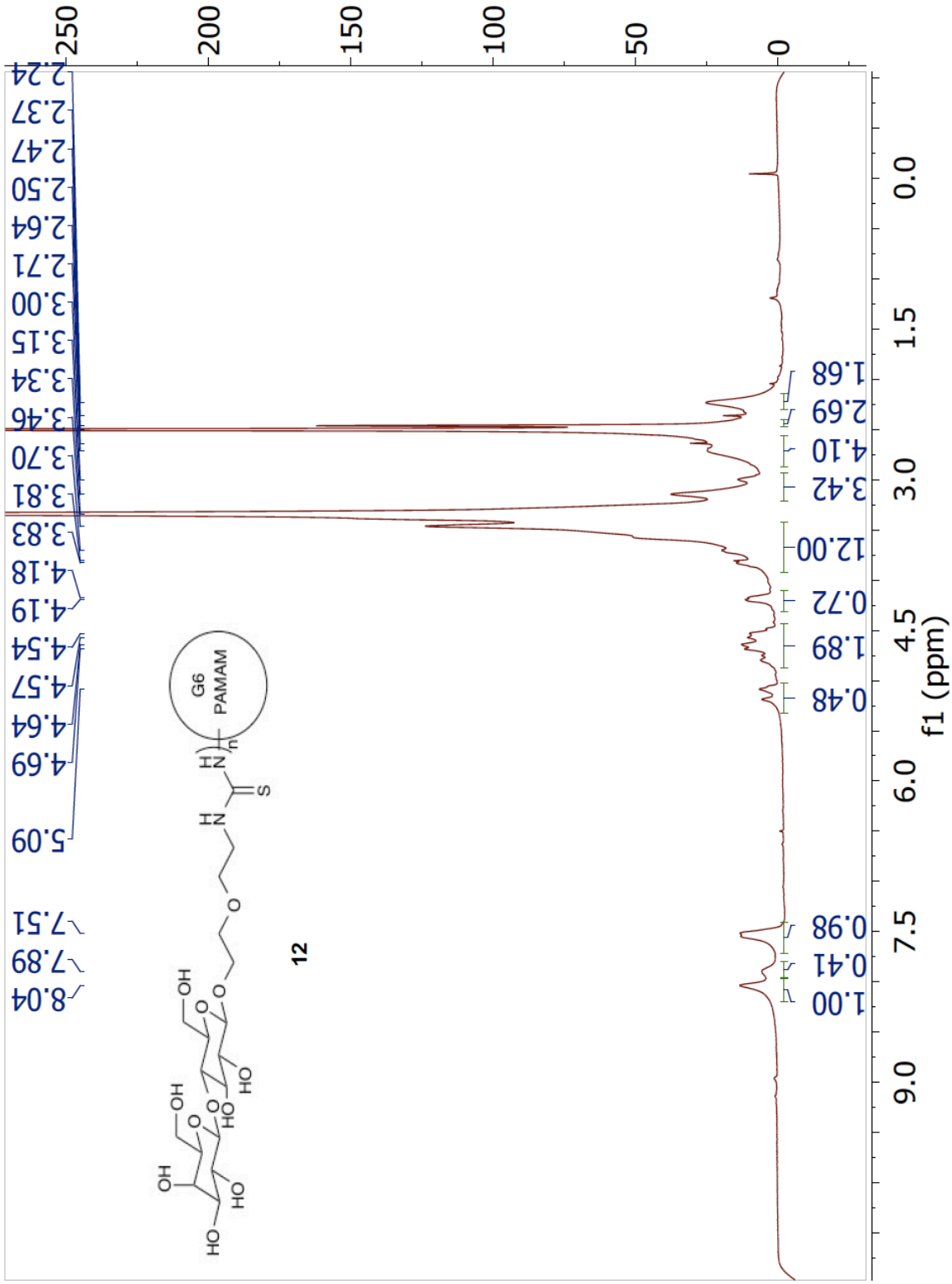


Figure 43. Full ^{1}H NMR spectrum for compound **12**.

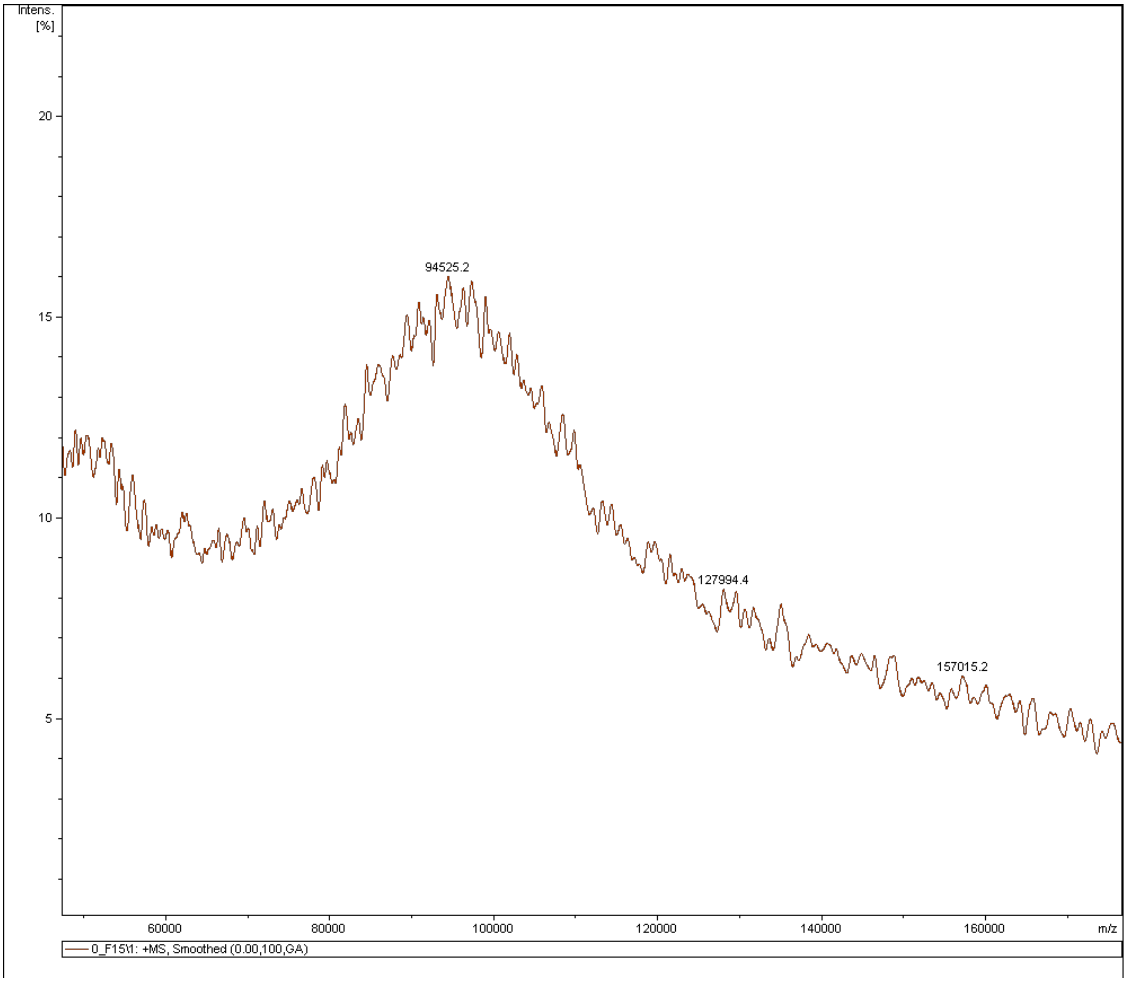


Figure 44. Smoothed MALDI-TOF spectrum for **12**. M_W = 95,962 g/mol.

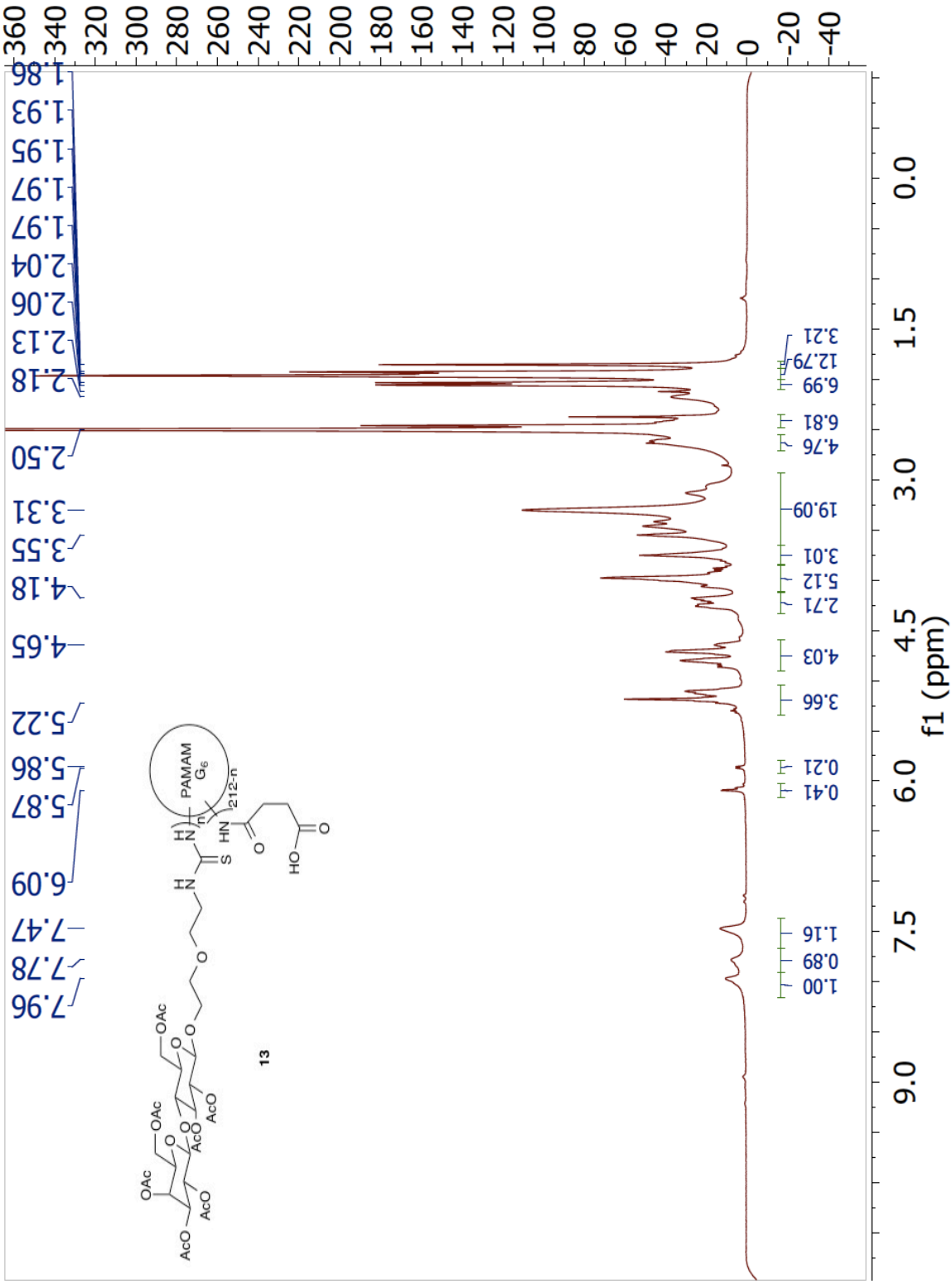


Figure 45. Full ^{1}H NMR spectrum for compound **13**.

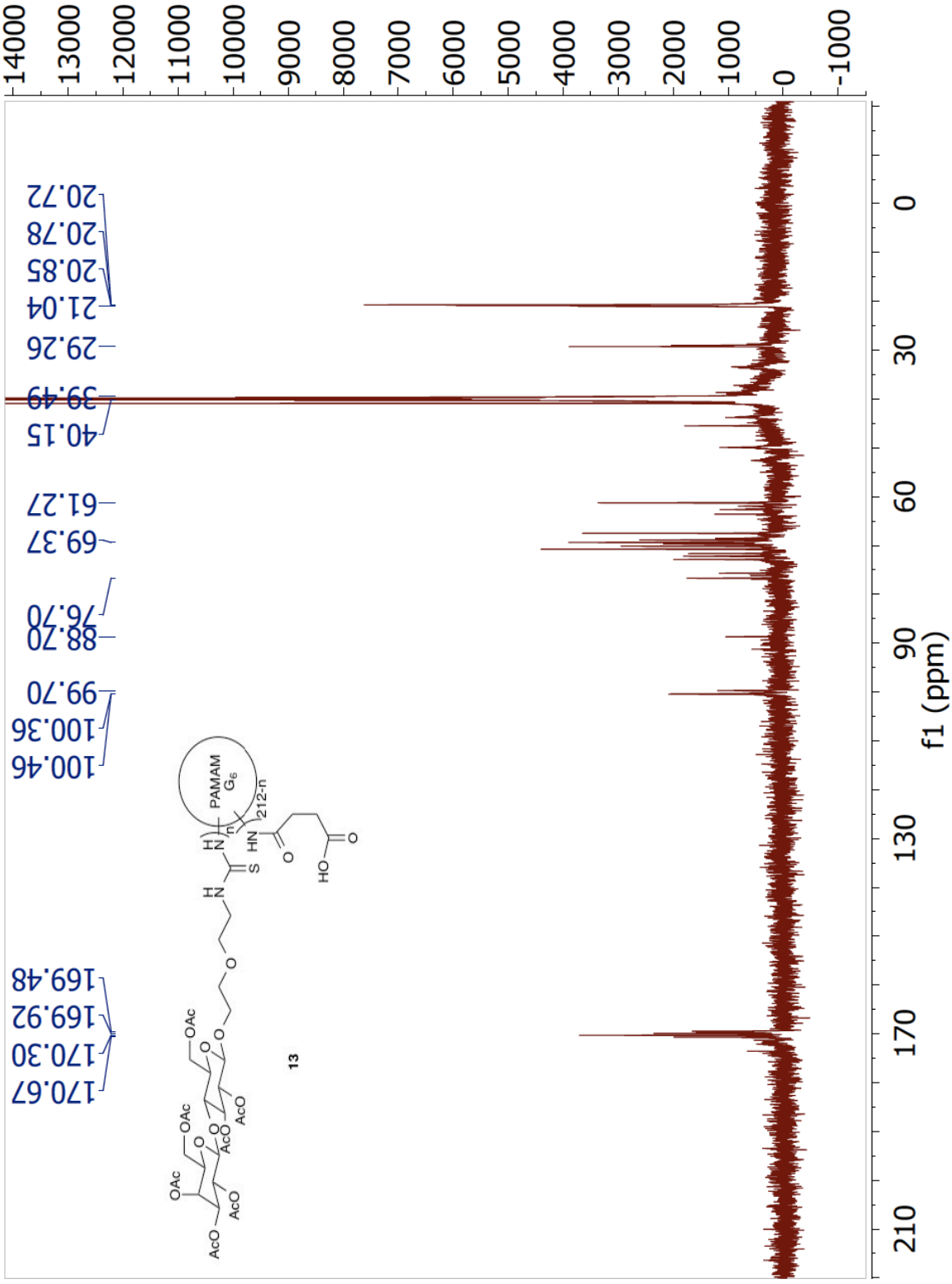


Figure 46. Full ^{13}C NMR spectrum for compound **13**.

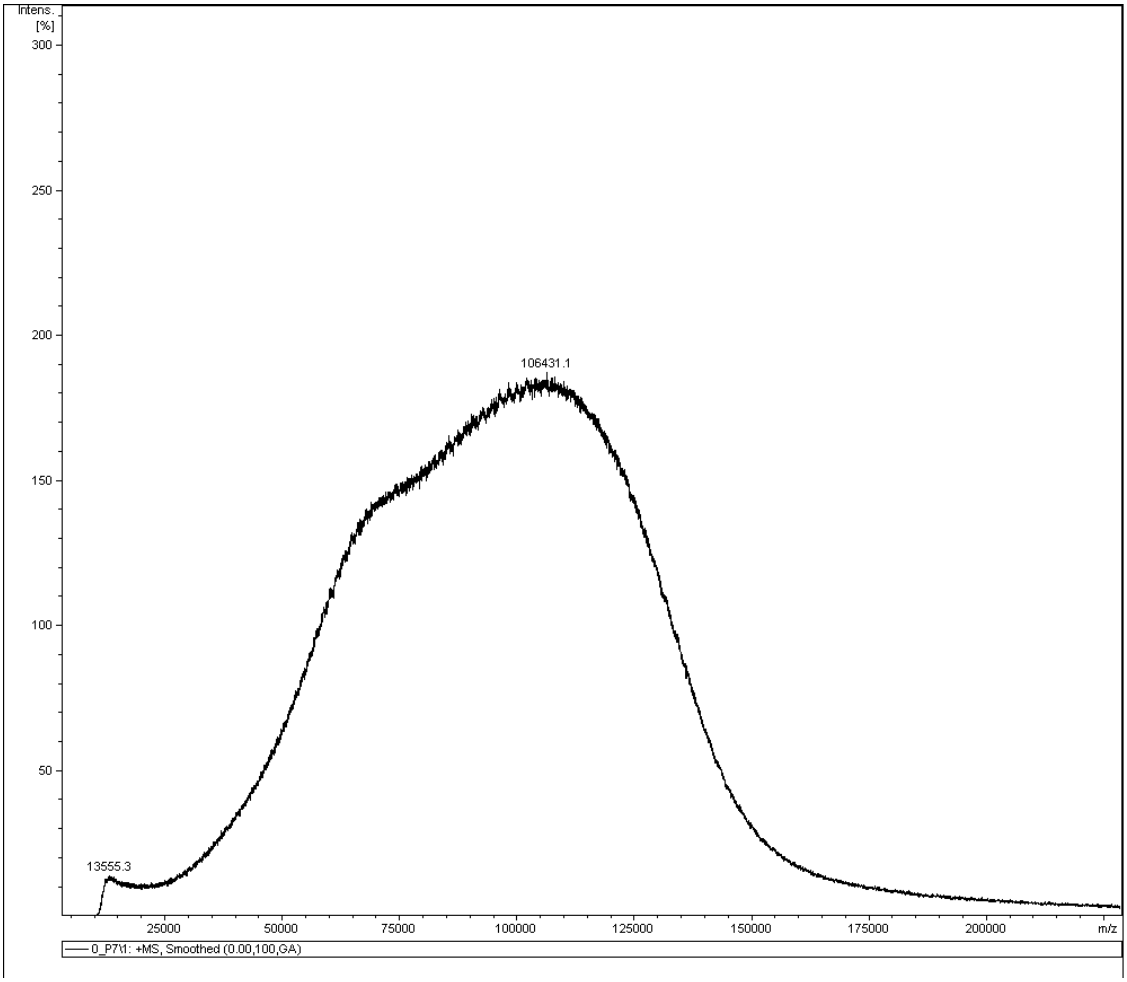


Figure 47. Smoothed MALDI-TOF spectrum for **13**. M_W = 104,000 g/mol.

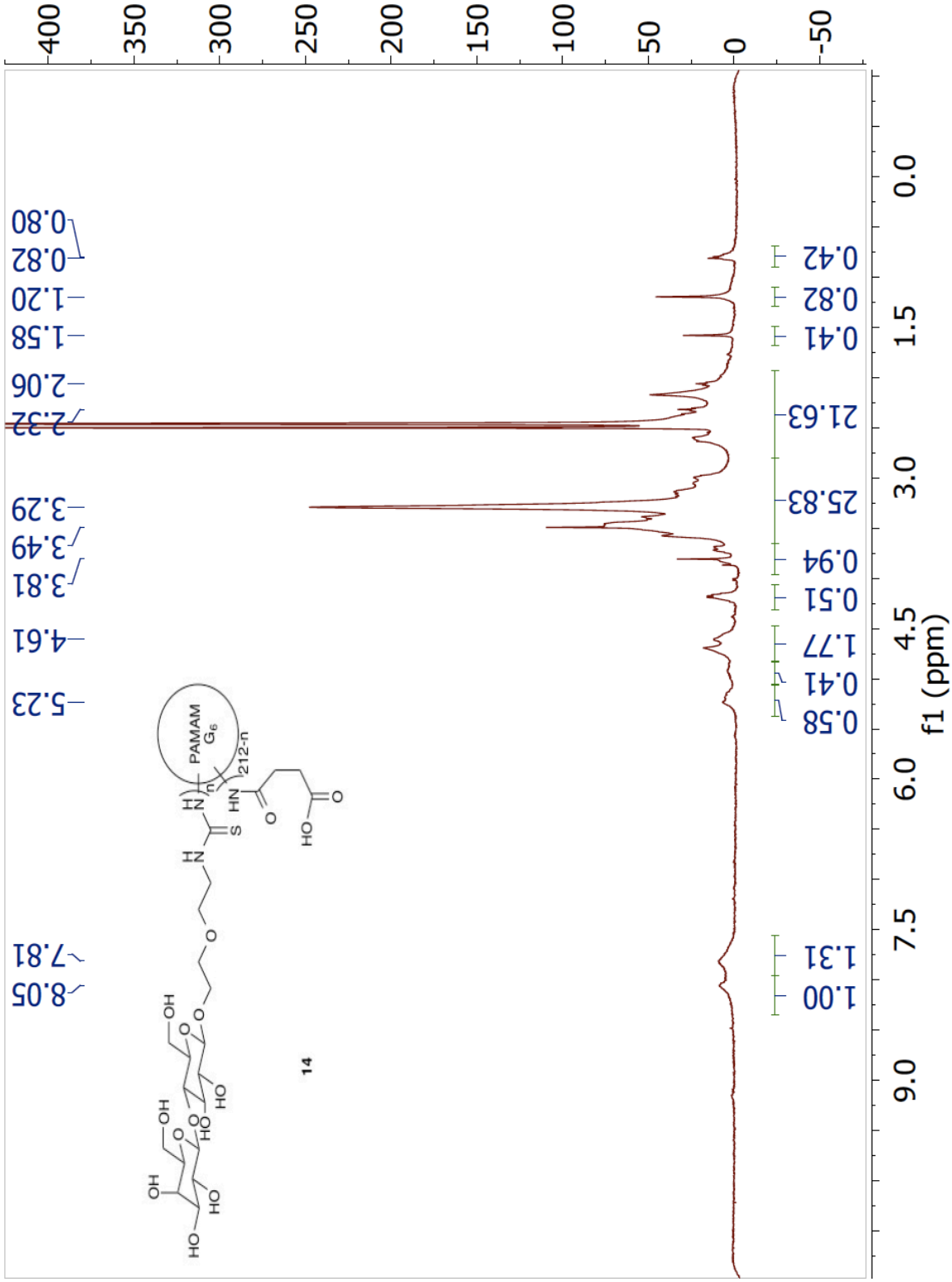


Figure 48. Full ^{1}H NMR spectrum for compound **14**.

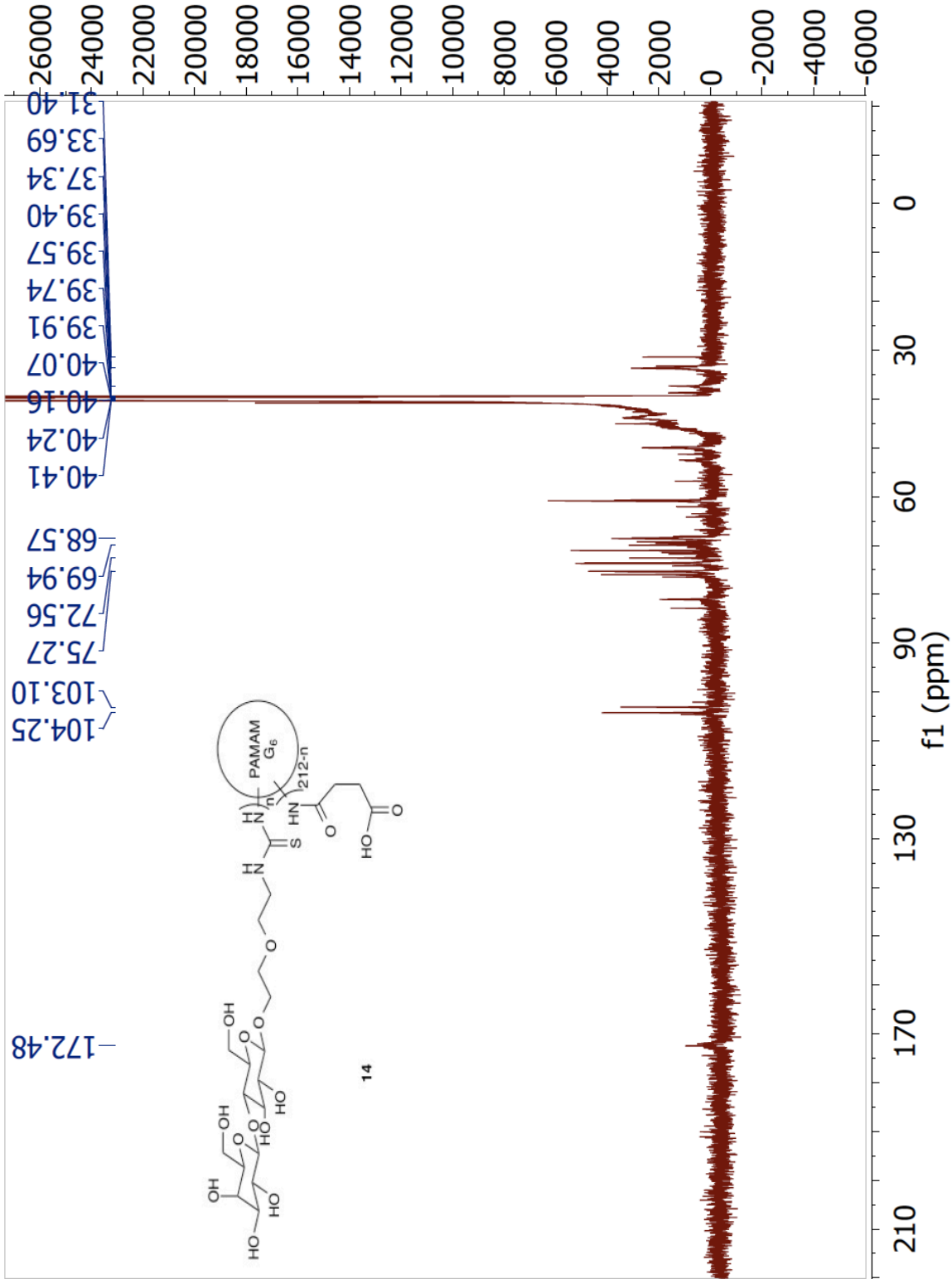


Figure 49. Full ^{13}C NMR spectrum for compound **14**.

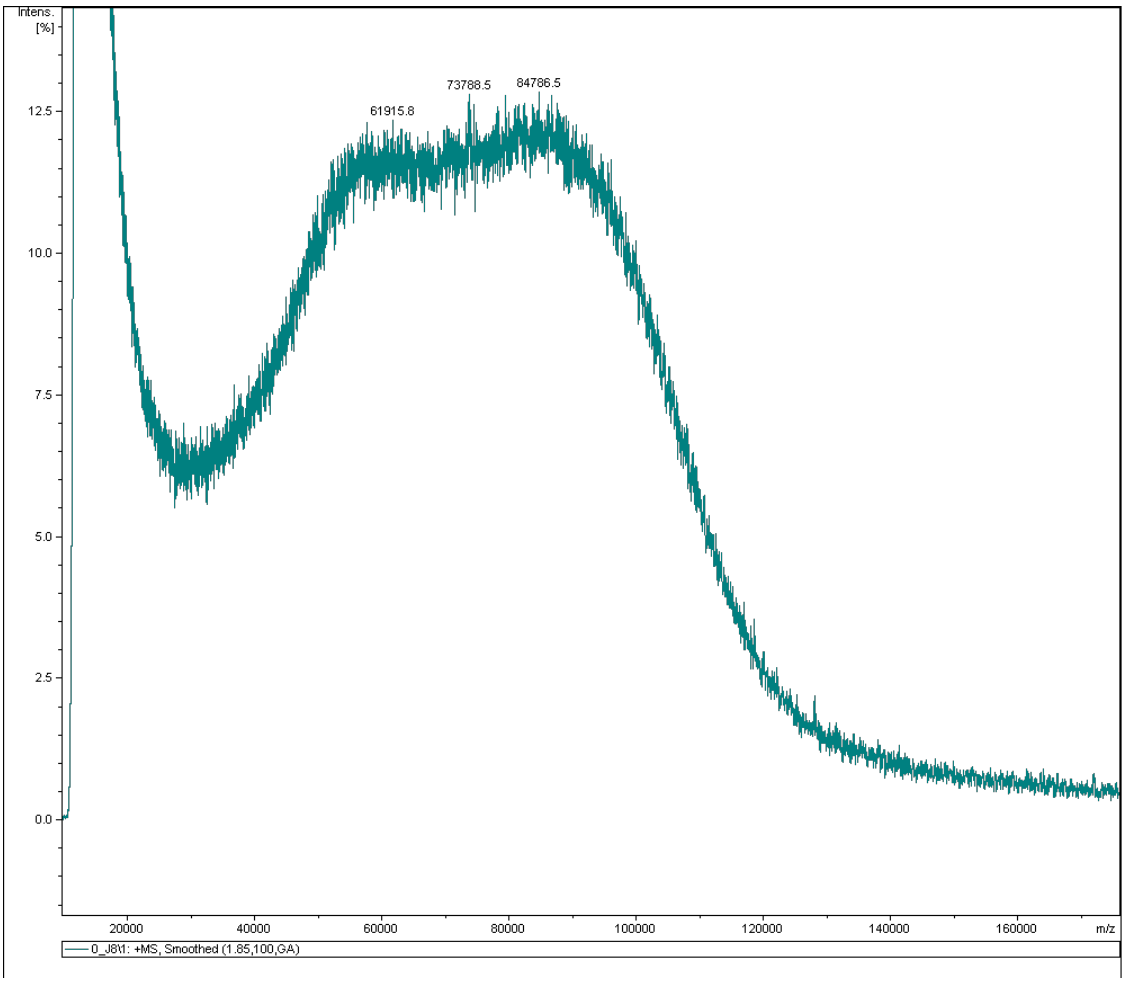


Figure 50. Smoothed MALDI-TOF spectrum for **14**. M_W = 85,200 g/mol.

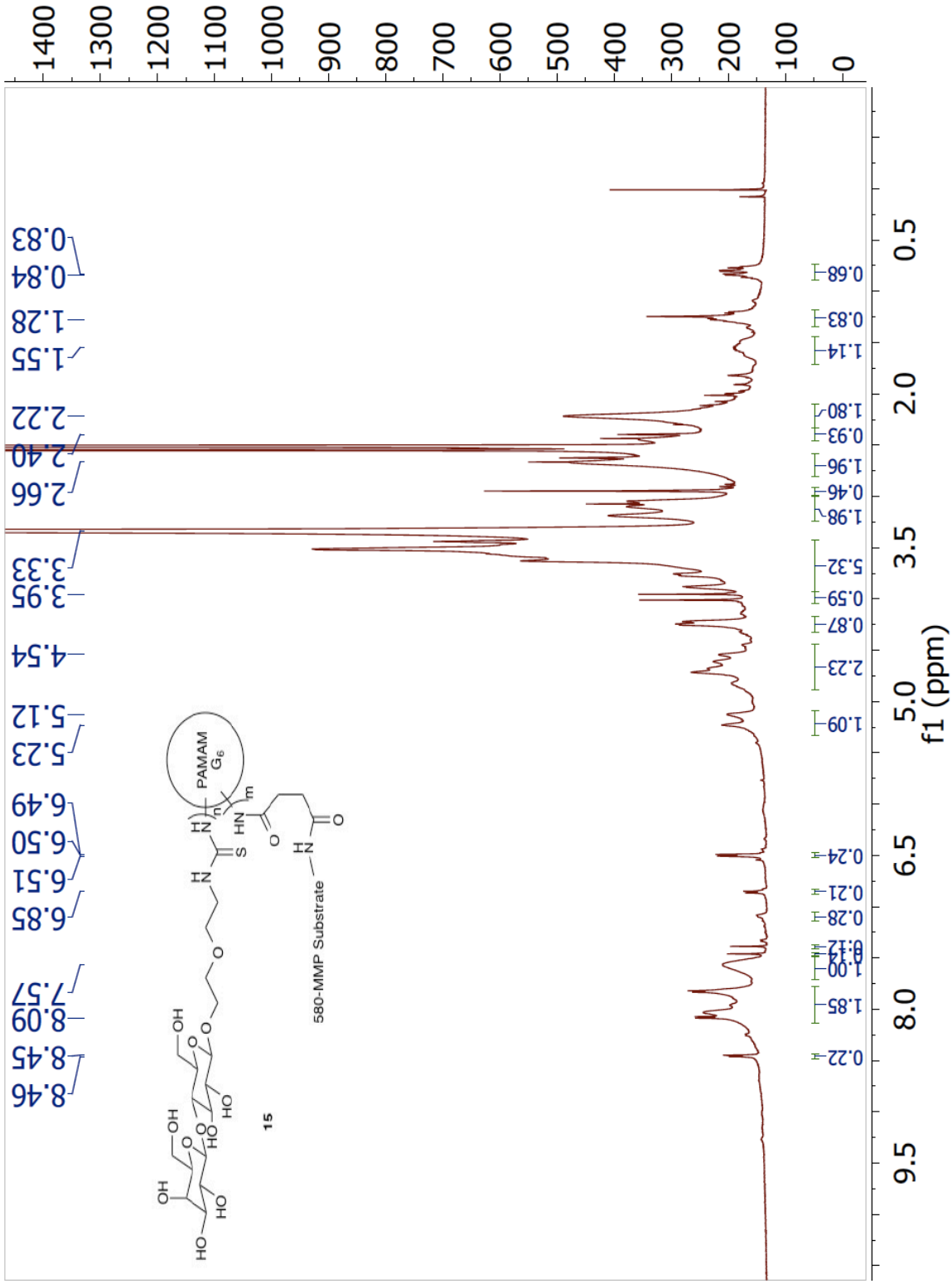


Figure 51. Full ^{1}H NMR spectrum for compound **15**.

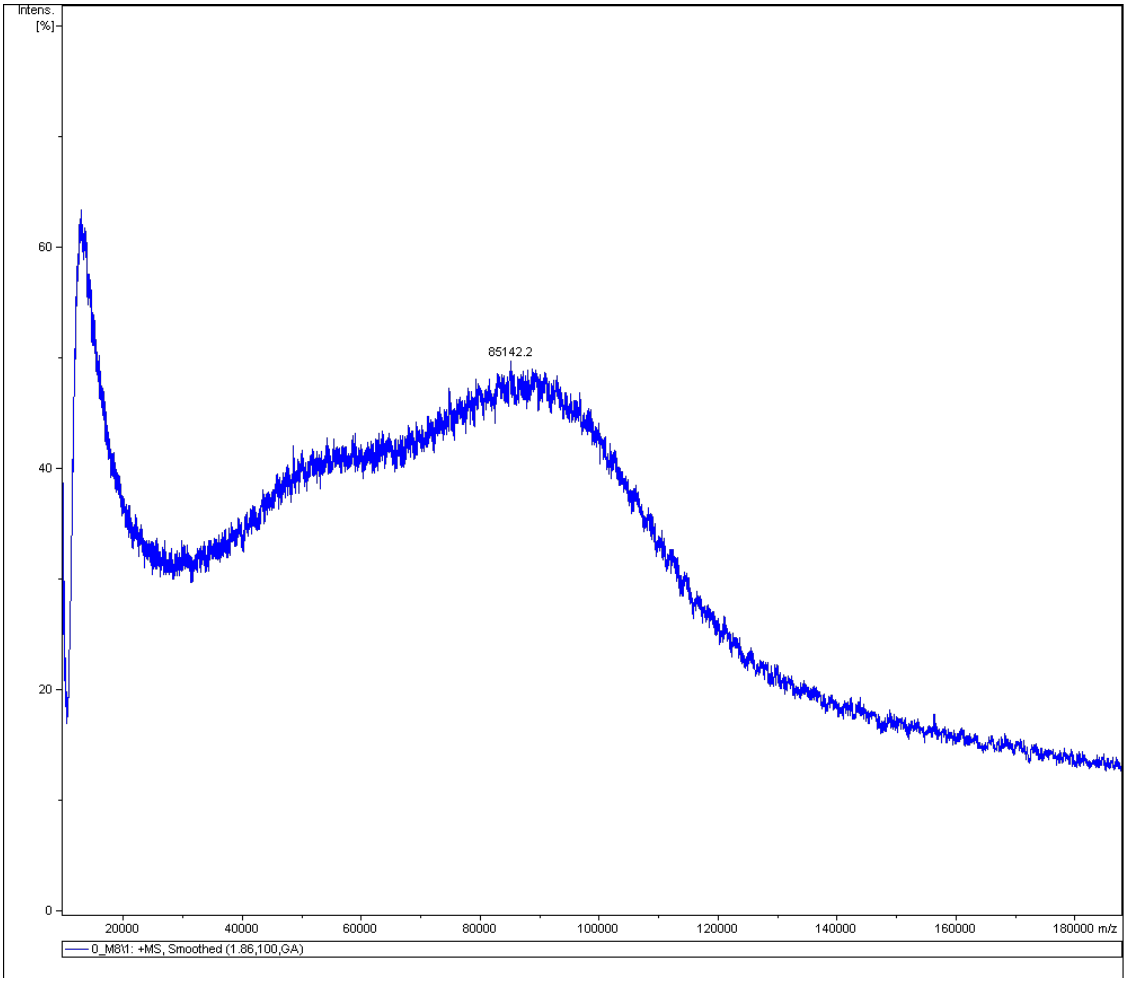


Figure 52. Smoothed MALDI-TOF spectrum for **15**. M_W = 83,500 g/mol.

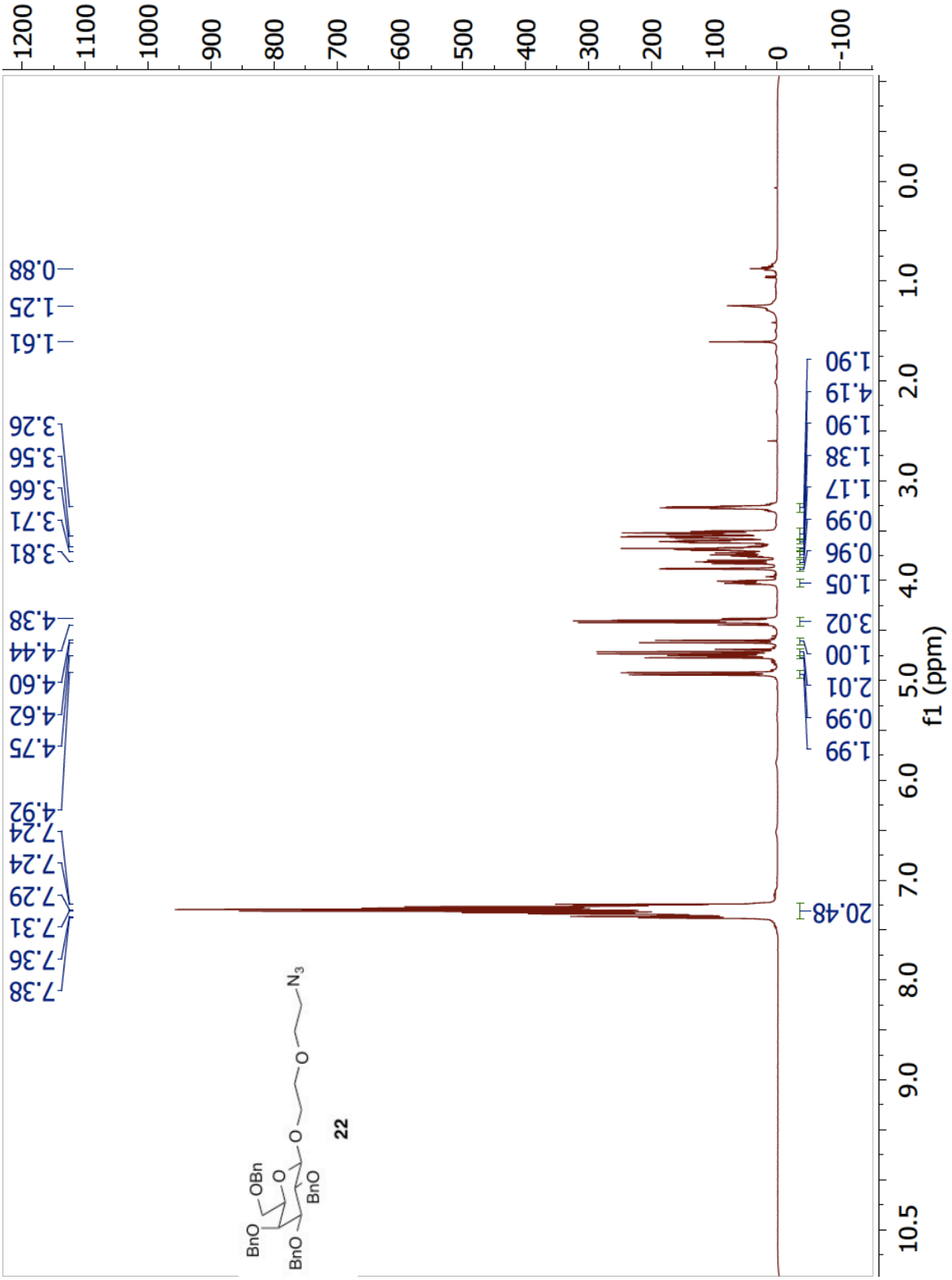


Figure 53. Full ^{1}H NMR spectrum for compound **22.**

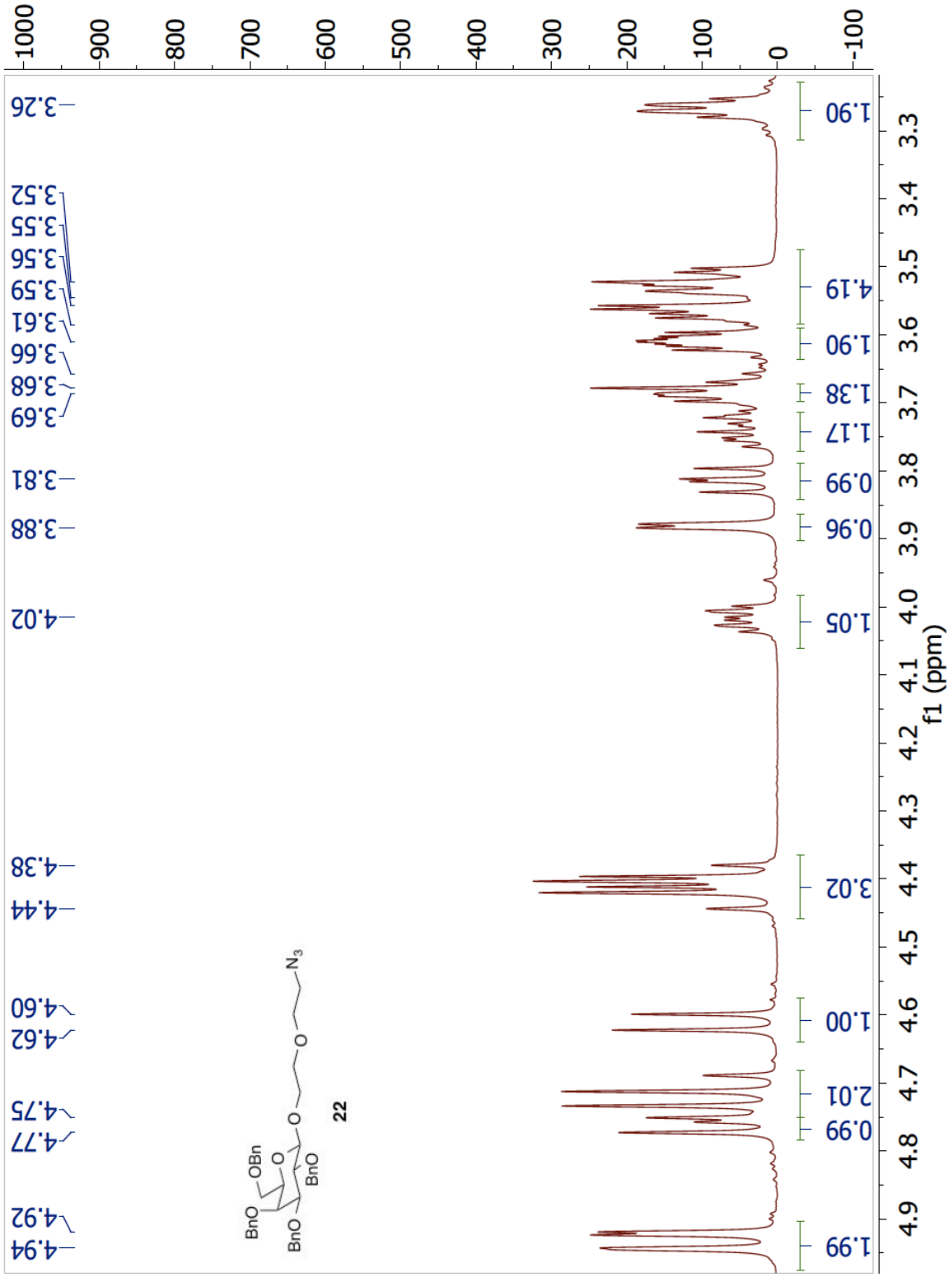


Figure 54. Expansion of the ^{1}H NMR carbohydrate region for compound **22**.

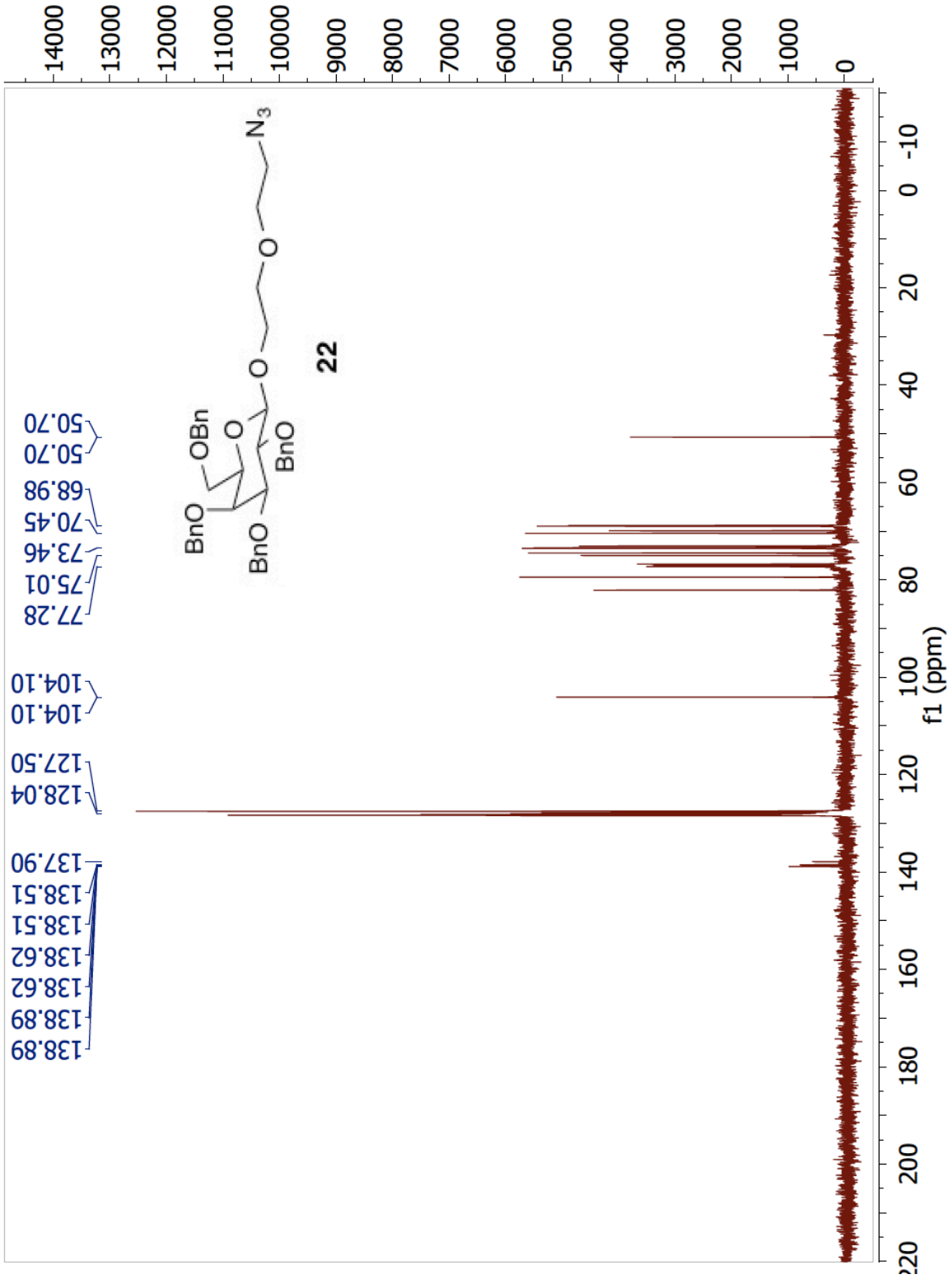


Figure 55. Full ^{13}C NMR spectrum for compound **22**.

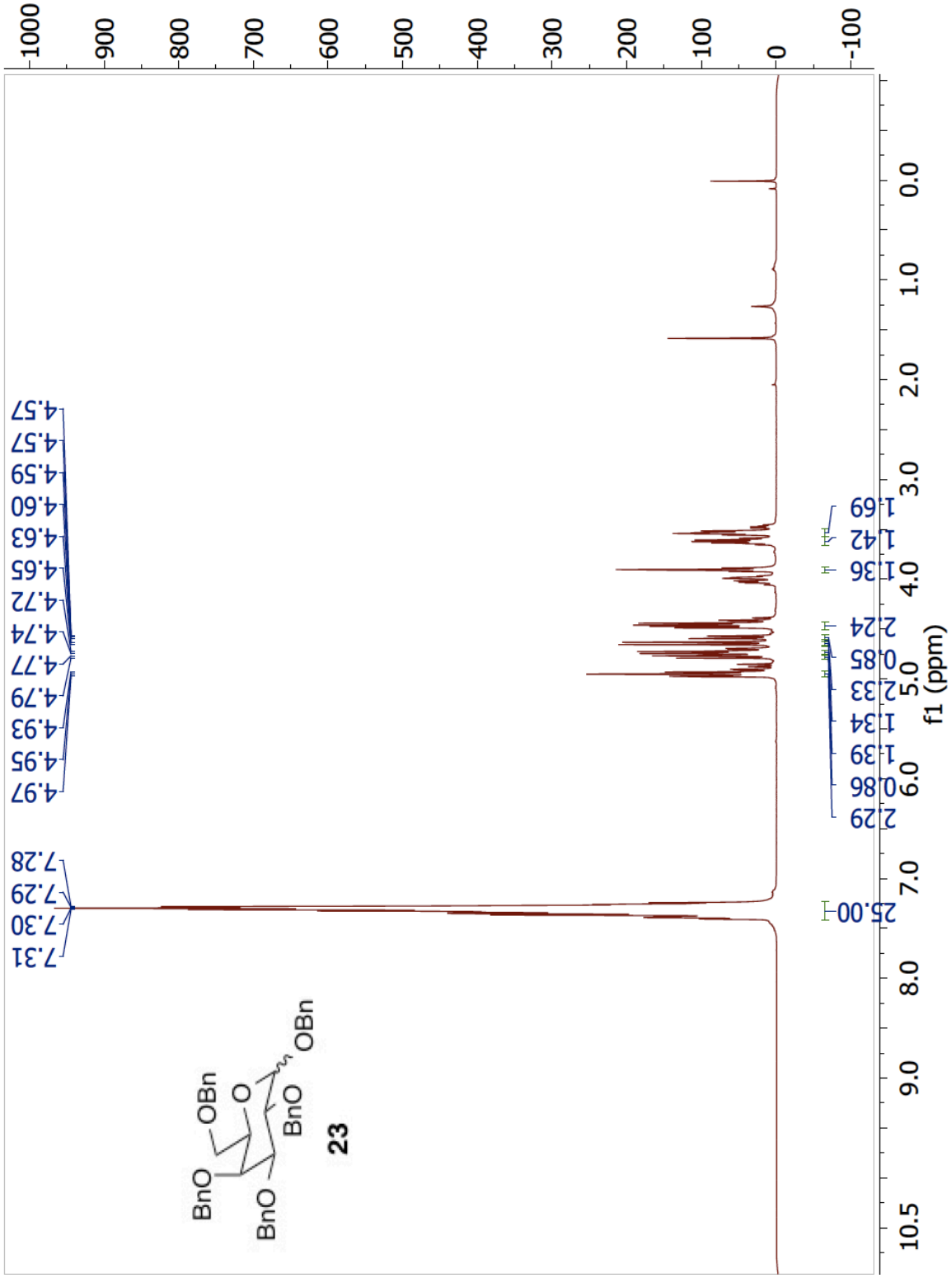


Figure 56. Full ^{1}H NMR spectrum for compound **23**.

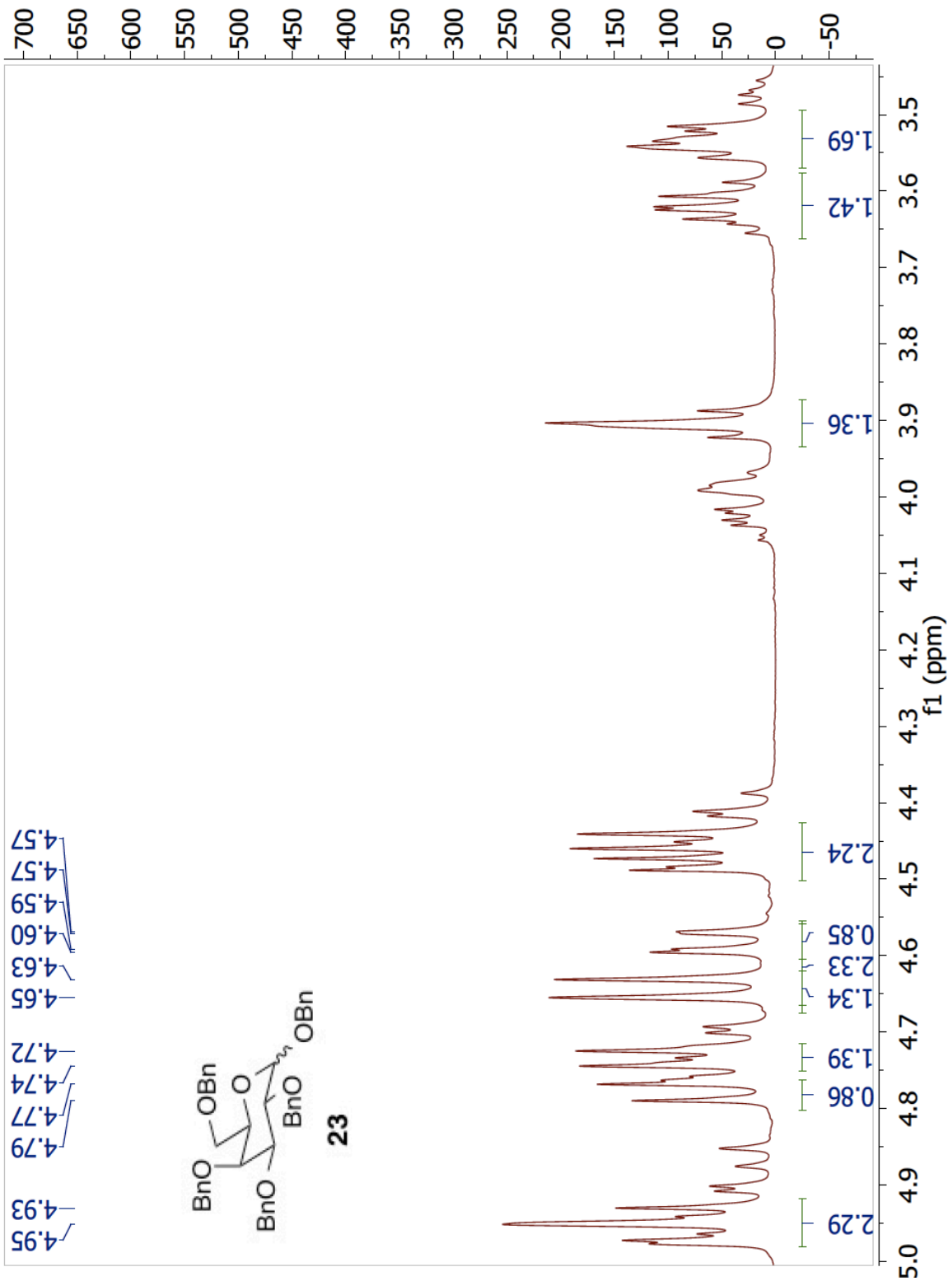


Figure 57. Expansion of ^{1}H NMR carbohydrate region for compound **23**.

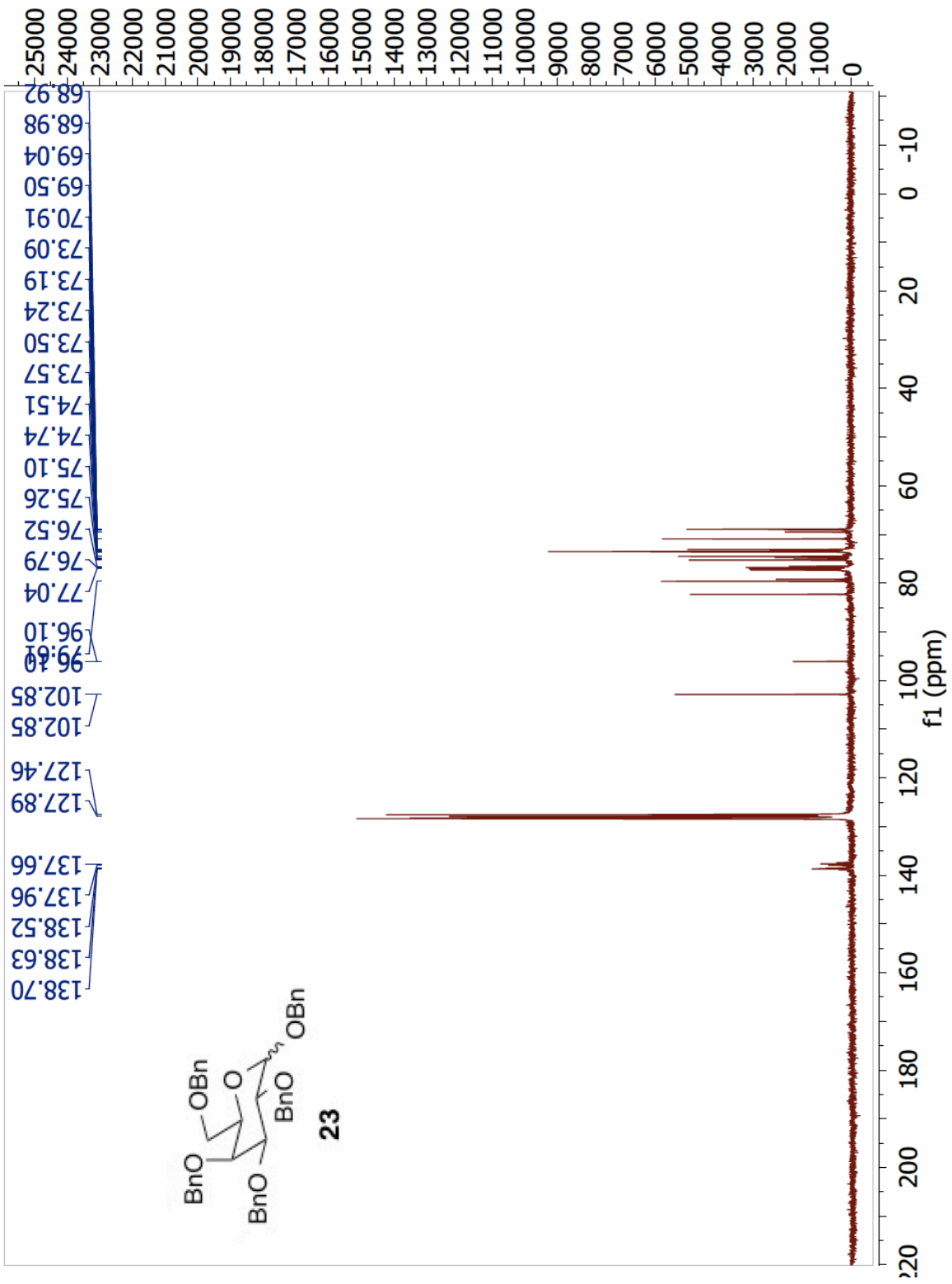


Figure 58. Full ^{13}C NMR spectrum for compound **23**.

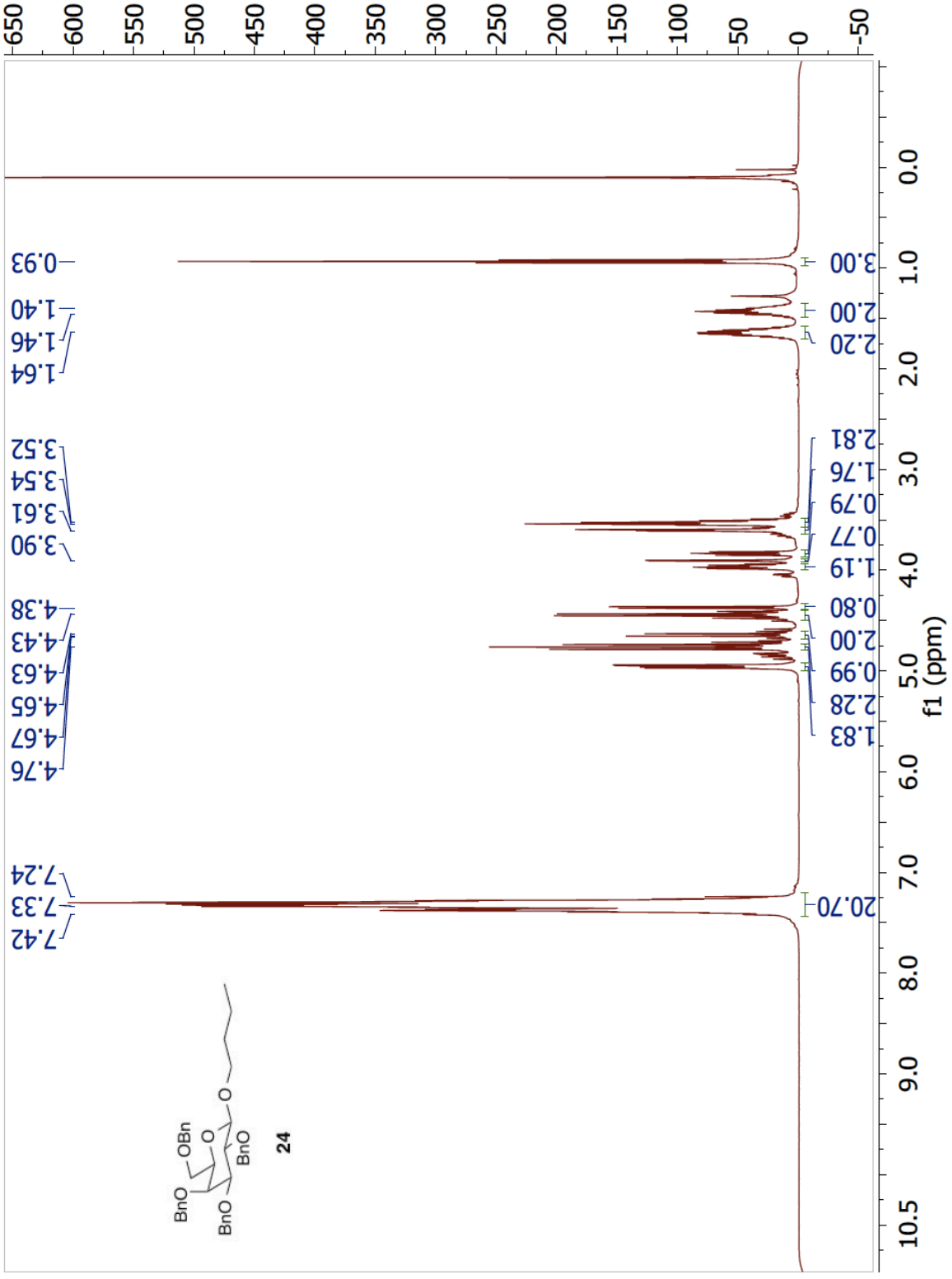


Figure 59. Full ^{1}H NMR spectrum for compound **24**.

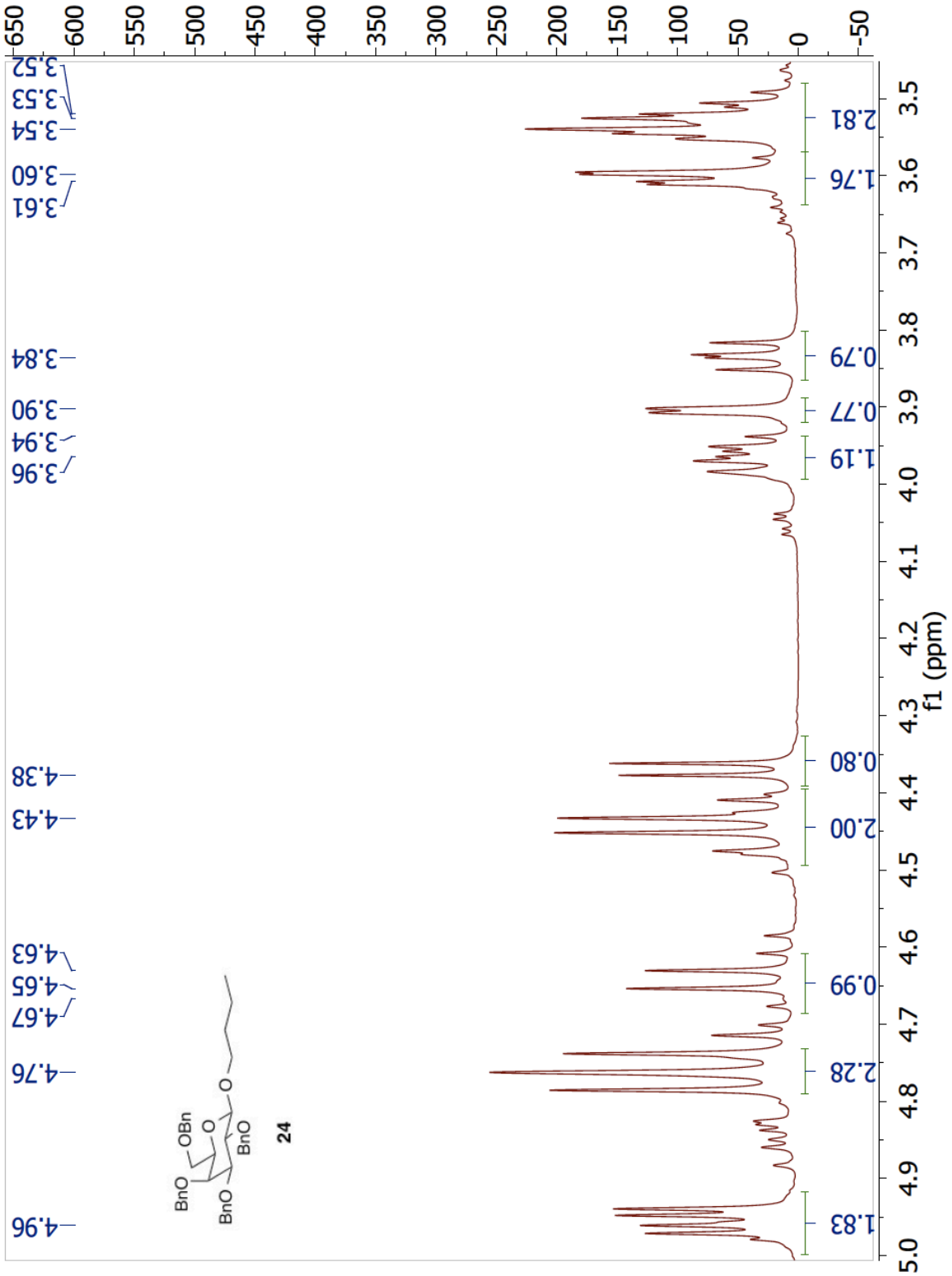


Figure 60. Expansion of the ^{1}H NMR carbohydrate region for compound **24**.

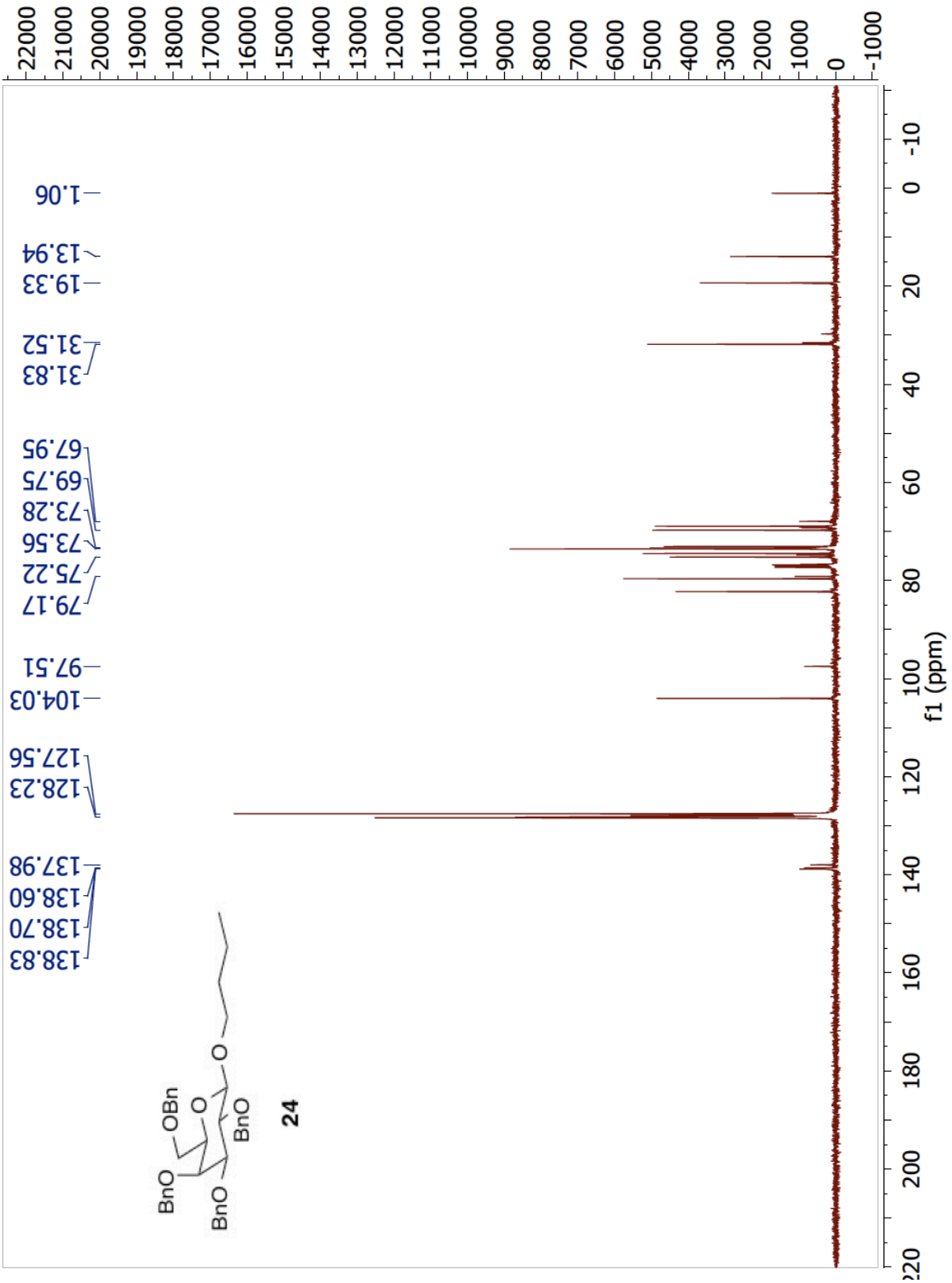


Figure 61. Full ^{13}C NMR spectrum for compound **24**.

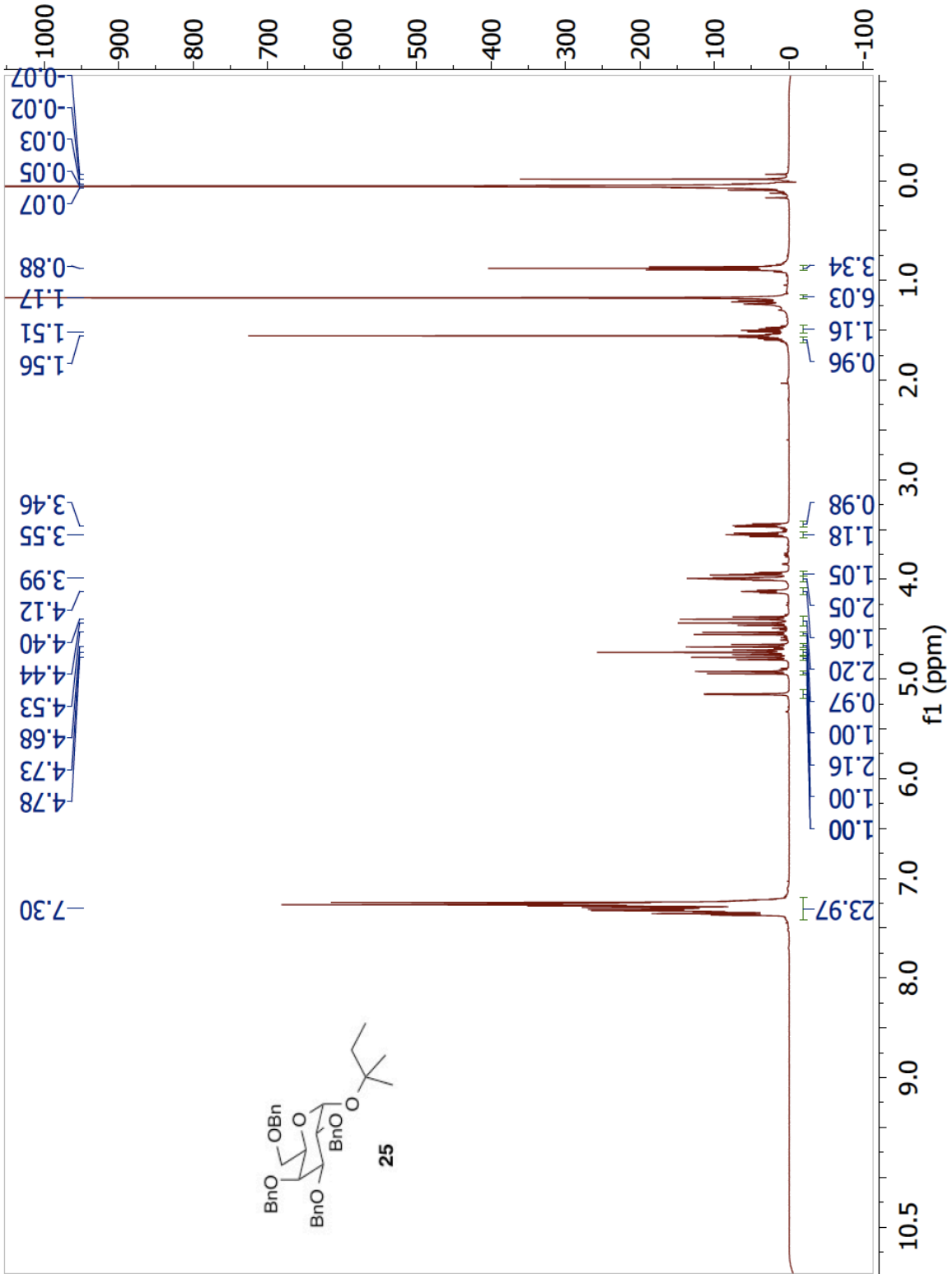


Figure 62. Full ^{1}H NMR spectrum for compound **25**.

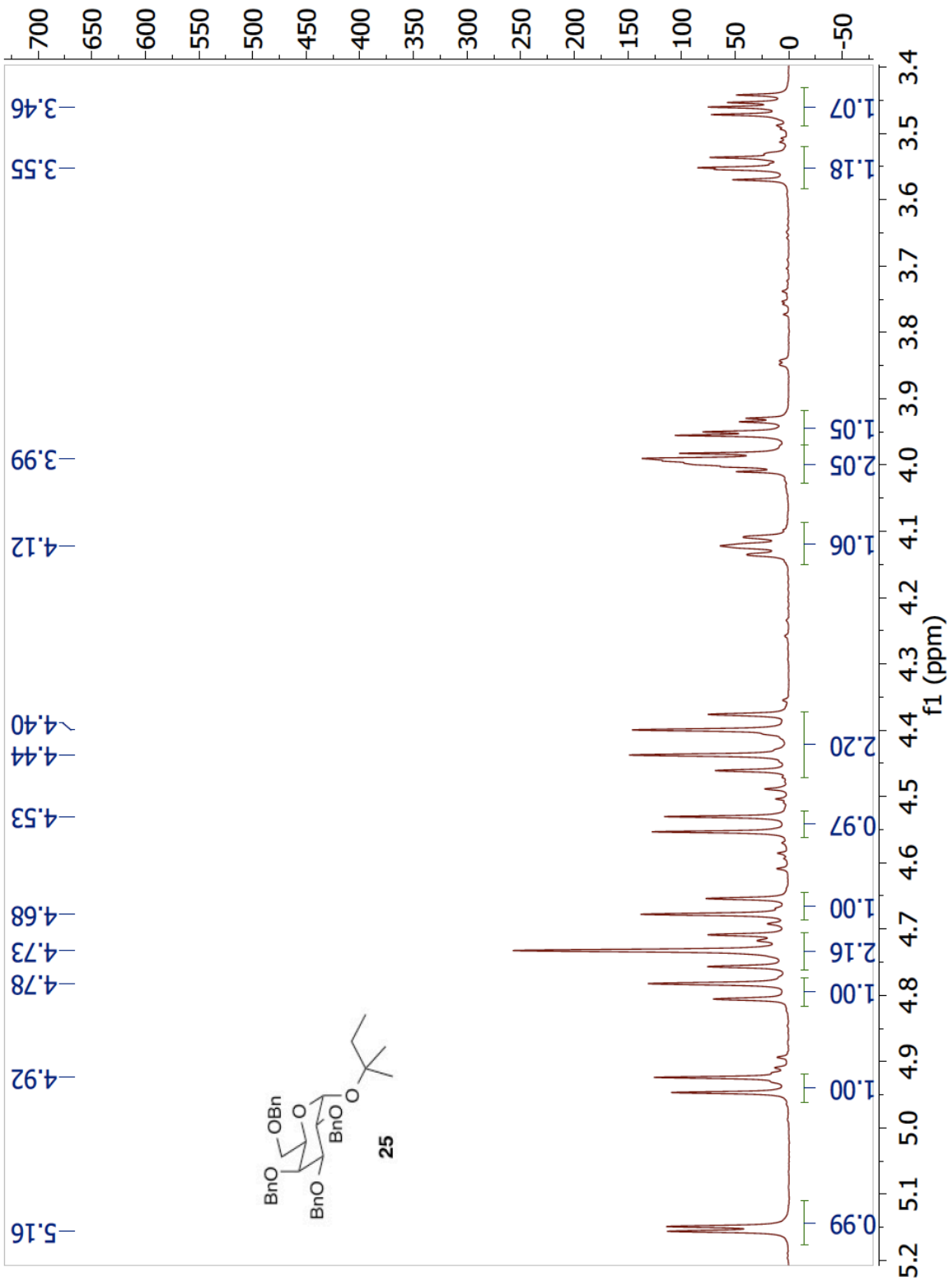


Figure 63. Expansion of the ^{1}H NMR carbohydrate region for compound **25**.

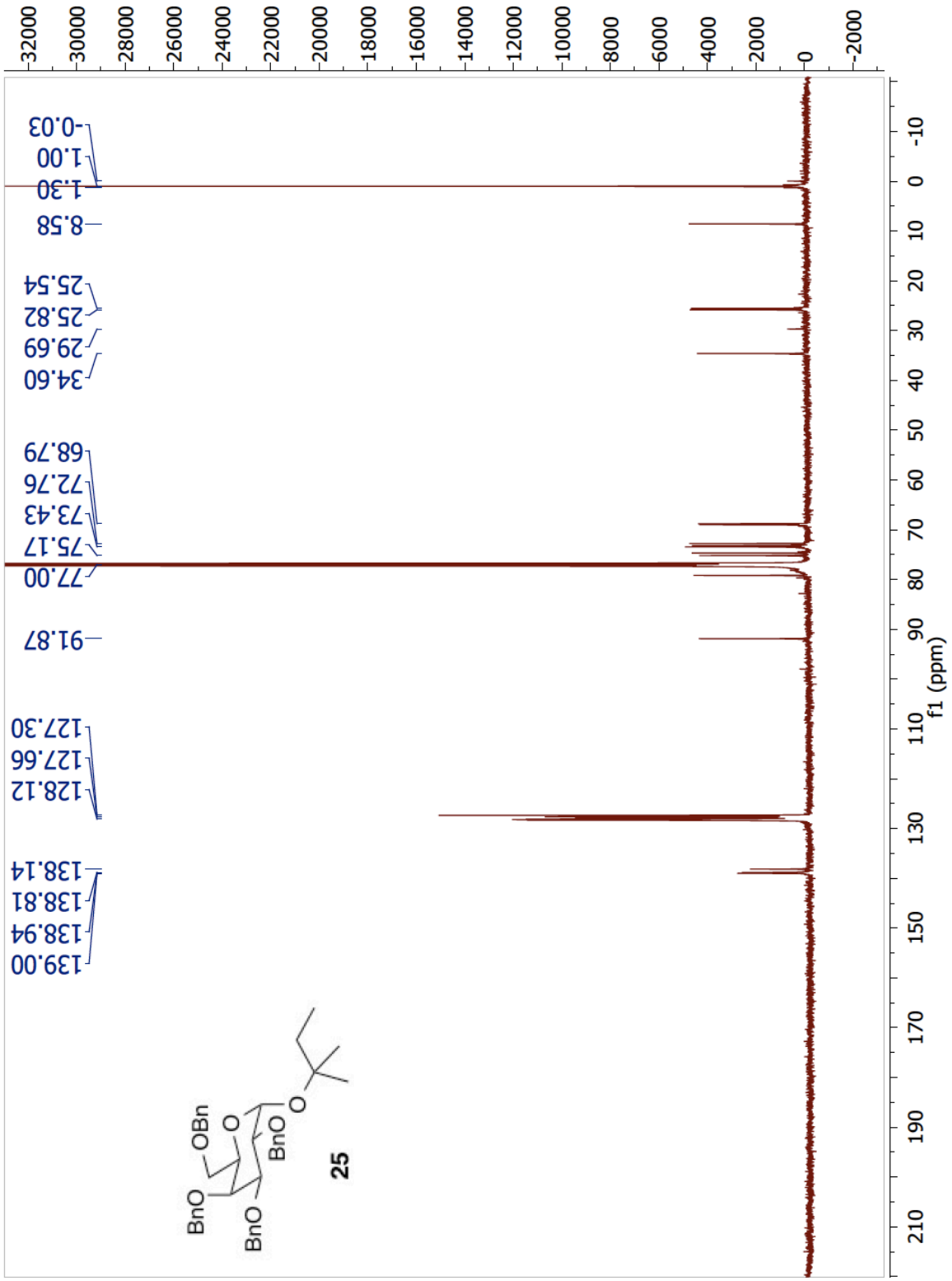


Figure 64. Full ^{13}C NMR spectrum for compound **25.**

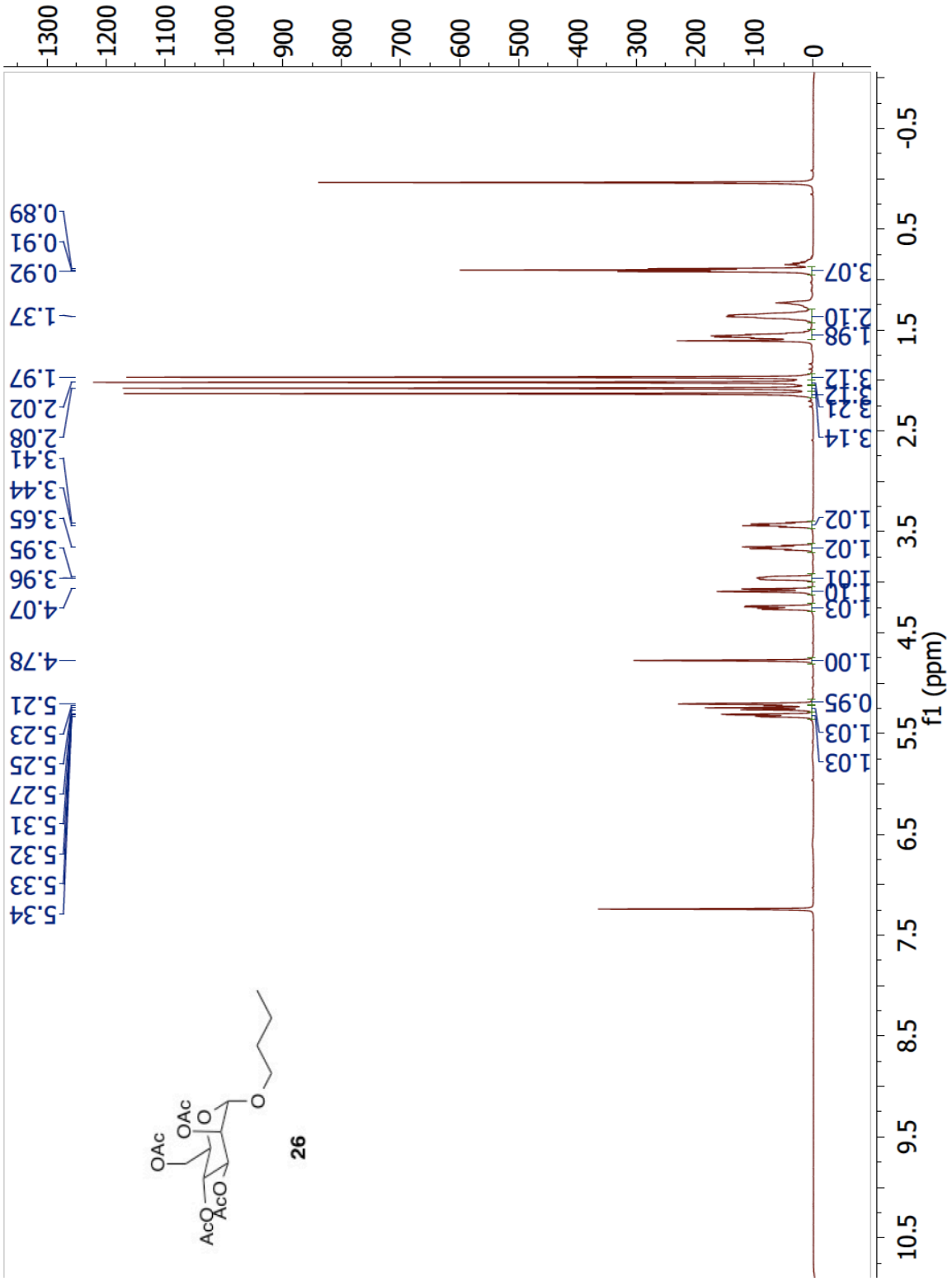


Figure 65. Full ^{1}H NMR spectrum for compound **26**.

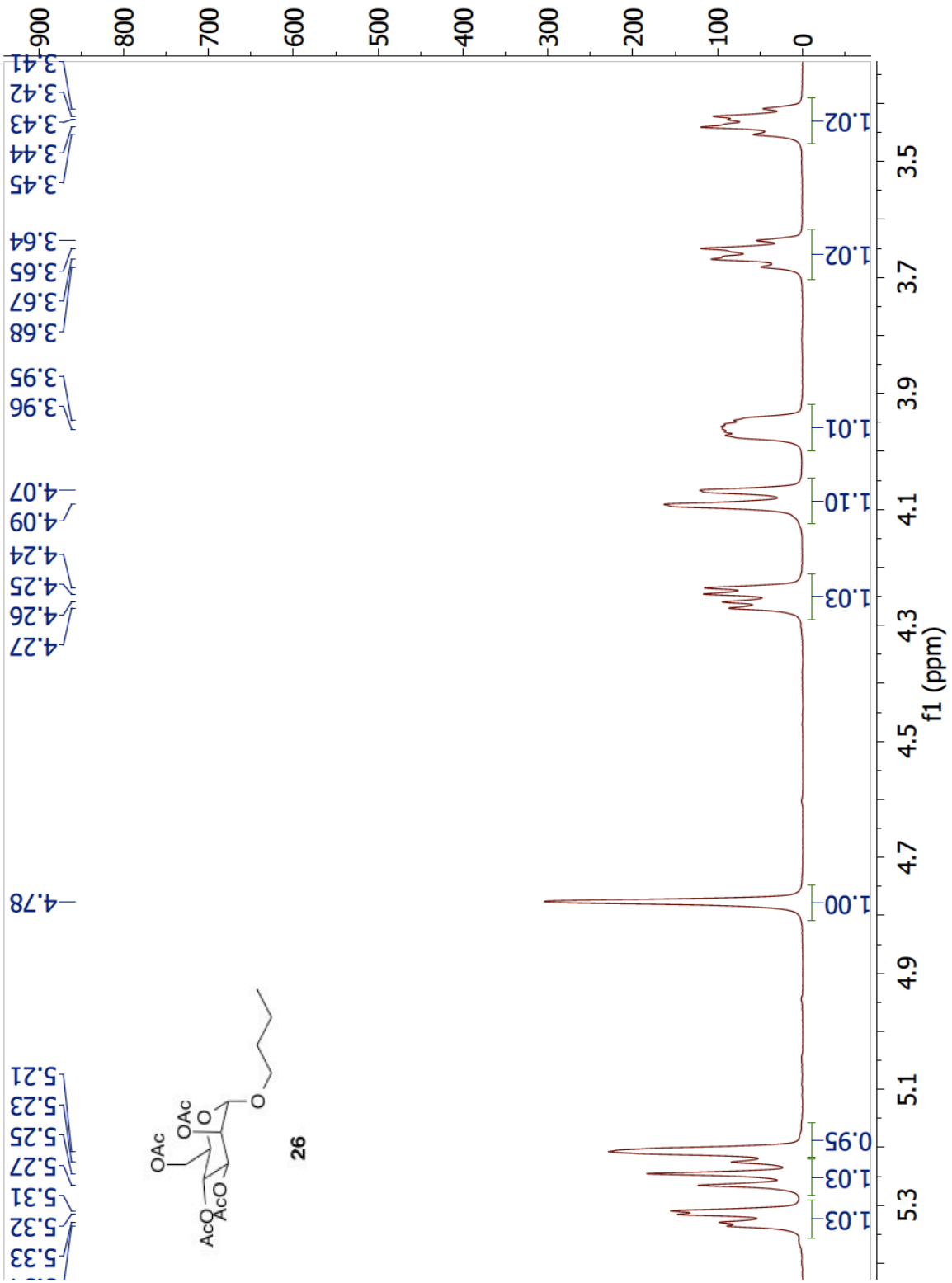


Figure 66. Expansion of ^{1}H NMR carbohydrate region for compound **26**.

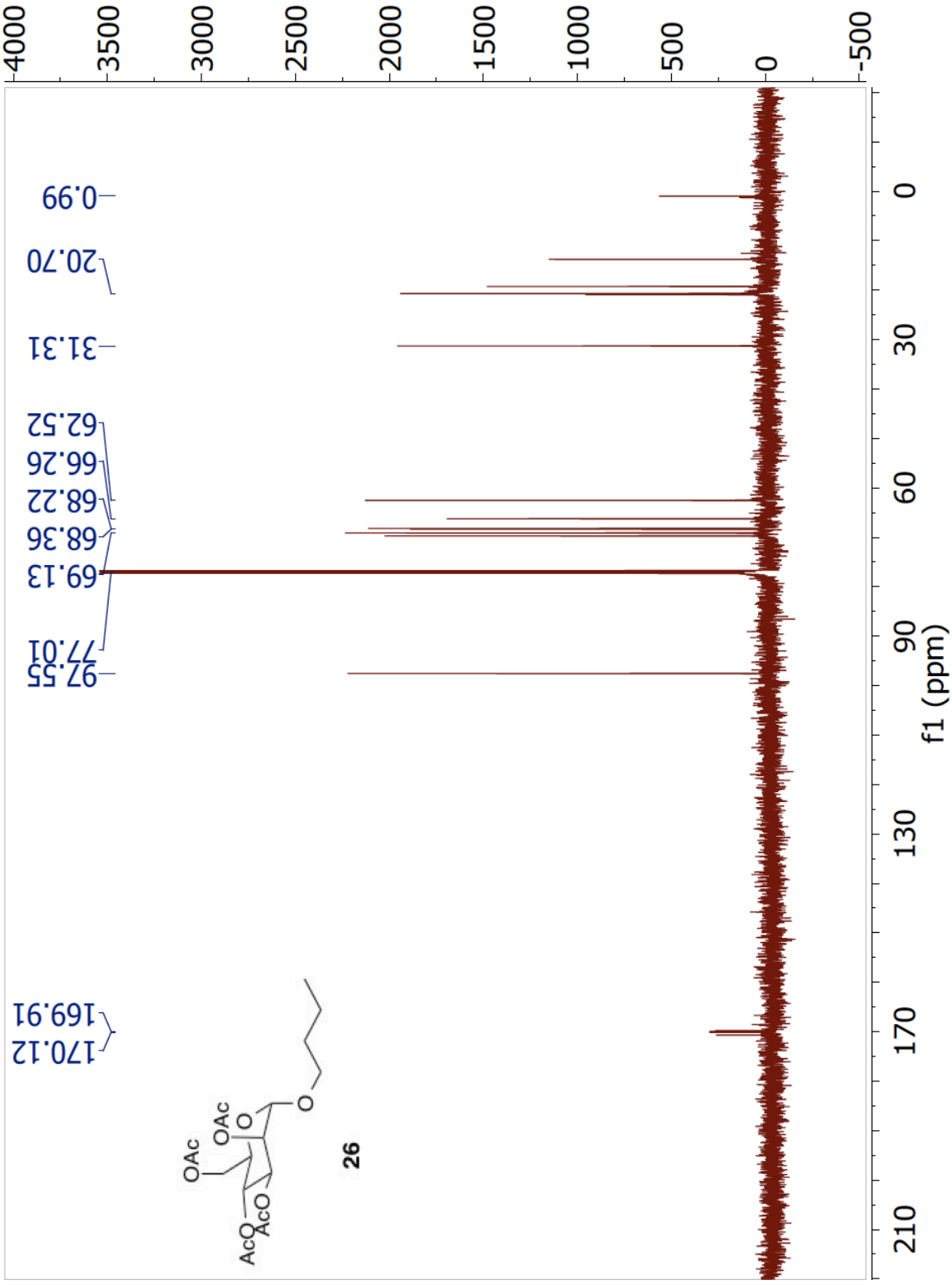


Figure 67. Full ^{13}C NMR spectrum for compound **26**.

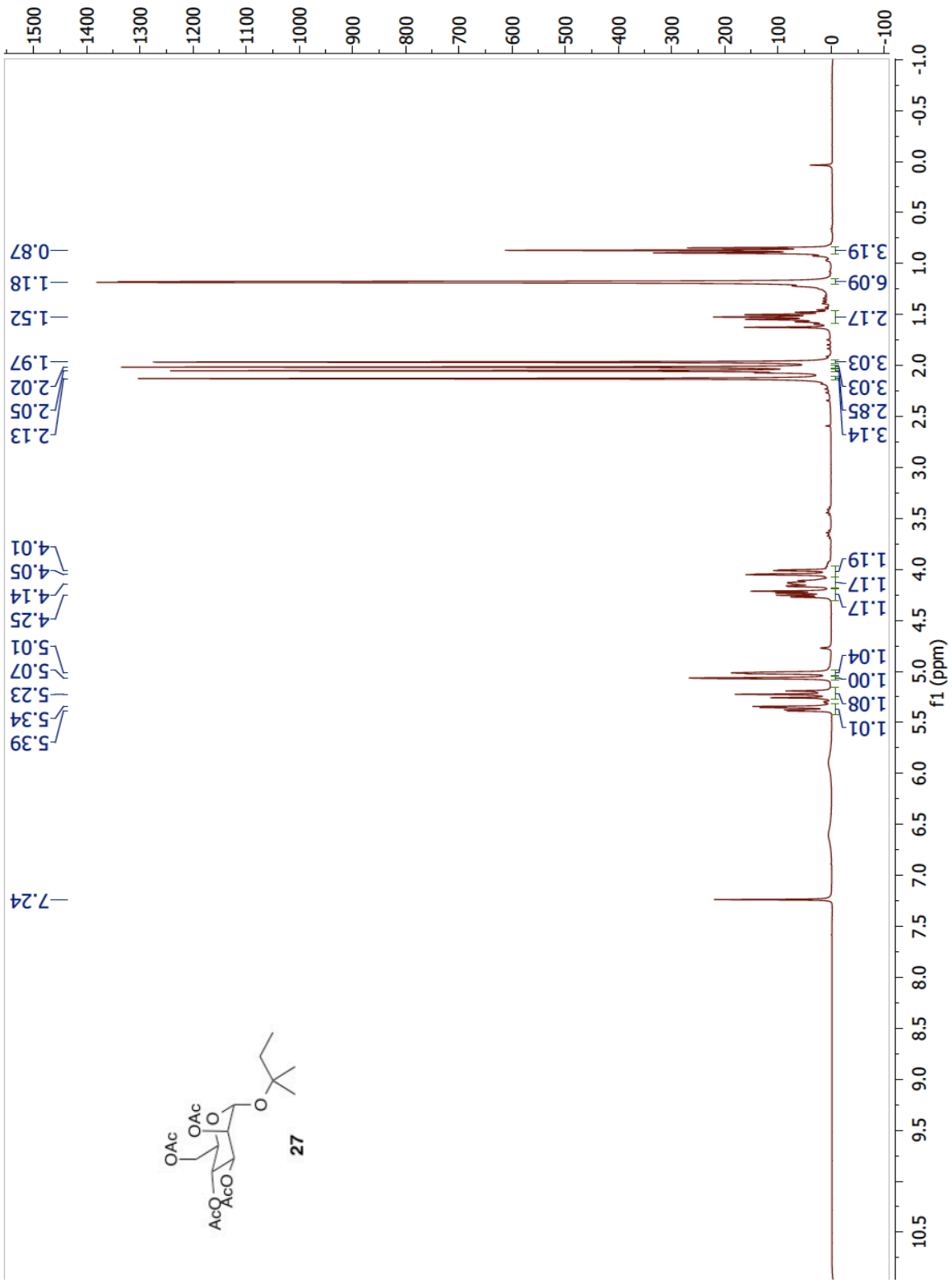


Figure 68. Full ^{1}H NMR spectrum for compound **27**.

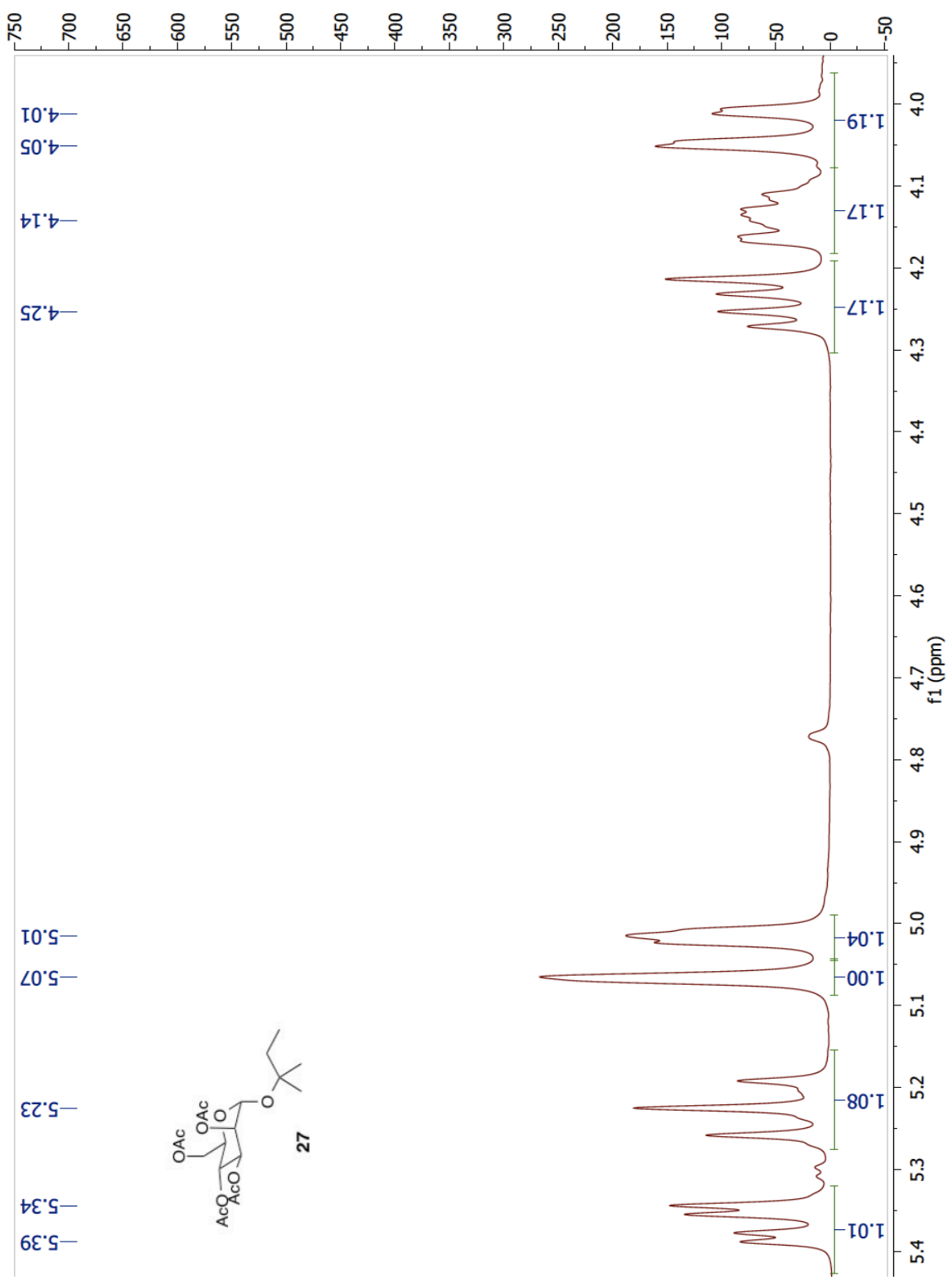


Figure 69. Expansion of the ^{1}H NMR carbohydrate region for compound **27**.

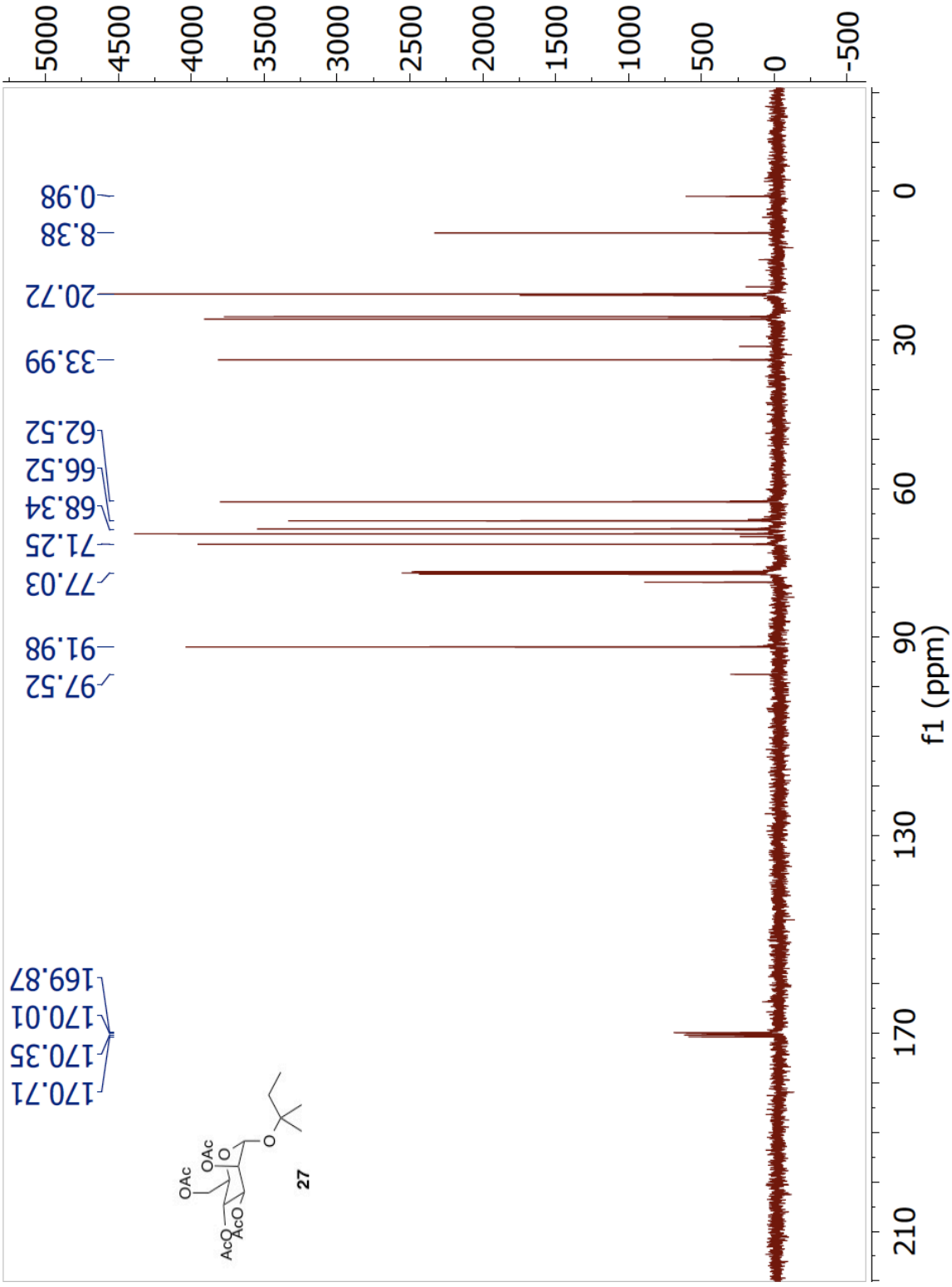


Figure 70. Full ^{13}C NMR spectrum for compound **27**.

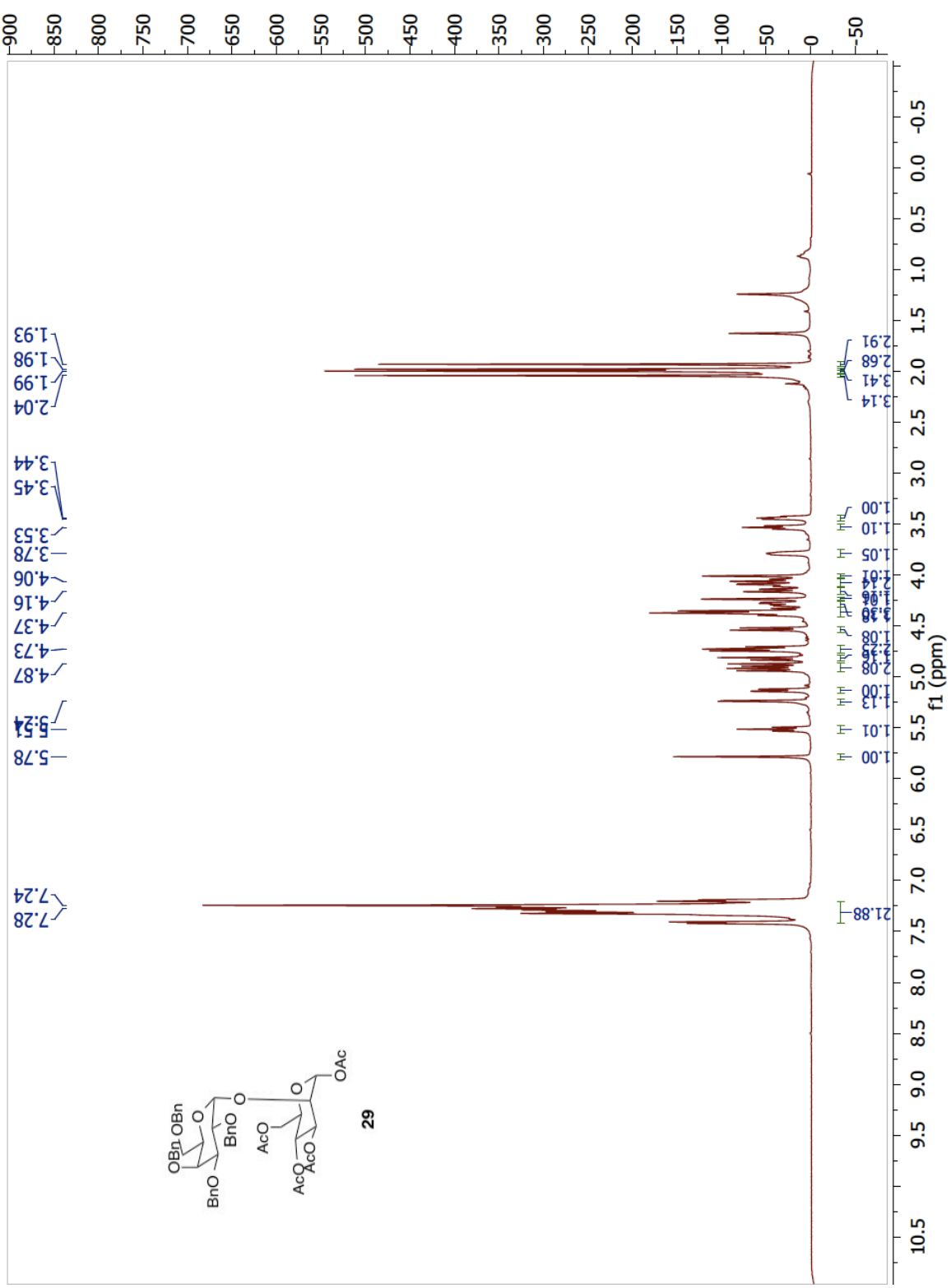


Figure 71. Full ^{1}H NMR spectrum for compound **29**.

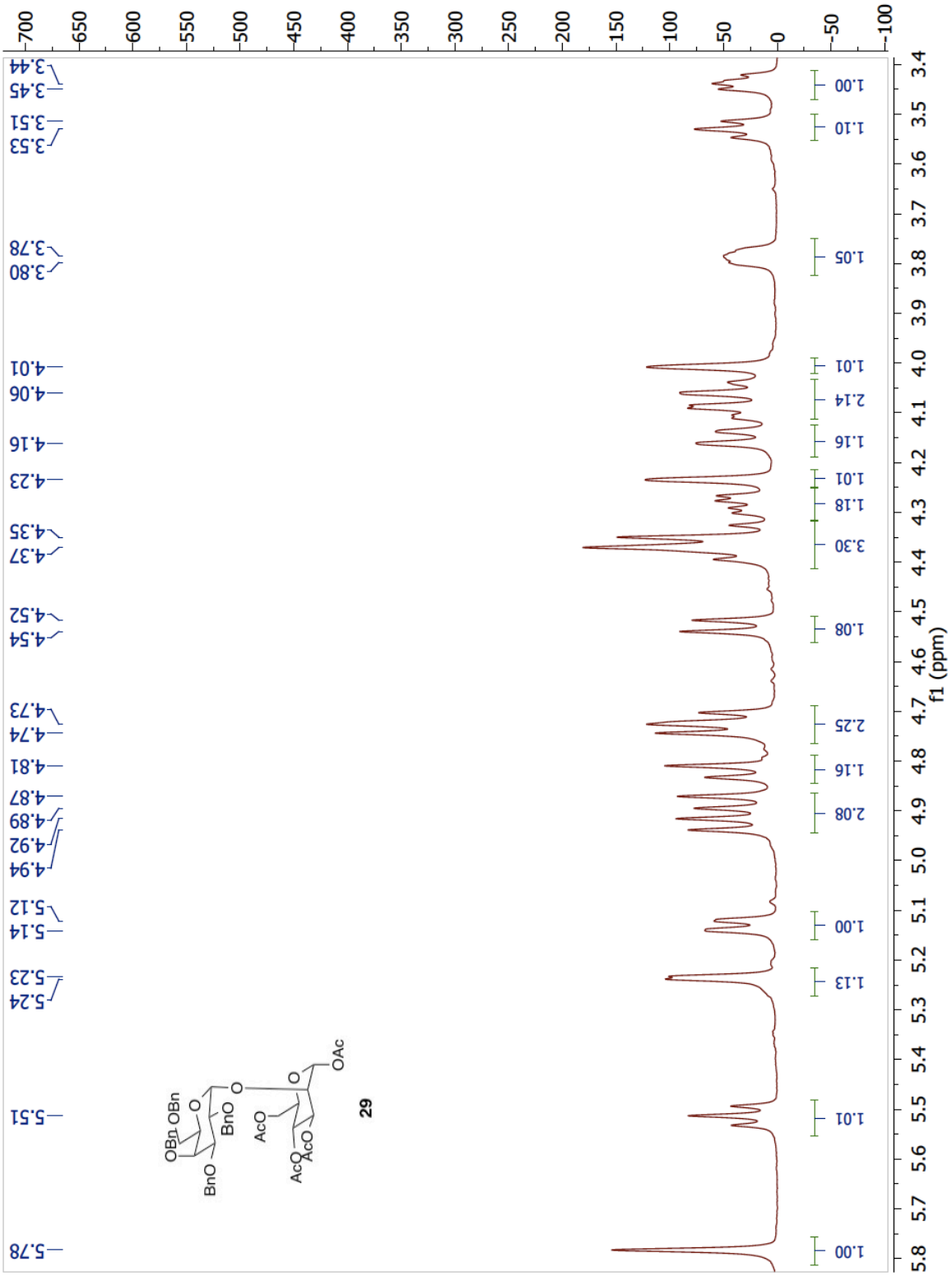


Figure 72. Expansion of the ^{1}H NMR carbohydrate region for compound **29**.

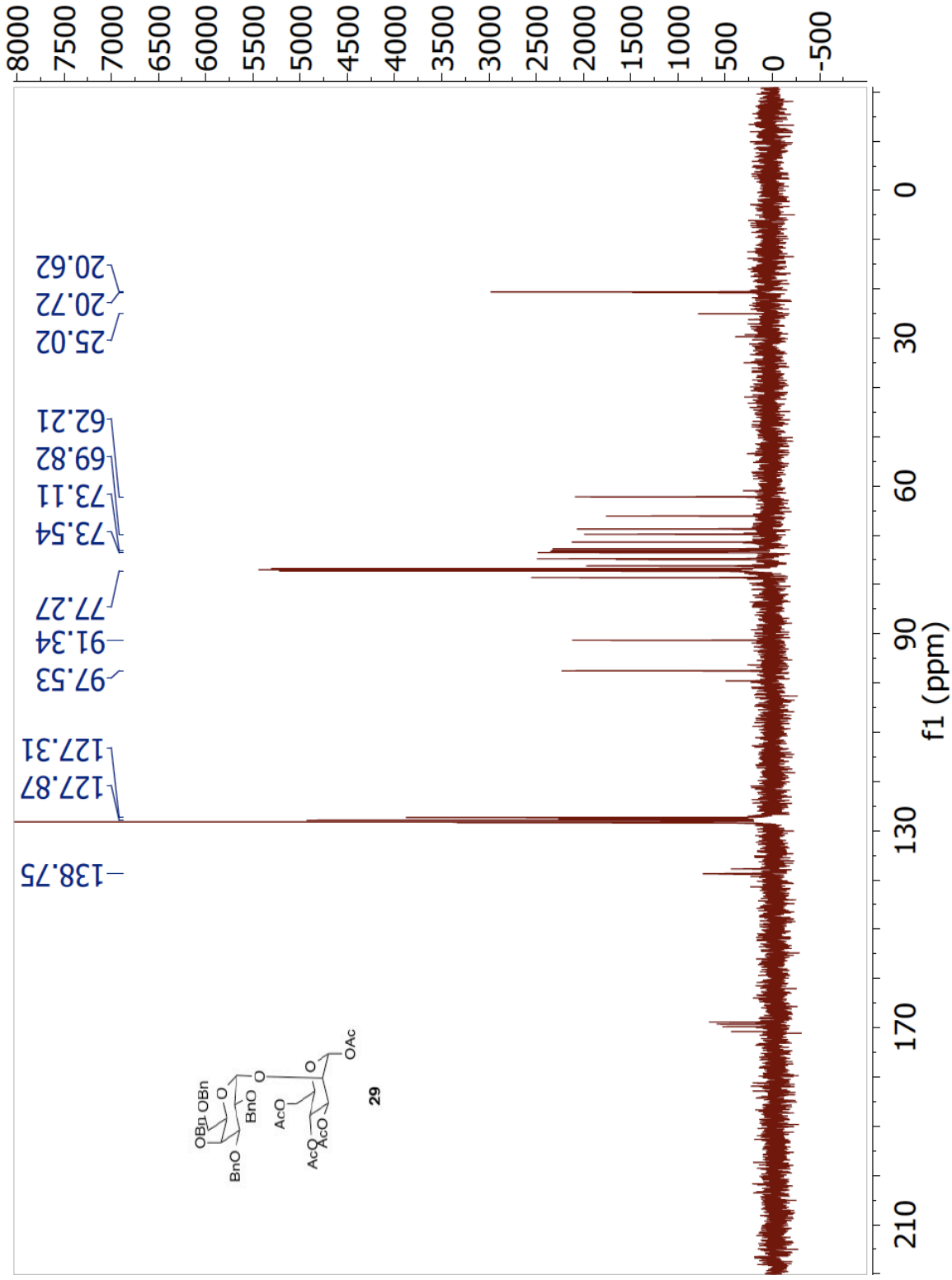


Figure 73. Full ^{13}C NMR spectrum for compound **29.**

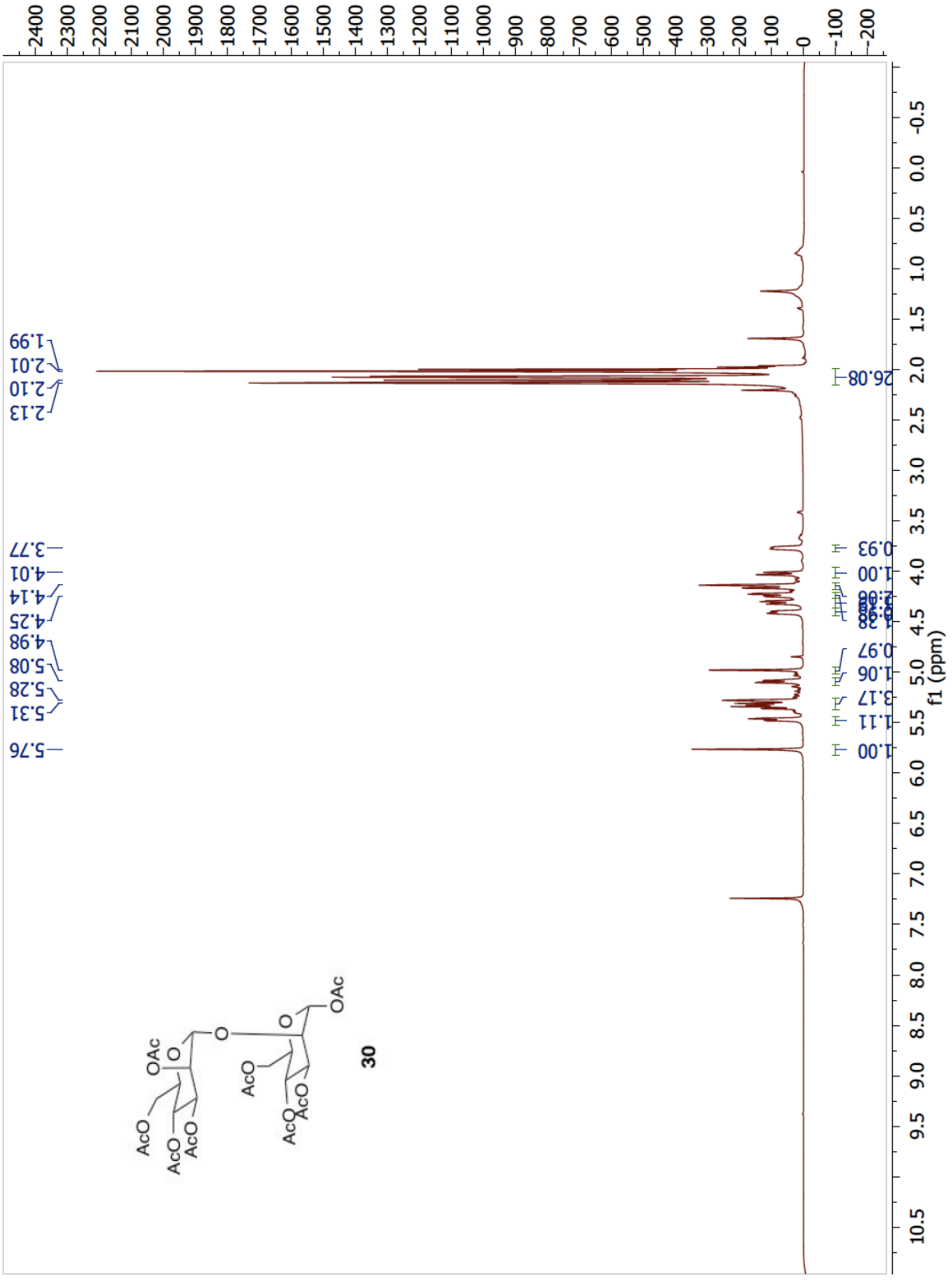


Figure 74. Full ^{1}H NMR spectrum for compound **30.**

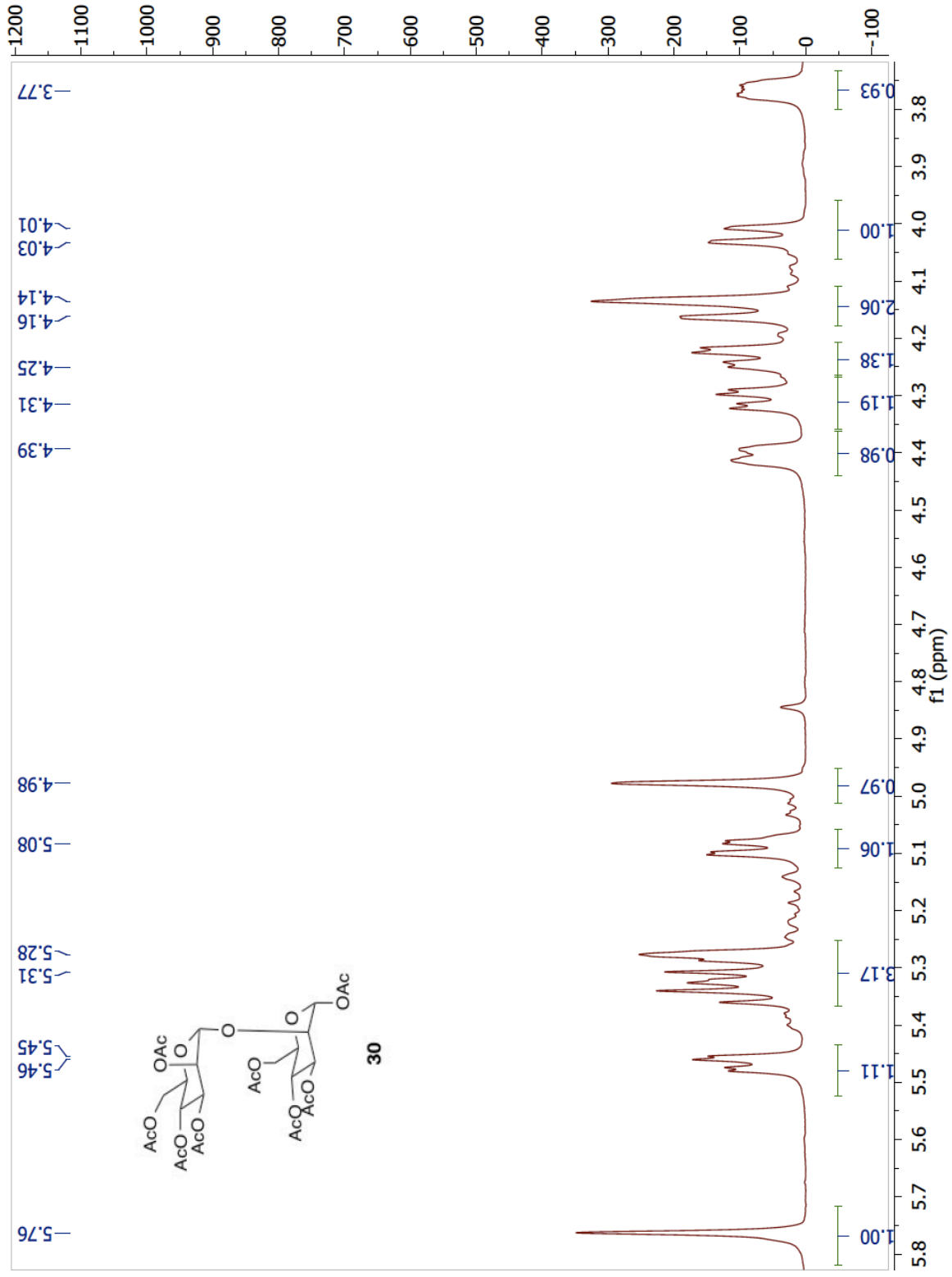


Figure 75. Expansion of the ^{1}H NMR carbohydrate region for compound **30**.

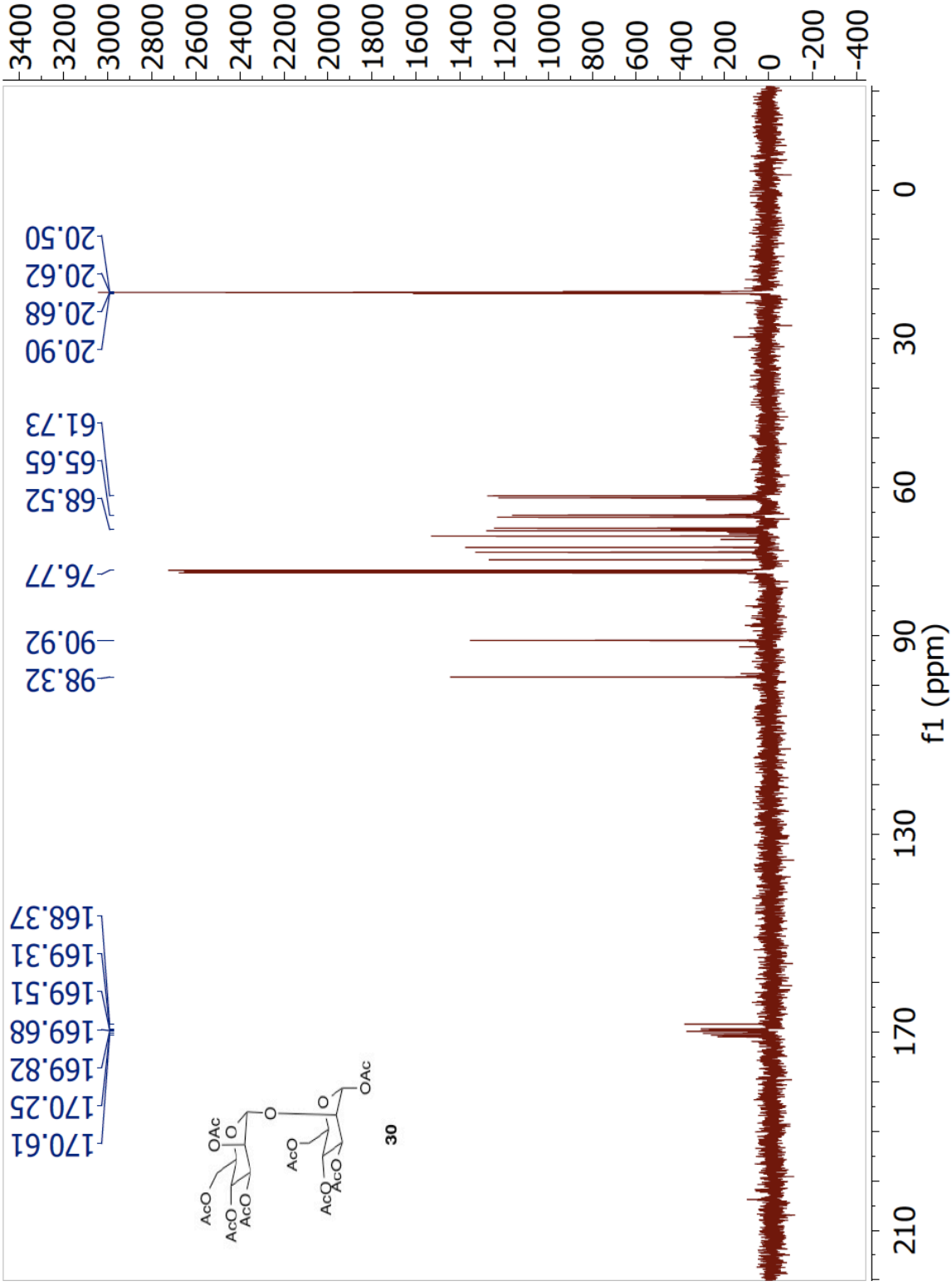


Figure 76. Full ^{13}C NMR spectrum for compound **30**.

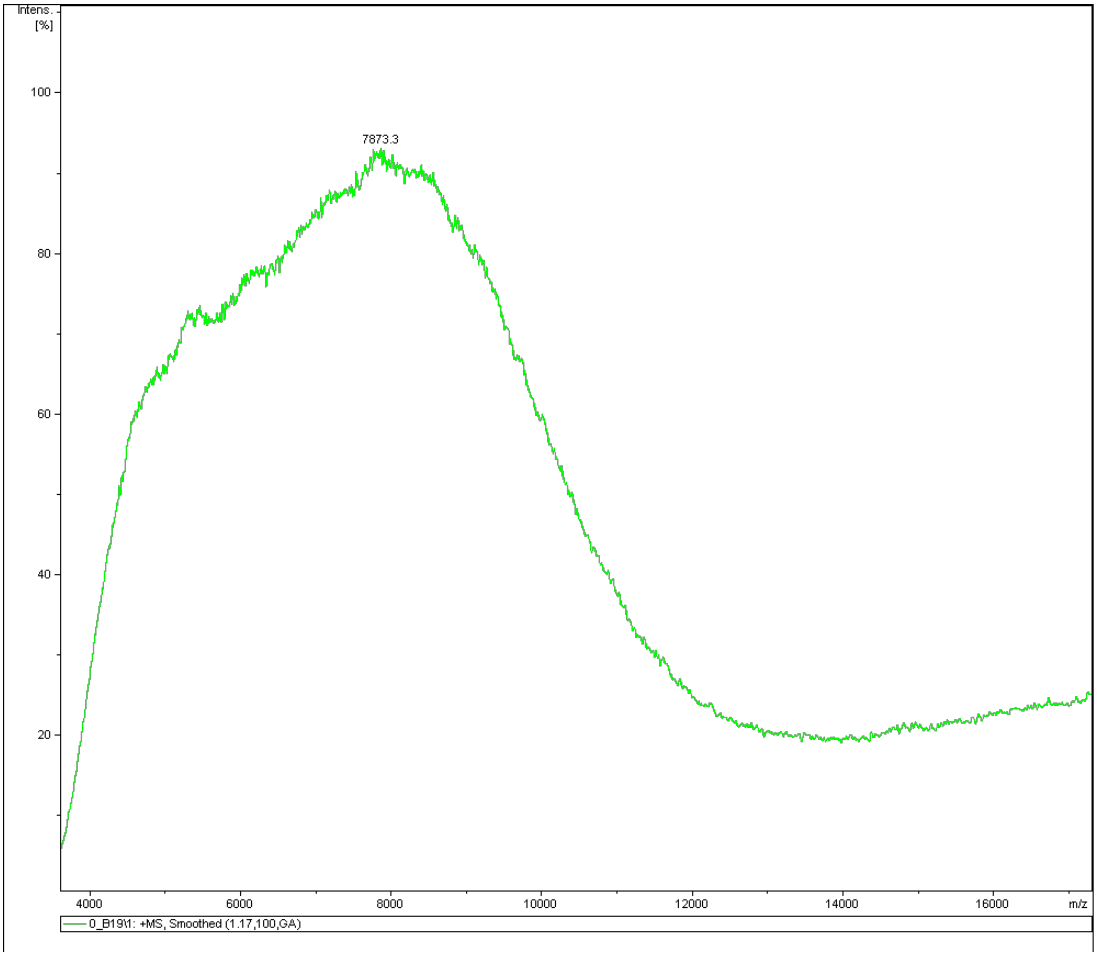


Figure 77. Smoothed MALDI-TOF spectrum for **31**. M_W = 8,536 g/mol.

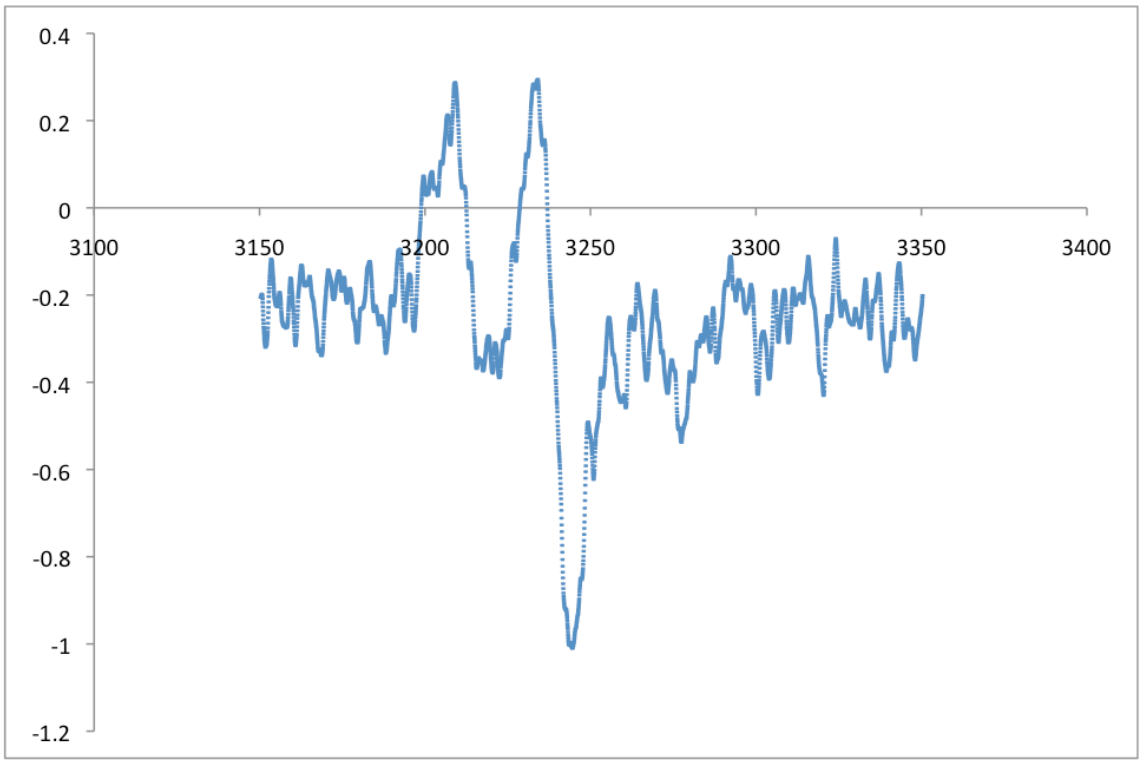


Figure 78. EPR spectrum for **31.**

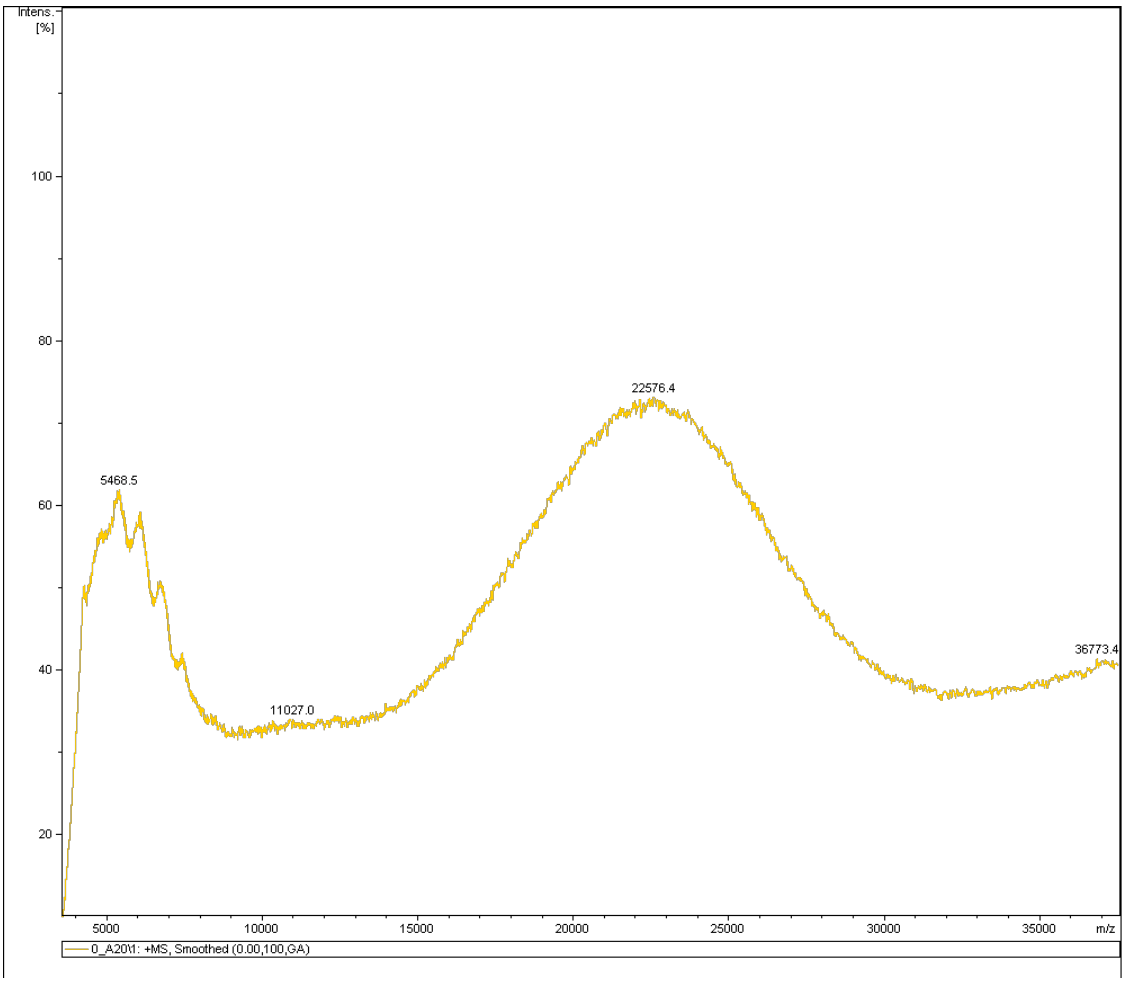


Figure 79. Smoothed MALDI-TOF spectrum for **32**. M_W = 22,834 g/mol.

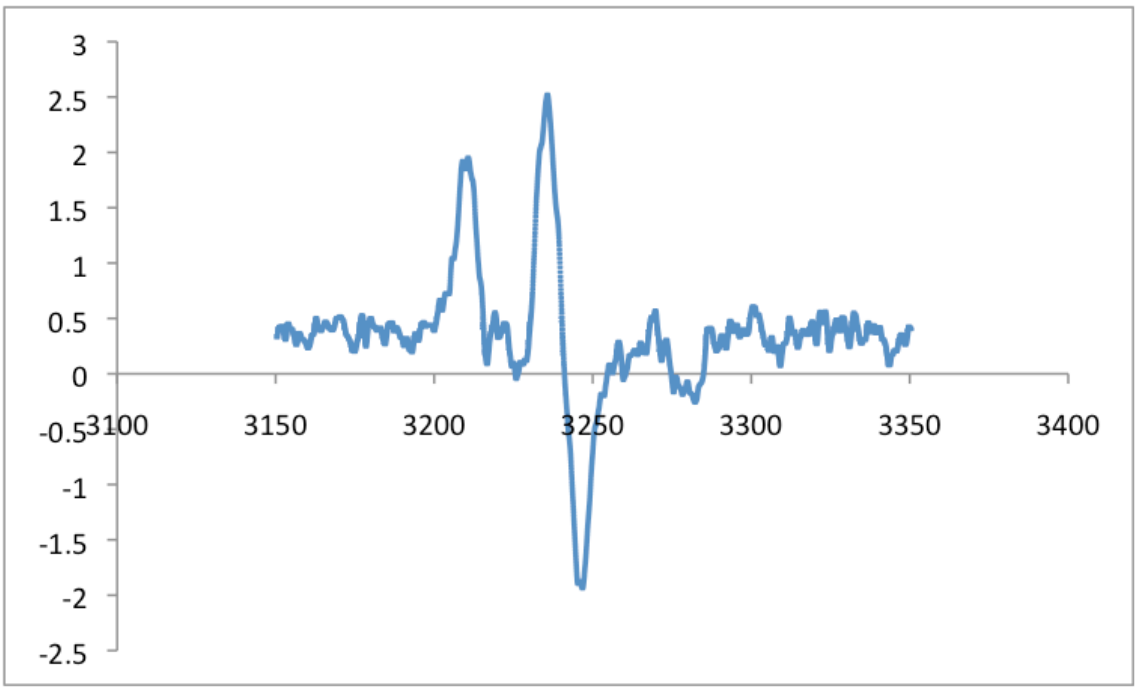


Figure 80. EPR spectrum for **32.**

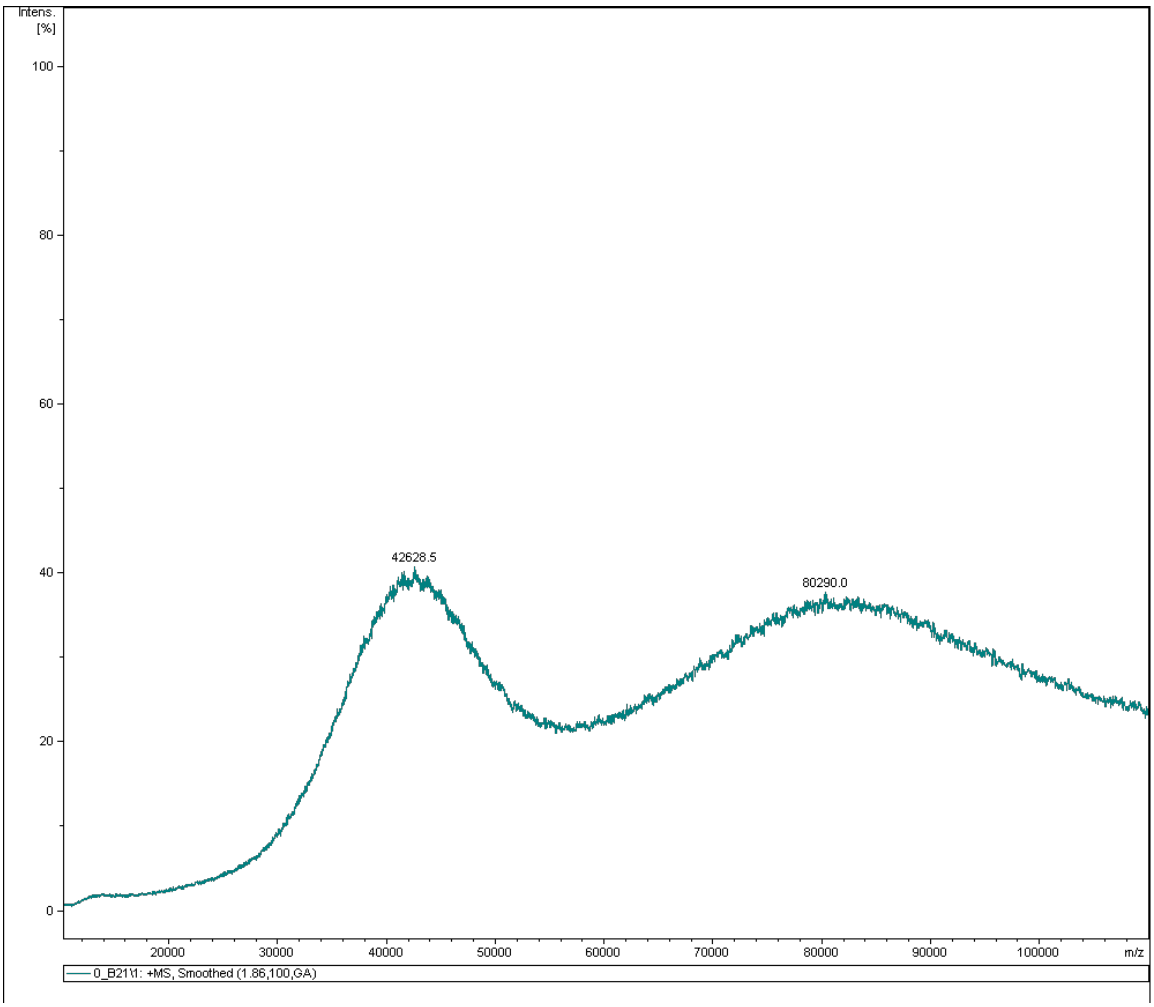


Figure 81. Smoothed MALDI-TOF spectrum for **33**. M_W = 42,796 g/mol.

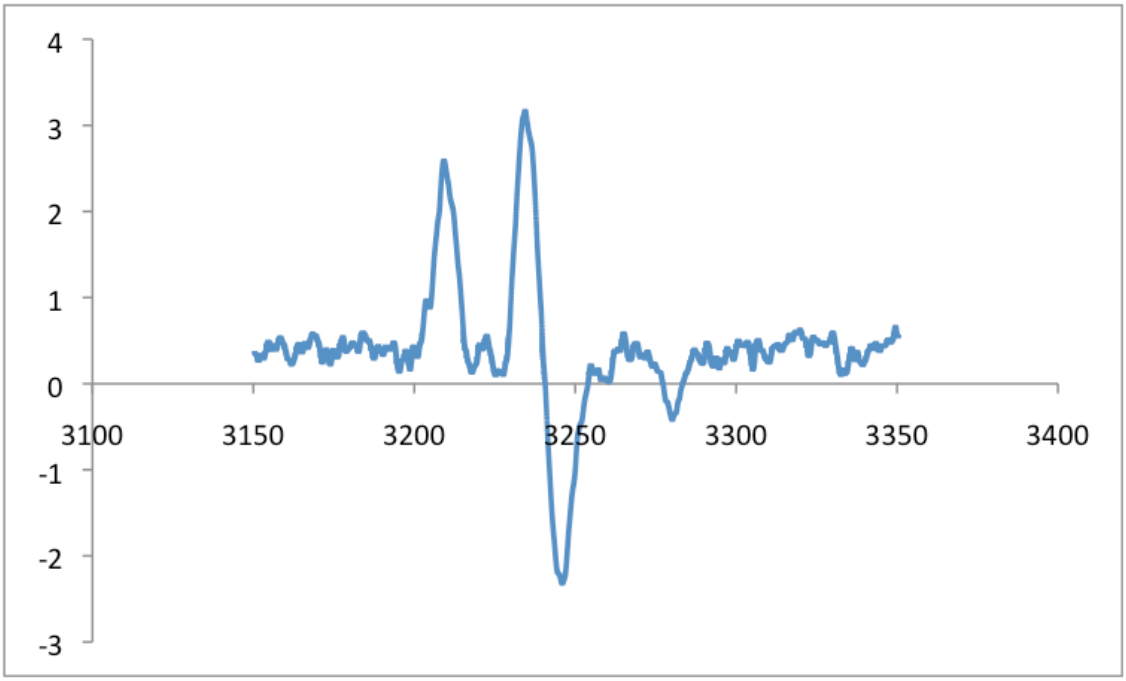


Figure 82. EPR spectrum for **33.**

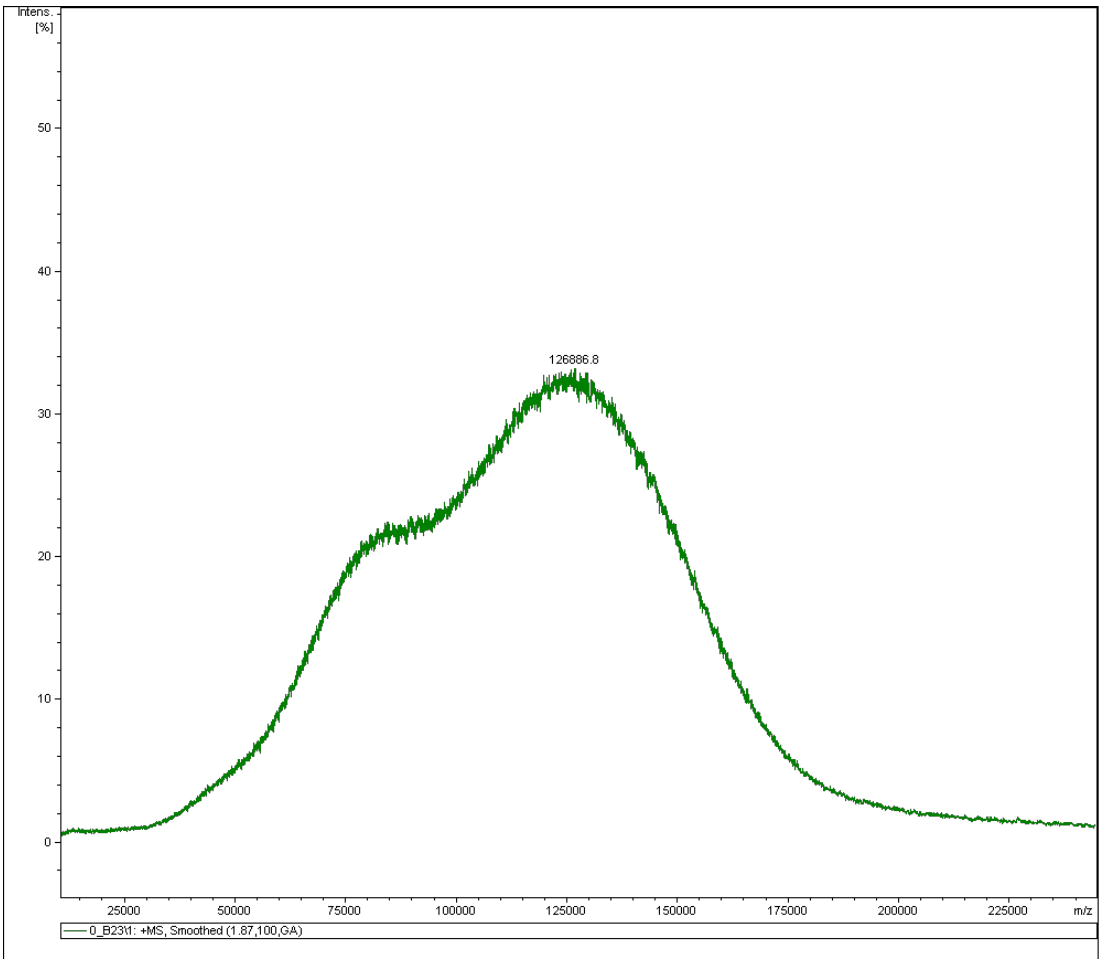


Figure 83. Smoothed MALDI-TOF spectrum for **34**. M_W = 116,587 g/mol.

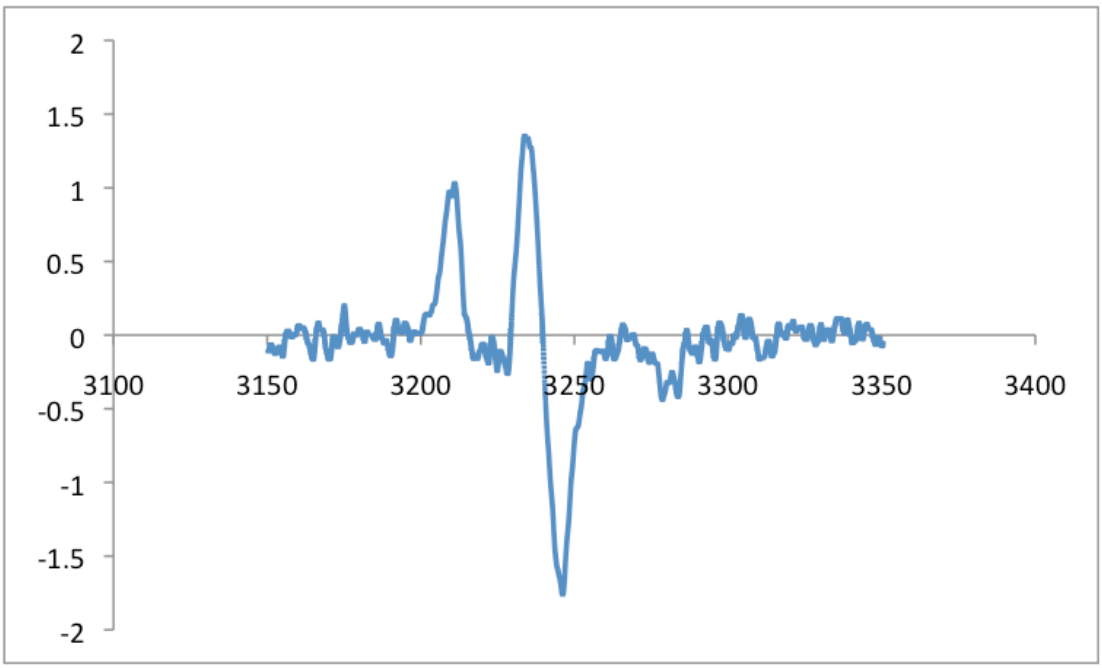


Figure 84. EPR spectrum for **34**.

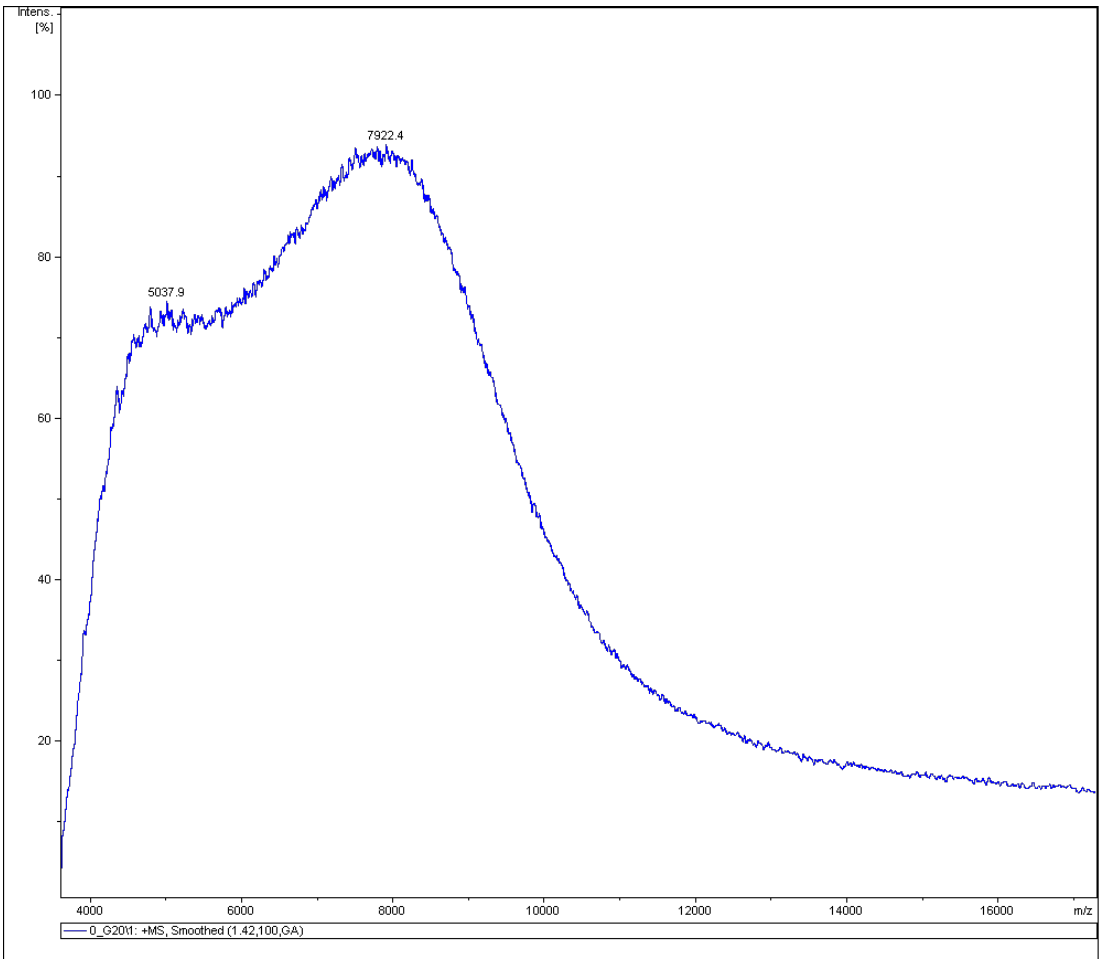


Figure 85. Smoothed MALDI-TOF spectrum for **35**. M_W = 6,854 g/mol.

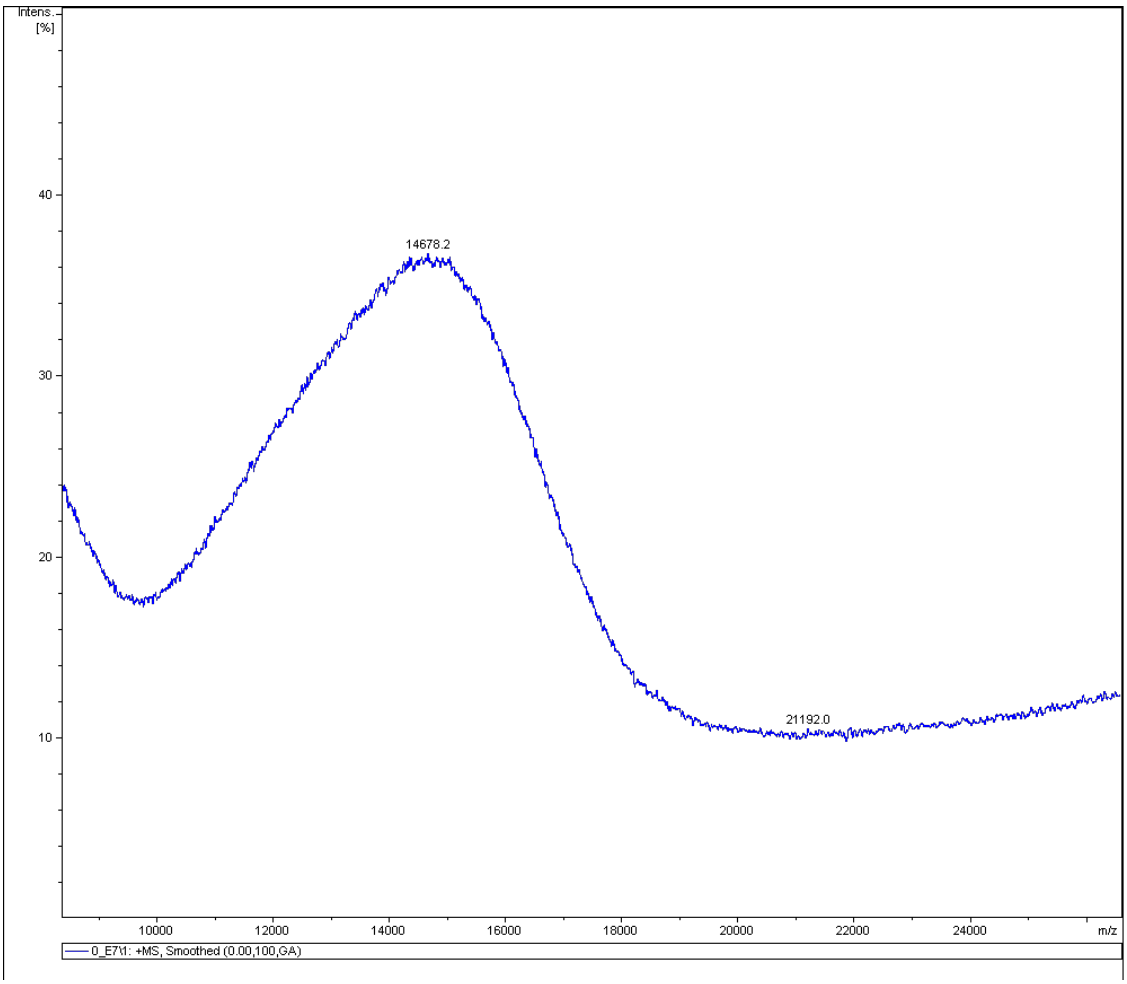


Figure 86. Smoothed MALDI-TOF spectrum for **36**. M_W = 16,330 g/mol.

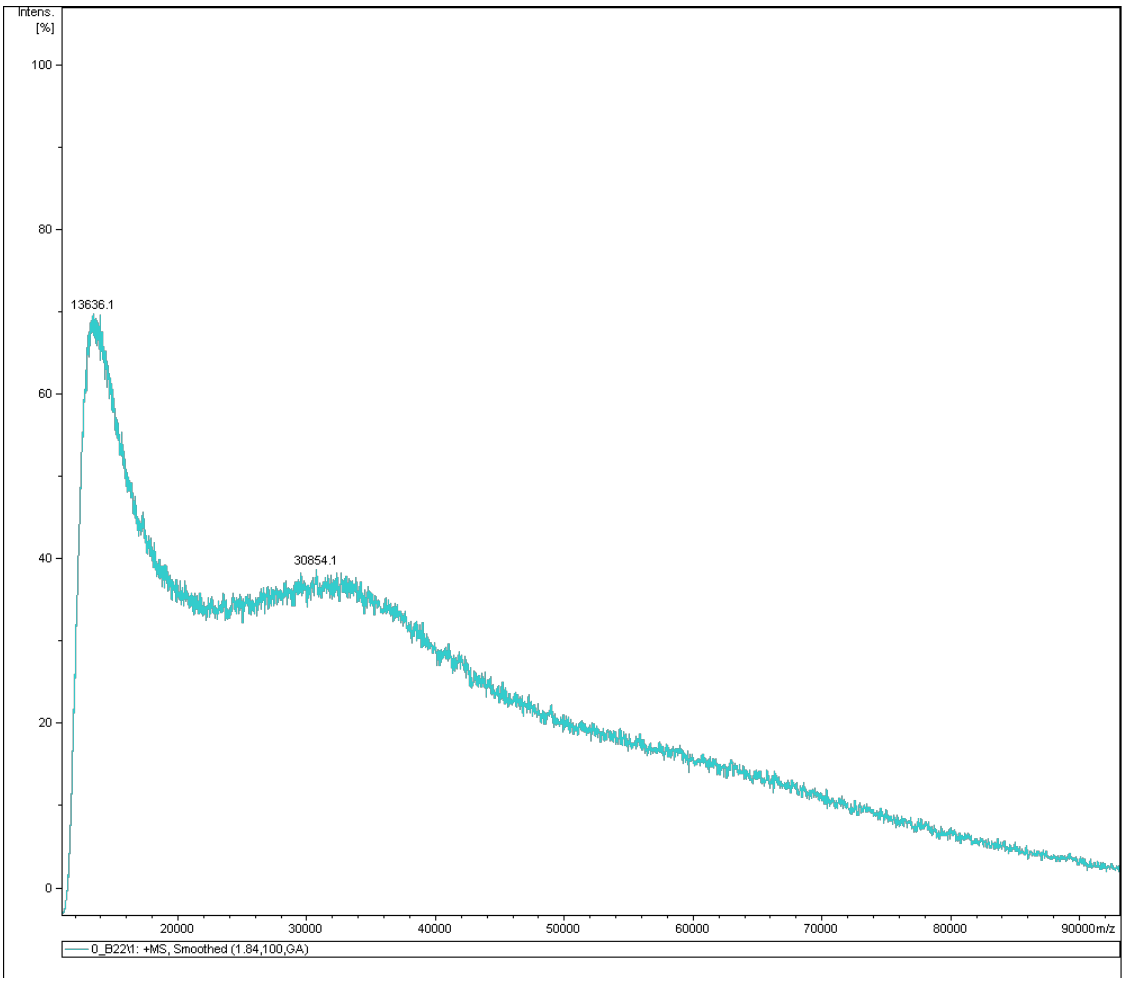


Figure 87. Smoothed MALDI-TOF spectrum for **37**. M_W = 30,791 g/mol.

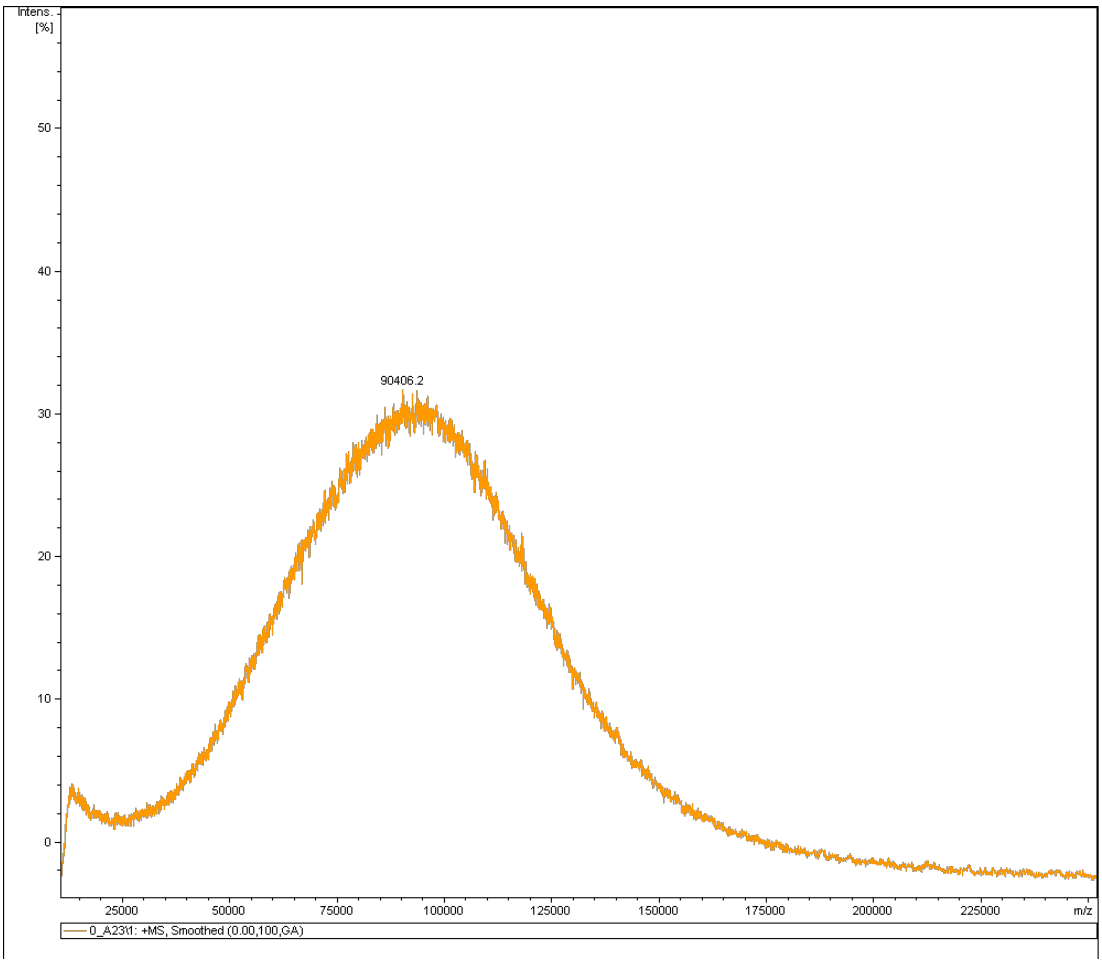


Figure 88. Smoothed MALDI-TOF spectrum for **38**. M_W = 91,055 g/mol.

APPENDIX C

COPYRIGHT INFORMATION FOR REPRINTED FIGURES

Figure 2 has been reprinted with permission from the RCSB Protein Data bank:

> *Data files contained in the PDB archive (**ftp://ftp.wwpdb.org**) are free of all copyright restrictions and made fully and freely available for both non-commercial and commercial use…Molecular images from RCSB PDB Structure Summary pages are available under the same conditions. The authors of the structural data producing the image and the RCSB PDB should be cited.*

Figure 5 has been reprinted with permission from Elsevier, publisher of *Clinica Chimica Acta.* From the General Terms conditions for the Copyright Clearance Center:

> *2. Elsevier hereby grants you permission to reproduce the aforementioned material subject to the terms and conditions indicated.*

Figure 6 has been reprinted with permission in accordance to the journal in which it was originally published (Reproductive Biology and Endocrinology, published by Biomed Central):

> *Reproduction of figures or tables from any article is permitted free of charge and without formal written permission from the publisher or the copyright holder, provided that the figure/table is original, BioMed Central is duly identified as the original publisher, and that proper attribution of authorship and the correct citation details are given as acknowledgment.*

REFERENCES CITED

1. Hirabayashi J, Kasai K. The family of metazoan metal-independent beta-galactoside-binding lectins - structure, function, and molecular evolution. Glycobiology. 1993;3: 297-304.

2. Zhao Y, Takahashi M, Gu J, et al. Functional roles of N-glycans in cell signaling and cell adhesion in cancer. Cancer Science. 2008;99: 1304-1310.

3. Kilpatrick D. Animal lectins: a historical introduction and overview. Biochimica Et Biophysica Acta-General Subjects. 2002;1572: 187-197.

4. Gabius H, Andre S, Jimenez-Barbero J, Romero A, Solis D. From lectin structure to functional glycomics: principles of the sugar code. Trends in Biochemical Sciences. 2011;36: 298-313.

5. Norling L, Perretti M, Cooper D. Endogenous galectins and the control of the host inflammatory response. Journal of Endocrinology. 2009;201: 169-184.

6. Balan V, Nangia-Makker P, Raz A. Galectins as Cancer Biomarkers. Cancers, 2010:592-610.

7. Wang B, Boons G-J. Carbohydrate Recognition: Biological Problems, Methods, and Applications. Hoboken, New Jersey: Wiley & Sons, 2011.

8. Than N, Romero R, Kim C, McGowen M, Papp Z, Wildman D. Galectins: guardians of eutherian pregnancy at the maternal-fetal interface. Trends in Endocrinology and Metabolism. 2012;23: 23-31.

9. Cooper D. Galectinomics: finding themes in complexity. Biochimica Et Biophysica Acta-General Subjects. 2002;1572: 209-231.

10. Sorme P, Arnoux P, Kahl-Knutsson B, Leffler H, Rini J, Nilsson U. Structural and thermodynamic studies on cation - II interactions in lectin-ligand complexes: High-affinity galectin-3 inhibitors through fine-tuning of an arginine-arene interaction. Journal of the American Chemical Society. 2005;127: 1737-1743.

11. Saraboji K, Hakansson M, Genheden S, Diehl C, Qvist J. The carbohydrate-binding site in galectin-3 is preorganized to recognize a sugarlike framework of oxygens: ultra-high-resolution structures and water dynamics. Biochemistry (Easton). 2012;51: 296-306.

12. http://www.rcsb.org/pdb/explore/explore.do?structureId=3zsj.

13. Dumic J, Dabelic S, Flogel M. Galectin-3: An open-ended story. Biochimica Et Biophysica Acta-General Subjects. 2006;1760: 616-635.

14. Ahmad N, Gabius H, Andre S, et al. Galectin-3 precipitates as a pentamer with synthetic multivalent carbohydrates and forms heterogeneous cross-linked complexes. Journal of Biological Chemistry. 2004;279: 10841-10847.

15. Dam T, Gabius H, Andre S, Kaltner H, Lensch M, Brewer C. Galectins bind to the multivalent glycoprotein asialofetuin with enhanced affinities and a gradient of decreasing binding constants. Biochemistry. 2005;44: 12564-12571.

16. Kubler D, Hung C, Dam T, et al. Phosphorylated human galectin-3: Facile large-scale preparation of active lectin and detection of structural changes by CD spectroscopy. Biochimica Et Biophysica Acta-General Subjects. 2008;1780: 716-722.

17. Hsu D, Kuwabara I, Liu F. Galectin-3 and regulation of cell function. Transfusion Medicine and Hemotherapy. 2005;32: 83-96.

18. Ochieng J, Platt, D, Tait, L, et al. Structure-function relationship of a recombinant human galactoside-binding protein. Biochemistry. 1993;32: 4455-4460.

19. Kuklinski S, Probstmeier R. Homophilic binding properties of galectin-3: Involvement of the carbohydrate recognition domain. Journal of Neurochemistry. 1998;70: 814-823.

20. Leffler H, Carlsson S, Hedlund M, Qian Y, Poirier F. Introduction to galectins. Glycoconjugate Journal. 2002;19: 433-440.

21. Mehul B, Bawumia S, Martin S, Hughes R. Structure of baby hamster-kidney carbohydrate-binding protein CBP30, an S-type animal lectin. Journal of Biological Chemistry. 1994;269: 18250-18258.

22. Hsu D, Zuberi R, Liu F. Biochemical and biophysical characterization of human recombinant IgE-binding protein, an S-type animal lectin. Journal of Biological Chemistry. 1992;267: 14167-14174.

23. Zhao Q, Guo X, Nash G, et al. Circulating Galectin-3 Promotes Metastasis by Modifying MUC1 Localization on Cancer Cell Surface. Cancer Research. 2009;69: 6799-6806.

24. Yu L, Andrews N, Zhao Q, et al. Galectin-3 interaction with Thomsen-Friedenreich disaccharide on cancer-associated MUC1 causes increased cancer cell endothelial adhesion. Journal of Biological Chemistry. 2007;282: 773-781.

25. Bian C, Zhang Y, Sun H, Li D, Wang D. Structural Basis for Distinct Binding Properties of the Human Galectins to Thomsen-Friedenreich Antigen. Plos One. 2011;6.

26. Glinskii O, Sud S, Mossine V, et al. Inhibition of Prostate Cancer Bone Metastasis by Synthetic TF Antigen Mimic/Galectin-3 Inhibitor Lactulose-L-Leucine. Neoplasia. 2012;14: 65-73.

27. Varki A, Cummings RD, Esko JD, Freeze HH, Hart GW, Etzler EM. Essentials of Glycobiology, Second Edition. Cold Spring Harbor, NY: Cold Spring Harbor Laboratory Press, 2009

28. Tejler J, Leffler H, Nilsson U. Synthesis of O-galactosyl aldoximes as potent LacNAc-mimetic galectin-3 inhibitors. Bioorganic & Medicinal Chemistry Letters. 2005;15: 2343-2345.

29. Califice S, Castronovo V, Van Den Brule F. Galectin-3 and cancer. International Journal of Oncology. 2004;25: 983-992.

30. Newlaczyl, Yu LG. Galectin-3-A jack-of-all-trades in cancer. Cancer letters. 2011;313: 123-128.

31. Zhao Q, Barclay M, Rhodes J, Yu L. Galectin-3-muc1 interaction promotes epithelial cancer cell aggregation: Potential role of circulating galectin-3 in colon cancer metastasis. Gastroenterology. 2007;132: A306-A306.

32. Chen C, Zhao Q, Rhodes J, Yu L. Galectin-3 induces secretion of cytokines from vascular endothelium that enhance cancer cell-endothelium adhesion: a novel mechanism for galectin-3-mediated metastasis promotion. Gut. 2012;61: A109-A110.

33. Chen C, Duckworth C, Zhao Q, Pritchard D, Rhodes J, Yu L. Increased Circulation of Galectin-3 in Cancer Induces Secretion of Metastasis-Promoting Cytokines from Blood Vascular Endothelium. Clinical Cancer Research. 2013;19: 1693-1704.

34. Cay T. Immunhistochemical Expression of Galectin-3 in Cancer: A Review of the Literature. Turkish Journal of Pathology, 2012:1-10.

35. Chiu C, Strugnell S, Griffith O, et al. Diagnostic Utility of Galectin-3 in Thyroid Cancer. American Journal of Pathology. 2010;176: 2067-2081.

36. Dancer J, Truong L, Zhai Q, Shen S. Expression of Galectin-3 in Renal Neoplasms A Diagnostic, Possible Prognostic Marker. Archives of Pathology & Laboratory Medicine. 2010;134: 90-94.

37. Lee J, Song S, Choi J, et al. Decreased galectin-3 expression during the progression of cervical neoplasia. Journal of Cancer Research and Clinical Oncology. 2006;132: 241-247.

38. Merseburger A, Kramer M, Hennenlotter J, et al. Involvement of decreased galectin-3 expression in the pathogenesis and progression of prostate cancer. Prostate. 2008;68: 72-77.

39. Song L, Tang J-w, Owusu L, Sun M-Z, Wu J, Zhang J. Galectin-3 in cancer. Clinica Chimica Acta, 2014:185-191.

40. Miyazaki J, Hokari R, Kato S, et al. Increased expression of galectin-3 in primary gastric cancer and the metastatic lymph nodes. Oncology Reports. 2002;9: 1307-1312.

41. Choi J, Il Cho S, Do N, Kang C, Lim S. Clinical Significance of the Expression of Galectin-3 and Pim-1 in Laryngeal Squamous Cell Carcinoma. Journal of Otolaryngology-Head & Neck Surgery. 2010;39: 28-34.

42. Yamaki S, Fujii T, Yajima R, et al. Clinicopathological significance of decreased galectin-3 expression and the long-term prognosis in patients with breast cancer. Surgery Today. 2013;43: 901-905.

43. Shekhar M, Nangia-Makker P, Tait L, Miller F, Raz A. Alterations in galectin-3 expression and distribution correlate with breast cancer progression - Functional analysis of galectin-3 in breast epithelial-endothefial interactions. American Journal of Pathology. 2004;165: 1931-1941.

44. Idikio H. Galectin-3 expression in human breast carcinoma: correlation with cancer histologic grade. International Journal of Oncology. 1998;12: 1287-1290.

45. Song S, Ji B, Ramachandran V, et al. Overexpressed Galectin-3 in Pancreatic Cancer Induces Cell Proliferation and Invasion by Binding Ras and Activating Ras Signaling. Plos One. 2012;7.

46. Kim Y, Jung J, Kim H, et al. Galectin-3 binding protein promotes cell motility in colon cancer by stimulating the shedding of protein tyrosine phosphatase kappa by proprotein convertase. Biochemical and Biophysical Research Communications. 2011;404: 96-102.

47. Kim S, Shin J, Lee K, et al. Galectin-3 Facilitates Cell Motility in Gastric Cancer by Up-Regulating Protease-Activated Receptor-1(PAR-1) and Matrix Metalloproteinase-1(MMP-1). Plos One. 2011;6.

48. Cheng Y, Huang W, Chen C, et al. Increased galectin-3 facilitates leukemia cell survival from apoptotic stimuli. Biochemical and Biophysical Research Communications. 2011;412: 334-340.

49. Nangia-Makker P, Wang Y, Raz T, et al. Cleavage of galectin-3 by matrix metalloproteases induces angiogenesis in breast cancer. International Journal of Cancer. 2010;127: 2530-2541.

50. Nangia-Makker P, Balan V, Raz A. Regulation of Tumor Progression by Extracellular Galection-3. Cancer Microenvironment, 2008:43-51.

51. Inohara H, Akahani S, Koths K, Raz A. Interactions between galectin-3 and Mac-2-binding protein mediate cell-cell adhesion. Cancer Research. 1996;56: 4530-4534.

52. Yu L. The oncofetal Thomsen-Friedenreich carbohydrate antigen in cancer progression. Glycoconjugate Journal. 2007;24: 411-420.

53. Guzman A, Argueso P. Structure and Biological Roles of Mucin-type O-glycans at the Ocular Surface. The ocular surface. 2010;8: 8-17.

54. Rapoport E, Andre S, Kurmyshkina O, et al. Galectin-loaded cells as a platform for the profiling of lectin specificity by fluorescent neoglycoconjugates: A case study on galectins-1 and-3 and the impact of assay setting. Glycobiology. 2008;18: 315-324.

55. Rapoport E, Pochechueva T, Kurmyshkina O, et al. Solid-phase assays for study of carbohydrate specificity of galectins. Biochemistry-Moscow. 2010;75: 310-319.

56. Song X, Xia B, Stowell S, Lasanajak Y, Smith D, Cummings R. Novel Fluorescent Glycan Microarray Strategy Reveals Ligands for Galectins. Chemistry & Biology. 2009;16: 36-47.

57. Chen J, Zhang M. The Par3/Par6/aPKC complex and epithelial cell polarity. Experimental Cell Research. 2013;319: 1357-1364.

58. Alberts B, Johnson A, Lewis J. Molecular Biology of the Cell. 4th ed. New York, New York: Garland Science, 2002.

59. Liu Y, Chen L. The regulation of cell polarity in the progression of lung cancer. Journal of Cancer Research and Therapeutics. 2013;9: S80-S85.

60. Martin-Belmonte F, Perez-Moreno M. Epithelial cell polarity, stem cells and cancer. Nature Reviews Cancer. 2012;12: 23-38.

61. Fedeles S, Gallagher A. Cell polarity and cystic kidney disease. Pediatric Nephrology. 2013;28: 1161-1172.

62. Brayman M, Thathiah A, Carson D. MUC1: A multifunctional cell surface component of reproductive tissue epithelia. Reproductive Biology and Endocrinology, 2004.

63. Linden S, Sheng Y, Every A, et al. MUC1 Limits Helicobacter pylori Infection both by Steric Hindrance and by Acting as a Releasable Decoy. Plos Pathogens. 2009;5.

64. Singh P, Hollingsworth M. Cell surface-associated mucins in signal transduction. Trends in Cell Biology. 2006;16: 467-476.

65. Van Elssen C, Frings P, Bot F, et al. Expression of aberrantly glycosylated Mucin-1 in ovarian cancer. Histopathology. 2010;57: 597-606.

66. Savla R, Taratula O, Garbuzenko O, Minko T. Tumor targeted quantum dot-mucin 1 aptamer-doxorubicin conjugate for imaging and treatment of cancer. Journal of Controlled Release. 2011;153: 16-22.

67. Lee Y, Townsend RR, Hardy MR, Lonngren J, Arnarp J. Binding of synthetic oligosaccharides to the hepatic Gal/GalNAc lectin. Dependence on fine structural features. The Journal of biological chemistry. 1983;258: 199-202.

68. Lee YC. Biochemistry of carbohydrate-protein interaction. The FASEB journal. 1992;6: 3193-3200.

69. Lee YC. Binding modes of mammalian hepatic Gal/GalNAc receptors: JOHN WILEY & SONS LTD, 1989:80-93, discussion 93-85.

70. Chabre Y, Roy R, Horton D. Design and creativity in synthesis of multivalent neoglucoconjugates. Advances in Carbohydrate Chemistry and Biochemistry, Vol 63. 2010;63: 165-393.

71. Vrasidas I, Andre S, Valentini P, et al. Rigidified multivalent lactose molecules and their interactions with mammalian galectins; a route to selective inhibitors. Organic & Biomolecular Chemistry. 2003;1: 803-810.

72. Newkome GR, Moorefield CN, Vögtle F. Dendrimers and dendrons : concepts, syntheses, applications. Weinheim ; New York: Wiley-VCH, 2001.

73. Cloninger M. Biological applications of dendrimers. Current Opinion in Chemical Biology. 2002;6: 742-748.

74. Lee C, MacKay J, Frechet J, Szoka F. Designing dendrimers for biological applications. Nature Biotechnology. 2005;23: 1517-1526.

75. Chabre Y, Roy R. Recent trends in glycodendrimer syntheses and applications. Current Topics in Medicinal Chemistry. 2008;8: 1237-1285.

76. Hulikova K, Benson V, Svoboda J, Sima P, Fiserova A. N-Acetyl-D-glucosamine-coated polyamidoamine dendrimer modulates antibody formation via natural killer cell activation. International Immunopharmacology. 2009;9: 792-799.

77. Lundquist J, Toone E. The cluster glycoside effect. Chemical Reviews. 2002;102: 555-578.

78. Woller E, Walter E, Morgan J, Singel D, Cloninger M. Altering the strength of lectin binding interactions and controlling the amount of lectin clustering using mannose/hydroxyl-functionalized dendrimers. Journal of the American Chemical Society. 2003;125: 8820-8826.

79. Niederhafner P, Sebestik J, Jezek J. Glycopeptide dendrimers. Part I. Journal of Peptide Science. 2008;14: 2-43.

80. Goodman C, Wolfenden M, Nangia-Makker P, Raz A, Cloninger M. Multivalent Scaffolds Induce Galectin-3 Aggregation into Nanoparticles, 2014.

81. Furuike T, Aiba S, Nishimura SI. A Highly Practical Synthesis of Cyclodextrin-Based Glycoclusters Having Enhanced Affinity with Lectins. Tetrahedron. 2000;56: 9909-9915.

82. Vrasidas, de Mol NJ, Liskamp RMJ, Pieters RJ. Synthesis of lactose dendrimers and multivalency effects in binding to the cholera toxin B subunit. European journal of organic chemistry. 2001: 4685-4692.

83. Hatano K, Yamazaki T, Yoshino K, Ohyama N, Koyama T. Synthesis and lectin-binding activity of luminescent silica particles peripherally functionalized with lactose. Tetrahedron letters. 2008;49: 5593-5596.

84. Seah N, Santacroce PV, Basu A. Probing the lactose.GM3 carbohydrate-carbohydrate interaction with glycodendrimers. Organic letters. 2009;11: 559-562.

85. Wolfenden ML. Using PAMAM Dendrimer Frameworks to Investigate Multivalent Binding in Protein:Carbohydrate Interactions. Chemistry. Bozeman, MT: Montana State University, 2009.

86. Bizier N, Atkins S, Helland L, Colvin S, Twitchell J, Cloninger M. Indium triflate catalyzed peracetylation of carbohydrates. Carbohydrate Research. 2008;343: 1814-1818.

87. http://www.dendritech.com/pamam.html.

88. Consorzio Interuniversitario Nazionale Per la Bio-Oncologia I, Cumashi A, Sherman AA, Tsvetkov YE, Tinari N. Synthetic inhibitors of galectin-1 and -3 selectively modulate homotypic cell aggregation and tumor cell apoptosis. Anticancer research. 2009;29: 403-410.

89. Zou J, Glinsky VV, Landon LA, Matthews L, Deutscher SL. Peptides specific to the galectin-3 carbohydrate recognition domain inhibit metastasis-associated cancer cell adhesion. Carcinogenesis (New York). 2005;26: 309-318.

90. Andre S, Ortega P, Perez M, Roy R, Gabius H. Lactose-containing starburst dendrimers: influence of dendrimer generation and binding-site orientation of receptors (plant/animal lectins and immunoglobulins) on binding properties. Glycobiology. 1999;9: 1253-1261.

91. Otsuji E, Park Y, Tashiro K, Kojima N, Toyokuni T, Hakomori S. Inhibition of B16 melanoma metastasis by administration of G(M3)- or GG3- liposomes - blocking adhesion of melanoma-cells to endothelial-cells (antiadhesion therapy) via inhibition of G(M3)-GG3CER or G(M3)-LACCER interaction. International Journal of Oncology. 1995;6: 319-327.

92. Lieber M, Smith B, Szakal A, Nelsonrees W, Todaro G. Continuous tumor-cell line from a human lung carcinoma with properties of type-II alveolar epithelial cells. International Journal of Cancer. 1976;17: 62-70.

93. Giard D, Aaronson S, Todaro G, et al. In-vitro cultivation of human tumors - establishment of cell lines derived from a series of solid tumors. Journal of the National Cancer Institute. 1973;51: 1417-1423.

94. Rasheed S, Nelsonre W, Toth E, Arnstein P, Gardner M. Characterization of a newly derived human sarcoma cell line (HT-1080). Cancer. 1974;33: 1027-1033.

95. Nangia-Makker P, Balan V, Raz A. Galectin-3 binding and Metastasis. Methods Mol Biol., 2012:251-266.

96. Smith PK, Krohn RI, Hermanson GT, et al. Measurement of Protein Using Bicinchoninic Acid. Analytical Biochemistry, 1985:76-85.

97. Allen T, Cullis P. Drug delivery systems: Entering the mainstream. Science. 2004;303: 1818-1822.

98. Malik N, Evagorou E, Duncan R. Dendrimer-platinate: a novel approach to cancer chemotherapy. Anti-Cancer Drugs. 1999;10: 767-776.

99. Kolonko E, Kiessling L. A polymeric domain that promotes cellular internalization. Journal of the American Chemical Society. 2008;130: 5626-+.

100. Saovapakhiran A, D'Emanuele A, Attwood D, Penny J. Surface Modification of PAMAM Dendrimers Modulates the Mechanism of Cellular Internalization. Bioconjugate Chemistry. 2009;20: 693-701.

101. Malik N, Wiwattanapatapee R, Klopsch R, et al. Dendrimers: Relationship between structure and biocompatibility in vitro, and preliminary studies on the biodistribution of I-125-labelled polyamidoamine dendrimers in vivo. Journal of Controlled Release. 2000;65: 133-148.

102. Gupta U, Agashe HB, Asthana A, Jain NK. A review of in vitro-in vivo investigations on dendrimers: the novel nanoscopic drug carriers. Nanomedicine. 2006;2: 66-73.

103. Gillies E, Dy E, Frechet J, Szoka F. Biological evaluation of polyester dendrimer: Poly(ethylene oxide) "Bow-Tie" hybrids with tunable molecular weight and architecture. Molecular Pharmaceutics. 2005;2: 129-138.

104. Kolonko E, Pontrello J, Mangold S, Kiessling L. General Synthetic Route to Cell-Permeable Block Copolymers via ROMP. Journal of the American Chemical Society. 2009;131: 7327-7333.

105. Nanjwade B, Bechra HM, Derkar GK, Manvi FV, Nanjwade VK. Dendrimers: emerging polymers for drug-delivery systems. European journal of pharmaceutical sciences. 2009;38: 185-196.

106. Wiwattanapatapee R, Lomlim L, Saramunee K. Dendrimers conjugates for colonic delivery of 5-aminosalicylic acid. Journal of controlled release. 2003;88: 1-9.

107. Kukowska-Latallo J, Candido KA, Cao ZY, Nigavekar SS, Majoros IJ. Nanoparticle targeting of anticancer drug improves therapeutic response in animal model of human epithelial cancer. Cancer research (Chicago, Ill.). 2005;65: 5317-5324.

108. Gullotti E, Yeo Y. Extracellularly activated nanocarriers: a new paradigm of tumor targeted drug delivery. Molecular pharmaceutics. 2009;6: 1041-1051.

109. Rowsell S, Hawtin P, Minshull CA, Jepson H, Brockbank SMV. Crystal structure of human MMP9 in complex with a reverse hydroxamate inhibitor. Journal of molecular biology. 2002;319: 173-181.

110. Tallant C, Marrero A, Xavier Gomis-Ruth F. Matrix metalloproteinases: fold and function of their catalytic domains. Biochimica et biophysica acta. Molecular cell research. 2010;1803: 20-28.

111. Meyer B, Rademann J. Extra- and Intracellular Imaging of Human Matrix Metalloprotease 11 (hMMP-11) with a Cell-penetrating FRET Substrate. Journal of Biological Chemistry. 2012;287.

112. Zhang M, Teng X-d, Guo X-x, Li Z-g, Han J-g. Expression of tissue levels of matrix metalloproteinases and their inhibitors in breast cancer. Breast (Edinburgh). 2013;22: 330-334.

113. http://www.anaspec.com/products/productcategory.asp?id=174.

114. Lindhorst TK. Essentials of Carbohydrate Chemistry and Biochemistry. Weinheim, Germany: Wiley-VCH Verlag GmbH & Co. KGaA, 2007.

115. Koenigs W, Knorr E. On some derivatives of dextrose and galactose. Berichte Der Deutschen Chemischen Gesellschaft. 1901;34: 957-981.

116. Garegg P. Synthesis and reactions of glycosides. Advances in Carbohydrate Chemistry and Biochemistry, Vol 59. 2004;59: 69-134.

117. Schmidt R, Michel J. Facile synthesis of alpha-O-glycosyl and beta-O-glycosyl imidates - preparation of glycosides and disaccharides. Angewandte Chemie-International Edition in English. 1980;19: 731-732.

118. Schmidt R. New methods for the synthesis of glycosides and oligosaccharides - are there alternatives to the Koenigs-Knorr method. Angewandte Chemie-International Edition in English. 1986;25: 212-235.

119. Stick RV. Carbohydrates: The Sweet Molecules of Life. London: Academic Press, 2001.

120. Loh T, Chua G. Discovery of indium complexes as water-tolerant Lewis acids. Chemical Communications. 2006: 2739-2749.

121. Frost C, Hartley J. New applications of indium catalysts in organic synthesis. Mini-Reviews in Organic Chemistry. 2004;1: 1-7.

122. Bandini M, Cozzi P, Giacomini M, Melchiorre P, Selva S, Umani-Ronchi A. Sequential one-pot InBr3-catalyzed 1,4-then 1,2-nucleophilic addition to enones. Journal of Organic Chemistry. 2002;67: 3700-3704.

123. Mattson A, Michel AK, Cloninger MJ. Using In(III) as a promoter for glycosylation. Carbohydrate research. 2012;347: 142-146.

124. Kaneko M, Hayashi R, Cook GR. Intermolecular friedel-crafts reaction catalyzed by InCl3. Tetrahedron Letters. 2007;48: 7085-7087.

125. Thirupathi P, Kim SS. InBr3: A Versatile Catalyst for the Different Types of Friedel-Crafts Reactions. Journal of Organic Chemistry. 2009;74: 7755-7761.

126. Fukase K, Kinoshita T, Naki Y, Hasuoka A, Kusumoto S. A novel method for the stereoselective glycosidation with thioglycosides: promotion by hypervalent iodine, reagents prepared from HIO and various acids. Tetrahedron Letters, 1996:3897-3904.

127. Adinolfi M, Barone G, Iadonisi A, Schiattarella M. Iodine/triethylsilane as a convenient promoter system for the activation of disarmed glycosyl trichloro- and N-(phenyl)trifluoroacetimidates. Synlett. 2002: 269-270.

128. Ren T, Liu D. Synthesis of targetable cationic amphiphiles. Tetrahedron Letters. 1999;40: 7621-7625.

129. Gros EG, Gruneiro EM. Methylation of carbohydrates bearing base-labile substituents, with diazomethane-boron trifluoride etherate. Carbohydrate research. 1970;14: 409-411.

130. Kim S, Song S, Lee T, Jung S, Kim D. Practical synthesis of KRN7000 from phytosphingosine. Synthesis-Stuttgart. 2004: 847-850.

131. Stanca-Kaposta E, Gamblin D, Cocinero E, et al. Solvent interactions and conformational choice in a core N-glycan segment: Gas phase conformation of the central, branching trimannose unit and its singly hydrated complex. Journal of the American Chemical Society. 2008;130: 10691-10696.

132. Decoster E, Lacombe JM, Strebler JL, Ferrari B, Pavia AA. Another Approach to the Synthesis of Benzyl Derivatives of Reducing Monosaccharides - Study of Pyranose-Furanose Equilibria by C-13 Nmr. Journal of Carbohydrate Chemistry. 1983;2: 329-341.

133. Mangold SL, Morgan JR, Strohmeyer GC, Gronenborn AM, Cloninger MJ. Cyanovirin-N binding to Man alpha 1-2Man functionalized dendrimers. Organic & Biomolecular Chemistry. 2005;3: 2354-2358.

134. Excoffier G, Gagnaire DY, Vignon MR. Synthèse du nigérose et du laminarabiose sur polymère support. Carbohydrate research. 1976;51: 280-286.

135. Blattner R, Furneaux RH, Pakulski Z. 1,3-Dideoxynojirimycin-3-yl glycosides of beta-(1-->3)- and beta-(1-->6)-linked gluco-oligosaccharides. Carbohydrate research. 2006;341: 2115-2125.

136. Macdonald JM, Hrmova M, Fincher GB, Stick RV. The Synthesis of 3-O-(β-D-Glucopyranosyl)- and 3-O-(β-Laminaribiosyl)-isofagomines, Potent Inhibitors of a 1,3-β-D-Glucan endo-Hydrolase. Australian journal of chemistry. 2004;57: 187-191.